Int J Thermophys (2023) 44:178
https://doi.org/10.1007/s10765-023-03263-6

# EOS-CG-2021: A Mixture Model for the Calculation of Thermodynamic Properties of CCS Mixtures

Tobias Neumann[1,2] · Stefan Herrig[1] · Ian H. Bell[3] · Robin Beckmüller[1] · Eric W. Lemmon[3] · Monika Thol[1] · Roland Span[1]

Received: 4 August 2023 / Accepted: 16 September 2023 / Published online: 16 November 2023


## Abstract

Thermodynamic properties for CCS-relevant mixtures can be calculated with the fundamental equation of state presented in this work over wide ranges of pressure, temperature, and composition for gas, liquid, and supercritical states, as well as for phase equilibria. The mixture model is formulated in terms of the Helmholtz energy and is based on the EOS-CG model of Gernert and Span (J Chem Thermodyn 93:274, 2016]. The new model presented here (EOS-CG-2021) is an update and extension of the previous version, and covers the following sixteen components: carbon dioxide, water, nitrogen, oxygen, argon, carbon monoxide, hydrogen, methane, hydrogen sulfide, sulfur dioxide, monoethanolamine, diethanolamine, hydrogen chloride, chlorine, ammonia, and methyl diethanolamine. Previously published elements of the model are summarized, and new elements are validated and analyzed with the use of comparisons to experimental data and by assessing the physical and extrapolation behavior of the equations. A comprehensive study on the representation of multicomponent mixture data was carried out to show the high accuracy and application range of the EOS-CG-2021.

**Keywords** Carbon capture and storage (CCS) · Carbon dioxide-rich · Fundamental equation of state · Helmholtz energy · Multiparameter mixture model · Thermodynamic properties

✉ Roland Span
roland.span@thermo.rub.de

[1] Lehrstuhl für Thermodynamik, Ruhr-Universität Bochum, Universitätsstraße 150, 44801 Bochum, Germany

[2] Department of Chemical Engineering, Norwegian University of Science and Technology, 7491 Trondheim, Norway

[3] Applied Chemicals and Materials Division, National Institute of Standards and Technology, Boulder, CO, USA

## 1 Introduction

The effects of global climate change and its severe negative impacts on the earth have been studied for several decades, and an increasing number of actions have been taken to reduce its effects. One of the major milestones was the Kyoto Protocol in 1997 [1], which aimed to reduce the emissions of greenhouse gases, in particular, the most abundant one—carbon dioxide ($CO_2$). In 2015, the Paris Agreement [2] was negotiated to renew and extend previous decisions. The goal was set to remain below a 1.5 °C temperature increase. Global $CO_2$ emissions, however, continued to increase [3] leading to the formulation of four pathways in a dedicated IPCC report [4] to avoid the 1.5 °C increase. Three of the four included large-scale deployment of carbon capture and storage (CCS) processes. This technology has been successfully applied on an industrial scale since 1996 at the Sleipner gas field in Norway, where over 20 million tons of $CO_2$ have already been stored. Such processes for implementing separation, transportation, and storage of $CO_2$ are associated with large costs for the operators.

With or without proper political incentives, a viable approach to make CCS more economically attractive to industry is the increase of the efficiency of the technology. The knowledge of thermodynamic properties plays a crucial role in this undertaking. The ability to accurately calculate properties, e.g., phase boundaries, densities, speeds of sound, or heat capacities, with a single model increases production and safety and reduces costs as a result of the lower uncertainties, higher efficiencies, and fewer inconsistencies at interfaces between process steps. The EOS-CG model of Gernert and Span [5], based on the functional form of the GERG-2008 [6] model for natural gases, was developed in 2016 as the first step to meet these needs. It is formulated in terms of state-of-the-art Helmholtz energy equations of state (EOS), where the multicomponent mixture model is based on the combination of all possible binary mixture models of the constituents. The binary-specific models are built on highly accurate pure-fluid Helmholtz energy equations of state, which are then combined with interaction parameters fitted to experimental data for each binary mixture. The full mixture model, built on the combination of these models for the binary mixtures, makes possible the calculation of multicomponent mixture properties.

The EOS-CG model consistently and accurately describes thermodynamic properties in all fluid regions for $CO_2$-rich mixtures containing nitrogen ($N_2$), oxygen ($O_2$), argon (Ar), water ($H_2O$), and carbon monoxide (CO). Due to the planned and executed application of CCS to additional sources of $CO_2$ and to the used separation technologies, the CCS stream may contain various other impurities. The present work extends the mixture model through the inclusion of hydrogen ($H_2$), methane ($CH_4$), hydrogen sulfide ($H_2S$), sulfur dioxide ($SO_2$), monoethanolamine (MEA), diethanolamine (DEA), hydrogen chloride (HCl), chlorine ($Cl_2$), ammonia ($NH_3$), and methyl diethanolamine (MDEA) by incorporating all corresponding binary-specific models. New experimental data published recently made it possible to update and refit several binary mixture models, some of which are reported here and others are reported elsewhere [7, 8].

## 2 Background and Fundamentals

The origins of the mixture models presented in this work are discussed in the 2017 report [9] on the DETAIL model of AGA8 [10] published in 1992. Although the DETAIL model was originally published as equation for the compression factor, it was developed in terms of the Helmholtz energy with density, temperature, and composition as independent variables. Lemmon [11] expanded the model to use pure-fluid equations of state and mixing rules, see also [12]. With this new structure, Kunz et al. [13] developed the multicomponent mixture model, known as GERG-2004, focusing on natural gas mixtures. The GERG-2008 model of Kunz and Wagner [6] is an extension of the latter and includes the same 21 components as in the AGA8 [9] model. Although GERG-2008 [6] includes several CCS-relevant fluids, they are only considered as minor components and not all of the corresponding binary mixtures were fitted to experimental data. The uncertainties in the calculation of thermodynamic properties of a mixture with these components can exceed the uncertainties of published measurements. The work here aimed to reduce the uncertainty to match those of measurements. The development of the new model for humid gas and CCS-relevant mixtures began with the same mathematical framework of the EOS-CG published by Gernert and Span [5]. Its mathematical structure is briefly summarized in the next section.

### 2.1 Functional Form

The mixture model is formulated in terms of the molar Helmholtz energy $a$ with the independent variables density $\rho$, temperature $T$, and composition $\vec{x}$. The Helmholtz energy is reduced by the temperature of the fluid and the gas constant ($R$= 8.314462618 J·mol$^{-1}$·K$^{-1}$ [14]) and split into two parts:

$$\frac{a\left(\rho, T, \vec{x}\right)}{RT} = \alpha\left(\delta, \tau, \vec{x}\right) = \alpha^{\mathrm{o}}\left(\rho, T, \vec{x}\right) + \alpha^{\mathrm{r}}\left(\delta, \tau, \vec{x}\right). \tag{1}$$

The ideal-gas part

$$\alpha^{\mathrm{o}}\left(\rho, T, \vec{x}\right) = \sum_{i=1}^{N} x_i \left[\alpha_i^{\mathrm{o}}(\rho, T) + \ln x_i\right] \tag{2}$$

consists of the ideal-gas parts $\alpha_i^{\mathrm{o}}$ of the pure-fluid EOS of the $N$ components in the mixture, the mole fraction $x_i$ of component $i$, and the dimensionless ideal-gas entropy of mixing $x_i \ln x_i$. The gas constants used for the reduction of the ideal part can be taken from the original publications listed in Sect. 3.

The residual part $\alpha^{\mathrm{r}}$ describes the actual behavior of the mixture.

$$\alpha^{\mathrm{r}}\left(\delta, \tau, \vec{x}\right) = \sum_{i=1}^{N} x_i \alpha_i^{\mathrm{r}}(\delta, \tau) + \Delta\alpha^{\mathrm{r}}\left(\delta, \tau, \vec{x}\right) \tag{3}$$

It contains the linear combination of the residual parts of the pure component EOS $\alpha_i^r$ evaluated at a reduced temperature and a reduced density that are representative for the mixture (this part can be understood as an extended corresponding states approach) and a departure term $\Delta\alpha^r$, which can be understood as a correction to the corresponding states part. As introduced by Klimeck [15], density and temperature are reduced by reducing functions according to

$$\delta = \frac{\rho}{\rho_r(\overrightarrow{x})} \text{ and } \tau = \frac{T_r(\overrightarrow{x})}{T}. \tag{4}$$

The reducing functions are given by

$$\frac{1}{\rho_r(\overrightarrow{x})} = \sum_{i=1}^{N} \frac{x_i^2}{\rho_{c,i}} + \sum_{i=1}^{N-1} \sum_{j=i+1}^{N} 2x_i x_j \beta_{v,ij} \gamma_{v,ij} \frac{x_i + x_j}{\beta_{v,ij}^2 x_i + x_j} \frac{1}{8} \left( \frac{1}{\rho_{c,i}^{1/3}} + \frac{1}{\rho_{c,j}^{1/3}} \right)^3 \tag{5}$$

and

$$T_r(\overrightarrow{x}) = \sum_{i=1}^{N} x_i^2 T_{c,i} + \sum_{i=1}^{N-1} \sum_{j=i+1}^{N} 2x_i x_j \beta_{T,ij} \gamma_{T,ij} \frac{x_i + x_j}{\beta_{T,ij}^2 x_i + x_j} \left( T_{c,i} T_{c,j} \right)^{0.5}. \tag{6}$$

They are dependent on the critical parameters of the pure fluids, the composition, and the four binary-specific adjustable parameters $\beta_{T,ij}$, $\gamma_{T,ij}$, $\beta_{v,ij}$, and $\gamma_{v,ij}$. In the further course, these parameters are called reducing parameters. The parameters are related to the order of the two components. A change in the order is defined by:

$$\beta_{T,ij} = \frac{1}{\beta_{T,ji}}, \beta_{v,ij} = \frac{1}{\beta_{v,ji}}, \gamma_{T,ij} = \gamma_{T,ji}, \text{ and } \gamma_{v,ij} = \gamma_{v,ji}. \tag{7}$$

Lemmon and Jacobsen [16] developed the departure term in Eq. 3, which reads as

$$\Delta\alpha^r(\delta, \tau, \overrightarrow{x}) = \sum_{i=1}^{N-1} \sum_{j=i+1}^{N} x_i x_j F_{ij} \alpha_{ij}^r(\delta, \tau). \tag{8}$$

This function is required when sufficient knowledge is available but the four interaction parameters in Eqs. 5 and 6 are insufficient to represent the true properties of the mixture, due either to deficiencies in the model or strong mixing effects in dissimilar fluids, allowing lower uncertainties in calculated properties. If a comprehensive database is available, a generalized or binary-specific departure function $\alpha_{ij}^r$ can be developed. The binary-specific weighting factor $F_{ij}$ is generally set to zero when a comprehensive database is not available. It is set to one if the database is sufficient to develop a binary-specific departure function $\alpha_{ij}^r$. And it is used as binary-specific adjustable parameter, if generalized departure functions $\alpha_{ij}^r$ are used for different binary systems. The departure functions in this work consist of varying numbers of polynomial-like (pol), exponential (exp), special exponential (spec), and Gaussian bell-shaped (GBS) terms, which can be written as:

$$\alpha_{ij}^{\mathrm{r}}(\delta,\tau)=\sum_{k=1}^{K_{\mathrm{pol},ij}} n_{ij,k}\delta^{d_{ij,k}}\tau^{t_{ij,k}}+\sum_{k=K_{\mathrm{pol},ij}+1}^{K_{\mathrm{pol},ij}+K_{\mathrm{exp},ij}} n_{ij,k}\delta^{d_{ij,k}}\tau^{t_{ij,k}}\exp\left(-\delta^{l_{ij,k}}\right)$$
$$+\sum_{k=K_{\mathrm{pol},ij}+K_{\mathrm{exp},ij}+1}^{K_{\mathrm{pol},ij}+K_{\mathrm{exp},ij}+K_{\mathrm{spec},ij}} n_{ij,k}\delta^{d_{ij,k}}\tau^{t_{ij,k}}\cdot\exp\left[-\eta_{ij,k}\left(\delta-\varepsilon_{ij,k}\right)^2-\beta_{ij,k}\left(\delta-\gamma_{ij,k}\right)\right]$$
$$+\sum_{k=K_{\mathrm{pol},ij}+K_{\mathrm{exp},ij}+K_{\mathrm{spec},ij}+1}^{K_{\mathrm{pol},ij}+K_{\mathrm{exp},ij}+K_{\mathrm{spec},ij}+K_{\mathrm{GBS},ij}} n_{ij,k}\delta^{d_{ij,k}}\tau^{t_{ij,k}}$$
$$\cdot\exp\left[-\eta_{ij,k}\left(\delta-\varepsilon_{ij,k}\right)^2-\beta_{ij,k}\left(\tau-\gamma_{ij,k}\right)^2\right]. \tag{9}$$

The terms include the adjustable coefficients $n_{ij,k}$, $\eta_{ij,k}$, $\varepsilon_{ij,k}$, $\gamma_{ij,k}$, $\beta_{ij,k}$, and exponents $d_{ij,k}$, $t_{ij,k}$, and $l_{ij,k}$. The adjustment process of all parameters, coefficients, and exponents is described in Sect. 2.2.

## 2.2 Calculation of Thermodynamic Properties

The Helmholtz energy is a fundamental quantity, and therefore all thermodynamic properties can be calculated through a combination of their derivatives with respect to the independent variables. The most relevant properties and their expressions in terms of derivatives of the Helmholtz energy are given in Table 1. Additional details and other properties can be found in Kunz et al. [13], Span [17], or in the 2017 version of AGA8 that presents the equations in a modified format [9]. The derivatives are abbreviated as follows:

$$\alpha_\delta=\left(\frac{\partial\alpha}{\partial\delta}\right)_{\tau,\vec{x}},\alpha_\tau=\left(\frac{\partial\alpha}{\partial\tau}\right)_{\delta,\vec{x}},\alpha_{\delta\delta}=\left(\frac{\partial^2\alpha}{\partial\delta^2}\right)_{\tau,\vec{x}},\alpha_{\tau\tau}=\left(\frac{\partial^2\alpha}{\partial\tau^2}\right)_{\delta,\vec{x}},\alpha_{\delta\tau}=\left(\frac{\partial^2\alpha}{\partial\delta\partial\tau}\right)_{\vec{x}}. \tag{10}$$

**Table 1** Thermodynamic properties relevant in this work and their relation to the reduced Helmholtz energy $\alpha$

| Property | Relation to the reduced Helmholtz energy and its derivatives | |
|---|---|---|
| Pressure | $p=\rho RT\left(1+\delta\alpha_\delta^{\mathrm{r}}\right)$ | (11) |
| Isobaric heat capacity | $c_p=R\left[-\tau^2\alpha_{\tau\tau}^{\mathrm{o}}-\tau^2\alpha_{\tau\tau}^{\mathrm{r}}+\frac{\left(1+\delta\alpha_\delta^{\mathrm{r}}-\delta\tau\alpha_{\delta\tau}^{\mathrm{r}}\right)^2}{1+2\delta\alpha_\delta^{\mathrm{r}}+\delta^2\alpha_{\delta\delta}^{\mathrm{r}}}\right]$ | (12) |
| Speed of sound | $w=\sqrt{\frac{RT}{M}\left[1+2\delta\alpha_\delta^{\mathrm{r}}+\delta^2\alpha_{\delta\delta}^{\mathrm{r}}-\frac{\left(1+\delta\alpha_\delta^{\mathrm{r}}-\delta\tau\alpha_{\delta\tau}^{\mathrm{r}}\right)}{\tau^2\alpha_{\tau\tau}^{\mathrm{o}}+\tau^2\alpha_{\tau\tau}^{\mathrm{r}}}\right]}$ | (13) |
| With the molar mass | $M=\sum_{i=1}^{N}x_iM_i$ | (14) |
| Fugacity coefficient of component $i$ | $\varphi_i=\exp\left[\left(\frac{\partial n\alpha^{\mathrm{r}}}{\partial n_i}\right)_{T,V,n_{j\neq i}}-\ln\left(1+\delta\alpha_\delta^{\mathrm{r}}\right)\right]$ | (15) |

Because the independent thermodynamic variables of the Helmholtz energy are temperature, density, and molar composition, the derivatives are also functions of these variables. If thermodynamic properties are calculated with other independent variables, e.g., pressure and temperature or pressure and enthalpy, an iterative transformation to the natural variables density and temperature is required. More details of these calculations are given in Gernert et al. [18]. For computational implementation, the numerical values of the derivatives can alternatively be determined by automatic differentiation with libraries, e.g., teqp [19].

### 2.3 Optimization Procedure

Binary mixture models in terms of the Helmholtz energy can be quite complex with many adjustable parameters. Although the addition of adjustable parameters increases the flexibility of the EOS and allows for better representation of the experimental database, additional care must be used to ensure reasonable physical behavior, including extrapolated states far beyond the range of the available database. The adjustable parameters are fitted based on experimental data, where the quality and quantity of the data help define the extent of non-linear mixing effects and thus the complexity of the departure function. The use of the minimal number of adjustable parameters that are required for accurate representation of measurements aids in reasonable physical and extrapolation behavior.

The multicomponent approach requires the evaluation of all possible binary combinations of the components in the mixtures. It may not be possible to correlate binary-specific mixture models when there is a lack of experimental data. In this situation, simple predictive combining rules without a departure function can be applied. For the Lorentz-Berthelot combining rule [13], the four reducing parameters of Eqs. 5 and 6 are set to unity:

$$\gamma_{T,ij} = 1, \gamma_{v,ij} = 1, \beta_{T,ij} = 1, \text{ and } \beta_{v,ij} = 1. \tag{16}$$

Reducing parameters that use a linear combining rule result in reducing functions that linearly connect the critical values of the pure fluids as given by

$$\gamma_{T,ij} = \frac{1}{2}\frac{\left(T_{\mathrm{c},i} + T_{\mathrm{c},j}\right)}{\left(T_{\mathrm{c},i} \cdot T_{\mathrm{c},j}\right)^{0.5}}, \gamma_{v,ij} = 4 \cdot \left(\frac{1}{\rho_{\mathrm{c},i}} + \frac{1}{\rho_{\mathrm{c},j}}\right)\left(\frac{1}{\rho_{\mathrm{c},i}^{1/3}} + \frac{1}{\rho_{\mathrm{c},j}^{1/3}}\right)^{-3}, \tag{17}$$

where $\beta_{T,ij}$ and $\beta_{v,ij}$ have been set to one. These combining rules for use in the calculation of mixture properties are still based on the combination of the pure-fluid equations of state. For mixtures with a symmetric mixing behavior, the prediction is usually quite reasonable. In CCS applications, the systems described with combining rules typically belong to components with very low concentrations and their influence on the overall multicomponent model is small. Nevertheless, these binary-specific equations should be used with caution with higher concentrations of the constituents.

For systems described by experimental data, up to four of the parameters of the reducing functions, Eqs. 5 and 6, can be adjusted to fit the data. The available

database must contain vapor–liquid-equilibrium (VLE) data to properly define the phase boundaries of the system. In general, no restrictions regarding the possible values of the four parameters are known, aside from being larger than zero. Most of the mixture models are comprised only adjusted reducing parameters, where the parameters are slightly different than the ones obtained by the linear or Lorentz-Berthelot combining rules. Exceptions can occur for binary mixtures, e.g., with large differences in the critical properties of the pure components, such as mixtures including hydrogen.

If the database features highly accurate and comprehensive datasets over wide ranges of temperature, pressure, and composition for various thermodynamic properties, e.g., VLE, density, and speed of sound, or if the mixture exhibits strong interactions, a departure function can be adjusted, with the weighing factor $F_{ij}$ set to unity. The number and type of terms are chosen during the adjustment process. For mixtures that behave similarly, it is possible to apply a generalized departure function and adjust $F_{ij}$, cf. Kunz and Wagner [6].

The optimization of the reducing parameters $\beta_{T,ij}$, $\gamma_{T,ij}$, $\beta_{v,ij}$, and $\gamma_{v,ij}$, as well as of the coefficients and exponents of the departure function $n_{ij,k}$, $\eta_{ij,k}$, $\varepsilon_{ij,k}$, $\gamma_{ij,k}$, $\beta_{ij,k}$, $d_{ij,k}$, $t_{ij,k}$, and $l_{ij,k}$ was carried out with the non-linear fitting algorithm originally developed by Lemmon and Jacobsen [20] and subsequently modified extensively by Lemmon. The algorithm iteratively minimizes the deviations between selected data points and the EOS by varying the adjustable parameters. The weights on the data points depend mainly on their experimental uncertainty. To ensure reasonable physical and extrapolation behavior where no experimental data are available, as well as to limit values of the parameters, constraints were used.

### 2.3.1 Experience, Considerations, and Thoughts Regarding the Fitting Process

The following summarizes new insights acquired during the development of the binary-specific models used in this work and can enlighten others who attempt to fit different systems with the same type of model. A more comprehensive and thorough investigation is still necessary to assess the benefits of the use of certain types of terms or the need to develop new models to better represent mixture properties.

(1) Fitting the reducing parameters of the mixture model without a departure function to data only for VLE states requires close inspection of the changes in density. Herrig [21] fitted four reducing parameters, shown in Table 2, for the MEA + $H_2O$ system to VLE data only.
However, he did not monitor the influence of the reducing parameters on calculated values of homogeneous densities. His EOS describes the VLE data accurately but the value for $\gamma_{v,\mathrm{MEA+H_2O}}$ is quite small compared to that from the Lorentz-Berthelot combining rule, cf. Eq. 16, resulting in the very high deviations of the mixture model to the experimental density data as shown in Fig. 1.
The deviations are one order of magnitude larger than those calculated with the Lorentz-Berthelot combining rule. Similar deviations were found for speed of sound data. The EOS developed in this work includes a departure function and

**Table 2** Binary reducing parameters and $F_{ij}$ of the mixture EOS for MEA + $H_2O$ developed by Herrig [21]

| $i+j$ | $\beta_{T,ij}$ | $\gamma_{T,ij}$ | $\beta_{v,ij}$ | $\gamma_{v,ij}$ | $F_{ij}$ |
|---|---|---|---|---|---|
| MEA + $H_2O$ [21] | 1.025500 | 1.052467 | 1.236603 | 0.482099 | 0 |

These values are given for demonstration only; the values obtained in this work are given in Table 4

moderate values of the reducing parameters (close to 1, see Sect. 3). Among other properties, the EOS was adjusted to VLE and density data, resulting in comparably small deviations as shown in Fig. 1a).

(2) In this work, the curve of critical loci as a function of composition was analyzed using the phase envelope algorithm as implemented in TREND [49] for the new EOS, a preliminary EOS for the MEA + $H_2O$ system (which satisfactorily described all experimental data) and the EOS of Herrig [21], as shown in Fig. 2.

Since no experimental data, and in particular no VLE data, are available in the critical region, the departure function of the preliminary EOS was too flexible and caused unreasonable physical behavior, such as the large temperature maximum that is greater than both critical temperatures of the pure components (cf. Deiters and Bell [50]). In this case, decreasing the absolute values of the coefficients of the exponential terms in the departure function from around 1.5 down to 0.04 moved the critical line towards smaller

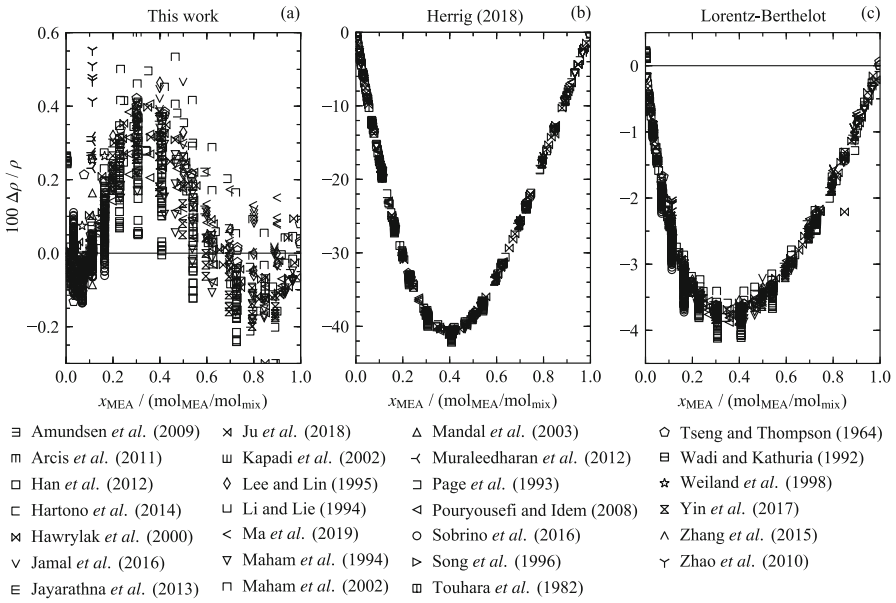


**Fig. 1** Relative deviations $\Delta\rho/\rho=(\rho_{data}-\rho_{EOS})/\rho_{data}$ between experimental homogeneous density data [22–48] and values calculated with the present EOS (a), the EOS of Herrig [21] (b), and the Lorentz-Berthelot combining rule (c) as a function of composition for the system MEA + $H_2O$

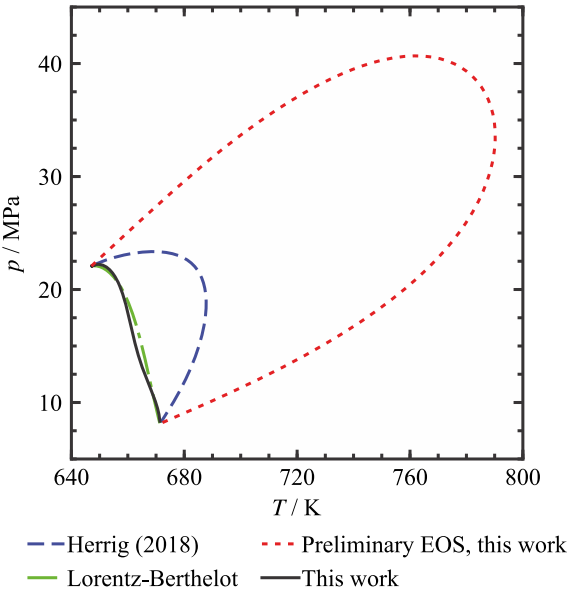


**Fig. 2** *p,T* diagram showing the critical lines calculated with the present EOS, a preliminary EOS developed in this work, the EOS of Herrig [21], and the Lorentz-Berthelot combining rule for the system MEA + $H_2O$

temperatures and ultimately corrected the unphysical temperature maximum. This gives rise to the hypothesis that the coefficients in the fitted departure functions should be less than one. Figure 2 shows the large influence of the low value of $\gamma_{v,ij}$ in the EOS of Herrig [21], resulting in an unreasonable temperature maximum, even though no departure function was included.

(3) A different example that validates the assumption that moderate reducing parameters (close to unity) are essential for the accurate calculation of multicomponent properties is the EOS for $CO_2 + H_2$ of Beckmüller et al. [7]. While assessing the EOS-CG-2021, the Ph.D. thesis of Al-Siyabi [51] was found reporting speed of sound data of binary and multicomponent mixtures. This dataset was not known during the development of the $CO_2 + H_2$ EOS [7] and the EOS deviates by up to 16% from the data of the binary system. This is cause by a rather high $\gamma_{T,CO_2+H_2} = 1.961$ and a GBS term with a large coefficient $n_{CO_2+H_2,2} = 12.38$. However, despite this high value for $\gamma_{T,CO_2+H_2}$, the speed of sound data of Al-Siyabi [51] in the $CO_2 + N_2 + H_2 + CH_4$ system are in good agreement with the EOS (average absolute deviation from the present equation of state is 0.581%, cf. Table 9). Decreasing $\gamma_{T,CO_2+H_2}$ by 0.1 without additional fitting of other reducing parameters improves the description of the multicomponent data of Al-Siyabi [51] while the deviations of the binary speed of sound data remain almost constant. This demonstrates the influence of the reducing parameter on calculated properties of multicomponent mixtures. To further investigate the influence of the coefficient of the second GBS term, the value was manually reduced, which, in this case, led to a better representation of the binary speed of sound data without distorting the multicomponent speed of sound data; however, this change resulted in a

distortion of other properties to which the coefficient was fitted. Other cases will be different, but most will show that the potentially negative impact on the calculation of other properties, which could not be considered in the fit, will be higher when the coefficients in the departure function are larger than necessary.

(4) The development of the EOS-LNG [52] brought about more than just a new model, but new insights into mixture modeling. The same functional form with the Helmholtz energy EOS developed in this work was used, but the work focused on the description of liquefied natural gas (LNG) components. In this case models were used for the binary systems, which consist of the four adjustable reducing parameters and a binary-specific departure function containing two polynomial terms and five exponential terms. The EOS-LNG authors realized that one reducing parameter in the methane+butane binary mixture caused large deviations in calculated density values in typical LNG multicomponent systems. A change from $\gamma_{v,CH_4+C_4H_{10}} = 0.9976$ to $\gamma_{v,CH_4+C_4H_{10}} = 1.0176$ had only a slight effect on the binary mixture as shown in Fig. 3. However, a value of $\gamma_v > 1$ decreased the density deviations in all of the multicomponent mixtures discussed in Thol et al. [52], also shown in Fig. 3. The AARD improved by nearly an order of magnitude in the LNG Oman system, as illustrated in Fig. 4.

The most significant influence of the binary-specific EOS for $CH_4+C_4H_{10}$ is related to the Oman system because the butane concentration is higher than that in the other multicomponent mixtures. This new knowledge shows that a small change in $\gamma_v$ (e.g., 0.02) may have a negligible effect on binary density calculations, but it can significantly influence calculations in multicomponent systems.

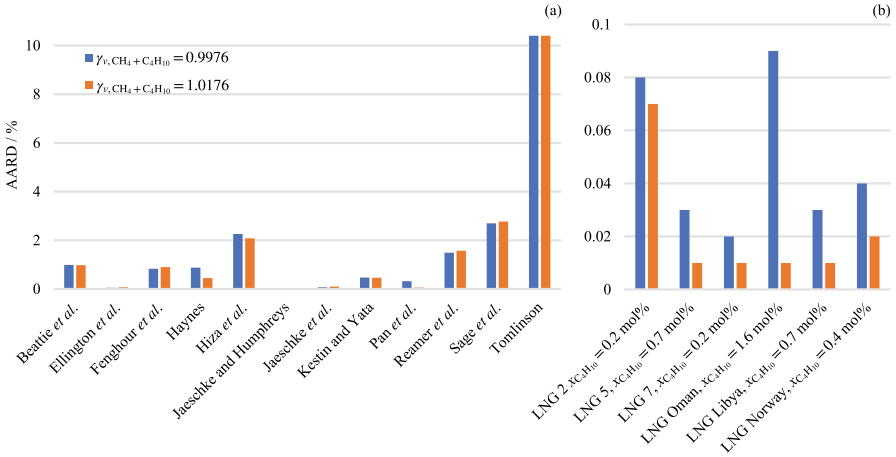


**Fig. 3** The AARD $= \frac{1}{n}\sum_{i=1}^{n}\left|100\left(\rho_{i,\text{data}} - \rho_{i,\text{EOS}}\right)/\rho_{i,\text{data}}\right|$ of density data [53–64] of the $CH_4+C_4H_{10}$ mixture (a) and various LNG multicomponent mixtures [65, 66] (b). Values are calculated with the EOS included in the EOS-LNG [52] except for the $CH_4+C_4H_{10}$ system for which two preliminary equations differing only in the reducing parameter $\gamma_v$ were used

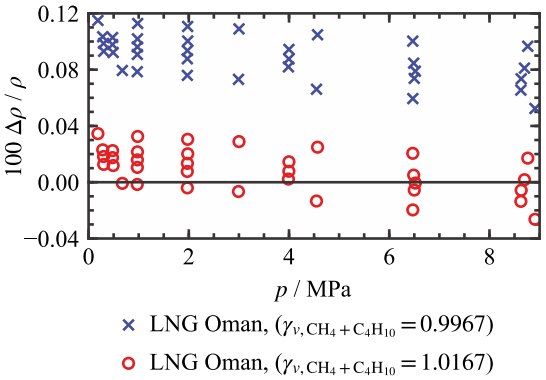


**Fig. 4** Relative deviations $\Delta\rho/\rho = (\rho_{data}-\rho_{EOS})/\rho_{data}$ between experimental homogeneous density data for the LNG Oman mixture [65] and values calculated with the EOS-LNG [52] except for the $CH_4+C_4H_{10}$ system for which two preliminary equations differing only in the reducing parameter $\gamma_v$ were used

The parameters of the binary mixture models developed in this work were kept in accordance with these new boundaries except for the MDEA + $H_2O$ system (cf. Sect. 3). Since MDEA is typically an impurity with a low concentration in the $CO_2$ transport segment, the influence of $\gamma_{v,MDEA+H_2O} < 1$ on calculated properties for CCS multicomponent mixtures is expected to be negligible.

## 3 The EOS-CG-2021 Mixture Model

Multicomponent mixture models explicit in the Helmholtz energy and of the type described here are primarily based on Helmholtz energy equations of state for the pure fluids (as described in Sect. 2.1); an overview of the equations used in the EOS-CG-2021 model is presented in Table 3. In addition to the reference, the range of validity and the critical point for each of the fluids are given. To accurately implement this type of model, the pure-fluid equations of state must be as accurate as possible. The validity of the EOS in terms of temperature and pressure is generally based on the ranges of the experimental data used in their development. Because the mixture model is based on the reduced properties (temperature and density) of the mixture, the EOS for those fluids that have a large value of reduced temperature or small value of reduced density of the triple point *must* extrapolate far beyond the lowest measurements available. Properties at low temperatures calculated from the mixture model are often evaluated outside the range of the pure fluid limits for at least one of the fluids. Such state points should be treated with care.

For example, the triple-point ratio ($T_{trp}/T_c$) for carbon dioxide is 0.712 and that for propane is 0.231. At high propane concentrations and temperatures close to the triple point of propane, the reduced temperatures used in Eqs. 1 to 3 approach the triple-point ratio of propane. The reduced temperature is used to calculate the pure fluid contributions from each equation of state. This means that values are calculated from the carbon dioxide equation at temperatures of about 0.23 $T_c$, far below the triple point of this fluid (which is also the lower limit of all experimental liquid-phase data that have been measured). The $CO_2$ equation must be extrapolated to 40% of its triple-point temperature to accurately model carbon dioxide/propane mixtures at high propane concentrations and low temperatures.

**Table 3** Pure-fluid equations of state in terms of the Helmholtz energy used in this work

| Component | Reference | Year | Range of validity | | Critical parameters | | |
|---|---|---|---|---|---|---|---|
| | | | ($T_{min}$–$T_{max}$)/K | $p_{max}$/MPa | $T_c$/K | $\rho_c$/(mol·dm$^{-3}$) | $p_c$/MPa |
| $CO_2$ | Span and Wagner [70] | 1996 | 216.592–1100 | 800 | 304.128 | 10.625 | 7.3773 |
| $H_2O$ | Wagner and Pruß [67] | 2002 | $T_{melt}(p)$–2000 | 1000 | 647.096 | 17.874 | 22.064 |
| $N_2$ | Span et al. [72] | 2000 | 63.151–2000 | 2200 | 126.192 | 11.184 | 3.3958 |
| $O_2$ | Schmidt and Wagner [73] | 1985 | 54.361–2000 | 82 | 154.581 | 13.63 | 5.043 |
| Ar | Tegeler et al. [74] | 1999 | 83.806–2000 | 1000 | 150.687 | 13.407 | 4.863 |
| CO | Lemmon and Span [75] | 2006 | 68.16–500 | 100 | 132.86 | 10.85 | 3.494 |
| $H_2$ | Leachman et al. [76] | 2009 | 13.957–1000 | 2000 | 33.145 | 15.508 | 1.2964 |
| $CH_4$ | Setzmann and Wagner [77] | 1991 | 90.694–625 | 1000 | 190.564 | 10.139 | 4.5992 |
| $H_2S$ | Lemmon and Span [75] | 2006 | 187.7–760 | 170 | 373.1 | 10.19 | 9.000 |
| $SO_2$ | Gao et al. [78] | 2016 | 197.7–525 | 35 | 430.64 | 8.078 | 7.8866 |
| MEA | Herrig [21][a] | 2018 | 283.7–675 | 9 | 671.4 | 5.39 | 8.125 |
| DEA | Kortmann [79][a] | 2016 | 301.7–740 | 5 | 736.5 | 3.3 | 4.9508 |
| HCl | Thol et al. [80] | 2018 | 159.07–670 | 200 | 324.68 | 11.87 | 8.3135 |
| $Cl_2$ | Thol et al. [81] | 2021 | 172.17–440 | 20 | 416.865 | 8.06 | 7.6424 |
| $NH_3$ | Gao et al. [82] | 2023 | 159.49–725 | 1000 | 405.56 | 13.696 | 11.363 |
| MDEA | Neumann et al. [83] | 2022 | 281.85–741 | 100 | 741.00 | 2.72 | 4.6899 |

[a]Details about the structure and the parameters of the EOS can be found in the supplementary material

The corresponding effect occurs at high reduced temperature of the mixture for fluids with large critical temperature. In this case, the reduced temperature of the mixture frequently exceeds the highest reduced temperature, for which experimental data are available for the pure fluid.

The difference in the values of the critical points for binary mixtures is an indicator of mixing behavior. Larger differences generally result in mixtures whose properties are less linear and deviate more from a corresponding states basis.

For state points described above, it is important that the underlying equation of state of the pure fluid exhibits correct extrapolation behavior. Older equations of state may have deficiencies at this point, which may cause numerical problems when

evaluated in the mixture. An example is the equation of state of water [67] for temperatures lower than 230 K ($T/T_c < 0.36$). In this range, the algorithms fail in the evaluation of the pure-fluid equation because of numerical issues in the extrapolated fluid phase, which then also means that a mixture cannot be evaluated. Unfortunately, this also affects calculations of the phase equilibrium, where the liquid density must be calculated as well. Thus, also every flash calculation determining the density from a specified temperature and pressure, where it is checked whether a point is in the gaseous or liquid-phase, is affected. Especially in recent years, the development of empirical Helmholtz energy equations has focused strongly on this aspect, so that at least numerical problems no longer play a role. But due to the lack of experimental data in this area, no reliable statements can be made about the accuracy of the equations in this region. The largest extrapolation, however, usually occurs when a component is present in the mixture only at low concentrations. In these cases, it can be assumed that the influence on the accuracy of the calculated property is limited. Besides possible loss of accuracy, phase-equilibrium calculations must be treated with caution. When evaluating the equations of state in software packages such as TREND [49], REFPROP [68], or CoolProp [69], a fluid phase equilibrium is always assumed. In areas below the triple-point temperatures of the pure substances, however, solid phases become relevant. That means, even if a numerical value results from the evaluation of a fluid phase equilibrium, this does not mean that it is correct. In TREND such solid phases are considered at least for the components water [67], $CO_2$ [70], and benzene [71] (The solid EOS for benzene will be implemented in upcoming versions of TREND). For other substances there are no corresponding solid equations available, yet.

In this work, the Helmholtz energy framework is built upon the pure-fluid equations of state, where any pure-fluid EOS could be used. Switching the specified equation that was used in the mixture model development with either older (and generally published) equations or newer (and often preliminary) equations will almost always increase the uncertainty in calculated properties, even if the newer equation has lower uncertainties for the pure-fluid calculations. The most accurate mixture calculations from this work can only be obtained when the pure-fluid equations of state in Table 3 are used in conjunction with the fitted mixing parameters reported here. The use of other pure-fluid equations may cause larger deviations than typical experimental uncertainties.

The development of the EOS-CG-2016 specified that the most accurate pure-fluid EOS at that time would be used in the mixture models. This is particularly important for binary mixtures containing water because numerical deficiencies resulting from the complex functional form of the EOS for pure $H_2O$ and $CO_2$ are often corrected with a departure function. Since this complexity is not needed in natural gas applications, GERG-2004 used significantly simpler equations of state for $H_2O$ and $CO_2$ [13]. This work re-fitted the interaction parameters for the existing binary mixture models for $CH_4 + H_2O$ and $H_2S + H_2O$ in GERG-2004 [13] for use with the reference EOS given in Table 3.

According to Eqs. 5, 6, and 8, the calculation of properties from multicomponent mixture models requires the binary combinations of all the constituents. For the 16

components relevant to CCS included in the EOS-CG-2021, this results in 120 binary-specific mixtures as shown in Fig. 5.

The modular framework of the multicomponent mixture model in terms of the Helmholtz energy allows binary-specific equations of state from different references to be used if they are based on the same functional form. Binary-specific equations from several sources are summarized within the EOS-CG-2021 model. The goal in this work was to develop a mixture model with the most accurate available pure-fluid equations of state and to represent the available thermodynamic property mixture data within their experimental uncertainty. The EOS-CG-2021 adopts 18 binary formulations from the GERG-2008 model [6], 12 binary-specific EOS for mixtures with $NH_3$ from Neumann et al. [84], 10 binary formulations from the original EOS-

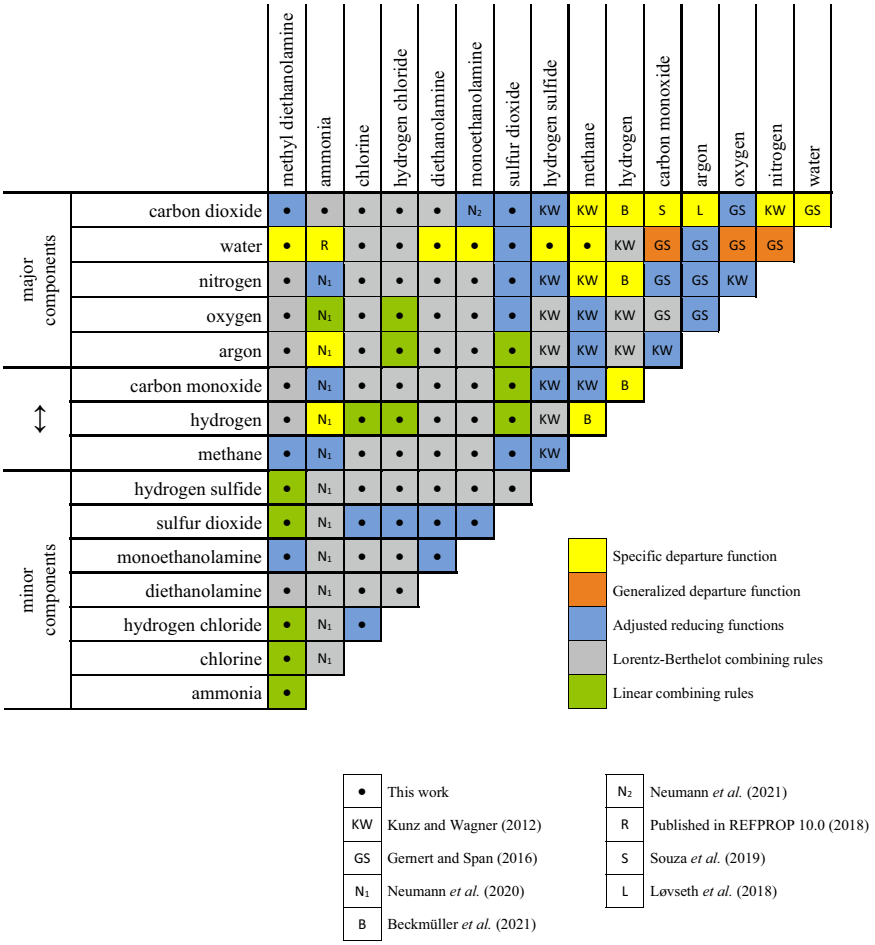


**Fig. 5** Overview of the 120 binary combinations resulting from the 16 components considered in the development of the mixture model for CCS-relevant mixtures. According to their mole fractions in typical CCS-mixtures, the components are classified as major or minor components. Carbon monoxide, hydrogen, and methane occur as major or minor components depending on the CCS application

CG-2016 model [5], 4 binary-specific EOS for mixtures with $H_2$ from Beckmüller et al. [7], and 1 each from Neumann et al. [85], REFPROP [68], Souza et al. [86], and Løvseth et al. [87]. Within the scope of this work, 72 updated or newly developed sets of parameters for different binary mixtures were added; in part, these new parameter sets have already been published in the PhD thesis of Herrig [21]. In total, 18 binary formulations contain a specific departure function and three include a generalized departure function. The reducing parameters were adjusted without a departure function for 32 of the binary mixture equations. The remaining 67 systems are formulated in terms of simple combining rules due to the lack of sufficiently accurate and comprehensive data.

The reducing parameters for each binary mixture are given in Table 4 and the parameters of the binary-specific departure functions are given in Table 5. Only the models developed in this work are evaluated in Sect. 3.1. A comprehensive analysis of the other binary mixtures is given in their corresponding publications.

The complete multicomponent mixture model including all pure-fluid and binary-specific EOS is implemented in the open source software package TREND [49], which enables the calculation of all thermodynamic properties, as well as in upcoming releases of REFPROP [68] and CoolProp [69]. Test values can be calculated with the use of TREND [49] as described in the supplementary material.

### 3.1 Comparison to Experimental Data

The performance of the mixture models developed in this work is analyzed with the use of comparisons of calculations to experimental data and evaluation of the extrapolation behavior at conditions outside the range of validity. Comparisons with experimental data use the percentage deviation

$$100\frac{\Delta X}{X} = 100\left(\frac{X_{\text{data}} - X_{\text{EOS}}}{X_{\text{data}}}\right) \tag{18}$$

for single data points and the average absolute relative deviation

$$\text{AARD} = \frac{1}{n}\sum_{i=1}^{n}|100\Delta X_i/X_i| \tag{19}$$

for datasets, where $n$ is the number of datapoints in one set. The datasets are subdivided into composition ranges, if possible, to view the compositional dependence. Relative deviations in calculated values of bubble- and dew-point compositions can be misleading; for example, comparably high values arise for components that exist as trace elements in the mixture. VLE data are thus evaluated with the average absolute deviation in terms of mole fraction,

$$\text{AAD} = \frac{1}{n}\sum_{i=1}^{n}|\Delta X_i|. \tag{20}$$

Comparisons to the data for the mixture models not developed here but adopted from other works are given in their respective publications [5–8, 68, 86–88]; the

**Table 4** Reducing parameters and $F_{ij}$ values for all binary mixtures required to implement the full mixture model

| $i+j$ | $\beta_{T,ij}$ | $\gamma_{T,ij}$ | $\beta_{v,ij}$ | $\gamma_{v,ij}$ | $F_{ij}$ | $i+j$ | $\beta_{T,ij}$ | $\gamma_{T,ij}$ | $\beta_{v,ij}$ | $\gamma_{v,ij}$ | $F_{ij}$ |
|---|---|---|---|---|---|---|---|---|---|---|---|
| $CO_2+H_2O$ [5] | 1.030538 | 0.828472 | 1.021392 | 0.895156 | 1 | DEA+Ar[a] | 1.000000 | 1.000000 | 1.000000 | 1.000000 | 0 |
| $N_2+CO_2$ [6] | 1.005895 | 1.107654 | 0.977795 | 1.047578 | 1 | HCl+Ar[b] | 1.000000 | 1.074563 | 1.000000 | 1.001236 | 0 |
| $CO_2+O_2$ [5] | 1.000000 | 1.031986 | 1.000000 | 1.084460 | 0 | $Cl_2$+Ar[a] | 1.000000 | 1.000000 | 1.000000 | 1.000000 | 0 |
| $CO_2$+Ar [87] | 0.998705 | 1.039675 | 1.003766 | 1.013833 | 1 | Ar+$NH_3$ [84] | 1.146326 | 0.998353 | 0.756526 | 1.041113 | 1 |
| $CO_2$+CO [86] | 0.989782 | 1.162130 | 1.033802 | 1.000162 | 1 | MDEA+Ar[a] | 1.000000 | 1.000000 | 1.000000 | 1.000000 | 0 |
| $CO_2+H_2$ [7] | 0.979000 | 1.961000 | 1.198000 | 0.842000 | 1 | CO+$H_2$ [7] | 1.078000 | 1.105000 | 1.037000 | 1.040000 | 1 |
| $CH_4+CO_2$ [6] | 1.022624 | 0.975665 | 0.999518 | 1.002807 | 1 | $CH_4$+CO [6] | 0.987412 | 0.987473 | 0.997341 | 1.006103 | 0 |
| $CO_2+H_2S$ [6] | 1.016035 | 0.926019 | 0.906631 | 1.024086 | 0 | CO+$H_2S$ [6] | 1.025537 | 1.022750 | 0.795660 | 1.101731 | 0 |
| $CO_2+SO_2$ | 1.020063 | 1.007975 | 0.889865 | 1.005778 | 0 | $SO_2$+CO[b] | 1.000000 | 1.177903 | 1.000000 | 1.007241 | 0 |
| MEA+$CO_2$ [8] | 1.000000 | 1.070000 | 1.000000 | 1.000000 | 0 | MEA+CO[a] | 1.000000 | 1.000000 | 1.000000 | 1.000000 | 0 |
| DEA+$CO_2$[a] | 1.000000 | 1.000000 | 1.000000 | 1.000000 | 0 | DEA+CO[a] | 1.000000 | 1.000000 | 1.000000 | 1.000000 | 0 |
| HCl+$CO_2$[a] | 1.000000 | 1.000000 | 1.000000 | 1.000000 | 0 | HCl+CO[a] | 1.000000 | 1.000000 | 1.000000 | 1.000000 | 0 |
| $Cl_2$+$CO_2$[a] | 1.000000 | 1.000000 | 1.000000 | 1.000000 | 0 | $Cl_2$+CO[a] | 1.000000 | 1.000000 | 1.000000 | 1.000000 | 0 |
| $NH_3$+$CO_2$[a] | 1.000000 | 1.000000 | 1.000000 | 1.000000 | 0 | CO+$NH_3$ [84] | 1.057512 | 0.952705 | 0.739937 | 1.707000 | 0 |
| MDEA+$CO_2$ | 1.081000 | 1.386000 | 1.000000 | 1.000000 | 0 | MDEA+CO[a] | 1.000000 | 1.000000 | 1.000000 | 1.000000 | 0 |
| $N_2+H_2O$ [5] | 1.048054 | 0.805147 | 0.926245 | 0.733443 | 1 | $CH_4+H_2$ [7] | 1.010000 | 1.440000 | 1.086000 | 0.804000 | 1 |
| $O_2+H_2O$ [5] | 1.253060 | 0.807842 | 1.028197 | 0.873460 | 0.6017 | $H_2+H_2S$ [6][a] | 1.000000 | 1.000000 | 1.000000 | 1.000000 | 0 |
| $H_2O$+Ar [5] | 0.679104 | 0.921000 | 0.940398 | 1.050952 | 0 | $SO_2+H_2$[b] | 1.000000 | 1.940852 | 1.000000 | 1.035171 | 0 |
| CO+$H_2O$ [5] | 0.956090 | 0.823984 | 0.940426 | 0.766756 | 0.9897 | MEA+$H_2$[a] | 1.000000 | 1.000000 | 1.000000 | 1.000000 | 0 |
| $H_2+H_2O$ [6][a] | 1.000000 | 1.000000 | 1.000000 | 1.000000 | 0 | DEA+$H_2$[a] | 1.000000 | 1.000000 | 1.000000 | 1.000000 | 0 |
| $CH_4+H_2O$ | 1.263000 | 0.748000 | 1.176000 | 1.038000 | 1 | HCl+$H_2$[b] | 1.000000 | 1.724556 | 1.000000 | 1.005948 | 0 |
| $H_2S+H_2O$ | 0.960526 | 0.924026 | 0.945818 | 1.189702 | 1 | $Cl_2+H_2$[b] | 1.000000 | 1.914078 | 1.000000 | 1.035410 | 0 |
| $SO_2+H_2O$ | 1.019562 | 0.916311 | 1.094032 | 0.962547 | 0 | $H_2$+$NH_3$ [84] | 0.988240 | 1.126600 | 1.010300 | 0.729800 | 1 |
| MEA+$H_2O$ | 1.00400 | 0.957300 | 1.007600 | 1.089160 | 1 | MDEA+$H_2$[a] | 1.000000 | 1.000000 | 1.000000 | 1.000000 | 0 |
| DEA+$H_2O$ | 0.993200 | 0.973400 | 1.006000 | 1.123000 | 1 | $CH_4+H_2S$ [6] | 1.011090 | 0.961156 | 1.012599 | 1.040161 | 0 |

**Table 4** continued

| $i+j$ | $\beta_{T,ij}$ | $\gamma_{T,ij}$ | $\beta_{v,ij}$ | $\gamma_{v,ij}$ | $F_{ij}$ | $i+j$ | $\beta_{T,ij}$ | $\gamma_{T,ij}$ | $\beta_{v,ij}$ | $\gamma_{v,ij}$ | $F_{ij}$ |
|---|---|---|---|---|---|---|---|---|---|---|---|
| $HCl+H_2O$[a] | 1.000000 | 1.000000 | 1.000000 | 1.000000 | 0 | $SO_2+CH_4$ | 0.999432 | 1.115714 | 1.315534 | 1.119543 | 0 |
| $Cl_2+H_2O$[a] | 1.000000 | 1.000000 | 1.000000 | 1.000000 | 0 | $MEA+CH_4$[a] | 1.000000 | 1.000000 | 1.000000 | 1.000000 | 0 |
| $NH_3+H_2O$ [68] | 0.933585 | 1.015826 | 1.044759 | 1.189754 | 1 | $DEA+CH_4$[a] | 1.000000 | 1.000000 | 1.000000 | 1.000000 | 0 |
| $MDEA+H_2O$ | 0.970000 | 1.010000 | 0.980000 | 1.268700 | 1 | $HCl+CH_4$[a] | 1.000000 | 1.000000 | 1.000000 | 1.000000 | 0 |
| $N_2+O_2$ [6] | 0.997191 | 0.995157 | 0.999522 | 0.997082 | 0 | $Cl_2+CH_4$[a] | 1.000000 | 1.000000 | 1.000000 | 1.000000 | 0 |
| $N_2+Ar$ [5] | 0.999442 | 0.989311 | 1.006697 | 1.001549 | 0 | $CH_4+NH_3$ [84] | 1.022371 | 0.940156 | 1.006058 | 1.069834 | 0 |
| $N_2+CO$ [5] | 1.002409 | 0.994100 | 1.000000 | 1.001317 | 0 | $MDEA+CH_4$ | 1.000000 | 1.625000 | 1.074000 | 1.000000 | 0 |
| $N_2+H_2$ [7] | 1.027000 | 1.240000 | 0.993000 | 0.773000 | 1 | $SO_2+H_2S$[a] | 1.000000 | 1.000000 | 1.000000 | 1.000000 | 0 |
| $CH_4+N_2$ [6] | 0.998099 | 0.979273 | 0.998721 | 1.013950 | 1 | $MEA+H_2S$[a] | 1.000000 | 1.000000 | 1.000000 | 1.000000 | 0 |
| $N_2+H_2S$ [6] | 1.004692 | 0.960174 | 0.910394 | 1.256844 | 0 | $DEA+H_2S$[a] | 1.000000 | 1.000000 | 1.000000 | 1.000000 | 0 |
| $SO_2+N_2$ | 1.045874 | 1.194659 | 0.903625 | 1.215581 | 0 | $HCl+H_2S$[a] | 1.000000 | 1.000000 | 1.000000 | 1.000000 | 0 |
| $MEA+N_2$[a] | 1.000000 | 1.000000 | 1.000000 | 1.000000 | 0 | $Cl_2+H_2S$[a] | 1.000000 | 1.000000 | 1.000000 | 1.000000 | 0 |
| $DEA+N_2$[a] | 1.000000 | 1.000000 | 1.000000 | 1.000000 | 0 | $NH_3+H_2S$ [84][a] | 1.000000 | 1.000000 | 1.000000 | 1.000000 | 0 |
| $HCl+N_2$[a] | 1.000000 | 1.000000 | 1.000000 | 1.000000 | 0 | $MDEA+H_2S$[b] | 1.000000 | 1.059430 | 1.000000 | 1.140800 | 0 |
| $Cl_2+N_2$[a] | 1.000000 | 1.000000 | 1.000000 | 1.000000 | 0 | $MEA+SO_2$ | 1.021293 | 1.200045 | 1.000000 | 1.000000 | 0 |
| $N_2+NH_3$ [84] | 1.057512 | 0.952705 | 0.739937 | 1.447261 | 0 | $DEA+SO_2$ | 1.021293 | 1.200045 | 1.000000 | 1.000000 | 0 |
| $MDEA+N_2$[a] | 1.000000 | 1.000000 | 1.000000 | 1.000000 | 0 | $SO_2+HCl$ | 1.002605 | 1.048380 | 1.000000 | 1.000000 | 0 |
| $O_2+Ar$ [5] | 0.999039 | 0.988822 | 1.006502 | 1.001341 | 0 | $Cl_2+SO_2$ | 1.015678 | 0.927820 | 1.024354 | 1.016621 | 0 |
| $O_2+CO$ [5][a] | 1.000000 | 1.000000 | 1.000000 | 1.000000 | 0 | $NH_3+SO_2$ [84][a] | 1.000000 | 1.000000 | 1.000000 | 1.000000 | 0 |
| $H_2+O_2$ [6][a] | 1.000000 | 1.000000 | 1.000000 | 1.000000 | 0 | $MDEA+SO_2$[b] | 1.000000 | 1.037046 | 1.000000 | 1.097897 | 0 |
| $CH_4+O_2$ [6] | 1.000000 | 0.950000 | 1.000000 | 1.000000 | 0 | $DEA+MEA$ | 1.015703 | 1.020484 | 0.766762 | 0.852448 | 0 |
| $O_2+H_2S$ [6][a] | 1.000000 | 1.000000 | 1.000000 | 1.000000 | 0 | $MEA+HCl$[a] | 1.000000 | 1.000000 | 1.000000 | 1.000000 | 0 |
| $SO_2+O_2$ | 0.927961 | 1.035878 | 1.219246 | 1.660632 | 0 | $MEA+Cl_2$[a] | 1.000000 | 1.000000 | 1.000000 | 1.000000 | 0 |
| $MEA+O_2$[a] | 1.000000 | 1.000000 | 1.000000 | 1.000000 | 0 | $NH_3+MEA$ [84][a] | 1.000000 | 1.000000 | 1.000000 | 1.000000 | 0 |
| $DEA+O_2$[a] | 1.000000 | 1.000000 | 1.000000 | 1.000000 | 0 | $MDEA+MEA$ | 1.000000 | 0.805000 | 1.000000 | 1.000000 | 0 |

**Table 4** continued

| $i+j$ | $\beta_{T,ij}$ | $\gamma_{T,ij}$ | $\beta_{v,ij}$ | $\gamma_{v,ij}$ | $F_{ij}$ | $i+j$ | $\beta_{T,ij}$ | $\gamma_{T,ij}$ | $\beta_{v,ij}$ | $\gamma_{v,ij}$ | $F_{ij}$ |
|---|---|---|---|---|---|---|---|---|---|---|---|
| $HCl+O_2$[b] | 1.000000 | 1.069638 | 1.000000 | 1.001592 | 0 | DEA+HCl[a] | 1.000000 | 1.000000 | 1.000000 | 1.000000 | 0 |
| $Cl_2+O_2$[a] | 1.000000 | 1.000000 | 1.000000 | 1.000000 | 0 | DEA+$Cl_2$[a] | 1.000000 | 1.000000 | 1.000000 | 1.000000 | 0 |
| $NH_3+O_2$ [84][b] | 1.000000 | 1.118566 | 1.000000 | 1.000002 | 0 | $NH_3$+DEA [84][a] | 1.000000 | 1.000000 | 1.000000 | 1.000000 | 0 |
| MDEA+$O_2$[a] | 1.000000 | 1.000000 | 1.000000 | 1.000000 | 0 | MDEA+DEA[a] | 1.000000 | 1.000000 | 1.000000 | 1.000000 | 0 |
| CO+Ar [6] | 1.000000 | 0.954216 | 1.000000 | 1.159721 | 0 | $Cl_2$+HCl | 1.007373 | 0.968865 | 0.928100 | 0.917288 | 0 |
| $H_2$+Ar [6][a] | 1.000000 | 1.000000 | 1.000000 | 1.000000 | 0 | $NH_3$+HCl [84][a] | 1.000000 | 1.000000 | 1.000000 | 1.000000 | 0 |
| $CH_4$+Ar [6] | 0.990954 | 0.989843 | 1.034630 | 1.014679 | 0 | MDEA+HCl[b] | 1.000000 | 1.086325 | 1.000000 | 1.173873 | 0 |
| $H_2S$+Ar [6][a] | 1.000000 | 1.000000 | 1.000000 | 1.000000 | 0 | $NH_3+Cl_2$ [84][a] | 1.000000 | 1.000000 | 1.000000 | 1.000000 | 0 |
| $SO_2$+Ar[b] | 1.000000 | 1.141020 | 1.000000 | 1.021291 | 0 | MDEA+$Cl_2$[b] | 1.000000 | 1.041648 | 1.000000 | 1.096224 | 0 |
| MEA+Ar[a] | 1.000000 | 1.000000 | 1.000000 | 1.000000 | 0 | MDEA+$NH_3$[b] | 1.000000 | 1.045755 | 1.000000 | 1.207629 | 0 |

[a]Calculated from the Lorentz-Berthelot combining rules

[b]Calculated according to the linear combining rules

**Table 5** Parameters of the departure functions

| $k$ | Type | $n_{ij,k}$ | $t_{ij,k}$ | $d_{ij,k}$ | $l_{ij,k}$ | $\eta_{ij,k}$ | $\beta_{ij,k}$ | $\gamma_{ij,k}$ | $\varepsilon_{ij,k}$ |
|---|---|---|---|---|---|---|---|---|---|
| $CO_2+H_2O$ [5] | | | | | | | | | |
| 1 | pol | 0.39440467 | 0.88 | 1 | | | | | |
| 2 | pol | −1.7634732 | 2.932 | 1 | | | | | |
| 3 | pol | 0.14620755 | 2.433 | 3 | | | | | |
| 4 | exp | 0.008752232 | 1.33 | 0 | 1 | | | | |
| 5 | exp | 2.0349398 | 4.416 | 2 | 1 | | | | |
| 6 | exp | −0.09035025 | 5.514 | 3 | 1 | | | | |
| 7 | exp | −0.21638854 | 5.203 | 1 | 2 | | | | |
| 8 | exp | 0.03961217 | 1 | 5 | 2 | | | | |
| $N_2+CO_2$ [6] | | | | | | | | | |
| 1 | pol | 0.28661625028399 | 1.85 | 2 | | | | | |
| 2 | pol | −0.10919833861247 | 1.4 | 3 | | | | | |
| 3 | spec | −1.137403208227 | 3.2 | 1 | | 0.25 | 0.75 | 0.5 | 0.5 |
| 4 | spec | 0.76580544237358 | 2.5 | 1 | | 0.25 | 1 | 0.5 | 0.5 |
| 5 | spec | 0.0042638000926819 | 8 | 1 | | 0 | 2 | 0.5 | 0.5 |
| 6 | spec | 0.17673538204534 | 3.75 | 2 | | 0 | 3 | 0.5 | 0.5 |
| $CO_2$+Ar [87] | | | | | | | | | |
| 1 | pol | −0.0656 | 3.22 | 2 | | | | | |
| 2 | pol | 0.0237 | 2.9 | 3 | | | | | |
| 3 | spec | 3.5217 | 1.9 | 1 | | 1.243 | 1.208 | 0.5 | 0.65 |
| 4 | spec | −2.831 | 1.57 | 1 | | 1.072 | 0.82 | 0.5 | 0.727 |
| 5 | spec | −1.406 | 2.73 | 1 | | 1.465 | 1.527 | 0.5 | 0.648 |
| 6 | spec | 0.864 | 1.08 | 2 | | 0.946 | 0.86 | 0.5 | 0.706 |
| $CO_2$+CO [86] | | | | | | | | | |
| 1 | pol | 1.861 | 2.82 | 1 | | | | | |
| 2 | pol | −4.017 | 3.26 | 1 | | | | | |
| 3 | exp | 0.2734 | 0.94 | 2 | 1 | | | | |
| 4 | exp | 2.393 | 3.944 | 4 | 1 | | | | |
| 5 | GBS | 26.46 | 2.53 | 1 | | 0.385 | 0.144 | 5.1 | 0.109 |
| 6 | GBS | −1.213 | 4.38 | 1 | | 0.295 | 0.31 | 1.661 | 2.596 |
| $CO_2+H_2$ [7] | | | | | | | | | |
| 1 | pol | 3.56 | 1.47 | 1 | | | | | |
| 2 | pol | −1.036 | 1.17 | 2 | | | | | |
| 3 | GBS | −4.835 | 1.95 | 1 | | 0.58 | 0.465 | 0.17 | 0.52 |
| 4 | GBS | 12.38 | 0.31 | 2 | | 0.2 | 0.82 | 2.11 | 0.15 |
| 5 | GBS | −2.65 | 1.412 | 3 | | 0.292 | 0.52 | 1.49 | 0.24 |
| 6 | GBS | −3.3 | 2.28 | 1 | | 0.12 | 1 | 1.73 | 0.15 |

**Table 5** continued

| | | | | | | | | | |
|---|---|---|---|---|---|---|---|---|---|
| $CH_4+CO_2$ [6] | | | | | | | | | |
| 1 | pol | −0.10859387354942 | 2.6 | 1 | | | | | |
| 2 | pol | 0.080228576727389 | 1.95 | 2 | | | | | |
| 3 | pol | −0.0093303985115717 | 0 | 3 | | | | | |
| 4 | spec | 0.040989274005848 | 3.95 | 1 | | 1 | 1 | 0.5 | 0.5 |
| 5 | spec | −0.24338019772494 | 7.95 | 2 | | 0.5 | 2 | 0.5 | 0.5 |
| 6 | spec | 0.23855347281124 | 8 | 3 | | 0 | 3 | 0.5 | 0.5 |
| $N_2+H_2O$, $O_2+H_2O$, $CO+H_2O$ [5] | | | | | | | | | |
| 1 | pol | 4.0142079 | 0.547 | 1 | | | | | |
| 2 | exp | −1.1573939 | 0.055 | 1 | 1 | | | | |
| 3 | exp | −7.2102425 | 1.925 | 1 | 1 | | | | |
| 4 | exp | −5.3251223 | 0.552 | 2 | 1 | | | | |
| 5 | exp | −2.2155867 | 1 | 4 | 1 | | | | |
| $CH_4+H_2O$ | | | | | | | | | |
| 1 | pol | 3.3 | 1.1 | 1 | | | | | |
| 2 | pol | −2.88 | 0.8 | 1 | | | | | |
| 3 | exp | 9.6 | 0.8 | 1 | 1 | | | | |
| 4 | exp | −11.7 | 1 | 1 | 1 | | | | |
| 5 | exp | 2.13 | 4 | 2 | 1 | | | | |
| 6 | exp | −0.53 | 3.4 | 4 | 1 | | | | |
| $H_2S+H_2O$ | | | | | | | | | |
| 1 | pol | 0.17 | 0.9 | 1 | | | | | |
| 2 | pol | −0.1116 | 4.04 | 1 | | | | | |
| 3 | exp | 0.121 | 6.88 | 2 | 1 | | | | |
| 4 | exp | −0.002352 | 8.15 | 4 | 1 | | | | |
| 5 | exp | −0.0431 | 5.35 | 8 | 2 | | | | |
| 6 | exp | 0.7764 | 2.7 | 1 | 1 | | | | |
| $MEA+H_2O$ | | | | | | | | | |
| 1 | exp | 0.0436 | 0.1 | 1 | 2 | | | | |
| 2 | exp | 0.0437 | 0.1 | 3 | 2 | | | | |
| 3 | GBS | −0.0217 | 3.06 | 2 | | 0.69 | 0.55 | 2.42 | 2.8 |
| 4 | GBS | −0.0187 | 4.39 | 1 | | 0.25 | 1.83 | 1.42 | 2.16 |
| $DEA+H_2O$ | | | | | | | | | |
| 1 | exp | 0.151 | 0.58 | 1 | 2 | | | | |
| 2 | GBS | −0.0817 | 4.19 | 2 | | 1.36 | 0.72 | 1.9 | 2.1 |
| 3 | GBS | 0.326 | 3.03 | 1 | | 2.4 | 1.32 | 2.29 | 2.33 |

**Table 5** continued

| | | | | | | | | | |
|---|---|---|---|---|---|---|---|---|---|
| $NH_3+H_2O$ [68] | | | | | | | | | |
| 1 | exp | −2.00211 | 0.25 | 1 | 2 | | | | |
| 2 | exp | 3.0813 | 2 | 1 | 1 | | | | |
| 3 | GBS | −1.75352 | 0.5 | 1 | | 0 | 0.27 | 2.8 | 0 |
| 4 | GBS | 2.9816 | 2 | 1 | | 0.746 | 0.86 | 1.8 | 2 |
| 5 | GBS | −3.82588 | 1 | 1 | | 4.25 | 3 | 1.5 | −0.25 |
| 6 | GBS | −1.7385 | 4 | 1 | | 0.7 | 0.5 | 0.8 | 1.85 |
| 7 | GBS | 0.42008 | 4 | 3 | | 3 | 4 | 1.3 | 0.3 |
| $MDEA+H_2O$ | | | | | | | | | |
| 1 | exp | 0.058 | 3.3 | 1 | 2 | | | | |
| 2 | exp | 0.0497 | 1.66 | 2 | 2 | | | | |
| 3 | GBS | 0.02 | 3.1 | 3 | | 2.6 | 2.09 | 1.96 | 2.129 |
| 4 | GBS | −0.063 | 1.44 | 2 | | 2.6 | 2.6 | 1.0 | 2.486 |
| 5 | GBS | 0.00316 | 3.5 | 1 | | 0.4 | 1.89 | 2.6 | 2.254 |
| $N_2+H_2$ [7] | | | | | | | | | |
| 1 | exp | −1.659 | 0.724 | 1 | 1 | | | | |
| 2 | exp | −0.268 | 0.097 | 2 | 1 | | | | |
| 3 | exp | −0.502 | 2.953 | 1 | 2 | | | | |
| 4 | exp | 0.323 | 3.5 | 2 | 2 | | | | |
| 5 | GBS | 2.976 | 2.939 | 1 | | 1.86 | 0.93 | 1.3 | 2.51 |
| 6 | GBS | 5.084 | 0.694 | 1 | | 0.03 | 0.36 | 0.8 | 0.39 |
| 7 | GBS | −3.866 | 2.329 | 1 | | 1.85 | 0.99 | 1.5 | 2.51 |
| 8 | GBS | −5.474 | 1.066 | 1 | | 0.13 | 0.24 | 2.3 | 1.22 |
| $CH_4+N_2$ [6] | | | | | | | | | |
| 1 | pol | −0.0098038985517335 | | 0 | 1 | | | | |
| 2 | pol | 0.00042487270143005 | | 1.85 | 4 | | | | |
| 3 | spec | −0.034800214576142 | | 7.85 | 1 | | 1 | 1 | 0.5 | 0.5 |
| 4 | spec | −0.13333813013896 | | 5.4 | 2 | | 1 | 1 | 0.5 | 0.5 |
| 5 | spec | −0.011993694974627 | | 0 | 2 | | 0.25 | 2.5 | 0.5 | 0.5 |
| 6 | spec | −0.069243379775168 | | 0.75 | 2 | | 0 | 3 | 0.5 | 0.5 |
| 7 | spec | −0.31022508148249 | | 2.8 | 2 | | 0 | 3 | 0.5 | 0.5 |
| 8 | spec | 0.24495491753226 | | 4.45 | 2 | | 0 | 3 | 0.5 | 0.5 |
| 9 | spec | 0.22369816716981 | | 4.25 | 3 | | 0 | 3 | 0.5 | 0.5 |
| $Ar+NH_3$ [84] | | | | | | | | | |
| 1 | exp | 0.2350785 | 2.3 | 3 | 1 | | | | |
| 2 | GBS | −1.913776 | 1.65 | 1 | | 1.3 | 0.6 | 0.9 | 0.31 |
| 3 | GBS | 1.624062 | 0.42 | 1 | | 1.5 | 0.5 | 1.5 | 0.39 |

**Table 5** continued

| | | | | | | | | | |
|---|---|---|---|---|---|---|---|---|---|
| $CO+H_2$ [7] | | | | | | | | | |
| 1 | pol | −0.521 | 2.25 | 1 | | | | | |
| 2 | pol | −0.387 | 0.473 | 2 | | | | | |
| 3 | GBS | −2.59 | 0.585 | 1 | | 0.647 | 0.751 | 1.86 | 1.38 |
| 4 | GBS | 4.35 | 0.091 | 2 | | 0.344 | 0.66 | 2.23 | 0.773 |
| $CH_4+H_2$ [7] | | | | | | | | | |
| 1 | pol | 1.28 | 0.34 | 1 | | | | | |
| 2 | pol | −0.774 | 0.42 | 2 | | | | | |
| 3 | exp | −0.914 | 0.8 | 1 | 1 | | | | |
| 4 | exp | 0.36 | 3.29 | 2 | 1 | | | | |
| 5 | GBS | −2.45 | 0.05 | 1 | | 0.83 | 0.97 | 0.77 | 1.36 |
| 6 | GBS | 4.462 | 0.254 | 2 | | 0.34 | 0.2 | 1.74 | 1.44 |
| 7 | GBS | −0.972 | 0.41 | 3 | | 0.57 | 0.26 | 0.79 | 1.69 |
| 8 | GBS | −2.07 | 2.63 | 1 | | 0.44 | 0.18 | 0.4 | 1.53 |
| $H_2+NH_3$ [84] | | | | | | | | | |
| 1 | exp | −3.73558 | 1.28 | 1 | 1 | | | | |
| 2 | exp | −7.47092 | 2.05 | 2 | 1 | | | | |
| 3 | GBS | 1.98413 | 2.6 | 1 | | 0.61 | 2.06 | 0.79 | 0.8 |
| 4 | GBS | 1.87191 | 3.13 | 2 | | 1.6 | 1.74 | 2.1 | 1.62 |

The labels of the parameters $\eta_{ij,k}$, $\varepsilon_{ij,k}$, $\gamma_{ij,k}$, $\beta_{ij,k}$ are not correct in Table 8 of reference [84]. The correct labels are given in this work

datasets that formed the basis for the models are summarized in Table S1 in the supplementary material. The AAD and AARD tables for the data used in the development of the EOS in this work are given in Table 7 in the "Appendix". All experimental data were converted to molar-based SI units with temperatures on the International Temperature Scale of 1990 (ITS-90) and pressures converted to MPa.

In the following sections, comparisons between the mixture model with experimental data, including ternary and multicomponent mixtures, are analyzed. Only the most accurate and comprehensive datasets are discussed for brevity.

Systems, which could not be fitted due to the scarce data situation and which are described accordingly only with a combination rule, are not discussed in this section. As Herrig [21] shows, no general statements can be made about which accuracies can be expected for these systems, because this differs very strongly binary-specifically from each other. For example, the prediction of phase equilibria depends on the combination rule not only quantitatively but also qualitatively (e.g., $CH_4+Cl_2$), see Herrig [21].

### 3.1.1 $H_2O + CH_4$

A reduced Helmholtz energy explicit formulation for the binary system $H_2O+CH_4$ is included in the GERG-2008 model of Kunz and Wagner [6]. Since $CH_4$ is the most relevant component in that mixture model, the binary formulation for $H_2O+CH_4$ is considered to yield reliable results, although binary mixtures with water are normally not accurately described within GERG-2008 [6]. For the binary model in GERG-2008 [6], all four reducing parameters were fitted but no binary-specific departure function was used. Because $CH_4$ was not considered in the original EOS-CG model of Gernert and Span [5], no binary formulation for $H_2O+CH_4$ is included in that model.

Compared to many other binary mixtures, the experimental database for $H_2O+CH_4$ is comprehensive. VLE data are available in many publications in addition to data for homogeneous densities and, in some cases, values for isobaric heat capacities, virial coefficients, and excess enthalpies. Although none of the data sets published after the development of the GERG-2008 model [6] is regarded as very accurate, the work of Herrig [21] improved the description of this system by developing a binary-specific departure function. In this section, data calculated from this model are compared to the available experimental data.

Even with the mathematical flexibility of a departure function, the system $H_2O+CH_4$ is exceptionally challenging to describe. In the VLE region, the coexisting phases are almost pure fluids. As a result, even small compositional uncertainties of the data lead to high deviations in pressure. In Fig. 6, *p,x* diagrams for four isotherms illustrate this type of mixing behavior. The phase boundaries were calculated from the new model and GERG-2008 [6]. Selected experimental data are shown for comparisons.

Due to the almost pure coexisting phases, absolute deviations in composition between the new model and GERG-2008 [6] are quite small. Nevertheless, the new model provides a more accurate description of the data. Results calculated from GERG-2008 [6] do not follow the trend of the bubble-point data at lower temperatures. For the two lowest isotherms, the GERG-2008 model [6] drastically underestimates the solubility of $CH_4$ in $H_2O$ and yields a saturated-liquid that is almost pure $H_2O$. Deviations between values calculated from both models and experimental VLE data from various sources are shown in Fig. 7. Additional data were found in the literature, see Table 7 in the "Appendix"; however, those data exhibit extremely large deviations from GERG-2008 [6], the present model, and all its preliminary versions. These large deviations are presumably caused by high composition uncertainties; thus, only the data sets found to be reliable are included in Fig. 7. As mentioned before, deviations in pressure are not meaningful for a system with steep *p,x* phase boundaries, but the deviations in composition give a good impression of the accuracy of both models.

At temperatures between 255 K and 400 K, the present model represents most of the data with deviations below 0.0015 $mol_{CH_4}/mol_{mix}$. The overall representation of the data in this temperature range is more accurate than with GERG-2008 [6], especially with regard to the saturated-liquid data of Awan et al. [91], Chapoy et al. [89], and Frost *et al.* [93]. At elevated temperatures between 400 K and 600 K, the

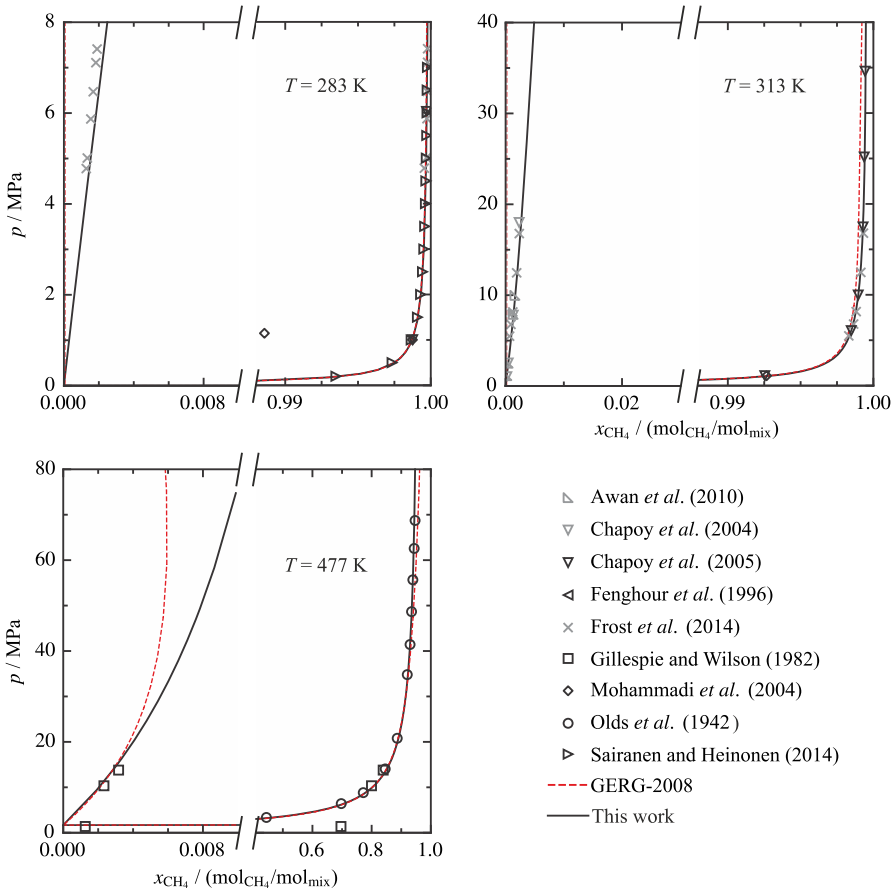


**Fig. 6** *p,x* diagrams showing selected experimental phase equilibrium data [89–97] at 283 K, 313 K, and 477 K in comparison to phase boundaries calculated with the EOS of this work and GERG-2008 [6] for the system $H_2O+CH_4$

data are mostly described within 0.01 $mol_{CH_4}/mol_{mix}$. In this temperature region, the accuracy of both models is comparable, although GERG-2008 [6] exhibits some higher deviations.

For this mixture, it is only partially possible to compare deviations between calculated and experimental data with given or estimated experimental uncertainties. None of the references included in Fig. 7 provides combined uncertainties in composition. Many references do not even state the uncertainties in composition. Instead, less meaningful information on the reproducibility or the calibration precision of the gas chromatograph is given. These uncertainty specifications are not sufficient for the validation of the present model but are not surprising with respect to the shape of phase boundaries, which are characterized by extremely small mole fractions of one component.

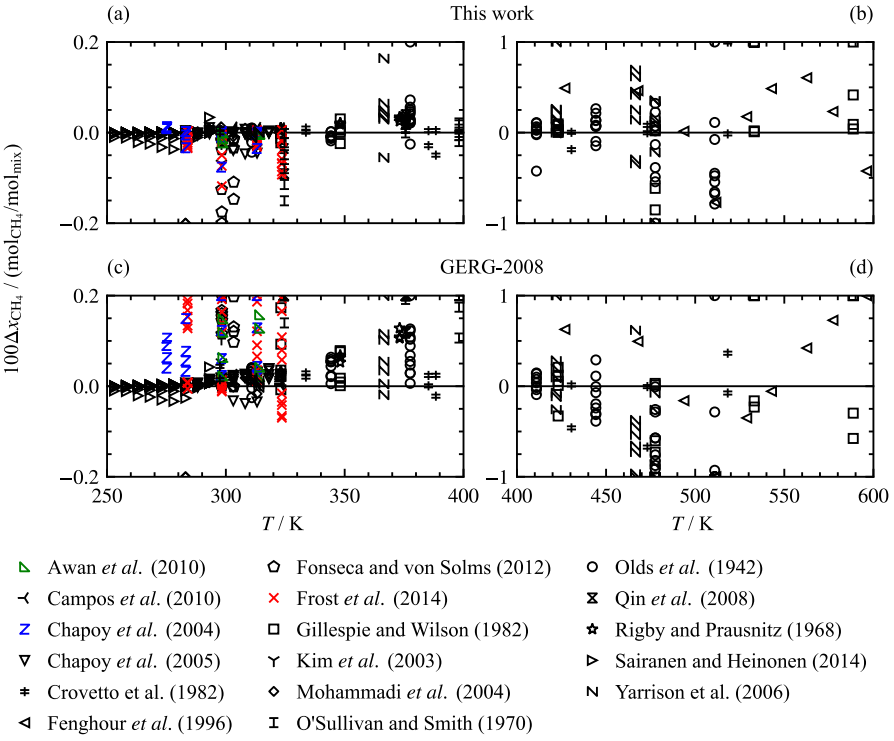


**Fig. 7** Absolute deviations $\Delta x_{CH_4}=(x_{CH_4,data}-x_{CH_4,EOS})$ between experimental phase equilibrium data [89–102] and values calculated with the EOS of this work (a, b) and GERG-2008 [6] (c, d) as a function of temperature for the system $H_2O+CH_4$

Complete VLE data sets including the compositions of both phases are only given by Gillespie and Wilson [94], Fonseca and von Solms [98], Qin et al. [100], and Frost et al. [93]. All these data sets were obtained by withdrawing samples from the coexisting phases and analyzing them in a gas chromatograph. The experimental set-up of Frost et al. [93] was developed by Fonseca and von Solms [98], whose data result from the first measurements with that apparatus. The measurements of Frost et al. [93] consequently supersede the data of Fonseca and von Solms [98]. They cover a temperature range from 284 K to 324 K and are among the most valuable data sets for the development of the present model. The data of Gillespie and Wilson [94] were useful to fit the model at elevated temperatures up to 589 K, although they exhibit some scatter and cannot be considered as highly accurate.

The solubility of $CH_4$ in $H_2O$, which is equivalent to the saturated-liquid-phase in VLE, was measured at temperatures above 275 K by Awan et al. [91], Campos et al. [102], Chapoy et al. [89], and Kim et al. [99]. In all these works, the mole fractions of $CH_4$ in the saturated-liquid were measured instead of the bubble-point with known composition. All data sets are in good agreement with the VLE data of Frost et al. [93]. The deviations of the data of Chapoy et al. [89] correspond to the representation

of their data for $H_2O+CO_2$ by the original EOS-CG model of Gernert and Span [5], who report a maximum deviation of 0.002 $mol_{H_2O}/mol_{mix}$.

Solubilities of $H_2O$ in $CH_4$, and thus the saturated-vapor states of the VLE, were investigated by Chapoy et al. [103], Fenghour et al. [92], Sairanen and Heinonen [97], Mohammadi et al. [95], Olds et al. [96], and Rigby and Prausnitz [101]. In the latter work, the water mole fractions are estimated to be accurate within 1%. Considering the highest measured water concentration $x_{H_2O}=0.01992$ $mol_{H_2O}/mol_{mix}$, this uncertainty estimate is equivalent to an expanded ($k=2$) uncertainty of about 0.0004 $mol_{CH_4}/mol_{mix}$. The maximum deviation between these data and the present model is 0.00034 $mol_{CH_4}/mol_{mix}$ (AAD=0.00016 $mol_{CH_4}/mol_{mix}$). The data are consequently represented within their experimental uncertainty. The measurements of Olds et al. [96] were published in 1942 and are the oldest reliable experimental data found in the literature. Although they are not considered as highly accurate, they were important for the fitting process because they cover a temperature range from 310 K to 510 K. According to the authors, the mole fractions of water are accurate within 2%. At temperatures below 400 K, this corresponds to a maximum expanded ($k=2$) uncertainty of 0.0017 $mol_{CH_4}/mol_{mix}$. At higher temperatures, the maximum uncertainty increases up to 0.022 $mol_{CH_4}/mol_{mix}$. These uncertainties mostly agree with the deviations shown in Fig. 7. Fenghour et al. [92] investigated the high-temperature region up to almost 600 K. Dew points were obtained from isochoric $p\rho T$ measurements. The pressure of a mixture with known composition was continuously measured while varying the temperature. Discontinuities in the obtained pressure versus temperature diagram indicated that the dew-point of the mixture was reached. No uncertainties are given for those dew points. Neglecting one clear outlier, the data are represented with a maximum deviation of 0.006 $mol_{CH_4}/mol_{mix}$. At temperatures between 283 K and 318 K, very accurate dew points were published by Chapoy et al. [103] as a correction of an earlier work by the same authors. The data are represented with an AAD of 0.00 006 $mol_{CH_4}/mol_{mix}$ and a maximum deviation of 0.0005 $mol_{CH_4}/mol_{mix}$. The authors provide a maximum uncertainty in the mole fraction of water of 0.2%. Interpreting this value as the standard uncertainty of every state point leads to an average expanded ($k=2$) uncertainty of 0.00 006 $mol_{CH_4}/mol_{mix}$ and maximum uncertainty of 0.0004 $mol_{CH_4}/mol_{mix}$, which is both in close agreement with the deviations from the present model. The most recent saturated-vapor data were published by Sairanen and Heinonen [97] covering low temperatures between 253 K, which is close to the hydrate formation temperature, and 293 K. The data were used to fit the model in the low-temperature region but are not considered as highly accurate. At 283 K and 293 K, they are in close agreement with the measurements of Chapoy et al. [103] but exhibit some scatter with decreasing temperatures.

We do not provide estimated uncertainties in calculated VLE compositions because none of the discussed references provides a complete and reliable uncertainty analysis.

The development of the present model for $H_2O+CH_4$ was enhanced by a comprehensive database of homogenous densities. Deviations between the available experimental data, the present model, and the binary formulation included in GERG-

2008 [6] are shown in Fig. 8. The database is restricted to the gas and supercritical state regions. No liquid-phase data were found in the literature.

The most accurate data for homogeneous gas-phase densities were published by Joffrion and Eubank [105]. The authors investigated three mixtures with 0.5 $mol_{H_2O}/mol_{mix}$, 0.25 $mol_{H_2O}/mol_{mix}$, and 0.1 $mol_{H_2O}/mol_{mix}$ in a temperature range from 398 K to 498 K and at pressures up to 12 MPa. The combined standard uncertainty is stated to be 0.08%. The present model describes more than 95% of the data within deviations of 0.16%, which corresponds to the expanded ($k$=2) uncertainty of the data. The GERG-2008 model [6] represents the data mostly with comparable deviations; however, the deviations increase with increasing pressure. Above 3 MPa, deviations between the data and GERG-2008 [6] are higher than the experimental uncertainty. Another important data set was measured by Fenghour et al. [92], which also lead to the dew-point data discussed before. That work provides gas-phase densities for nine mixtures covering $H_2O$ contents between 0.076 $mol_{H_2O}/mol_{mix}$ and 0.676 $mol_{H_2O}/mol_{mix}$ at temperatures between 430 K and 700 K and pressures ranging from 7.5 MPa to 30 MPa. The given standard uncertainty of the data are 0.08% for the mixture with the lowest $H_2O$ content and 0.14% for the mixture with the highest $H_2O$ content. The expanded ($k$=2) uncertainties consequently range from 0.16% to 0.28%, which does not agree with the deviations of up to 1.2% from the present model. GERG-2008 [6] enables a more consistent description of the data but also exhibits deviations up to 0.84%. During

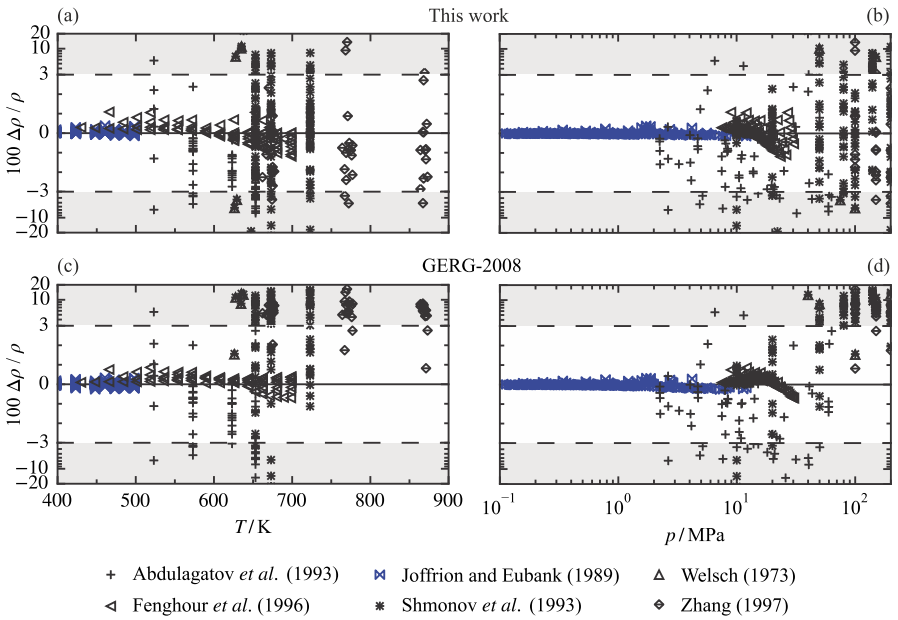


**Fig. 8** Relative deviations $\Delta\rho/\rho=(\rho_{data}-\rho_{EOS})/\rho_{data}$ between experimental homogeneous density data [92, 104–108] and values calculated with the EOS of this work (a, b) and GERG-2008 [6] (c, d) as a function of temperature (a, c) and pressure (b, d) for the system $H_2O+CH_4$. The ordinate is linearly scaled between the dashed lines and logarithmically scaled in the gray filled region

the development of the present model, many different functional forms for the departure function were applied and rejected before the final set of terms was obtained. None of these preliminary models provided higher accuracy to the data of Fenghour et al. [92] and a better description of the VLE data.

The high-temperature and high-pressure region of $H_2O+CH_4$ was investigated by Abdulagatov et al. [104] and Shmonov et al. [106]. The work of Abdulagatov et al. [104] presents data for various different mixtures covering the complete composition range at temperatures between 525 K and 653 K and at pressures between 2 MPa and 64 MPa. The claimed expanded ($k$=2) uncertainty of the data are 0.4%, which seems to be significantly underestimated. The data exhibit scatter of at least 6%. The work of Shmonov et al. [106] provides no information on experimental uncertainties. It includes measurements of four mixtures with 0.2 $mol_{H_2O}/mol_{mix}$, 0.4 $mol_{H_2O}/mol_{mix}$, 0.6 $mol_{H_2O}/mol_{mix}$, and 0.8 $mol_{H_2O}/mol_{mix}$ as well as results for both pure components. The measurements were carried out at temperatures between 653 K and 723 K and at pressures between 10 MPa and 200 MPa. The data deviate by more than 8% from the model. In order to check the reliability of the data, comparisons between the pure-fluid measurements and results calculated from the reference EOS of Setzmann and Wagner [77] (for $CH_4$) and Wagner and Pruß [67] (for $H_2O$) were made. The data exhibit deviations up to 9% for pure $CH_4$ and 2% for pure $H_2O$. Due to these high deviations, we consider the stated uncertainty of 0.4% to be implausible. Another high-pressure data set was published by Zhang [108]. It provides densities of the supercritical fluid at temperatures between 675 K and 873 K and pressures ranging from 100 MPa to 300 MPa. The data were not experimentally determined but are the result of calculations. The underlying method is only vaguely described as being based on "synthetic fluid inclusion data" and an equation fitted to $CH_4$ clathrate melting temperatures and pressures (see Zhang [108]). No uncertainties are given in the corresponding publication. The data were not used to fit the binary mixture model; nevertheless, they are mostly represented with deviations below 4%. Although none of the available high-temperature and high-pressure data sets is sufficiently accurate to allow for a quantitative validation of the present model, the deviations shown in Fig. 8 emphasize that the model yields qualitatively reasonable results in that state region, whereas GERG-2008 [6] exhibits much higher deviations from the data.

Estimated uncertainties of homogeneous densities calculated from the model can only be provided for gas-phase states. The uncertainties are based on the comparisons with the two reliable experimental data sets of Joffrion and Eubank [105] and Fenghour et al. [92]. For mixtures containing between 0.10 $mol_{H_2O}/mol_{mix}$ and 0.5 $mol_{H_2O}/mol_{mix}$, gas-phase densities for temperatures between 400 K and 495 K and at pressures up to 12 MPa can be calculated with an uncertainty of 0.16%. At higher temperatures up to 700 K and pressures between 7.5 MPa and 30 MPa, the uncertainty of calculated values is expected to be below 1.5%. This uncertainty estimate is also valid for mixtures containing higher fractions of water of up to 0.67 $mol_{H_2O}/mol_{mix}$.

Overall, the development of the departure function for $H_2O+CH_4$ resulted in a more accurate description of this mixture compared to the GERG-2008 model [6]. In

particular, the representation of the low-temperature VLE region has been improved. Nevertheless, the model for this important binary mixture could still be improved if additional accurate experimental data became available. Homogeneous liquid densities, high-temperature VLE data, and caloric data such as speed of sound would be beneficial for a refit of the present model.

### 3.1.2 $H_2O + H_2S$

The binary-specific departure function of Herrig [21] for the mixture $H_2O + H_2S$ is based on a limited experimental database. Accurate experimental values are restricted to VLE data, although some saturated-liquid densities and isobaric heat capacities are also available. The densities are briefly discussed within this section. The heat capacity measurements of Hnědkovský and Wood [109] were carried out in almost pure water ($x_{H_2S}$ =0.0067) and are, thus, not relevant for the validation of the mixture model. The system $H_2O + H_2S$ was also considered in the GERG-2008 model of Kunz and Wagner [6]. In that model, no binary-specific departure function was developed, but only two reducing parameters were fitted. The EOS-CG model of Gernert and Span [5] does not allow for the description of mixtures with $H_2S$.

As typical with binary mixtures containing water, the phase-equilibrium behavior of $H_2O + H_2S$ is complex. This is not only because solid water or hydrates might form, but also due to the possible split into vapor–liquid or liquid–liquid equilibria (LLE). The solubility of $H_2S$ in water is higher than that of $CH_4$, but still so limited that phase equilibria mostly consist of two phases rich in one of the components. At temperatures below the critical temperature of $H_2S$ ($T_{c,H_2S}$=373.1 K), the $H_2S$-rich phase in equilibrium may be liquid or gaseous depending on the pressure of the system. The resulting VLE and LLE regions are separated by a three-phase line along which a $H_2S$-rich vapor, a $H_2O$-rich liquid, and a $H_2S$-rich liquid are in a phase equilibrium (VLLE). This behavior is illustrated in Fig. 9. The phase boundaries for two exemplary isotherms ($T<T_{c,H_2S}$) were calculated from the new model and GERG-2008 [6]. Selected literature data are shown for comparisons.

Both models yield qualitatively comparable results, with almost congruent saturated-vapor lines. Figure 9 (left panel) indicates that the GERG-2008 model [6] underestimates the solubility of $H_2S$ in the liquid, whereas the new model is in excellent agreement with experimental data. The most distinct differences between the models are found in the prediction of the LLE region and VLLE line; however, no experimental data are available to validate these predictions. The representation of the VLE data are presented in more detail in Fig. 10. Deviations between literature data and bubble- and dew-point compositions calculated from the new model and GERG-2008 [6] are shown over the complete temperature range of the data.

The deviation plots confirm the impression obtained from the *p,x* diagrams: The new model is significantly more accurate in the calculation of bubble-point states and, thus, of the $H_2S$-solubility in the liquid than GERG-2008 [6]. Most of the data are represented with deviations below 0.002 $mol_{H_2S}/mol_{mix}$, whereas the same data deviate by up to 0.02 $mol_{H_2S}/mol_{mix}$ from the GERG-2008 [6]. The representation of

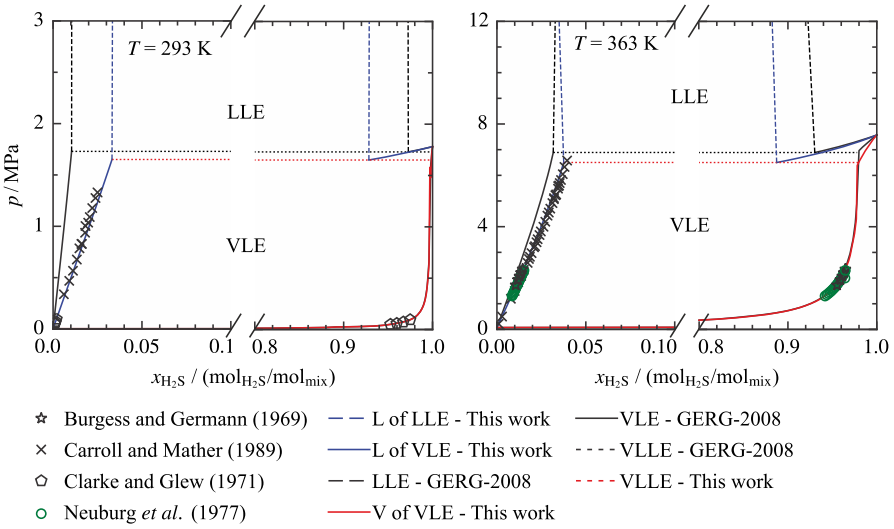


**Fig. 9** *p,x* diagrams showing selected experimental phase equilibrium data [110–113] at 293 K and 363 K in comparison to phase boundaries calculated with the EOS of this work and GERG-2008 [6] for the system $H_2O+H_2S$. Note that the VLE curves of the GERG-2008 [6] and this work are very similar in the vapor phase. Therefore, the solid black line is mostly covered by the solid red line

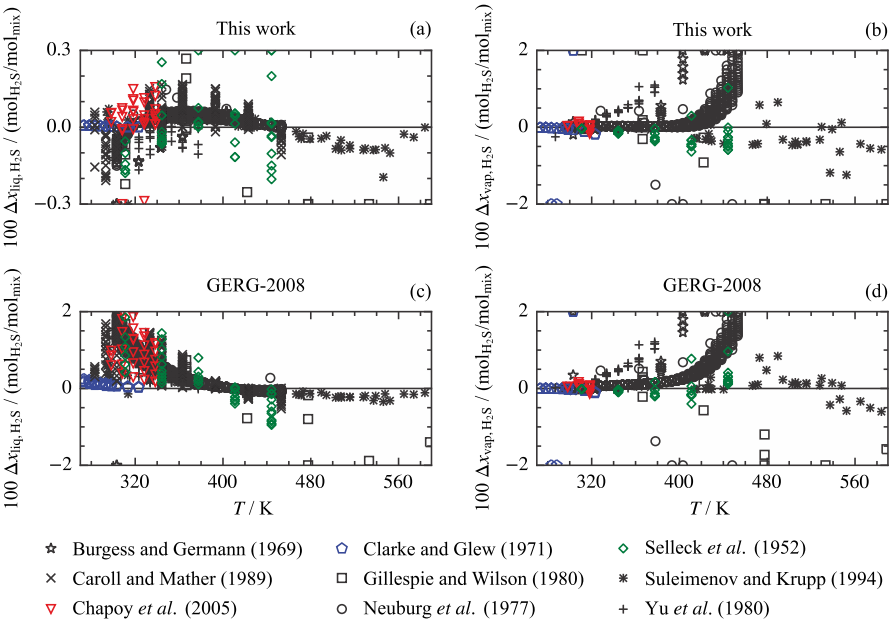


**Fig. 10** Absolute deviations $\Delta x_{H_2S}=(x_{H_2S,data}-x_{H_2S,EOS})$ between experimental bubble-point (a, c) and dew-point (b, d) data [94, 103, 110, 111, 113–117] and values calculated with the EOS of this work (a, b) and GERG-2008 [6] (c, d) as a function of temperature for the system $H_2O+H_2S$

the dew-point data are similar for both models, although the new model provides more consistent results at temperatures below 430 K.

Datasets containing values of both equilibrium phases were published by Burgess and Germann [110], Chapoy et al. [103, 118], Clarke and Glew [114], Gillespie and Wilson [94], Neuburg et al. [111], Selleck et al. [115], Suleimenov and Krupp [116], and Yu et al. [117]. The work of Carroll and Mather [113] is restricted to bubble-point data and is based on calculations. The most comprehensive data set was published by Neuburg et al. [111]. The data were not obtained experimentally but correlated based on data from various other sources. No uncertainty of these correlated values is given in the corresponding publication. The same applies to the data of Burgess and Germann [110] and Carroll and Mather [113], who also calculated data without providing uncertainties. Therefore, these three datasets do not allow for a quantitative validation of the mixture model. The data of Gillespie and Wilson [94] and Yu et al. [117] cannot be used for validation either. The results of Gillespie and Wilson [94] exhibit unreasonable large scatter, whereas the deviations of the dew-point data of Yu et al. [117] increase significantly with increasing pressure. Furthermore, both works do not include any uncertainty information.

Clarke and Glew [114] measured the solubility of $H_2S$ in water in a temperature range from 273 K to 323 K. The mole fractions are claimed to be accurate within 0.1%. Due to the small mole fractions of $H_2S$ in the liquid-phase, this leads to an extremely low expanded ($k$=2) uncertainty of 0.000006 $mol_{H_2S}/mol_{mix}$. The model represents the data with an AAD of 0.00004 $mol_{H_2S}/mol_{mix}$, which is about one order of magnitude higher than the claimed experimental uncertainty. Even though we assume that the uncertainty was underestimated by Clarke and Glew [114], the good agreement with the bubble-point data emphasizes the accuracy of the new model. Dew points from the same reference are also accurately represented; however, Clarke and Glew [114] obtained these values from phase-equilibrium calculations based on their bubble-point data without providing uncertainties.

Chapoy et al. [103, 118] measured the composition of both coexisting phases at temperatures between 298 K and 338 K. The measurements are based on a static-analytic method with fluid phase sampling. The corresponding publication does not provide combined uncertainties in composition; nevertheless, the data are in very good agreement with the present model. The bubble points are represented with a maximum deviation of 0.003 $mol_{H_2S}/mol_{mix}$ and an AAD of 0.0007 $mol_{H_2S}/mol_{mix}$, whereas the maximum deviation of the dew points is 0.0017 $mol_{H_2S}/mol_{mix}$ and the AAD 0.0007 $mol_{H_2S}/mol_{mix}$. These deviations are comparable with those of Chapoy's data for $H_2O+CO_2$ [119] and $H_2O+CH_4$ [89] from the original EOS-CG [5] and from the model presented in Sec. 3.1.1.

Selleck et al. [115] carried out measurements along five isotherms between 311 K and 444 K. The authors estimated the uncertainty in $H_2S$ mole fractions of the gas-phase to be 0.002 $mol_{H_2S}/mol_{mix}$, which leads to an expanded ($k$=2) uncertainty of 0.004 $mol_{H_2S}/mol_{mix}$. No experimental uncertainty is given for the bubble-point data. The model describes the dew-point data below the VLLE pressure with a maximum deviation of 0.0063 $mol_{H_2S}/mol_{mix}$ and an AAD of 0.0025 $mol_{H_2S}/mol_{mix}$ (excluding one clear outlier), which is in good agreement with the experimental uncertainty.

The publication also provides VLE data at pressures higher than the VLLE pressures calculated from the present model. The data are presented as extrapolation results (see Selleck et al. [115]). Since data in this region should be LLE data, these extrapolations are found to be unreasonable, and they exhibit large deviations from the present and the GERG-2008 model [6].

The high-temperature VLE region up to 584 K was investigated by Suleimenov and Krupp [116], whose data also include lower temperatures (down to 293 K). The authors give no useful information about the experimental uncertainty. The data are sufficiently consistent with comparative measurements at lower temperatures for use in validation of the model at temperatures between 445 K and 585 K. In this temperature range, the model represents most of the bubble- and dew-point data within 0.001 $mol_{H_2S}/mol_{mix}$ and 0.01 $mol_{H_2S}/mol_{mix}$, respectively.

Since the experimental studies used to develop the mixture model only provide vague information about the experimental uncertainty of the data, we do not provide uncertainty estimates for calculated VLE composition. However, the deviations shown in Fig. 10 give an impression of the accuracy of the mixture model.

The only low-temperature density data found in the literature are included in the VLE study of Selleck et al. [115] and were not measured at homogeneous states but at saturated-liquid states between 310 K and 445 K. Deviations between the data, the present mixture model, and GERG-2008 [6] are presented in Fig. 11.

The data deviate by approximately 1% up to 410 K and 3% at higher temperatures from the new model and by up to 5% from GERG-2008 [6]. Selleck et al. [115] estimated the uncertainty of their data to be within 3%, which is interpreted as a standard uncertainty. An expanded ($k$=2) uncertainty of 6% agrees with the deviations from both models. Nevertheless, this uncertainty is so high that it does not allow for a reasonable uncertainty estimate for calculated saturated-liquid densities.

High temperatures were investigated in the homogeneous state region by Zezin et al. [120] between 523 K and 674 K. These data were not available when the model was adjusted and were, thus, only used for comparison. Deviations with respect to the present model and the GERG-2008 [6] are in the same range ($AARD_{this\ work}$=19% and $AARD_{GERG}$=17%). Since both models are independent of each other, one could conclude that the high deviations are caused by measurement uncertainties of the data. However, a reliable statement is only possible if the data are

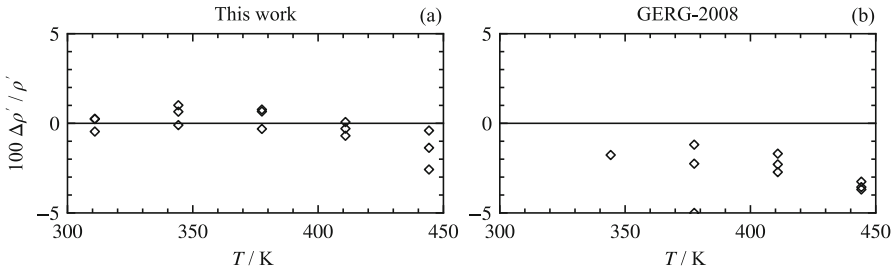


**Fig. 11** Relative deviations $\Delta\rho/\rho=(\rho_{data}-\rho_{EOS})/\rho_{data}$ between experimental saturated-liquid density data of Selleck et al. [115] and values calculated with the EOS of this work (a) and GERG-2008 [6] (b) as a function of temperature for the system $H_2O+H_2S$

included in the adjustment process. Therefore, a model error cannot be excluded here.

### 3.1.3 $SO_2 + CO_2$

With regard to the quantity of the available data, the binary system $SO_2 + CO_2$ is, aside from the system $SO_2 + H_2O$ (see Sec. 3.1.10), the experimentally best investigated system of the binary mixtures with $SO_2$ considered in the work of Herrig [21]. The development of the mixture model for this system was completed in mid-2017. The experimental database available at this point allowed the adjustment of all four parameters of the binary reducing functions. Two comprehensive *pvT* data sets were published later in 2017 and in 2018 by Nazeri et al. [121] and Gimeno et al. [122]. These two data sets consequently did not contribute to the fitting process, but comparisons to the mixture model are discussed in this section.

The most recent and also most accurate and consistent VLE data set was published by Coquelet et al. [123]. It covers two isotherms of the VLE region, 263 K and 333 K. The data result from the static-analytical method that is based on the extraction of the liquid and vapor phases from the two-phase equilibrium. The extracted samples were analyzed in a gas chromatograph to obtain the phase-equilibrium compositions. The equilibrium cell that was part of the experimental set-up of Coquelet et al. [123] was used before in the work of Lachet et al. [124]. However, the data of Lachet et al. [124] were only graphically reported in the corresponding publication. Coquelet et al. [123] re-measured the isotherms investigated by Lachet et al. [124]. Graphically obtained points from the publication of Lachet et al. [124] are included in the *p,x* diagrams shown in Fig. 12.

In addition to the data of Lachet et al. [124] and the data from Coquelet et al. [123], Fig. 12 also shows molecular-simulation data of Lachet et al. [124] as well as the experimental data of Blümcke [126] and Caubet [125]. The *p,x* diagrams do not include the data of Thiel and Schulte [127], who reported only two equilibrium points at atmospheric pressure with very low accuracy. The bubble- and dew-point data of Coquelet et al. [123] and Lachet et al. [124] are in very close agreement; Coquelet et al. [123] repeated the measurements of Lachet et al. [124] with a slightly modified apparatus. The mixture model was fitted to the data of Coquelet et al. [123] and, thus, represents the data accurately including the characteristic changes in curvature along the bubble curve at 263 K. The molecular simulation data of Lachet et al. [124] overall agree with the reliable experimental values, but the bubble points exhibit increasing offsets with increasing pressure. The old data of Blümcke [126] and Caubet [125] have systematic offsets to the other studies.

Deviations between the present model and the available VLE data are shown in Fig. 13. Due to their very large deviations, the data of Caubet [125] are not included in the deviation plots.

The model describes the most accurate data by Coquelet et al. [123] within a maximum deviation of 0.02 $mol_{SO_2}/mol_{mix}$. The corresponding publication states expanded ($k$=2) uncertainties of 0.0002 MPa (at $p \leq 1.6$ MPa) and 0.002 MPa (at $p >$ 1.6 MPa) in pressure and of 0.02 K in temperature. The uncertainty in composition of

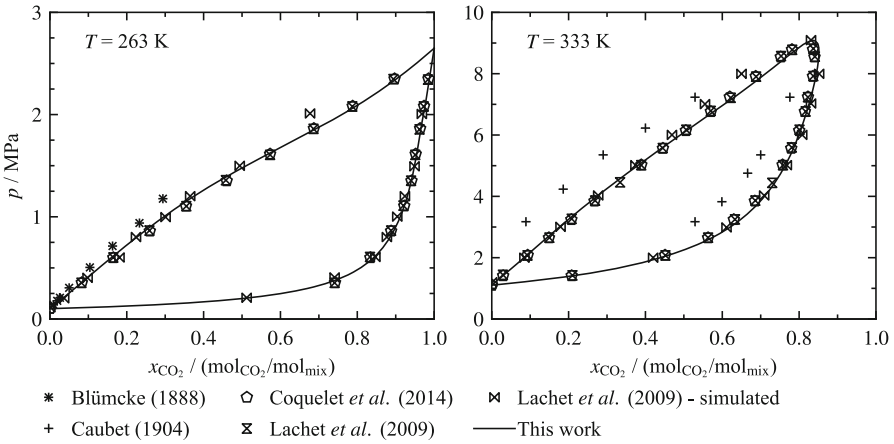


**Fig. 12** *p,x* diagrams showing selected experimental phase equilibrium data [123–126] at 263 K and 333 K in comparison to phase boundaries calculated with the EOS of this work for the system $SO_2+CO_2$

both phases is stated to be 0.6%. Because no *k*-factor is given, this value is interpreted as a standard uncertainty. The publication does not provide combined uncertainties in composition; thus, these uncertainties were calculated based on the given uncertainties in temperature, pressure, and composition. The obtained combined expanded uncertainties range from 0.0014 $mol_{SO_2}/mol_{mix}$ to 0.012 $mol_{SO_2}/mol_{mix}$ for the bubble points and from 0.004 $mol_{SO_2}/mol_{mix}$ to 0.012 $mol_{SO_2}/mol_{mix}$ for the dew points. They are included as error bars in the bottom panel of Fig. 13. The model represents most of the data within their experimental uncertainties for $x_{CO_2}>0.65$. At lower $CO_2$ concentrations, most deviations do not match the quite low uncertainties. Even intensive fitting of the data did not lead to significantly lower deviations. We therefore assume that the experimental uncertainties are to some extent underestimated. The uncertainty of calculated values is consequently estimated based on the deviations between the mixture model and the data. The uncertainty in both dew- and bubble-point compositions calculated from the new mixture model is 0.02 $mol_{SO_2}/mol_{mix}$ at temperatures between 260 K and 335 K. This uncertainty is estimated on the assumption that the model can be reasonably interpolated between the two isotherms investigated in the literature.

As mentioned at the beginning of this section, two $p\rho T$ data sets were published after the development of this binary mixture model. The only homogeneous density data available during the fitting process were the measurements of Wang et al. [128]. That study includes 12 data points along one single isotherm, 328 K, but no uncertainty analysis. Because no uncertainties of the instruments are given in the publication, no combined uncertainty in density could be estimated. Fitting the model to the data worsened the representation of the VLE data. The data were, therefore, not included in the fitting process; thus, the model was not adjusted to any density data. The deviations between calculated densities and the data of Wang et al. [128], Nazeri et al. [121], and Gimeno et al. [122] are shown in Fig. 14.

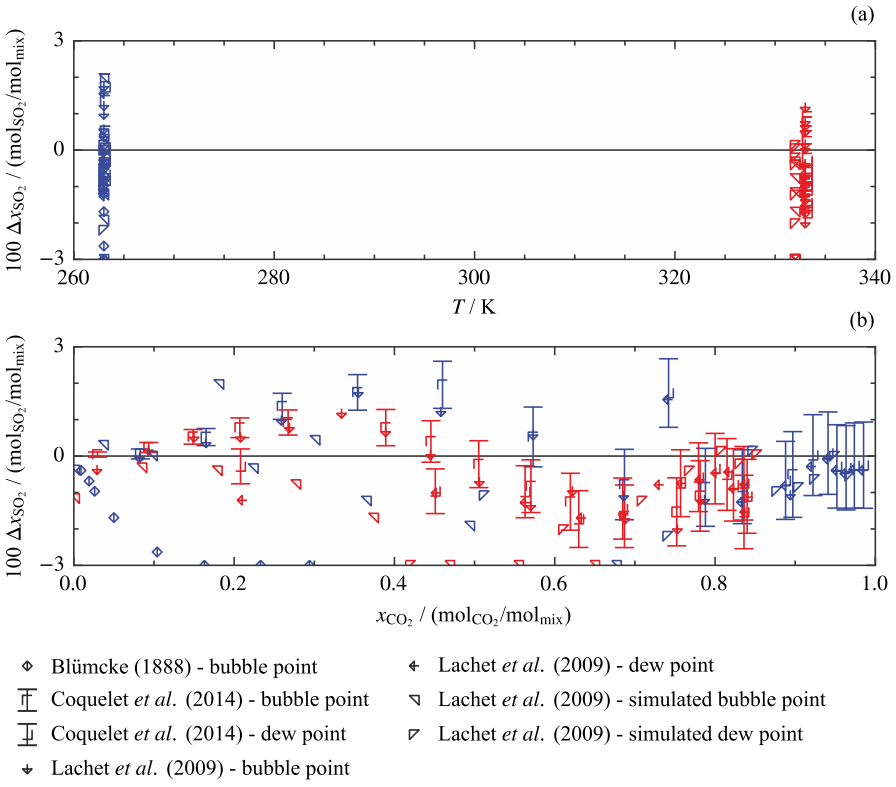


**Fig. 13** Absolute deviations $\Delta x_{SO_2} = (x_{SO_2,data} - x_{SO_2,EOS})$ between experimental phase equilibrium data and values calculated with the EOS of this work as a function of temperature (a) and $CO_2$ content (b) for the system $SO_2 + CO_2$. Error bars showing the estimated experimental uncertainty were only added to the data of Coquelet et al. [123]. The other references do not provide reliable information on the uncertainty of the data. Data measured at approximately 263 K are marked with blue symbols and data at approximately 333 K are marked with red symbols

The most recent work of Gimeno et al. [122] includes liquid and gas-phase densities for five $CO_2$-rich compositions ($0.8029 \leq x_{CO_2}/(mol_{CO_2}/mol_{mix}) \leq 0.9931$) along four isotherms ( $263 \leq T/K \leq 304$ K). Nazeri et al. [121] investigated the gas and liquid for only one composition ($x_{CO_2} \leq 0.9503$ $mol_{CO_2}/mol_{mix}$) along five isotherms ($273 \leq T/K \leq 353$ K). Both data sets were measured with vibrating-tube densimeters; thus, comparisons between the overlapping data for the mixture with 0.95 $mol_{CO_2}/mol_{mix}$ $CO_2$ at 273 K are of special interest. As shown in Fig. 15, both datasets agree within 0.26% in the liquid-phase at 20 MPa, which is the closest agreement of the data. With decreasing pressure, the deviations between the two datasets increase up to 0.68% at 4 MPa. The maximum expanded ($k=2$) uncertainty of the liquid-phase data between 4 MPa and 20 MPa stated by Gimeno et al. [122] and Nazeri et al. [121] is 0.08% and 0.1%, respectively. In Fig. 15, error bars illustrate the uncertainty of each state point. In the liquid-phase, the deviations between the two datasets are considerably higher than the reported uncertainties.

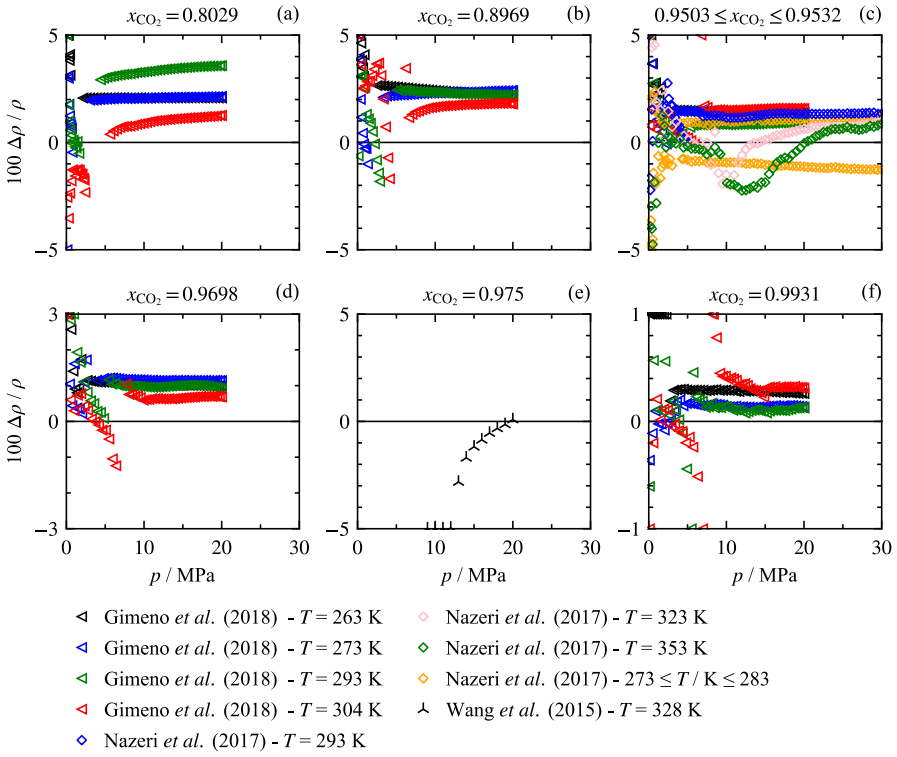


**Fig. 14** Relative deviations $\Delta\rho/\rho=(\rho_{data}-\rho_{EOS})/\rho_{data}$ between experimental density data [122, 128, 129] and values calculated with the EOS of this work as a function of pressure for the system $SO_2+CO_2$

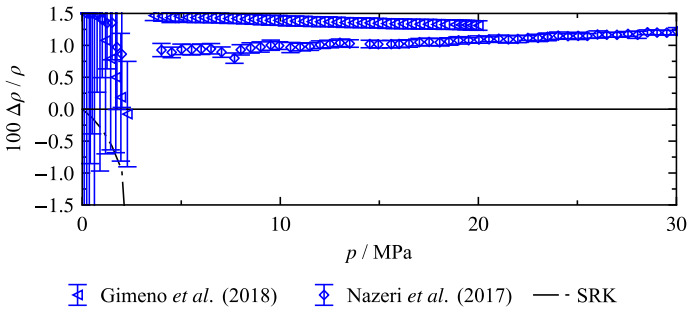


**Fig. 15** Relative deviations $\Delta\rho/\rho=(\rho_{data}-\rho_{EOS})/\rho_{data}$ between experimental density data [121, 122] and values calculated with the EOS of this work as a function of pressure for the system $SO_2+CO_2$ at 273 K; results calculated from SRK are included for comparisons

Although the experimental uncertainties of the data seem to be underestimated, they are certainly lower than their deviations from the binary mixture model developed here. Uncertainties of calculated densities are consequently equivalent to these deviations. Thus, the uncertainty in liquid-phase densities for $x_{CO_2} \ge 0.95$ is 1.5 % at temperatures up to 305 K. For lower $CO_2$ contents of $0.80 \le x_{CO_2} < 0.95$, the

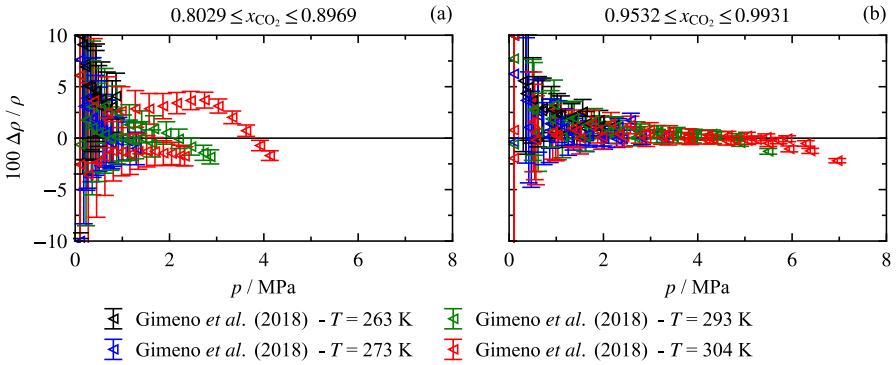


**Fig. 16** Relative deviations $\Delta\rho/\rho=(\rho_{data}-\rho_{EOS})/\rho_{data}$ between experimental density data [122] and values calculated with the EOS of this work as a function of pressure for the system $SO_2+CO_2$

uncertainty is conservatively estimated to be 3.5%. Densities decrease with decreasing pressure; thus, the relative uncertainties of the experimental data are larger. Figure 16 shows deviations of the gas-phase densities of Gimeno et al. [122] from the mixture model. The experimental uncertainties are indicated by error bars.

Excluding the 304 K isotherm of the mixture with $x_{CO_2}=0.8969$, most of the data are represented within their experimental uncertainties, which demonstrates the reliable predictive capabilities of the model because the data were not included in the fit. However, we do not provide relative uncertainties of calculated values from the deviations because, as evident in Fig. 16, the experimental uncertainties exhibit a significant pressure dependency. Based on the deviations of the experimental data, the uncertainty of the EOS seems to increase significantly with decreasing pressure; however, at very low pressures, the uncertainty of the EOS becomes small because the gas approaches the ideal-gas limit, and the EOS obeys this limit by design. Actually, the uncertainty of the measured data drastically increases at very low pressure.

Although the model for $SO_2+CO_2$ allows for a quantitatively correct description of the available VLE data and homogeneous density data in the gas-phase, it does not match the uncertainties of the experimental liquid densities. The accuracy of the model could be improved by fitting a short binary-specific departure function to the $p\rho T$ data sets published after the development of the present model.

### 3.1.4 $SO_2+N_2$

The experimental database for the binary system $SO_2+N_2$ is much more limited than for the previously discussed system $SO_2+CO_2$, but still considered sufficient to fit all four parameters of the binary reducing functions. The only data set providing information about both phases in equilibrium was published by El Ahmar et al. [130], who measured 49 VLE points along four isotherms. The data were determined with an analytical measurement technique, where the compositions of the coexisting phases at given conditions of temperature and pressure are analyzed in a gas

chromatograph. The data are shown in Fig. 17 together with the phase boundaries calculated from the new mixture model.

The *p,x* diagrams show that the model is in good agreement with the experimental data, especially along the $SO_2$-rich bubble curve. Along the dew curve, the data exhibit an increasing offset with increasing pressure and $N_2$ content. This is plausible with regard to the shape of the phase boundaries calculated from the new mixture model. Based on the underlying extended corresponding states principle, the model predicts a miscibility gap for the two lower temperatures investigated by El Ahmar et al. [130] but at pressures higher than measured (see Fig. 17 left). The phase boundaries do not match the trend of the dew-point data at pressures above 10 MPa. With increasing temperature, the calculated demixing curves that limit the high-pressure miscibility gap get closer and closer to each other until a closed VLE region is predicted (see Fig. 17 right). For a better overview, a three-dimensional *p,T, x* surface of the mixture is shown in Fig. 18.

The existence of a second high-pressure two-phase region was already reported by Tsiklis [132] in 1947. However, the publication does not provide experimental data, but *p,x* diagrams which qualitatively confirm the shape of the calculated phase boundaries.

The predicted mixing behavior seems only partly compatible with the representation of the experimental data of El Ahmar et al. [130], since even intensive fitting of these data did not reduce the deviations from the model significantly. By fitting all four adjustable parameters of the reducing functions, the mathematical flexibility of the model should be sufficient to allow for accurate calculations. The publication of El Ahmar et al. [130] does not provide combined experimental uncertainties of the VLE data, but individual uncertainties in temperature (0.1 K), pressure (0.4 kPa), and mole fraction (3.2%). Since the uncertainty in composition is not further specified, it is not clear whether this is the relative uncertainty (100 $\Delta x/x$) or the difference in mol % (100 $\Delta x$). Interpreting the value as a relative uncertainty of one component and conducting a propagation of uncertainties leads to a maximum combined expanded ($k$=2) uncertainty in both bubble- and dew-point compositions of

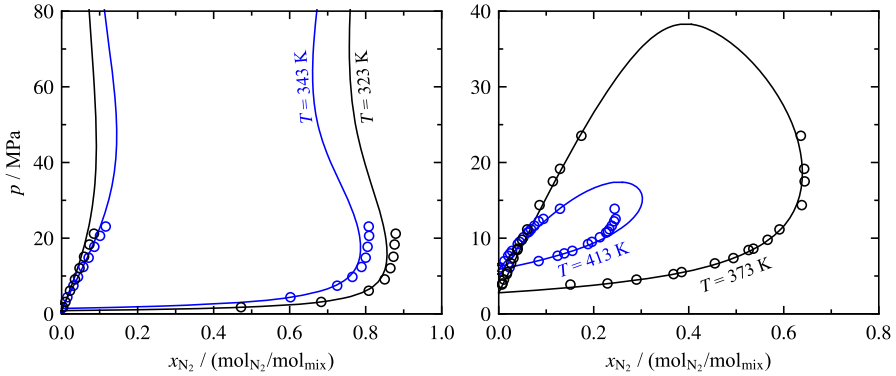


**Fig. 17** *p,x* diagrams showing the experimental phase equilibrium data of El Ahmar et al. [130] at 323 K, 343 K, 373 K, and 413 K in comparison to phase boundaries calculated with the EOS of this work for the system $SO_2+N_2$

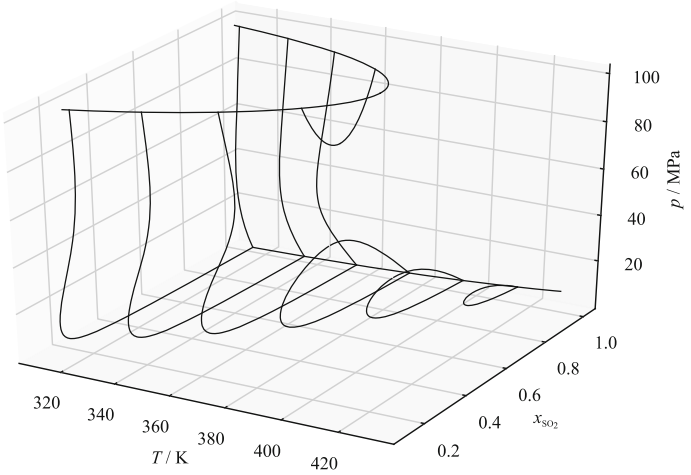


**Fig. 18** *p,T,x* diagram showing the phase boundary of the system $SO_2+N_2$ calculated with the EOS of this work. The *p,x* projections of the *p,T,x* surface were calculated at 315 K, 335 K, 355 K, 375 K, 395 K, and 415 K. The plot was calculated with the algorithm presented by Bell and Deiters [131]

0.0065 $mol_{SO_2}/mol_{mix}$. As evident in Fig. 19, this uncertainty does not match the deviations between the data and calculated results from the present mixture model. The deviation plots show absolute deviations in composition given in mol% as a function of temperature and composition ($x_{N_2}$).

The bubble-point data are represented with a maximum deviation of 0.02 $mol_{SO_2}/mol_{mix}$. The deviations between calculated dew points and the experimental data are mostly within 0.015 $mol_{N_2}/mol_{mix}$ for $N_2$ contents lower than in the retrograde regions of the phase boundaries. At higher mole fractions of $N_2$, the deviations increase up to 0.055 $mol_{SO_2}/mol_{mix}$. The best agreement between the data and the model was reached at 373 K, where the model predicts a closed phase boundary that matches the trend of the data (see right panel of Fig. 17). At 413 K, the data and the new model qualitatively agree on the shape of the VLE region, but the model predicts the two-phase region up to higher nitrogen contents. No reliable comparative data are available to validate this deviation. Dean and Walls [133] and Dornte and Ferguson [134] also measured a few VLE points, but both groups did not state any uncertainties and their data exhibit extremely large deviations from both the model and the data of El Ahmar et al. [130]. Both data sets were consequently not used for fitting, and it cannot be clarified whether the experimental uncertainties of El Ahmar's data are underestimated or not. Considering the discussed deviations of these data, the uncertainty of calculated phase-equilibrium compositions between 320 K and 415 K is conservatively estimated to be within 0.02 $mol_{SO_2}/mol_{mix}$ for bubble points and 0.05 $mol_{SO_2}/mol_{mix}$ for dew points.

No experimental densities are available in the literature; however, the discussed publication by El Ahmar et al. [130] includes molecular-simulation data obtained from Monte Carlo calculations. The data supplement the experimental VLE data with

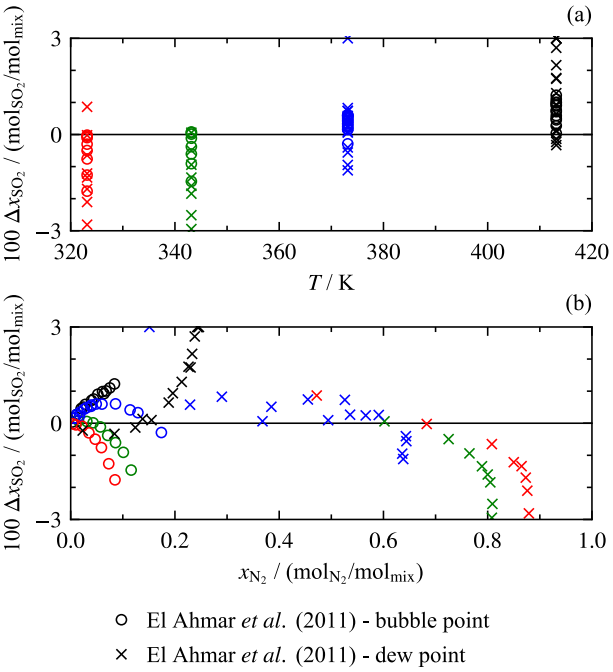


**Fig. 19** Absolute deviations $\Delta x_{SO_2} = (x_{SO_2,data} - x_{SO_2,EOS})$ between experimental phase equilibrium data and values calculated with the EOS of this work as a function of temperature (a) and $N_2$ content (b) for the system $SO_2 + N_2$

additional saturation densities. Köster and Vrabec [135] contributed to the development of the present mixture model with additional simulated homogeneous densities (gas and liquid-phase) over a wide composition range. Deviations of both data sets from the EOS are shown in Fig. 20.

The homogeneous density data obtained by Köster and Vrabec [135] are represented within a maximum deviation of approximately 6%. The approach of their molecular-simulations is based on a force field that describes the interactions between the molecules in the fluid. The effects of the like and unlike molecular interactions need to be separated. The like interactions were modeled with pure-substance force fields. For the unlike interactions, at least one experimental data point for a binary mixture must be used to obtain a binary interaction parameter. For this mixture, Köster and Vrabec [135] could use only the VLE data of El Ahmar et al. [130] for this purpose; resulting in reasonable deviations of up to 6%. For nitrogen concentrations higher than 0.5 $mol_{N_2}/mol_{mix}$, the data are mostly represented within 2.5%, whereas higher deviations occur with increasing $SO_2$ content. Because the pure-fluid EOS for $SO_2$ of Gao et al. [78], whose influence increases with increasing $SO_2$ content, yields very reliable results for calculated densities (uncertainties within 0.1% in the liquid-phase and 0.25% in the vapor phase), these higher deviations indicate shortcomings in the molecular model for pure $SO_2$. The saturated-vapor densities simulated by El Ahmar et al. [130] mostly deviate within 5% from our

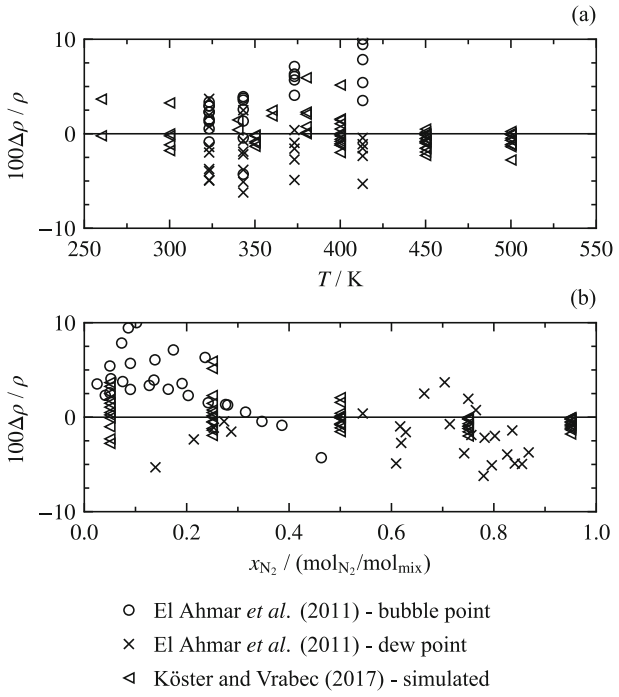


**Fig. 20** Relative deviations $\Delta\rho/\rho=(\rho_{data}-\rho_{EOS})/\rho_{data}$ between simulated density data and values calculated with the EOS of this work as a function of temperature (a) and $N_2$ content (b) for the system $SO_2+N_2$. The molecular-simulation data of El Ahmar et al. [130] describe phase equilibria, whereas Köster and Vrabec [135] simulated homogeneous density data in the gas and liquid-phase

mixture model, whereas the saturated-liquid points exhibit higher deviations of up to 10%. Since the mixture model was essentially fitted to the VLE data from the same group, the density data and the VLE data appear to be somewhat inconsistent. Neither the simulated data of Köster and Vrabec [135] nor of El Ahmar et al. [130] are accurate enough to sufficiently model the densities calculated from the binary model.

### 3.1.5 $SO_2+O_2$

The database for the binary system $SO_2+O_2$ corresponds to the previously discussed system $SO_2+N_2$; experimental VLE data and simulated homogeneous densities were published by El Ahmar et al. [130]. All four reducing parameters were adjusted to those data. The experimental apparatus used by El Ahmar et al. [130] to measure the VLE data was the same as for $SO_2+N_2$. The 27 points along the four investigated isotherms are shown in Fig. 21 together with the phase boundaries calculated from the binary mixture model.

The mixture model predicts a high-pressure miscibility gap for $SO_2+N_2$, whose composition range decreases with increasing temperature. At 413 K, the highest investigated temperature, the phase boundaries are closed as confirmed by the

experimental data. The deviations between experimental and calculated data with respect to composition are comparable to the previously discussed results for $SO_2+N_2$ and are presented in Fig. 22.

Except for two dew points in the critical region at 413 K, the model represents all the data within 0.03 $mol_{SO_2}/mol_{mix}$, which represents the estimated uncertainty of calculated VLE compositions between 320 K and 415 K. The combined expanded ($k=2$) uncertainties of the data were calculated considering the individual uncertainties in temperature, pressure, and composition as already discussed for $SO_2+N_2$ (see Sec. 3.1.4). As with $SO_2+N_2$, the experimental uncertainties for $SO_2+O_2$ do not match the deviations shown in Fig. 22. The calculated maximum uncertainty is 0.0063 $mol_{SO_2}/mol_{mix}$. No comparative data are available to clarify whether the experimental uncertainties are underestimated or whether the EOS needs to be improved.

The available database for densities is limited to the simulations of El Ahmar et al. [130] that provide densities of the saturated-liquid and vapor. Deviations of these data from the new model are shown in Fig. 23.

Compared to Fig. 20, the deviations for $SO_2+O_2$ data are slightly higher, especially for the dew-point densities that deviate by up to 16%. The mixture model should be much more accurate than these deviations indicate, especially with saturated-liquid densities at low temperatures, where the mixture is rich in $SO_2$ (which benefit from the high accuracy for liquid densities of pure $SO_2$ enabled by the EOS of Gao et al. [78]).

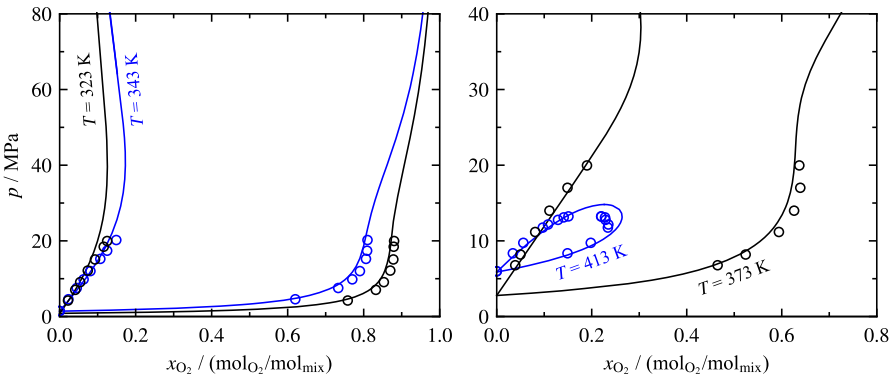


**Fig. 21** *p,x* diagrams showing the experimental phase equilibrium data of El Ahmar et al. [130] at 323 K, 343 K, 373 K, and 413 K in comparison to phase boundaries calculated with the EOS of this work for the system $SO_2+O_2$

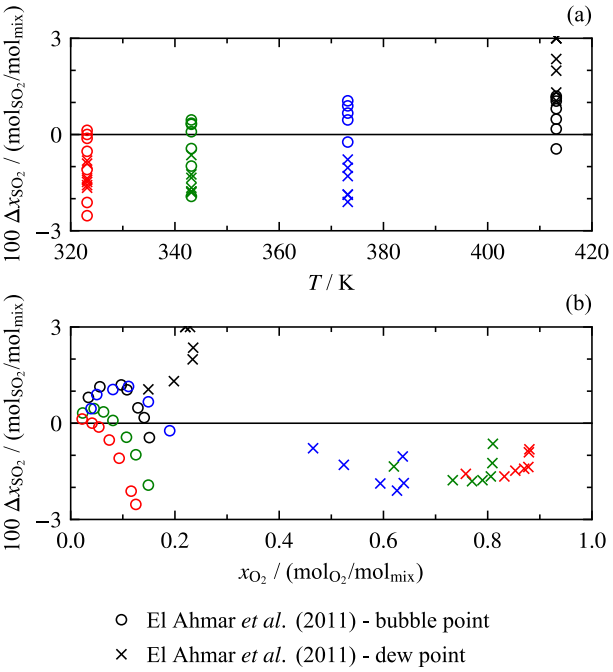


**Fig. 22** Absolute deviations $\Delta x_{SO_2} = (x_{SO_2,data} - x_{SO_2,EOS})$ between experimental phase equilibrium data [130] and values calculated with the EOS of this work as a function of temperature (a) and $O_2$ content (b) for the system $SO_2 + O_2$

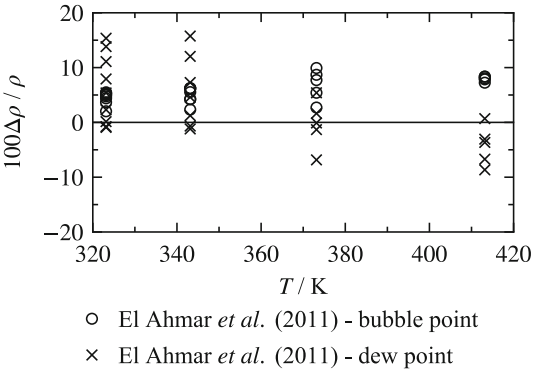


**Fig. 23** Relative deviations $\Delta\rho/\rho = (\rho_{data} - \rho_{EOS})/\rho_{data}$ between simulated saturated-liquid and saturated-vapor density data [130] and values calculated with the EOS of this work as a function of temperature for the system $SO_2 + O_2$

### 3.1.6 $SO_2 + CH_4$

Aside from $SO_2$+MEA and $SO_2$+DEA (see Sec. 3.1.9), the experimental database for the binary system $SO_2 + CH_4$ is surprisingly the most limited of the mixtures with $SO_2$ considered in this work. Only two publications with VLE data were found. These data sets by Dean and Walls [133] and Sayegh et al. [136] include a total of five points. Even with these limited data, all four parameters of the binary reducing

functions were required due to their mathematical flexibility to obtain the correct physical behavior along the phase boundaries.

Dean and Walls [133] investigated the solubility of $CH_4$ in $SO_2$ at two different temperatures (241 K and 302 K) with an analytical measuring technique. Their data are shown in Fig. 24 together with the data of Sayegh et al. [136] that are limited to a single VLE measurement at 318 K.

The *p,x* diagrams shown in Fig. 24 and the deviation plot presented in Fig. 25 emphasize how well the mixture model represents both experimental works. The available dew and bubble points differ within 0.015 $mol_{SO_2}/mol_{mix}$ and 0.005 $mol_{SO_2}/mol_{mix}$, respectively. When fitting a model to so few data points, achieving small deviations is usually not challenging; thus, the experimental uncertainty of the data are much more meaningful than their deviations. However, no information about experimental uncertainties is given in the publication of Dean and Walls [133] except for several vague statements about the purity of the pure components. The authors expect the $CH_4$ to be contaminated by approximately 0.5 vol% of $C_2H_6$ and state that the purity of the $SO_2$ sample was 99.6 vol%. Sayegh et al. [136] do not provide uncertainties in their measurements. Due to this lack of information and the very limited number of points for each investigated isotherm, the uncertainty in calculated VLE states from the model cannot be assessed.

Fitting the model to such a small number of experimental data points is also challenging due to the limited range of states that they cover (see Fig. 24); the accuracy of calculated values outside the range of data depends on the extrapolation behavior of the extended corresponding states principle. This aspect is especially relevant for the two isotherms investigated by Dean and Walls [133]. At a temperature of 241 K, the extrapolation behavior of the model predicts open phase boundaries at elevated pressures, whereas a closed VLE region is predicted for 302 K. This special mixing behavior was already discussed in detail for $SO_2+N_2$ (see Fig. 18) and for $SO_2+O_2$. The fitting process for $SO_2+CH_4$ showed that the

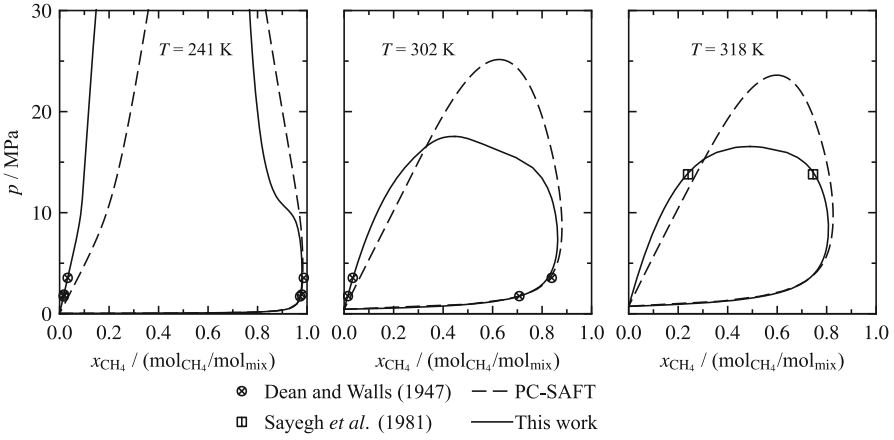


**Fig. 24** *p,x* diagrams showing selected experimental phase equilibrium data [133, 136] at 241 K, 302 K, and 318 K in comparison to phase boundaries calculated with the EOS of this work and PC-SAFT [137] for the system $SO_2+CH_4$

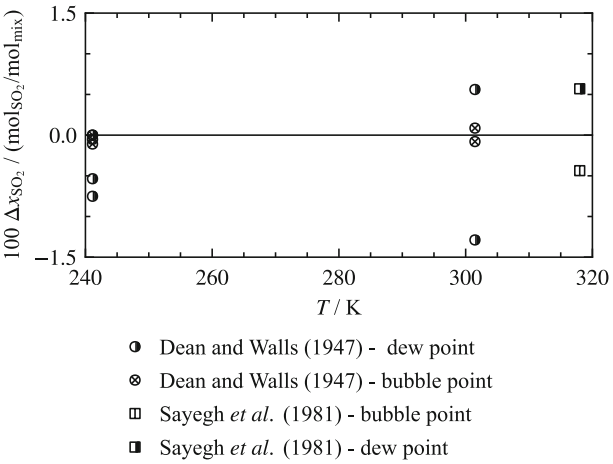


**Fig. 25** Absolute deviations $\Delta x_{SO_2} = (x_{SO_2,data} - x_{SO_2,EOS})$ between experimental phase equilibrium data [133, 136] and values calculated with the EOS of this work as a function of temperature for the system $SO_2 + CH_4$

shape of the phase boundaries calculated from the model was extremely sensitive to minor changes in the reducing parameters. Depending on the values of the parameters, the phase boundaries at 241 K and 301 K changed from a closed to an open form. In order to validate the phase-equilibrium behavior, comparisons with the more predictive PC-SAFT model of Gross and Sadowski [137] were carried out. It qualitatively confirms the shape of the phase boundaries, but yields significantly higher critical pressures at 302 K and 318 K; however, the predictive potential of the model is limited for this mixture because no binary interaction parameter was found for this fluid combination. Nevertheless, since the PC-SAFT model [137] considers the molecular structure of the mixture components and is thus to a certain degree physically based (though still empirical), the phase-equilibrium behavior predicted by this model was taken into account while constraining the mixture model of this work. However, the present model was not fitted to calculated values from PC-SAFT [137]; thus, new experimental data are crucial to further validate and improve the present model for $SO_2 + CH_4$.

### 3.1.7 $SO_2 + Cl_2$

For the binary mixture model for $SO_2 + Cl_2$, all four reducing parameters were fitted to the available experimental database, which consists of only two datasets. Both publications report VLE data, which are the most essential data for fitting mixture correlations. The data of Wilson and Wilding [138] cover the three isotherms 243 K, 273 K, and 323 K and the measurements of Gilot et al. [139] were carried out along four isobars 53 kPa, 67 kPa, 80 kPa, and 101.325 kPa. The isothermal data of Wilson and Wilding [138] are plotted in *p,x* diagrams shown in Fig. 26. The results of Gilot et al. [139] are depicted in *T,x* diagrams in Fig. 27. Both figures additionally include phase boundaries calculated from the mixture model.

The data indicate azeotropic mixing behavior, which is expected for two components with similar critical parameters ($T_{c,SO_2}$=430.64 K, $\rho_{c,SO_2}$= 8.078 mol·dm$^{-3}$, $p_{c,SO_2}$=7.887 MPa; $T_{c,Cl_2}$=416.865 K, $\rho_{c,Cl_2}$=8.06 mol·dm$^{-3}$, $p_{c,Cl_2}$=7.642 MPa), and for which one compound is dipolar and quadrupolar ($SO_2$) and the other ($Cl_2$) is only quadrupolar. It is remarkable that the extended corresponding states principle describes such complex mixing behavior with fitting only the reducing parameters but no binary-specific departure function. The model is in excellent agreement with the experimental data. Extrapolated to temperatures higher than experimentally investigated, it predicts the split of the azeotropic phase boundaries into two separated VLE regions, which is reported in the literature for mixtures with similar physical behavior such as $CO_2+C_2H_6$ (see for instance the experimental study of Ohgaki and Katayama [140]).

Both publications are quite limited regarding information about experimental uncertainties. Gilot et al. [139] do not provide any uncertainties but explain that the dew points at pressures lower than ambient pressure were measured through the use of a hygrometer. The dew- and bubble-point measurements at ambient pressure (101.325 kPa) were conducted with an ebulliometer. The vaguely described analysis of the phase compositions was done with chemical analysis and gas chromatography. Wilson and Wilding [138] state uncertainties in temperature (0.112 K) and pressure (0.67 kPa at $p \leq 150$ kPa, 1 kPa at $150 < p/\text{kPa} \leq 400$ kPa, and 0.25% at $p > 400$ kPa) but provide no uncertainties in the compositions of the coexisting phases. In the description of the experimental procedure, the authors explain that they filled the measuring cell with a known amount of the first component (most likely $SO_2$) and measured its vapor pressure. Increments of the second component were then added,

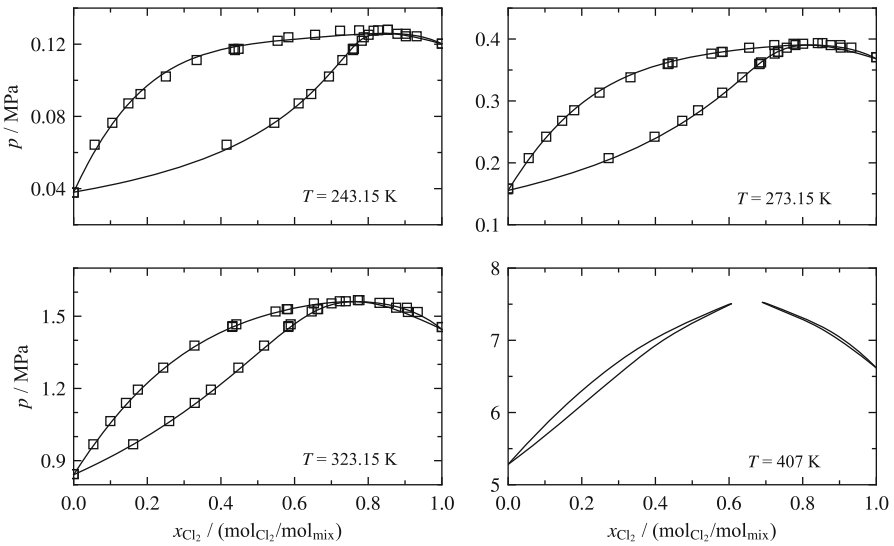


**Fig. 26** *p,x* diagrams showing the experimental phase equilibrium data of Wilson and Wilding [138] at 243.15 K, 273.15 K, 323 K, and 407 K in comparison to phase boundaries calculated with the EOS of this work for the system $SO_2+Cl_2$

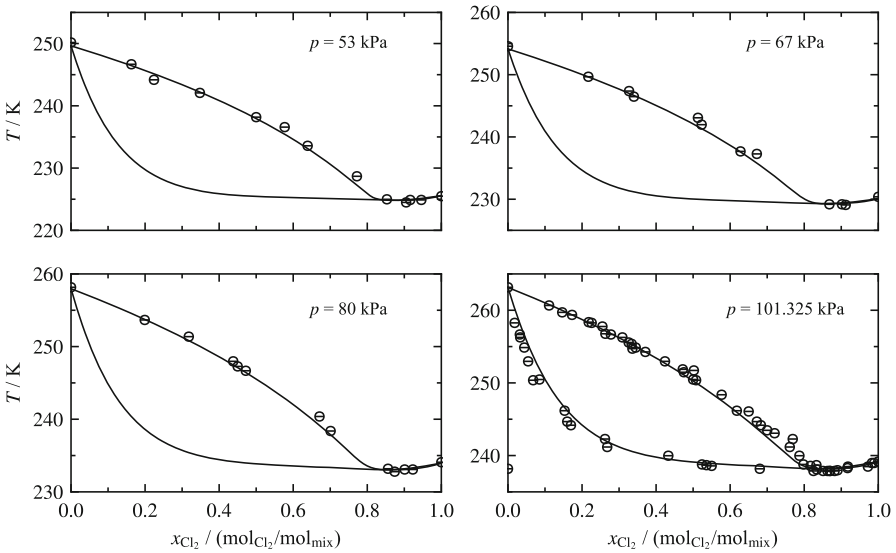


**Fig. 27** *T,x* diagrams showing the experimental phase equilibrium data of Gilot et al. [139] at 53 kPa, 67 kPa, 80 kPa, and 101.325 kPa in comparison to phase boundaries calculated with the EOS of this work for the system $SO_2+Cl_2$

the mixture was homogenized, and the pressure of the equilibrium state was measured. The measurements at saturation pressures below 150 kPa (at 243 K) were performed in a glass cell with a magnetic stirrer. The pressure was measured with a mercury manometer. The measurements at higher pressures were conducted in a stainless-steel cell whose content had to be stirred manually to ensure homogeneous mixing. In this set-up, saturation pressures were measured with pressure gauges that were calibrated with a dead-weight piston gauge. Both experimental procedures seem to be subject to quite large uncertainties in composition, as the manual stirring procedure probably did not ensure proper mixing of the two components during the measurements at high pressures. In addition, a degassing process was used after filling the cell with both components. If the sample was not carefully homogenized, this could have led to a loss of the more volatile component and consequently to a shift in composition. Because Wilson and Wilding [138] measured saturation pressures, deviations between their data and the mixture model were calculated with respect to pressure at given $T_{sat}$ and given composition; the data are shown in Fig. 28 together with isobaric results of Gilot et al. [139].

The majority of the isothermal data of Wilson and Wilding [138] are represented within deviations of 2.5% in pressure. Calculations generally agree with the data of Gilot et al. [139] to within 5%. As explained above, the experiments were conducted along isotherms with the temperature as the measured property. For that work, deviations in temperature are more meaningful (see Fig. 29).

The data of Gilot et al. [139] generally have deviations within 0.75% ($\Delta T<$ 1.95 K) in temperature with a distinct scatter of the data. The data of Wilson and Wilding [138] are almost completely represented within 0.25% ($\Delta T<0.8$ K), which emphasizes that this work is more reliable.

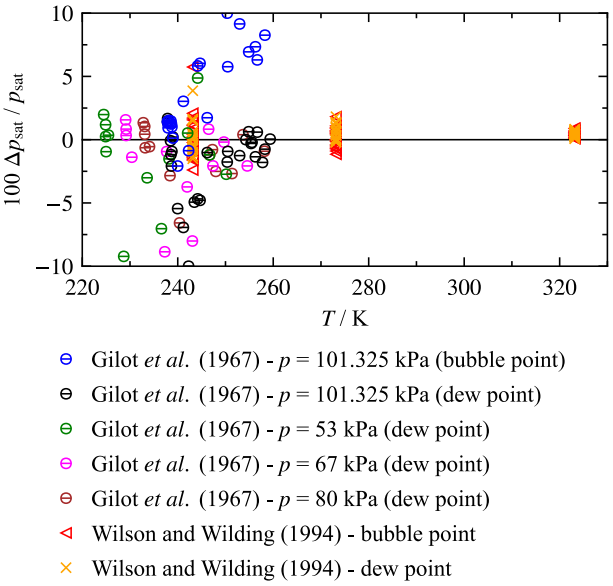


**Fig. 28** Relative deviations $\Delta p_{sat}=(p_{sat,data}-p_{sat,EOS})/p_{sat,data}$ between experimental phase equilibrium data [138, 139] and values calculated with the EOS of this work as a function of temperature for the system $SO_2+Cl_2$

Deviations between the experimentally investigated mixture compositions and calculated phase-equilibrium compositions at given temperature and pressure are presented in Fig. 30.

Since neither of the experimental works provided combined experimental uncertainties, the uncertainties in the model of calculated VLE states is difficult to ascertain. Wilson and Wilding [138] only state uncertainties of their temperature and pressure measurements. Considering these uncertainties and ignoring the potentially large additional uncertainty in the composition measurement, expanded combined uncertainties were calculated following the law of uncertainty propagation. Because the sensitivity of the composition with respect to temperature and pressure changes significantly along the phase boundary, the calculated uncertainties vary depending on the location of the VLE points. The average of the experimental uncertainties in bubble and dew points is about 0.012 $mol_{SO_2}/mol_{mix}$ and 0.007 $mol_{SO_2}/mol_{mix}$, respectively. Considering an unknown additional uncertainty in composition and the deviations plotted in Fig. 30, the conservatively estimated uncertainty of VLE data calculated from the EOS with respect to composition is 0.02 $mol_{SO_2}/mol_{mix}$ between 240 K and 325 K. At lower temperatures, between 225 K and 240 K, the uncertainty increases to 0.05 $mol_{SO_2}/mol_{mix}$ as estimated based on comparisons with the data of Gilot et al. [139].

Based on the deviations in saturation states, the uncertainty in saturation temperature is estimated to be 0.75% ($\Delta T$<2.4 K) at pressures up to 1.6 MPa and temperatures between 225 K and 325 K; saturation pressures in the same temperature range are expected to have a maximum uncertainty of 5%.

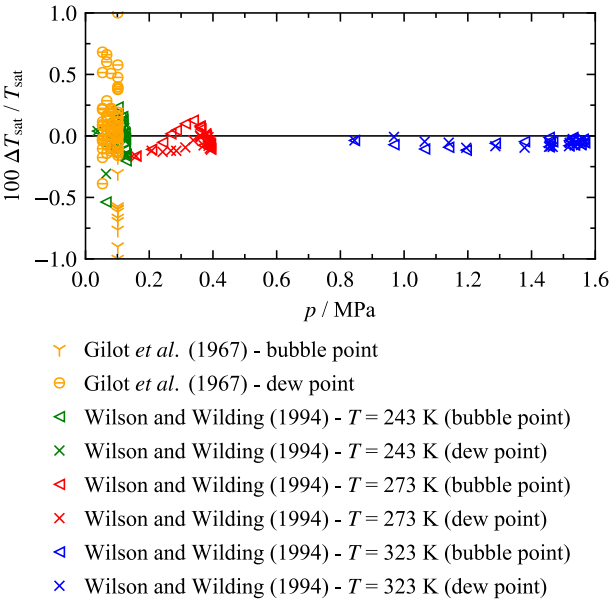


**Fig. 29** Relative deviations $\Delta T_{sat}=(T_{sat,data}-T_{sat,EOS})/T_{sat,data}$ between experimental phase equilibrium data [138, 139] and values calculated with the EOS of this work as a function of pressure for the system $SO_2+Cl_2$

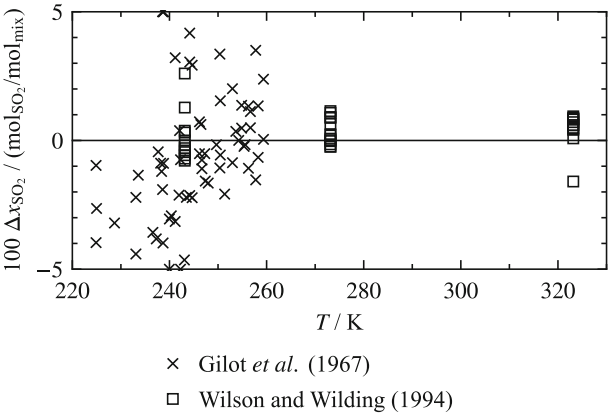


**Fig. 30** Absolute deviations $\Delta x_{SO_2} = (x_{SO_2,data} - x_{SO_2,EOS})$ between experimental phase equilibrium data [138] and values calculated with the EOS of this work as a function of temperature for the system $SO_2+Cl_2$

### 3.1.8 $SO_2 + HCl$

Fitting the parameters $\beta_T$ and $\gamma_T$ of the temperature-reducing function was sufficient to represent the available data for the system $SO_2+HCl$. For the density-reducing function, the quadratic combining rule of Lorentz-Berthelot was applied by setting $\beta_v$

and $\gamma_v$ to unity. The experimental database is limited to the VLE measurements of Wilson and Wilding [138] that were already discussed in Sect. 3.1.7. For this system, properties along two isotherms were measured, 203 K and 273 K. These data were supplemented with new molecular-simulation data of Köster and Vrabec [135], which include both VLE states and homogeneous densities. Köster and Vrabec [135] used the experimental data of Wilson and Wilding [138] to adjust the binary mixing parameter that accounts for interactions between unlike molecules. The molecular-simulation data are thus an extension of the experimental data and should not be considered an independent source of information. The experimental and simulated VLE data are shown in Fig. 31 together with the phase boundaries calculated from the mixture model.

The fitting process placed more emphasis on representing the experimental data at 203 K and 273 K. The fit was carefully extended to higher temperatures by additionally fitting the molecular-simulation data. At a temperature of 273 K, the simulated values can be validated with the experimental data. The *p,x* diagram given in Fig. 31 demonstrates the close agreement between both data sets, except for a section of the dew curve between about 0.65 $mol_{HCl}/mol_{mix}$ and 0.9 $mol_{HCl}/mol_{mix}$. The mixture model accurately describes the dew and bubble points over the whole temperature range. Deviations of the data from calculated values are shown in Fig. 32 (with respect to saturation pressure) and Fig. 33 (with respect to composition).

Figure 32 shows that the mixture model describes most of the experimental data of Wilson and Wilding [138] within 5%, except for a few (mostly bubble) points at

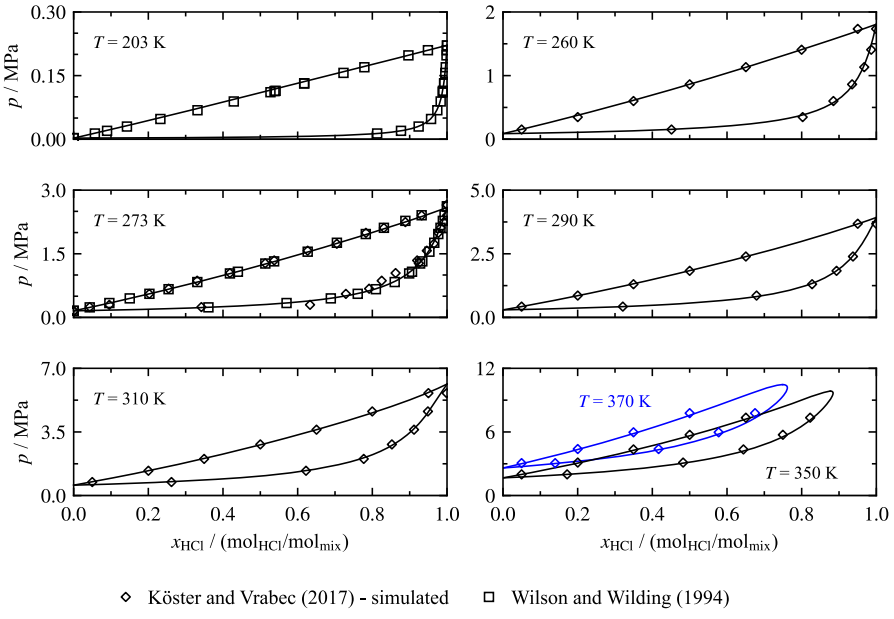


**Fig. 31** *p,x* diagrams showing selected experimental and simulated phase equilibrium data [135] at 203 K, 260 K, 273 K, 290 K, 310 K, 350 K, and 370 K in comparison to phase boundaries calculated with the EOS of this work for the system $SO_2+HCl$

203 K. The deviations of the molecular-simulation data of Köster and Vrabec [135] are of the same order of magnitude, which is expected, since they are partly based on the experimental data. Higher deviations occur along the dew curve at 273 K. Based on these deviations (with the exclusion of a few points with higher deviations) the estimated uncertainty of calculated saturation pressures between 200 K and 370 K is 5%.

The deviations in compositions are lower than for saturation pressures. As illustrated in Fig. 33, most of the data are represented within 0.03 $mol_{SO_2}/mol_{mix}$. The maximum of the calculated combined uncertainty of the experimental data of Wilson and Wilding [138] is 0.013 $mol_{SO_2}/mol_{mix}$. This value considers the given experimental uncertainties in temperature and pressure (see Sec. 3.1.7) but no uncertainty in composition. Consequently, a reproduction within 0.03 $mol_{SO_2}/mol_{mix}$ is considered to be reasonable. The estimated uncertainty of calculated phase-equilibrium compositions between 200 K and 370 K is 0.03 $mol_{SO_2}/mol_{mix}$. Deviations higher than this uncertainty estimate occur for the simulated dew points at 273 K, where the model was fitted to the experimental data that exhibit a slight offset from the simulated values.

No experimental data for homogeneous densities are available in the literature, but Köster and Vrabec [135] simulated liquid and gas-phase data over wide ranges in temperature, pressure, and composition. Deviations of these data from calculated values are shown in Fig. 34.

Except for a few points, the mixture model describes the data with deviations less than 3%. Consequently, this is a reasonable estimate for calculated homogeneous densities at temperatures between 200 K and 650 K, pressures up to 100 MPa, and HCl contents between 0.25 $mol_{HCl}/mol_{mix} \leq x_{HCl} < 0.75$ $mol_{HCl}/mol_{mix}$. The quality of the model for $SO_2+HCl$ was significantly improved by the molecular-simulation data.

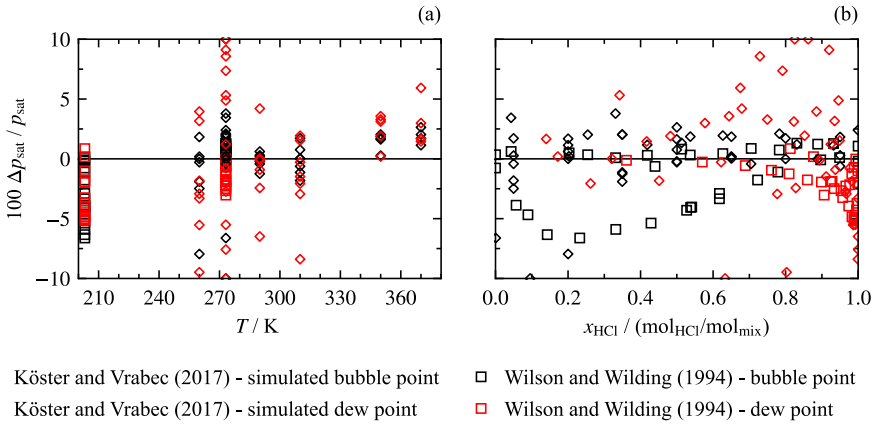


**Fig. 32** Relative deviations $\Delta p_{sat}=(p_{sat,data}-p_{sat,EOS})/p_{sat,data}$ between experimental and simulated phase equilibrium data [135, 138] and values calculated with the EOS of this work as a function of temperature (a) and composition (b) for the system $SO_2+HCl$

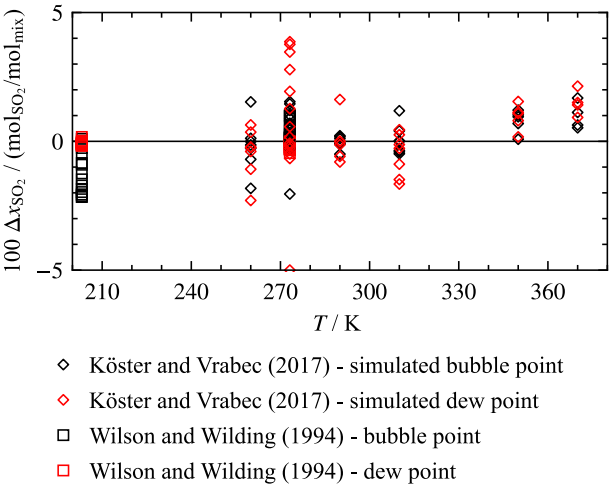


**Fig. 33** Absolute deviations $\Delta x_{SO_2} = (x_{SO_2,data} - x_{SO_2,EOS})$ between experimental and simulated phase equilibrium data [138, 141] and values calculated with the EOS of this work as a function of temperature for the system $SO_2 + HCl$

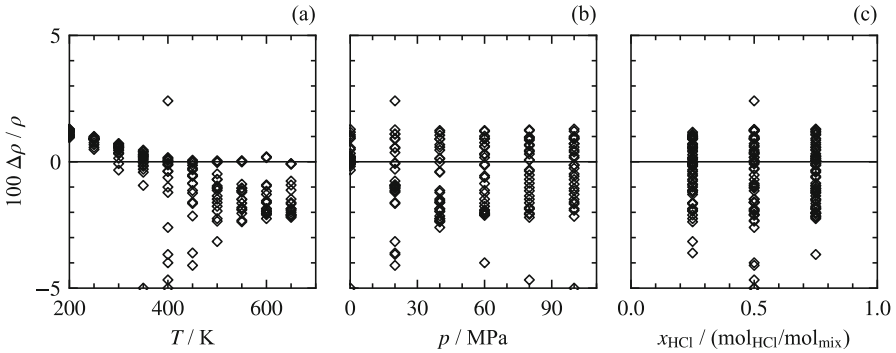


**Fig. 34** Relative deviations $\Delta\rho/\rho=(\rho_{data}-\rho_{EOS})/\rho_{data}$ between simulated density data of Köster and Vrabec [135] and values calculated with the EOS of this work as a function of temperature (a), pressure (b), and composition (c) for the system $SO_2 + HCl$

### 3.1.9 $SO_2$ + DEA and $SO_2$ + MEA

For the system $SO_2 + DEA$, the two parameters $\beta_T$ and $\gamma_T$ in the temperature-reducing function were fitted to limited experimental data. The parameters of the density-reducing function $\beta_v$ and $\gamma_v$ were not adjusted but set to unity. This set of parameters was adopted for the system $SO_2 + MEA$ for which experimental data are not available.

The only data set available for $SO_2 + DEA$ was published by Li et al. [142]. The study reports six bubble points at ambient pressure (0.101325 MPa). The compositions of the coexisting dew points are not given. The data of Li et al.

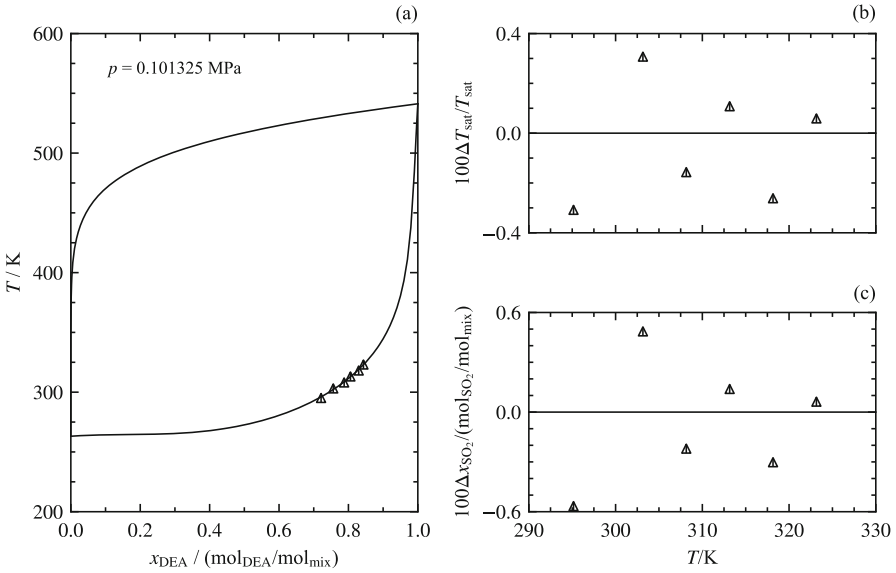


**Fig. 35** *T,x* diagram (a) showing the experimental phase equilibrium data of Li et al. [142] at 0.101 325 MPa in comparison to phase boundaries calculated with the EOS of this work for the system $SO_2$+HCl. Relative deviations $\Delta T_{sat}=(T_{sat,data}-T_{sat,EOS})/T_{sat,data}$ (b) and absolute deviations $\Delta x_{SO_2}=(x_{SO_2,data}-x_{SO_2,EOS})$ (c) between the phase equilibrium data of Li et al. [142] and values calculated with the EOS of this work as a function of temperature

[142] were obtained through a synthetic measurement technique in which bubble-point temperatures of prepared mixtures (with known compositions) are identified. The measured points are plotted in a *T,x* diagram shown in the left panel of Fig. 35. Deviations with respect to the saturation temperature and bubble-point composition between the data and values calculated from the mixture model are shown in the right panels, which show that the model accurately describes the data. All deviations with respect to temperature are within 0.4% ($0.2< \Delta T/K<1$); the deviations with respect to composition are within 0.006 $mol_{SO_2}/mol_{mix}$. Without additional measurements, a reliable uncertainty estimate for calculated VLE states cannot be made. Nevertheless, the comparisons presented here highlight that the model still adequately describes the phase boundaries.

Because experimental data for the binary system $SO_2$+MEA were not found in the literature, both the simple linear and quadratic combining rules were tested, which revealed considerable numerical problems. The fitting processes for the models for MEA+$H_2O$ and DEA+$H_2O$ suggested that parameter sets for one of these amines with another component are good starting points for fitting the other amine with the same second component. Since no further fitting of the parameters for $SO_2$+MEA was possible, the parameters for $SO_2$+DEA were adopted. The resulting model for $SO_2$+MEA cannot be quantitatively validated, but at least allows for numerically stable equilibrium calculations over a wide temperature range. Calculated *p,x* diagrams for selected isotherms are shown in Fig. 36.

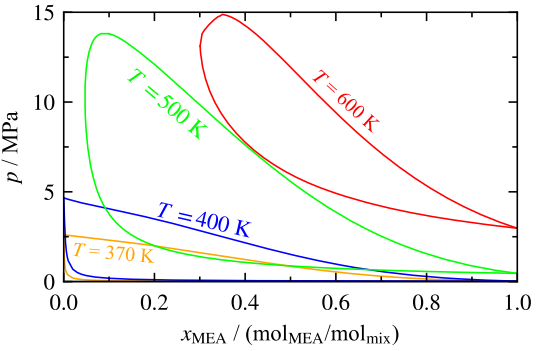


**Fig. 36** *p,x* diagrams showing selected phase boundaries at 370 K, 400 K, 500 K, and 600 K calculated with the EOS of this work for the system $SO_2$+MEA

### 3.1.10 $SO_2 + H_2O$

The binary system $SO_2$+$H_2O$ is one of the most complex mixtures considered in this work. Although the solubility of $SO_2$ in water is higher than that for many other gases, it is still limited. Phase equilibria mostly consist of one phase very rich in $SO_2$ and another phase very rich in $H_2O$. Below the critical temperature of $SO_2$ ($T_{c,SO_2}$ = 430.64 K) and above the normal melting point temperature of water, the $SO_2$-rich phase may undergo a phase transition from vapor to liquid with increasing pressure. As a result, the binary system splits into vapor–liquid-equilibrium or liquid–liquid-equilibrium (LLE) at higher pressures. The two equilibrium states are separated by a three-phase line along which a $SO_2$-rich vapor, a $H_2O$-rich liquid, and a $SO_2$-rich liquid are in equilibrium (VLLE). The complexity of the phase equilibria is further increased by the possible formation of solid phases at low temperatures. The formation of ice at temperatures below the normal melting point of water must be considered. $SO_2$ can also form a hydrate phase in water as reported in the work of van Berkum and Diepen [143]. Because Helmholtz-explicit mixture models as developed in this work are restricted to fluid phases, the binary model for $SO_2$+$H_2O$ does not allow the calculation of solid-phase properties. However, the algorithms implemented in the software package TREND [49] can predict the formation of ice and hydrates. The software also includes special equations for the calculation of solid phase properties, although $SO_2$-hydrates are currently not implemented in TREND [49]. For further information see Sect. 5.

The high solubility of $SO_2$ in water is increased by the formation of sulfurous acid ($H_2SO_3$), which is an intermediate species in the formation of sulfuric acid ($H_2SO_4$). So far, the functional form of the Helmholtz-explicit EOS is restricted to the description of the physical mixing behavior. It does not include special terms that account for chemical reactions. For specified mixtures, a new approach combining Helmholtz-explicit EOS with excess Gibbs energy models was developed by Neumann et al. [8] for this purpose (see Sect. 5). Although chemical reactions are not considered here mathematically, the effects are built into the mixing parameters from fitting experimental data (where the data already include the influence by chemical reactions). For $SO_2$+$H_2O$, the composition of the chemical equilibrium state is

clearly on the side of the educts; thus, only a small amount of sulfurous acid is formed [144].

Because the available experimental data for $SO_2+H_2O$ did not allow for the development of a binary-specific departure function, only the four parameters of the reducing functions were adjusted to the data. The validation of the binary model is therefore particularly interesting, since the mixing behavior is expected to deviate considerably from the corresponding states principle. A larger deviation from corresponding states usually requires a departure function to account for the non-ideal mixing effects.

Quantitatively, the system $SO_2+H_2O$ is the most experimentally investigated $SO_2$-system considered in this work. Many publications provide VLE data, two data sets for LLE, and two data sets with saturated-liquid densities are available. Unfortunately, none of the experimental studies of VLE states provide information for the coexisting phases; rather, only the $SO_2$ solubility in water is reported, which is equivalent to the composition of the saturated-liquid-phase. The uncertainties in most of the data are quite large, and it is not specified if the $SO_2$ concentration is given for the mixture or in pure water, which leads to different compositions of the saturated-liquid. Many publications present solubilities in terms of partial pressures of $SO_2$ without further specifications of the total pressure or composition. Only a subset of the available experimental data shown in this section; the data from many publications were omitted because they do not provide additional information that can be used to obtain the best fitted parameters.

Selected experimental solubility data are shown in Fig. 37. VLE and LLE phase boundaries calculated from the mixture model are plotted for comparisons. The pressures and compositions along the three-phase lines (VLLE) were calculated from the model with the three-phase-flash algorithms implemented in TREND [49]. No reliable literature data were found for these three-phase equilibria. The available LLE data are not shown because of their higher pressures. The complex mixing behavior of this system is evident in Fig. 37. For the four lowest isotherms ($T \leq 343$ K), the model predicts the characteristic wide composition range of the two-phase region with a transition from VLE to LLE at increasing pressures. Although only the shape of the VLE bubble line can be validated by comparisons with experimental results, the mixing behavior is qualitatively confirmed by the phase diagrams shown in the work of van Berkum and Diepen [143], who also provide experimental results that prove the existence of the LLE region and VLLE line. The two highest isotherms presented in Fig. 37 are above the critical temperature of pure $SO_2$ ($T_{c,SO_2} = 430.64$ K). For these isotherms, the model predicts only a VLE region; the model predicts extreme changes in slope and curvature of both phase boundaries in the critical region at 473 K. There is no experimental evidence for this behavior, but it is discussed in various publications on mixtures of $CO_2$ with alcohols, for example in the work of Hsieh et al. [145], who considered this behavior as a relic of the LLE at lower temperatures.

The mixture model is a compromise between accurately representing the available data at $T < T_{c,SO_2}$ and qualitatively mimicking the phase behavior at the higher temperatures. It was not possible to find a solution that could simultaneously describe

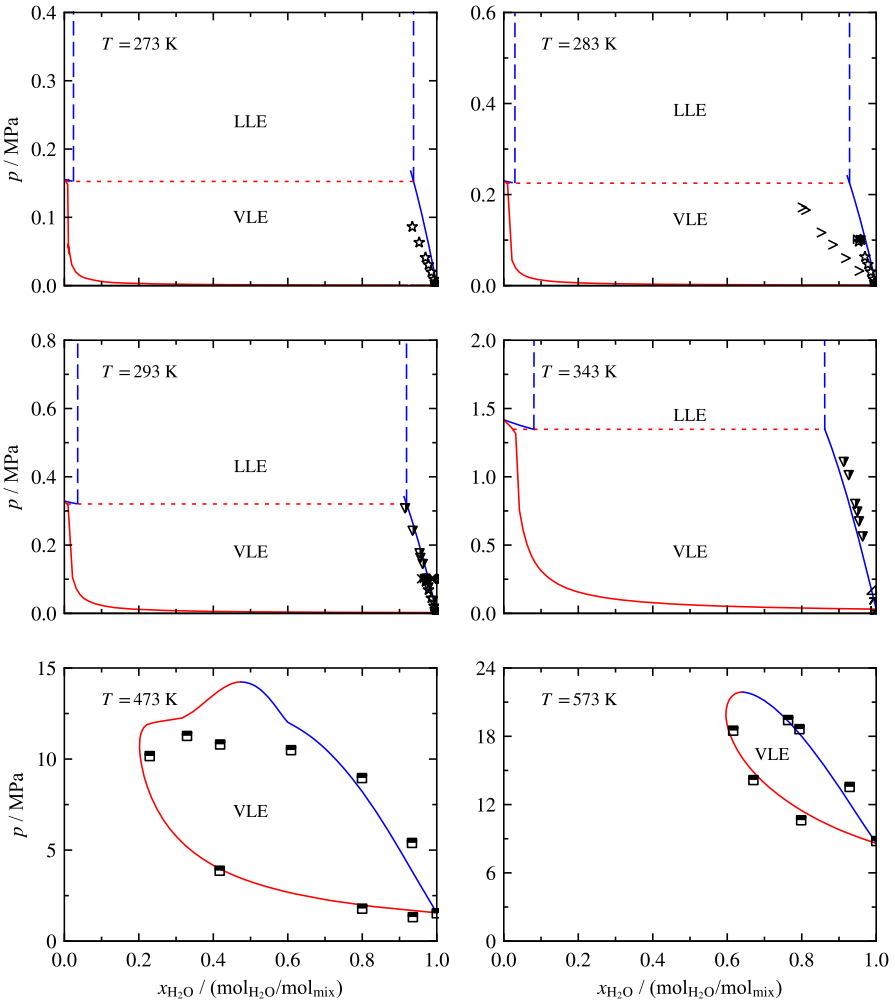


**Fig. 37** *p,x* diagrams showing selected experimental phase equilibrium data [146–158] at 273 K, 283 K, 293 K, 343 K, 473 K, and 573 K in comparison to phase boundaries calculated with the EOS of this work for the system $SO_2+H_2O$

the high-temperature data as well as the phase boundaries at low temperatures, as also discussed by Gernert and Span [5] for the similarly complex system $CO_2+H_2O$. The high-temperature data for $SO_2+H_2O$ by Spall [148] were graphically extracted

from low-quality phase diagrams shown in the publication, increasing the uncertainties for their data. At low temperatures, the most valuable datasets were measured by Sherwood [156] and Rumpf and Maurer [155]. At a temperature of 273 K (approximately the normal melting point of water), however, the data of Sherwood [156] indicate a higher $SO_2$ solubility than calculated from the model. Further fitting of the model led to larger deviations from the data of Rumpf and Maurer [155] and other references at higher temperature (see for example 293 K and 343 K).

Deviations between calculated phase-equilibrium compositions and selected experimental data are shown in Fig. 38. Most of the data at temperatures between 273 K and 393 K are represented with deviations below 0.03 $mol_{SO_2}/mol_{mix}$. At higher temperatures, the model deviates by up to 0.05 $mol_{SO_2}/mol_{mix}$ from the data of Spall [148]. None of the data sets presented in Fig. 38 were published with reliable information on the experimental uncertainties. The oldest works, published between 1862 and 1940, do not provide uncertainties at all, whereas some of the newer works state at least the uncertainties in saturation pressures; comparisons of these data are not discussed here and are in general not meaningful with respect to the mixing behavior shown in Fig. 37. The steep slope of the saturated-liquid curve leads to extremely large deviations in pressure when the calculated VLE composition

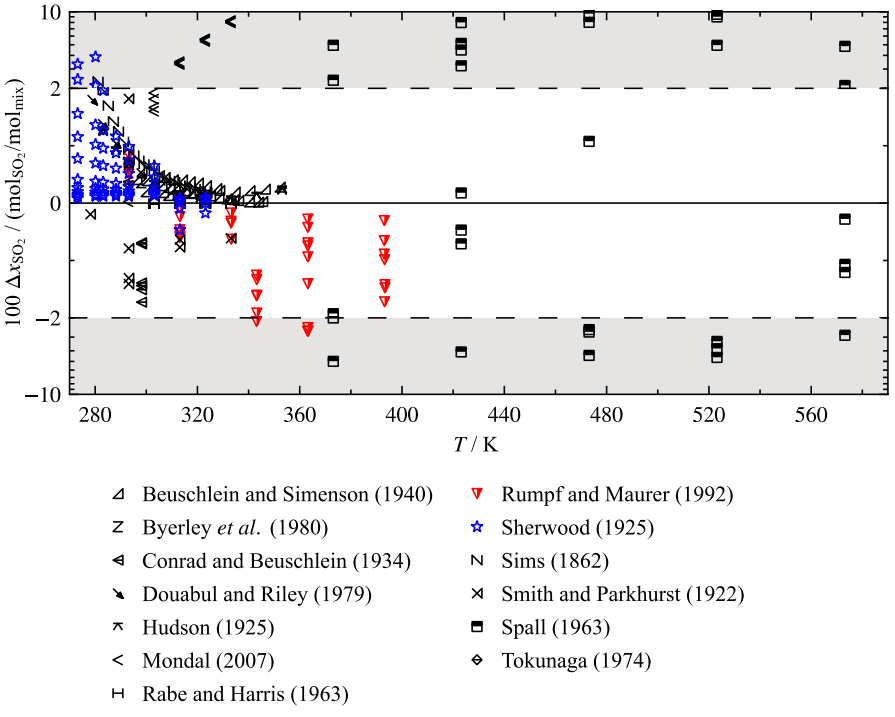


**Fig. 38** Absolute deviations $\Delta x_{SO_2} = (x_{SO_2,data} - x_{SO_2,EOS})$ between experimental phase equilibrium data [146–149, 151, 153–160] and values calculated with the EOS of this work as a function of temperature for the system $SO_2 + H_2O$

deviates slightly from the experimental result. The uncertainties of VLE compositions calculated from the mixture model are therefore based on the deviations shown above. The uncertainty in saturated-liquid compositions at temperatures from the normal-melting point of water to 390 K is 0.03 $mol_{SO_2}/mol_{mix}$. Between 390 K and 570 K, the uncertainty increases to 0.05 $mol_{SO_2}/mol_{mix}$. The uncertainty in calculated dew-point compositions cannot be estimated because of the lack of experimental data.

Densities of the saturated-liquid were measured by Campbell and Maass [152] and Beuschlein and Simenson [146]. The work of Beuschlein and Simenson [146] is limited to a single isotherm, 296 K, whereas the data of Campbell and Maass [152] cover temperatures from 293 K to 383 K. The compositions of the investigated solutions range from approximately 0.95 $mol_{H_2O}/mol_{mix}$ to almost 0.999 $mol_{H_2O}/mol_{mix}$. Deviations between the data and results obtained from the mixture model are plotted in Fig. 39.

The maximum deviation between the model and the data are 0.8%. Both publications do not provide information about the experimental uncertainties. Because the investigated samples are almost pure water, the uncertainty of saturated-liquid densities calculated from the reference EOS for water (IAPWS-95) by Wagner and Pruss [67] can be considered the lowest possible experimental uncertainty in the EOS. The maximum uncertainty stated by IAPWS [161] is 0.003%, which is far below the plotted deviations in Fig. 39. The deviations of up to 0.8% are likely not caused by inaccuracies of the dominating pure-fluid EOS for water; thus, we assume that the experimental uncertainty of the data are similar to the deviations. The uncertainty of calculated saturated-liquid densities between 295 K and 380 K is consequently estimated to be 1%.

The phase equilibria of $SO_2+H_2O$ were thoroughly investigated by van Berkum and Diepen [143]. Aside from different equilibria including hydrates, the authors also measured saturation pressures along a demixing curve at the given temperature and composition. The demixing curve is equivalent to the $H_2O$-rich saturated-liquid of the LLE. The data range from just above the normal melting point of water to 390 K at pressures up to 345 MPa. Because the data only provide information on one phase

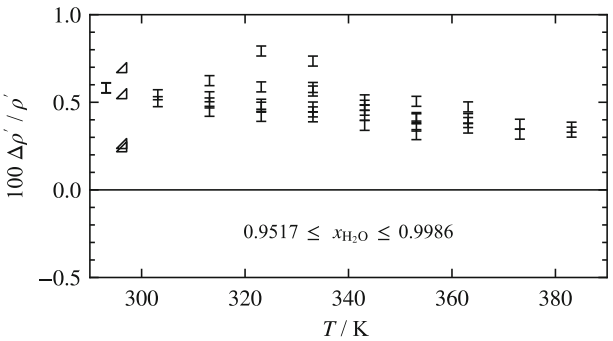


**Fig. 39** Relative deviations $\Delta\rho'/\rho' = (\rho'_{data} - \rho'_{EOS})/\rho'_{data}$ of experimental saturated-liquid density data [146, 152] and values calculated with the EOS of this work as a function of temperature for the system $SO_2+H_2O$

of the LLE, they could not be directly used in fitting. The non-linear fitting algorithm used in this work only allows fitting the model to complete LLE data sets. In order to enable, at least, a qualitatively correct representation of the LLE region, the missing phase composition was iteratively calculated from preliminary fits of the mixture model. These calculations were carried out with the phase-equilibrium algorithms implemented in TREND [49]. This stabilized the fit and improved the description of the-liquid-phase measured by van Berkum and Diepen [143]. The model represents the data with a maximum deviation of 0.05 $\mathrm{mol_{SO_2}/mol_{mix}}$, except for the saturated-liquid with the highest $SO_2$ content ($x_{H_2O}$=0.6147 $\mathrm{mol_{H_2O}/mol_{mix}}$). Deviations between the data of Berkum and Diepen [143] and values calculated from the mixture model are shown in Fig. 40. The additional dataset of Zhou et al. [162] (also only $H_2O$-rich saturated liquid-phase) became available after the model was completed and are only used for comparison here. The data exhibit an offset compared to those of van Berkum and Diepen [143] follow a different trend at higher temperatures ($T$>330 K).

The deviations indicate that the model reliably describes the $H_2O$-rich liquid in LLE. However, for a reliable statement on the uncertainty of the present equation, additional data including also the $SO_2$-rich saturation state are necessary.

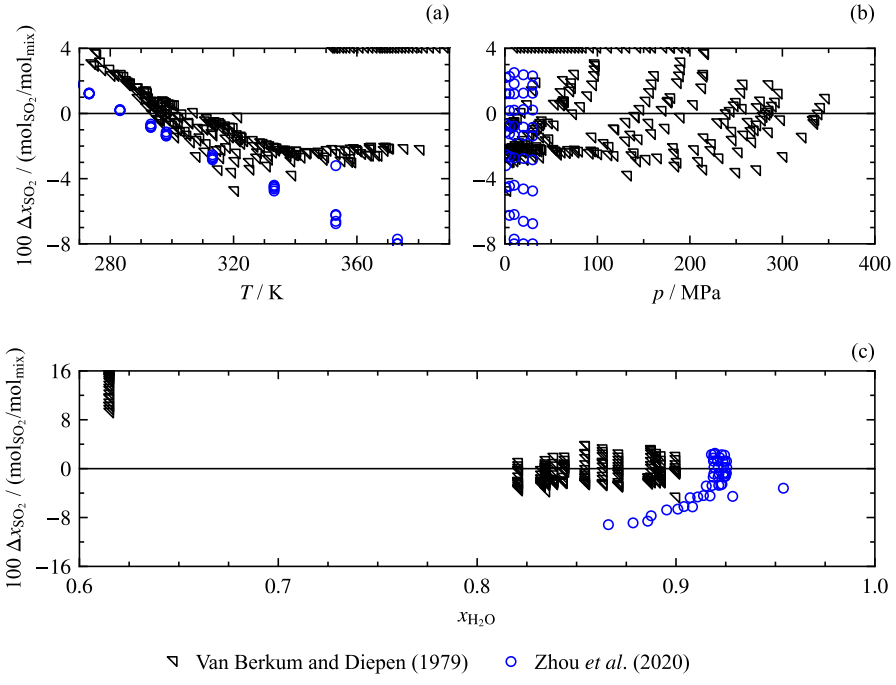


**Fig. 40** Absolute deviations $\Delta x_{SO_2} = (x_{SO_2,data} - x_{SO_2,EOS})$ between the experimental liquid–liquid-phase equilibrium data [143, 162] and values calculated with the EOS of this work as a function of temperature (a), pressure (b), and composition (c) for the system $SO_2$+$H_2O$

### 3.1.11 MEA + $H_2O$

Herrig [21] presented an EOS for the binary system MEA + $H_2O$ that did not contain a departure function, rather all four reducing parameters were adjusted to VLE data. The updated model in this work features a departure function, as presented in Table 5, to more accurately represent homogeneous density, speed of sound, and isobaric heat capacity data.

For VLE states, 11 datasets are available, which are comprehensive as compared to other mixtures containing amines. The temperature ranges from the melting point of MEA ($T_{melt}$=283.7 K) to approximately 470 K, with pressures up to 0.7 MPa. Different datasets show good consistency in the overlapping temperature and pressure regions. Only the bubble-point data of Wohland [163] exhibit significantly higher deviations with respect to the EOS. Most of the other datasets are represented within 0.05 $mol_{MEA}/mol_{mix}$ as shown in Fig. 41. There are more bubble-point than dew-point data available, also covering a wider composition range. If uncertainties are reported by the authors, they only comprise pressure, temperature, and composition measurements independently. As explained in detail in Herrig [21], the calculation of combined uncertainties ($k$=2) for many references leads to unreasonable low values.

The EOS was mainly fitted to the data of Kim et al. [166] covering a temperature range from 313 K to 374 K with an $AAD_x$ of 0.012 $mol_{MEA}/mol_{mix}$ and an $AAD_y$ of 0.0019 $mol_{MEA}/mol_{mix}$. According to Kim et al. [166], the experimental uncertainty in the composition measurement is between 2% and 4% because of the gas chromatographic analysis and the need to dilute some of the samples. The authors do not specify which substance was used for diluting. With the uncertainty of the pressure (0.3 kPa) and temperature (0.05 K) measurement, a combined expanded uncertainty ($k = 2$) was estimated in this work. The maximum uncertainties for the

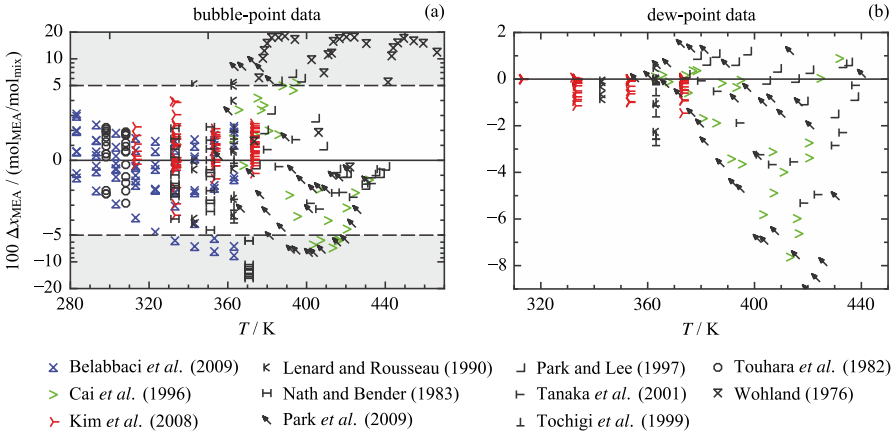


**Fig. 41** Absolute deviations in terms of composition $\Delta x_{MEA}=(x_{MEA,data}-x_{MEA,EOS})$ between bubble-point data (a) and dew-point data (b) [35, 163–171] and values calculated with the EOS of this work as a function of temperature for the binary system MEA + $H_2O$. The ordinate is linearly scaled between the dashed lines and logarithmically scaled in the gray filled region

bubble and dew points are 0.074 $mol_{MEA}/mol_{mix}$ and 0.013 $mol_{MEA}/mol_{mix}$, respectively. Most of the data points are represented within this uncertainty estimate.

To extend this range, data points of Belabbaci et al. [164] and Cai et al. [165] were used in the fit. The bubble points of Belabbaci et al. [164] are described with an $AAD_x$ of 0.019 $mol_{MEA}/mol_{mix}$. The bubble- and dew-point data of Cai et al. [165] are represented with $AAD_x$ of 0.036 $mol_{MEA}/mol_{mix}$ and $AAD_y$ of 0.023 $mol_{MEA}/mol_{mix}$, respectively. The qualitatively good agreement of the phase boundaries calculated with the new EOS is shown on selected isotherms in a *p,x* diagrams in Fig. 42.

Tochigi et al. [171] reported uncertainties in pressure (0.03 kPa), temperature (0.01 K), and composition (0.007 $mol_{MEA}/mol_{mix}$), which lead to combined expanded uncertainties $(k = 2)$ of approximately 0.018 $mol_{MEA}/mol_{mix}$ for bubble points and 0.043 $mol_{MEA}/mol_{mix}$ for dew points. Without fitting, these data are represented within 0.04 $mol_{MEA}/mol_{mix}$, which is in line with the datasets of Kim et al. [166] and Belabbaci et al. [164].

There are 27 datasets containing homogeneous density data in the literature. However, some state regions are comprehensively investigated by several authors, whereas other regions, such as the gas-phase, are uncovered. Except for four publications, measurements were carried out at atmospheric pressure only, cf. Fig. 43.

The datasets of Han et al. [34], Hawrylak et al. [43], and Sobrino et al. [32] were included in the fitting process because the data represent the maximum pressure, temperature, and composition ranges of the database. Han et al. [34] report an

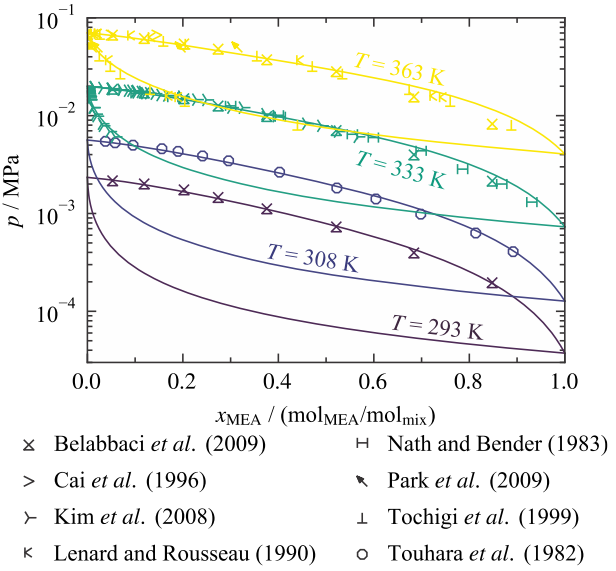


**Fig. 42** *p,x* diagrams showing selected experimental phase equilibrium data [35, 164–166, 169, 171–173] at 293 K, 308 K, 333 K, and 363 K in comparison to phase boundaries calculated with the EOS of this work for the system MEA + $H_2O$

uncertainty of the density measurements of 0.68 kg/m$^3$, which corresponds to a maximum uncertainty of 0.15% ($k$=2). More than half of the data are represented within this uncertainty, and the maximum deviation is 0.4%. The complete dataset is described with an AARD of 0.13%. Hawrylak et al. [43] do not state any uncertainty. However, their data cover the complete composition range and are represented with an AARD of 1.3%. Sobrino et al. [32] measured the most extensive dataset with 432 data points with a maximum temperature of 393 K, with pressures up to 120 MPa. The reported uncertainty of the density measurements is 0.35 kg/m$^3$, which corresponds to 0.075% ($k$=2). Approximately 80% of the datapoints are described within the experimental uncertainty, which results in an AARD of 0.046%. In general, almost all data points deviate by less than 0.5%. The estimated uncertainty of the EOS is approximately 0.1% in the region $293 \le T/\mathrm{K} \le 394$, $0.1 \le p/\mathrm{MPa} \le 120$, and $0.03 \le x_{\mathrm{MEA}}/(\mathrm{mol_{MEA}/mol_{mix}}) \le 0.16$ based on the data of Sobrino et al. [32] and 0.4% for the other regions covered with data ($298 \le T/\mathrm{K} \le 424$, $0.1 \le p/\mathrm{MPa} \le 0.7$, and $0.11 \le x_{\mathrm{MEA}}/(\mathrm{mol_{MEA}/mol_{mix}}) \le 0.73$), based on the data of Han et al. [34].

There are two datasets for the speed of sound available in the literature. The data are measured at atmospheric pressure and similar composition as well as temperature ranges. Figure 44 shows that the two datasets differ significantly from each other. Fitting the data of Jamal et al. [44] distorted the representation of the density data. Preliminary models fitting only density data resulted in much smaller deviations in

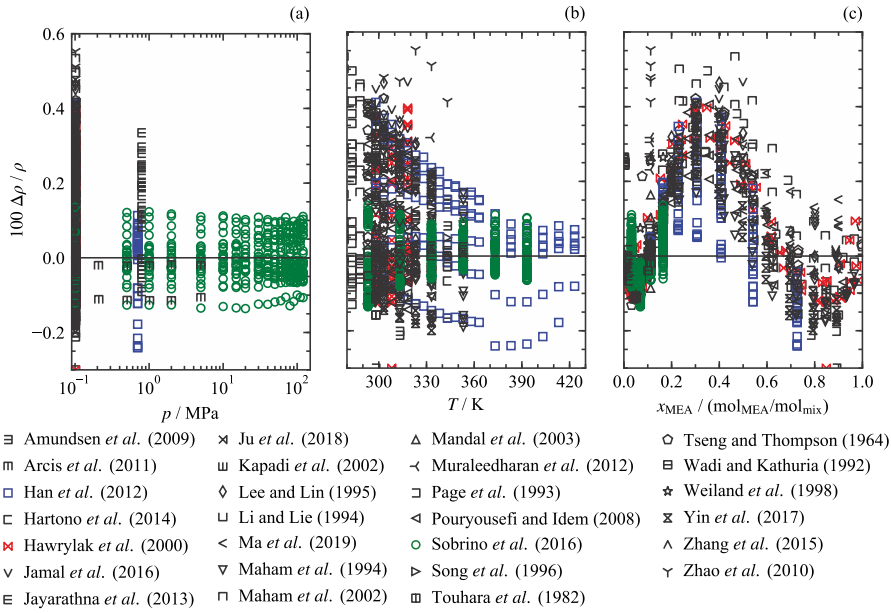


**Fig. 43** Relative deviations $\Delta\rho/\rho=(\rho_{\mathrm{data}}-\rho_{\mathrm{EOS}})/\rho_{\mathrm{data}}$ between calculated and experimental homogeneous density data [22–48] and values calculated with the EOS of this work as a function of pressure (a), temperature (b), and composition (c) for the system MEA+$H_2O$

the EOS with respect to the data of Hawrylak et al. [43]; these were chosen for the adjustment of the EOS parameters.

Deviations with respect to the EOS are within 1.5%. Since Hawrylak et al. [43] did not state experimental uncertainties, the uncertainty for the EOS can only be derived based on the deviations from the EOS, which is estimated to be 1.5% at atmospheric pressure for temperatures between 298.15 K and 318.15 K over the complete composition range.

Page et al. [30] and Vega-Maza [174] published the only experimental isobaric heat capacities. The percentage deviations from the EOS developed in this work are shown in Fig. 45.

Page et al. [30] do not report uncertainties, and thus the deviations, which are mainly within 2%, cannot be directly verified. However, the trend of higher deviations with increasing MEA concentrations indicates errors in the experiments because the main influence in the binary mixture model comes from the pure-fluid EOS at high concentrations and the pure-fluid EOS for MEA exhibits deviations of 2 % to the pure-fluid data from the same publication.

The uncertainty of the data of Vega-Maza [174] was reported through personal communication to be around 1%. This is confirmed for large parts of the datasets by an AARD of 0.7%, although the maximum deviations extend to 2%. In particular, the isotherm $T$=293.15 K at the lowest concentration of MEA of 0.0318 $\mathrm{mol_{MEA}/mol_{mix}}$ exhibits an offset. During the fitting process, it was not possible to align the data even if distortions in other properties were accepted. The uncertainty of the EOS in terms of the heat capacity is, therefore, estimated to be around 2% for up to 0.6 $\mathrm{mol_{MEA}/mol_{mix}}$ in the state regions covered by experimental data.

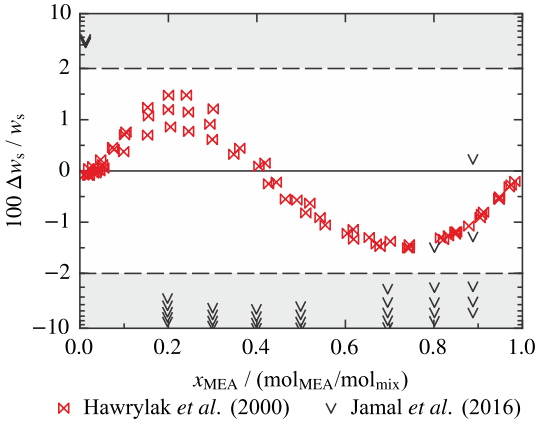


**Fig. 44** Relative deviations $\Delta w_s/w_s=(w_{s,data}-w_{s,EOS})/w_{s,data}$ between experimental homogeneous speed of sound data [43, 44] and values calculated with the EOS of this work as a function of composition for the system MEA+$H_2O$. The ordinate is linearly scaled between the dashed lines and logarithmically scaled in the gray filled region

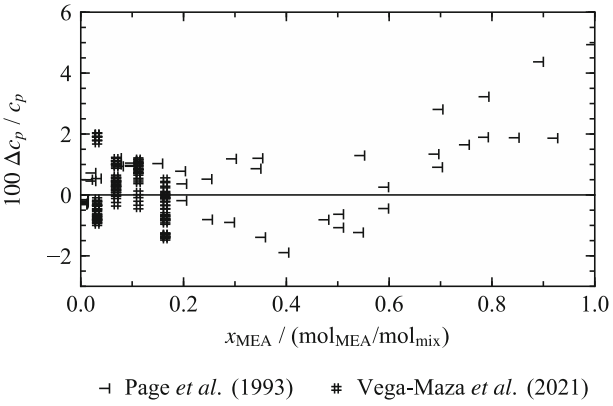


**Fig. 45** Relative deviations $\Delta c_p/c_p=(c_{p,\mathrm{data}}-c_{p,\mathrm{EOS}})/c_{p,\mathrm{data}}$ between experimental isobaric heat capacity data [30, 174] and values calculated with the EOS of this work as a function of composition for the mixture MEA + $H_2O$

### 3.1.12 DEA + $H_2O$

The binary mixture DEA + $H_2O$ is already described with an EOS developed by Herrig [21]. It was only adjusted to VLE data and did not consider density, speed of sound, or heat capacity data. An updated EOS with a fitted departure function is presented in this work. The VLE database consists of five publications. Sidi-Boumedine et al. [175] reported only four data points. The data of Abdi and Meisen [176] and Cai et al. [165] were measured along isobars and those of Horstmann et al. [177] and Wilding et al. [178] were measured along isotherms. Although there is little overlap in the temperature and pressure ranges of the datasets, good consistency was obtained when fitting the latter two, in particular the one of Cai et al. [165]. Deviations of experimental data from the EOS are shown in Fig. 46.

In general, all data are represented within 0.1 $\mathrm{mol_{DEA}/mol_{mix}}$, but the fitted data of Horstmann et al. [177] and Wilding et al. [178] at 373.15 K as well as all dew-point data deviate significantly less than this. Abdi and Meisen [176] reported a large number of bubble-point data without the corresponding vapor-phase composition and a few dew-point data. All VLE data points were measured with a dynamic technique, in which samples of both phases are analyzed in a gas chromatograph. The single bubble points were obtained with a synthetic measuring technique, where the composition of the liquid-phase was assumed to be almost identical to the overall composition of the mixture [21]. This generally results in higher deviations for the bubble-point data in comparison to the dew-point data of Abdi and Meisen [176] as visible in Fig. 46. At 365.15 K, the shift in composition is shown in the *p,x* diagram in Fig. 47.

Neither Abdi and Meisen [176], Wilding et al. [178], nor Cai et al. [165] report combined experimental uncertainties, and not even in all cases are individual uncertainties of temperature, pressure, and composition given so that a combined uncertainty could not be calculated. Horstmann et al. [177] state uncertainties of 0.03 K, 0.02 MPa, and 0.0001 in composition. Taking that information into account,

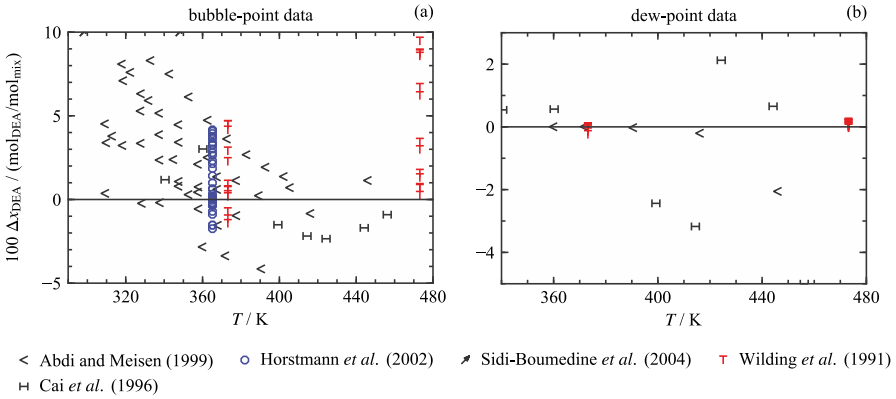


**Fig. 46** Absolute deviations in terms of composition $\Delta x_{DEA}=(x_{DEA,data}-x_{DEA,EOS})$ of bubble-point data (a) and dew-point data (b) [165, 175–178] from values calculated with the EOS of this work as a function of temperature for the binary system DEA + $H_2O$

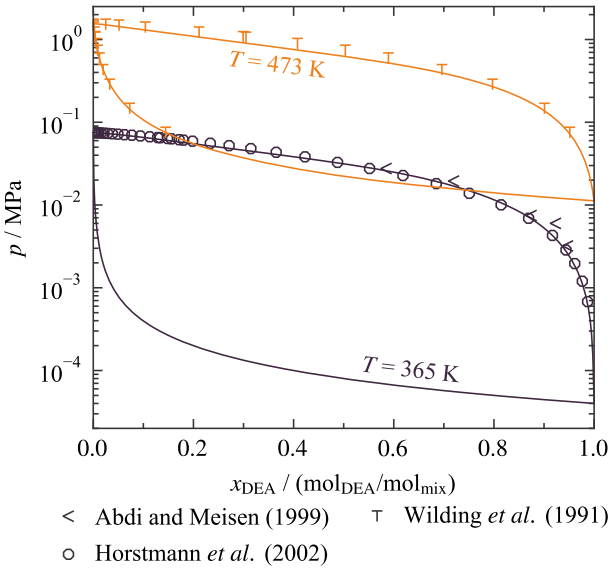


**Fig. 47** *p,x* diagrams showing selected experimental phase equilibrium data [176–178] at 365 K and 473 K in comparison to phase boundaries calculated with the EOS of this work for the system DEA + $H_2O$

the calculated combined uncertainties range from 0.08 mol% to 0.56 mol% which is between five to ten times smaller than the deviations from the EOS. However, the data of Horstmann et al. [177] and Wilding et al. [178] are consistent at approximately 360 K, see Fig. 46.

The coverage with respect to the available data and their accuracies is much worse for densities as compared to the MEA + $H_2O$ system. Measurements are not available in the gas-phase and most of the experimental pressures are at 1 atm. The highest

pressure was measured by Arcis et al. [179] (5 MPa), but, as shown in Fig. 48, these data exhibit an offset of 0.3% from the EOS.

The EOS was mainly fitted to the data of Han et al. [189] and Hawrylak et al. [43]. Similar to the MEA+$H_2O$ system, the data of Hawrylak et al. [43] deviate by up to 0.4%. The densities measured by Han et al. [189] are represented within 0.6%. During the fitting process, a better accuracy could not be achieved without distorting other datasets, although the final AARD is 0.26%. Both publications do not report experimental uncertainties. Since the deviations are similar to the MEA+$H_2O$ system, the uncertainty in terms of homogeneous densities can be estimated based on the deviations calculated with the EOS, which would be around 0.6% for calculations in the area where data are available.

Only Hawrylak et al. [43] measured speed of sound. These data are at atmospheric pressure along three isotherms: 298.15 K, 308.15 K, and 318.15 K. As depicted in Fig. 49, the new EOS describes the data within 1.5% with an AARD of 0.74%.

The authors do not report their experimental uncertainty and thus the uncertainty of the EOS in the range of the experimental data can only be estimated based on these deviations, which would be 1.5%.

The only dataset available with heat capacity measurements is that of Vega-Maza [174]. The percentage deviations calculated with the EOS are shown in Fig. 50.

The deviations between the data and the EOS are similar to the MEA+$H_2O$ mixture. Most of the data are described within 1% with a maximum deviation of 2%, which results in an AARD of 0.81%. The estimated uncertainty of the EOS is 2% over the region covered by experimental data.

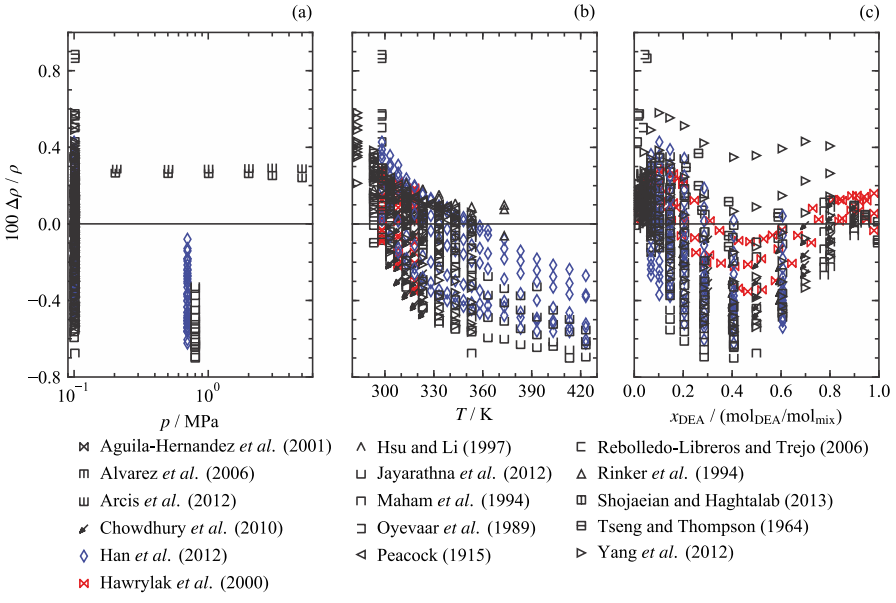


**Fig. 48** Relative deviations $\Delta\rho/\rho=(\rho_{data}-\rho_{EOS})/\rho_{data}$ between experimental homogeneous density data [26, 36, 43, 179–191] and values calculated with the EOS of this work as a function of pressure (a), temperature (b), and composition (c) for the system DEA+$H_2O$

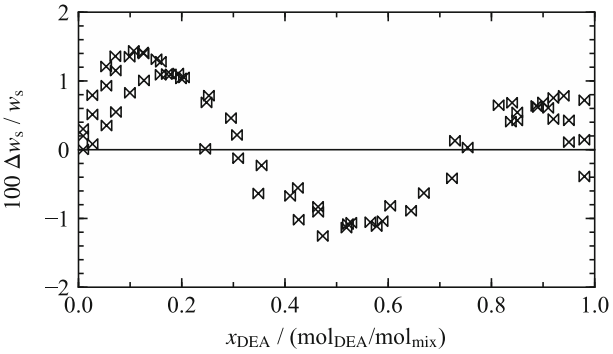


**Fig. 49** Relative deviations $\Delta w_s/w_s=(w_{s,data}-w_{s,EOS})/w_{s,data}$ between experimental speed of sound data of Hawrylak et al. [43] and values calculated with the EOS of this work as a function of composition for the system DEA + $H_2O$

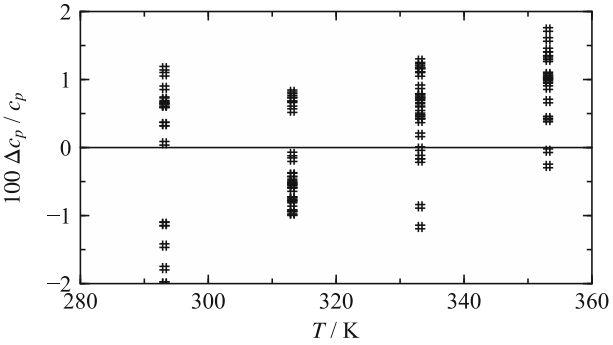


**Fig. 50** Relative deviations $\Delta c_p/c_p=(c_{p,data}-c_{p,EOS})/c_{p,data}$ between experimental isobaric heat capacity data of Vega-Maza et al. [174] and values calculated with the EOS of this work as a function of temperature for the mixture DEA + $H_2O$

### 3.1.13 MEA + DEA

Compared to the other binary systems containing amines discussed in this work, the mixing behavior of the binary mixture DEA + MEA is less complex because both components are chemically similar. Nevertheless, all four parameters of the binary reducing functions were required to accurately describe the limited available VLE data. Only two experimental studies by Cai et al. [165] and Tsintsarska et al. [192] were found in the literature. Each of these data sets includes results along a single isobar, 6.7 kPa or 1.8 kPa. The data and phase boundaries calculated from the mixture model are shown in *T,x* diagrams given in Fig. 51.

The *T,x* diagram emphasizes the good agreement between calculated VLE data and the experimental results, especially when considering the low saturation pressures that are overly sensitive to small temperature fluctuations and impurities. The resulting deviations between calculated phase-equilibrium compositions and the data are presented in Fig. 52.

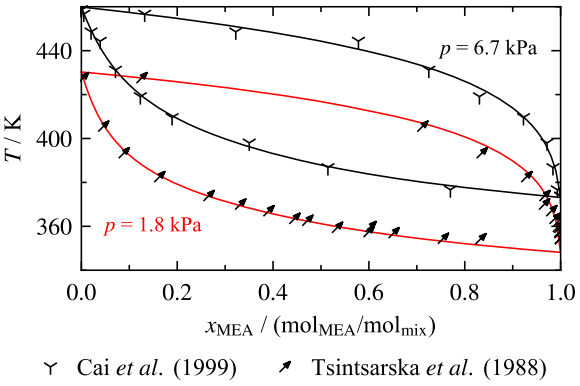


**Fig. 51** *T,x* diagrams showing the experimental phase equilibrium data [165, 192] at 1.8 kPa and 6.7 kPa in comparison to phase boundaries calculated with the EOS of this work for the system DEA + MEA

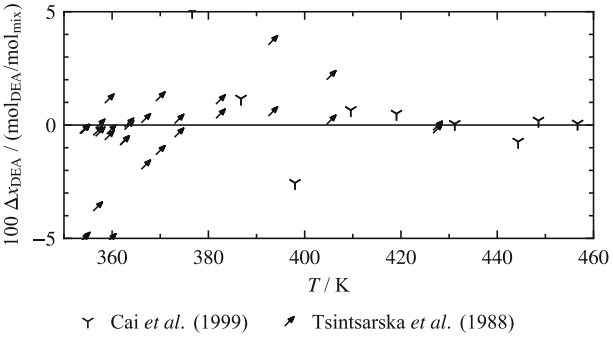


**Fig. 52** Absolute deviations $\Delta x_{MEA}=(x_{MEA,data}-x_{MEA,EOS})$ between experimental phase equilibrium data [165, 192] and values calculated with the EOS of this work as a function of temperature for the system DEA + MEA

Except for one outlier at 377 K, the model represents all the data of Cai et al. [165] within a maximum deviation of 0.026 $mol_{DEA}/mol_{mix}$. The deviations between the model and the measurements of Tsintsarska et al. [192] are mostly within 0.02 $mol_{DEA}/mol_{mix}$. As previously discussed, the experimental uncertainties seem to be underestimated in the publication of Cai et al. [165], whereas Tsintsarska et al. [192] do not provide any uncertainties.

### 3.1.14 MDEA + $H_2O$

The binary mixtures containing MDEA in this work are based on the pure-fluid EOS for MDEA of Neumann et al. [83]. For VLE states, the binary mixture parameters for MDEA + $H_2O$ were, for the most part, fitted to the data of Kim et al. [166] because it is the most comprehensive and accurate dataset covering both phases. As illustrated in Fig. 53, the deviations of the dew-point data from the new EOS are smaller than those of the bubble-point data.

Similar to the mixture of MEA + $H_2O$, the combined uncertainties ($k = 2$) of the data of Kim et al. [166] were calculated in this work. The maximum uncertainties for

the bubble- and dew-point measurements are 0.072 $mol_{MDEA}/mol_{mix}$ and 0.00012 $mol_{MDEA}/mol_{mix}$, respectively. Considering also the quite low purity of MDEA (99%), the representation of data of Kim et al. [166] is good in terms of the bubble-point data ($AAD_x = 0.027\ mol_{MDEA}/mol_{mix}$) and excellent with respect to the dew-point data ($AAD_y = 0.0001\ mol_{MDEA}/mol_{mix}$). Most data points deviate within the estimated combined uncertainties.

The data of Dell'Era et al. [195], which are visible in the *p,x* diagrams in Fig. 54, exhibit an offset to the data of Kim et al. [166] by around 0.05 $mol_{MDEA}/mol_{mix}$.

Therefore, these data were only fitted with small weights to shape the bubble curve at higher concentrations of MDEA. Nevertheless, they are still well represented by the EOS.

All available homogeneous density data were measured in the liquid-phase. Almost all data points are represented within 1% as shown in Fig. 55.

In general, the deviations of the density data are slightly worse than for the mixtures of MEA+$H_2O$ and DEA+$H_2O$ although various research groups investigated all three of these mixtures. The reasons for this could be the less pure samples of MDEA compared to MEA and DEA causing slight shifts in composition. The critical temperature and density of MDEA are quite different from the corresponding critical values of $H_2O$, more than those of MEA and DEA. This asymmetric mixture behavior is challenging to model with the extended corresponding states approach. In addition, convergence problems in the region close to the critical point occurred during the fitting process, which could only be solved by accepting tradeoffs in the representation of the experimental data. The most comprehensive dataset of Sobrino et al. [32] is still represented within 0.1% on average. Approximately half of the data points are reproduced within the previously discussed experimental uncertainty of 0.075%. The datasets of Han et al. [189] and Hawrylak et al. [43] were also included in the fitting process to cover the full

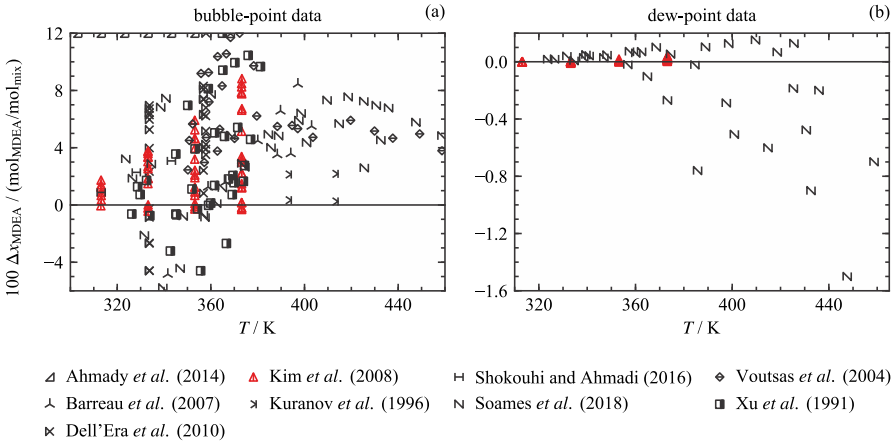


**Fig. 53** Absolute deviations $\Delta x_{MDEA}=(x_{MDEA,data}-x_{MDEA,EOS})$ of bubble-point data (a) and dew-point data (b) [166, 193–200] and values calculated with the EOS of this work as a function of temperature for the system MDEA+$H_2O$

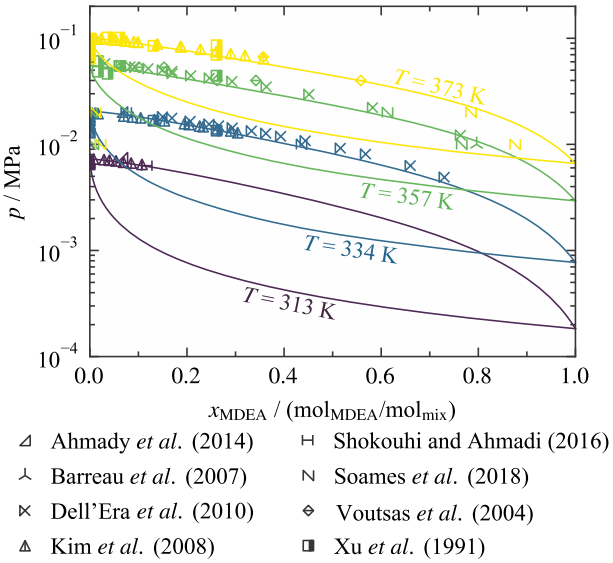


**Fig. 54** *p,x* diagrams showing selected experimental phase equilibrium data [166, 193–195, 197–200] at 313 K, 334 K, 357 K, and 373 K in comparison to phase boundaries calculated with the EOS of this work for the system MDEA + $H_2O$

composition range; however, the corresponding pressure range of 0.1 MPa to 0.7 MPa is rather narrow. Approximately a third of the data of Han et al. [189] are represented within their experimental uncertainty of 0.15% ($k$=2), which results in an AARD of 0.3%. The AARD calculated with the data of Hawrylak et al. [43] is 0.29%. Based on this, the estimated uncertainty of the calculation of homogeneous densities with the EOS developed in this work is 0.5% for the region experimentally investigated by Sobrino et al. [32] and 1% for all other regions covered by data.

Two datasets for the speed of sound were published by the same group. Hawrylak et al. [43] covers a wider composition range and these data were primarily used in the fitting process. Compared to the previous systems measured by the same authors, the deviations are significantly higher with a maximal deviation of around 7% (cf. Fig. 56).

The authors do not state any uncertainty but refer to the used apparatus called "Nusonics Model 6080". Based on the description of the other systems the uncertainties are expected to be within 2% and, therefore, in a similar range. This could not be achieved with this EOS because a decrease in deviations for one data type resulted in an increase of deviations in another, e.g., densities and isobaric heat capacities. As long as no other dataset is available in this state region, it cannot be clarified if the data are erroneous, or the present model has shortcomings.

Several datasets reported isobaric heat capacities in a temperature range between 278 K and 369 K, in a pressure range of 0.1 MPa to 25 MPa, and in the complete composition range. The most comprehensive dataset was measured by Zhang et al. [234] covering the full temperature and composition range, and thus these data were the basis for use in fitting isobaric heat capacities. Unfortunately, all measurements

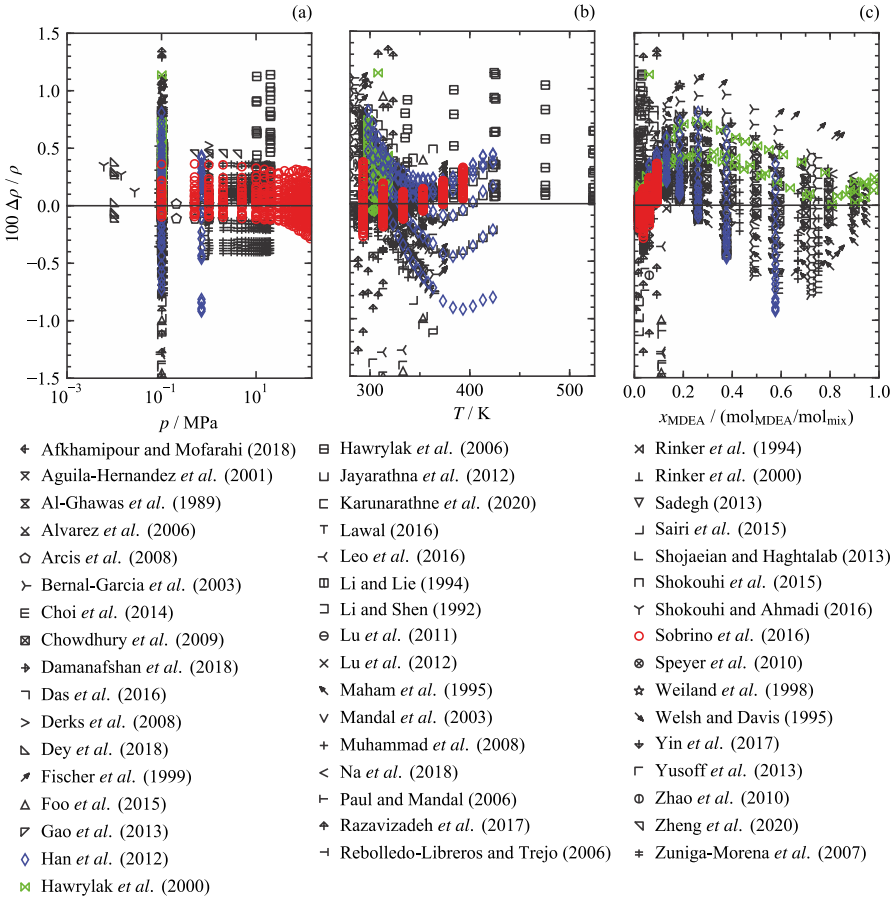


**Fig. 55** Relative deviations $\Delta\rho/\rho=(\rho_{data}-\rho_{EOS})/\rho_{data}$ between experimental homogeneous density data [24, 28, 32, 38, 39, 41, 43, 182–184, 186–189, 191, 197, 201–233] and values calculated with the EOS of this work as a function of pressure (a), temperature (b), and composition (c) for the system MDEA + $H_2O$

were conducted at atmospheric pressure and high-pressure data are not available. As shown in Fig. 57, the data deviate mostly within 2.5% with a maximum deviation of up to 5% at the highest temperature.

The authors state an uncertainty of 2% in terms of the isobaric heat capacity. However, this value is not based on measurement uncertainties but comparisons of deviations between measured isobaric heat capacities of water from tabulated values in the IAPWS formulation [67]. Since uncertainties in terms of mixtures are naturally higher due to the uncertainty in composition, the representation of the data in this work is assumed to be reasonable. To cover the higher pressures, the data of Vega-Maza et al. [174] were included in the fitting process. However, it was not possible to reach the same accuracy as for MEA + $H_2O$ without distorting other data or the physical behavior. Most of the data are described within 5% and the AARD is 3.4%. The other datasets are consistent with the data of Zhang et al. [234] except for

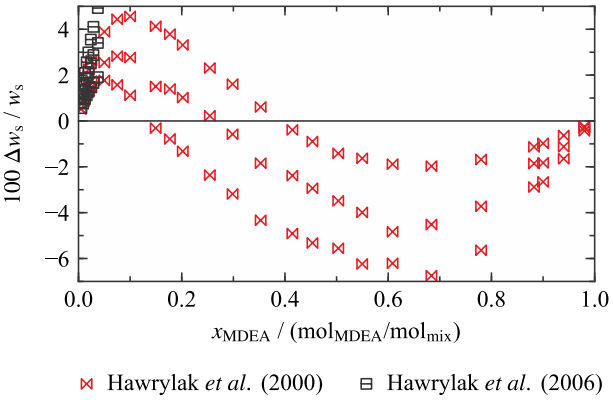


**Fig. 56** Relative deviations $\Delta w_s/w_s=(w_{s,data}-w_{s,EOS})/w_{s,data}$ between experimental homogeneous speed of sound data [43, 213] and values calculated with the EOS of this work as a function of composition for the system MDEA + $H_2O$

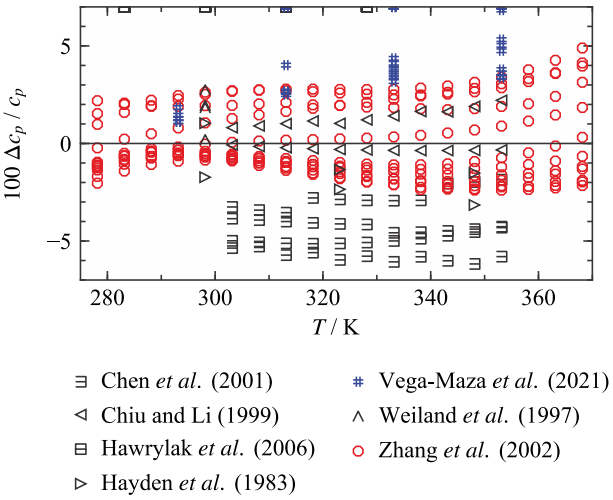


**Fig. 57** Relative deviations $\Delta c_p/c_p=(c_{p,data}-c_{p,EOS})/c_{p,data}$ between experimental isobaric heat capacity data [174, 213, 234–238] and values calculated with the EOS of this work as a function of temperature for the mixture MDEA + $H_2O$

Hawrylak et al. [213] and Chen et al. [235]. In Hawrylak et al. [213], the mixtures were already dissociated, which explains the high deviations and an AARD of 79%. Although Chen et al. [235] measured in the same state region as Zhang et al. [234], a clear offset is apparent. The uncertainties of the calculation of isobaric heat capacities with the EOS are 2.5% up to 340 K at atmospheric pressures and over the full composition range, and 5% for all other regions covered with experimental data.

### 3.1.15 MDEA + $CO_2$

The data situation for the MDEA + $CO_2$ mixture is significantly worse than for the MDEA + $H_2O$ system. Only two bubble-point datasets are available in the literature, and thus only two of the reducing parameters were adjusted. The data of Sadegh [226] are well represented ($AAD_x = 0.0076\,mol_{MDEA}/mol_{mix}$) as shown in Fig. 58.

The bubble-point data measured by Akbar [239] deviate by up to 0.12 $mol_{MDEA}/mol_{mix}$ from the phase boundary calculated with the EOS. This is due to the flat bubble curve in the composition region of the data. Comparing the data to the bubble curve in the *p,x* diagram in Fig. 59 shows the good agreement of the data and the EOS.

Akbar [239] used a synthetic isochoric method of absorption, where a constant volume of liquid MDEA is slowly exposed to gaseous $CO_2$. The amount of $CO_2$ and pressure of the system were measured. As soon as the pressure increases because $CO_2$ is no longer absorbed, equilibrium is reached. Based on the absorbed mass of $CO_2$, the solubility is calculated. The author does not state an uncertainty of this method. Comparisons to solubilities of $CO_2$ in other substances and other authors do not overlap. Therefore, no uncertainty can be estimated. However, since the deviations are in a similar range to the bubble-point deviations of the MDEA + $H_2O$ system, the results seem to be reasonable.

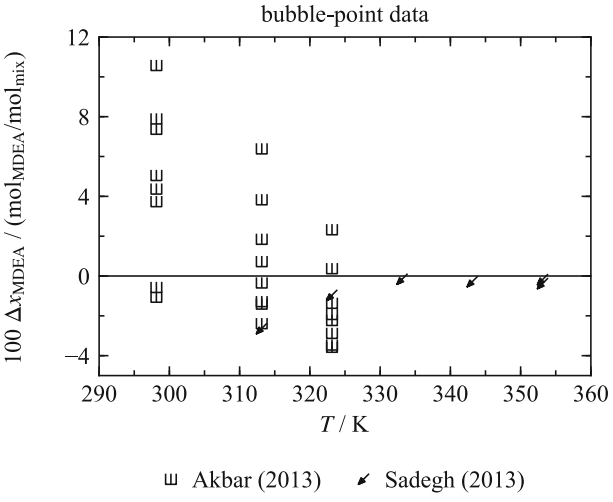


**Fig. 58** Absolute deviations $\Delta x_{MDEA}=(x_{MDEA,data}-x_{MDEA,EOS})$ between bubble-point data [226, 239] and values calculated with the EOS of this work as a function of temperature for the system MDEA + $CO_2$

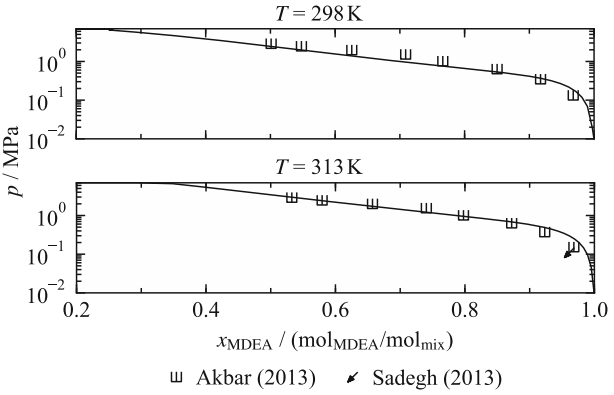


**Fig. 59** *p,x* diagrams showing selected experimental phase equilibrium data [226, 239] at 298 K and 313 K in comparison to phase boundaries calculated with the EOS of this work for the system MDEA + $CO_2$

### 3.1.16 MDEA + $CH_4$

The MDEA + $CH_4$ system is described with only one dataset consisting of 47 bubble points measured on 5 isotherms as presented in Fig. 60. Thus, only two reducing parameters were adjusted.

The data of Jou and Mather [240] deviate within 0.017 $mol_{MDEA}/mol_{mix}$, which results in an $AAD_x$ of 0.0035 $mol_{MDEA}/mol_{mix}$. The accurate description of the bubble curves is illustrated in Fig. 61.

The authors bubbled $CH_4$ through liquid MDEA for at least 4 h to ensure equilibrium. A liquid sample was then analyzed with a gas chromatograph. The uncertainty of the analysis was stated to be 3%, which is equal to 0.03 $mol_{MDEA}/mol_{mix}$. Although this uncertainty statement does not consider the uncertainties of the temperature and pressure measurements, the EOS reproduces the data well within the uncertainty in composition.

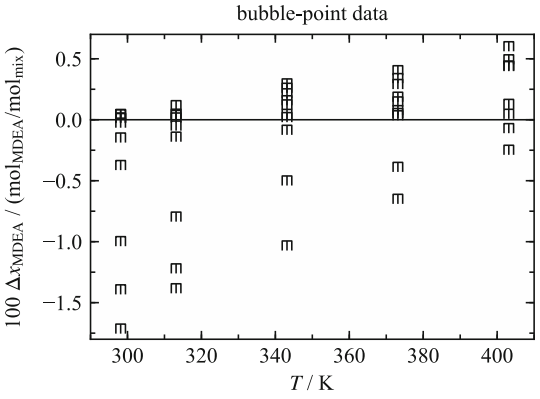


**Fig. 60** Absolute deviations $\Delta x_{MDEA}=(x_{MDEA,data}-x_{MDEA,EOS})$ between bubble-point data of Jou and Mather [240] and values calculated with the EOS of this work as a function of temperature for the binary system MDEA + $CH_4$

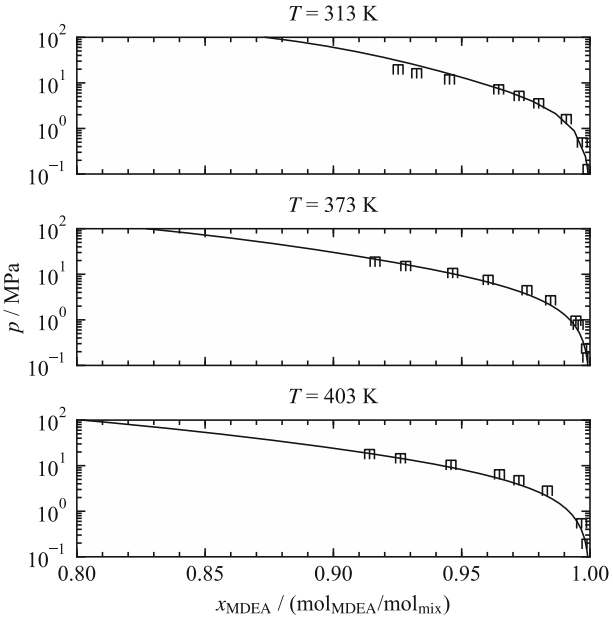


**Fig. 61** *p,x* diagrams showing selected experimental phase equilibrium data of Jou and Mather [240] at 313 K, 373 K, and 403 K in comparison to phase boundaries calculated with the EOS of this work for the system MDEA + $CH_4$

### 3.1.17 MDEA + MEA

Since only one isobaric heat capacity dataset is available in the literature for the MDEA + MEA system, only one reducing parameter was adjusted. The percentage deviations between calculated and measured values are shown in Fig. 62.

The data of Chen et al. [235] deviate within 4%, which is more accurate than for the MDEA + $H_2O$ system. Since an offset to the other datasets was apparent in the

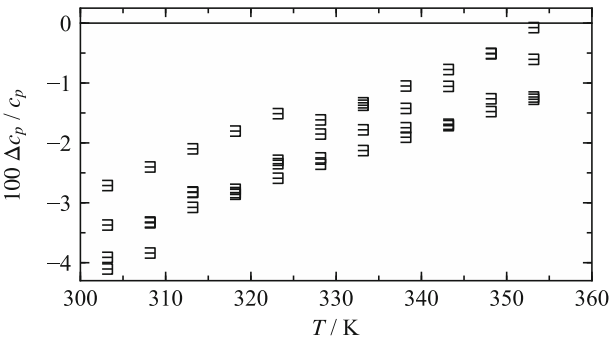


**Fig. 62** Relative deviations $\Delta c_p/c_p=(c_{p,\mathrm{data}}-c_{p,\mathrm{EOS}})/c_{p,\mathrm{data}}$ between experimental isobaric heat capacity data of Chen et al. [235] and values calculated with the EOS of this work as a function of temperature for the system MDEA + MEA

binary system with water, the same error happened most likely in this system. Therefore, the representation is considered to be reasonable.

### 3.1.18 $Cl_2 + HCl$

All four of the reducing parameters were used in fitting of the binary system $Cl_2 + HCl$. The database consists of the experimental VLE data of Wilson and Wilding [138], which was already discussed for the systems $SO_2 + Cl_2$ and $SO_2 + HCl$ (see Sects. 3.1.7 and 3.1.8), and an industrial study carried out at Höchst AG [241]. Molecular-simulation data for both VLE and homogeneous densities were contributed by Köster and Vrabec [135].

The VLE data of Wilson and Wilding [138] cover two isotherms, 213 K and 273 K. At 273 K, the data overlap with the measurements of Höchst AG [241], whose study includes three isotherms, 253 K, 273 K, and 293 K. These measurements were performed through a static-analytic method, in which the coexisting phases were sampled and analyzed. The report does not state any

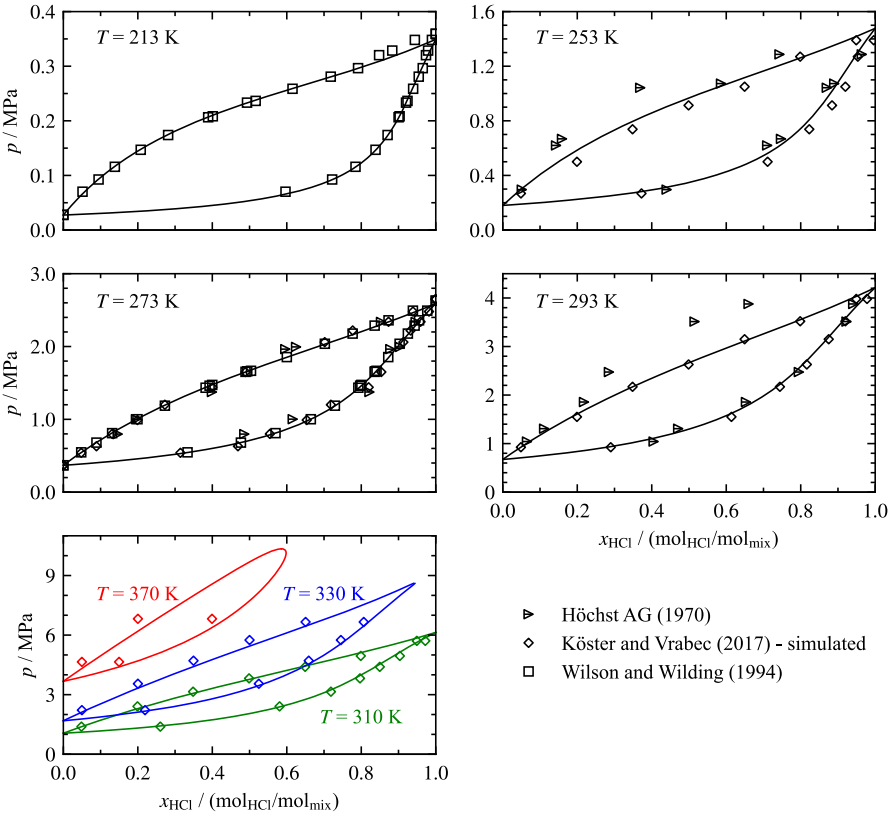


**Fig. 63** *p,x* diagrams showing selected experimental and simulated phase equilibrium data [135, 138, 241] at 213 K, 253 K, 273 K, 293 K, 310 K, 330 K, and 370 K in comparison to phase boundaries calculated with the EOS of this work for the system $Cl_2 + HCl$

uncertainties. As apparent from Fig. 63, considerable offset exists between the data of Höchst AG [241] and Wilson and Wilding [138]. Fitting the mixture model to the latter data set led to a more consistent and numerically stable model of the VLE region. The results obtained at Höchst AG were consequently omitted from the fitting process. Köster and Vrabec [135] used the VLE data of Wilson and Wilding [138] to adjust the unlike interaction parameter in the molecular-simulations so that their results are in close agreement with the data of Wilson and Wilding [138] at 273 K. With the simulations, Köster and Vrabec [135] extended the range of the available data up to 370 K.

Deviations between calculated VLE data, the experimental data, and simulated data are shown in Fig. 64. The figure presents deviations in both saturation pressure and phase-equilibrium composition. The deviations in pressure are of particular interest for the data of Wilson and Wilding [138], who measured pressures instead of analyzing the compositions of the phases in equilibrium.

Figure 64 shows similar deviations for dew and bubble points. Neglecting the measurements of Höchst AG [241], most of the data are fitted within 10% in saturation pressure and 0.05 $\mathrm{mol_{Cl_2}/mol_{mix}}$ in composition. These should be realistic estimates for the uncertainty of VLE data calculated from the model as well. These uncertainties are relatively large compared with other systems due to the quality of the available data. The reliable experimental data are limited to the two isotherms investigated by Wilson and Wilding [138]. Their combined experimental uncertainties were calculated based on given uncertainties in temperature and pressure (see Sec. 3.1.7); the maximum value is 0.015 $\mathrm{mol_{Cl_2}/mol_{mix}}$. At a temperature of 213 K, the data are generally represented within this uncertainty; however, the measurements at 273 K exhibit higher deviations, and the uncertainties may be underestimated. The molecular-simulation data are based on these experimental results and can thus not be used to independently assess the data.

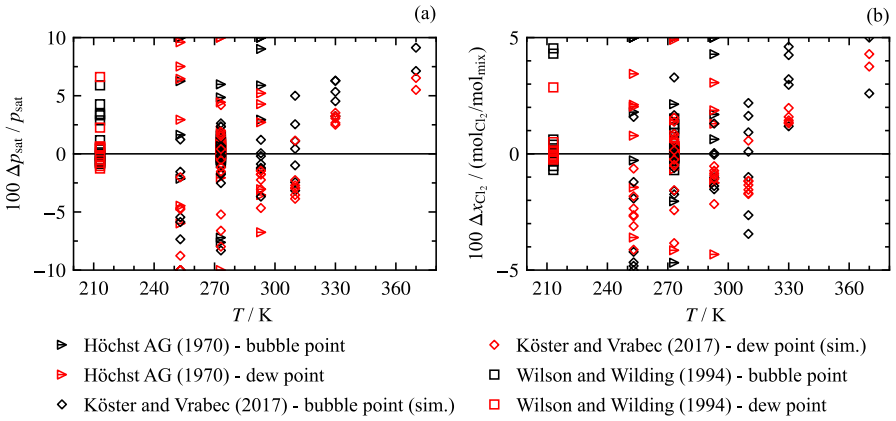


**Fig. 64** Relative deviations $p_{sat}=(p_{sat,data}-p_{sat,EOS})/p_{sat,data}$ (a) and absolute deviations $\Delta x_{Cl_2} = (x_{Cl_2,data} - x_{Cl_2,EOS})$ (b) between experimental phase equilibrium data [138, 141, 241] and values calculated with the EOS of this work as a function of temperature for the system $Cl_2+HCl$

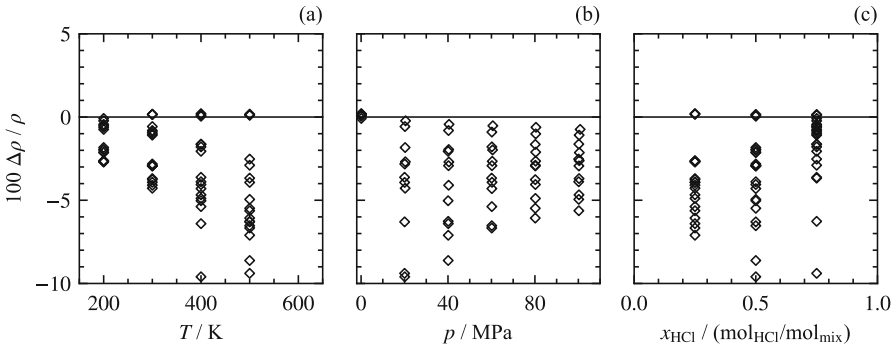


**Fig. 65** Relative deviations $\Delta\rho/\rho=(\rho_{data}-\rho_{EOS})/\rho_{data}$ between simulated density data of Köster et al. [141] and values calculated with the EOS of this work as a function of temperature (a), pressure (b), and composition (c) for the system $Cl_2+HCl$

The molecular-simulation results of Köster and Vrabec [141] for gas and liquid-phase densities cover three mixture compositions (0.25 $mol_{HCl}/mol_{mix}$, 0.5 $mol_{HCl}/mol_{mix}$, and 0.75 $mol_{HCl}/mol_{mix}$) at temperatures ranging from 180 K to 630 K and pressures up 100 MPa. The uncertainties in these data are high due to the lack of any comparative data and the questionable accuracy of the experimental VLE data that contributed to the molecular-simulation. The mixture model was consequently only fitted with low weights to a small number of these data points. Deviations between the data and calculated values are shown in Fig. 65.

The deviations increase with increasing temperature but show no clear trends with respect to pressure and composition. The latter aspect indicates that the molecular-simulation results are not more accurate for one of the pure components. In general, the plotted deviations are within 10%, which is clearly higher than desired for calculations of homogeneous densities with a Helmholtz-explicit EOS, and no definitive uncertainty estimate can be provided without additional experimental or comparative molecular-simulation data.

### 3.1.19 $NH_3+CO_2$

To calculate properties for multicomponent mixtures with ammonia as a minor impurity, an EOS for the $NH_3+CO_2$ system is needed. Neumann et al. [84] excluded this binary mixture because it is reactive and forms (depending on temperature, pressure, and composition) urea, water, and ammonia carbamate. The phase and chemical behavior is discussed in Lemkowitz et al. [242]. The experimental datasets available in the literature were measured at conditions where reactions occurred, e.g., Lemkowitz et al. [243], Briggs and Migrdichian [244], and Wormald and Wurzberger [245]. Since the equations and models used in this work are not able to describe reactive mixtures and because no experimental data are available at non-reactive conditions, the Lorentz-Berthelot combining rule was selected for use in the mixing rules until such time that these deficiencies can be addressed. This model should be used with caution for higher concentrations of ammonia.

### 3.2 Multicomponent Mixtures

Validating the model's ability to calculate accurate properties of multicomponent mixtures was based on a predictive combination of the binary-specific rules, and was carried out by Gernert and Span [5] and Ottøy et al. [246]. Gernert and Span [5] evaluated VLE data for the system $CO_2+N_2+O_2$ and concluded that the model describes the data accurately except for an offset at high oxygen concentrations. This behavior is related to the same issue in the binary $CO_2+O_2$. Ottøy et al. [246] investigated experimentally VLE states for the $CO_2+N_2+CH_4$ system. The performance of the EOS-CG-2021 model was evaluated based on these

**Table 6** Overview of the available thermodynamic property data of multicomponent systems of $CO_2$ combined with all components of the matrix (cf. Fig. 5)

| Ternary systems | Data types | References | Multicomponent systems | Data types | References |
|---|---|---|---|---|---|
| $CO_2+H_2O+CH_4$ | VLE | [100, 247–249] | $CO_2+H_2O+CO+H_2+CH_4$ | $p\rho T$ | [250, 251] |
| $CO_2+N_2+O_2$ | VLE | [252, 253] | $CO_2+N_2+O_2+Ar$ | $p\rho T$ | [121, 254] |
| | $p\rho T$ | [255, 256] | $CO_2+N_2+Ar+H_2$ | $p\rho T$ | [121] |
| $CO_2+N_2+Ar$ | VLE | [257] | $CO_2+N_2+H_2+CH_4$ | $w_s$ | [51] |
| | $p\rho T$ | [257, 258] | $CO_2+N_2+O_2+Ar+CO+H_2+CH_4$ | $p\rho T$ | [51, 254] |
| $CO_2+N_2+H_2$ | VLE | [259] | | | |
| | $p\rho T$ | [260] | | | |
| $CO_2+N_2+CH_4$ | VLE | [246, 261–266] | | | |
| | $p\rho T$ | [267, 268] | | | |
| $CO_2+O_2+H_2$ | $p\rho T$ | [256] | | | |
| $CO_2+O_2+Ar$ | VLE | [123] | | | |
| $CO_2+O_2+SO_2$ | VLE | [123] | | | |
| $CO_2+Ar+CO$ | $w_s$ | [51] | | | |
| $CO_2+Ar+H_2$ | VLE | [257] | | | |
| $CO_2+CO+H_2$ | VLE | [269, 270] | | | |
| | $p\rho T$ | [271] | | | |
| $CO_2+H_2+CH_4$ | VLE | [272] | | | |
| | $p\rho T$ | [272, 273] | | | |
| $CO_2+CH_4+H_2S$ | VLE | [274–279] | | | |
| | $p\rho T$ | [280] | | | |
| $CO_2+CH_4+SO_2$ | VLE | [281] | | | |
| | $p\rho T$ | [281] | | | |
| | $w_s$ | [281] | | | |

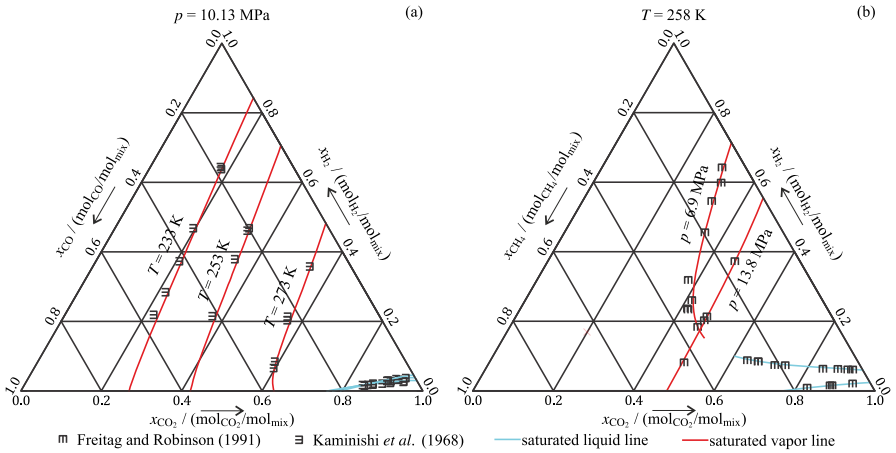


**Fig. 66** Ternary phase diagrams at selected states including experimental data [269, 272] for the mixtures $CO_2+CO+H_2$ (a) and $CO_2+H_2+CH_4$ (b)

measurements and other literature data. The deviations are "of the same order of magnitude as the deviations between the EOS-CG and the binary datasets" [246]. Their work also addressed the need for further measurements of other relevant systems to develop models with lower uncertainties.

In this work, a literature review was conducted to collect the available experimental thermodynamic data of multicomponent systems of $CO_2$ combined with all components of the matrix (cf. Fig. 5). VLE, density, and speed of sound data were found for 19 mixtures as shown in Table 6.

Mixtures of $CO_2+H_2O+MEA$, $CO_2+H_2O+DEA$, $CO_2+H_2O+NH_3$, and $CO_2+H_2O+MDEA$ are chemically reactive, forming new components not considered in this work. The EOS-CG-2021 model without extensions (cf. Sect. 5) is only able to describe these mixtures empirically if the concentrations of the products are negligible. This also applies to other reactive mixtures that do not contain $CO_2$. Therefore, these systems are excluded from the review and the following analysis.

In the "Appendix" in Tables 8 and 9, the AAD and AARD of the deviations of the EOS-CG-2021 model from the multicomponent experimental data are given. In general, the data situation is quite scarce; for example, VLE data are limited to ternary mixtures. For similar comparisons as carried out with the binary mixtures, a substantial amount of new data would be required due to the additional degree of freedom from the addition of a third component. Although a comprehensive validation of each multicomponent system is not possible, the typical low uncertainties in the EOS-CG-2021 model can still be proven with data from various sources covering wide temperature, pressure, and composition ranges. Two selected systems are shown in Fig. 66.

The deviations in terms of absolute molar concentrations between the VLE data and the model are calculated with the saturation points of the closest tie-line to the experimental data point. The procedure is discussed in detail in Ottøy et al. [246]. In Fig. 67, all VLE data of the various ternary and multicomponent mixtures are shown

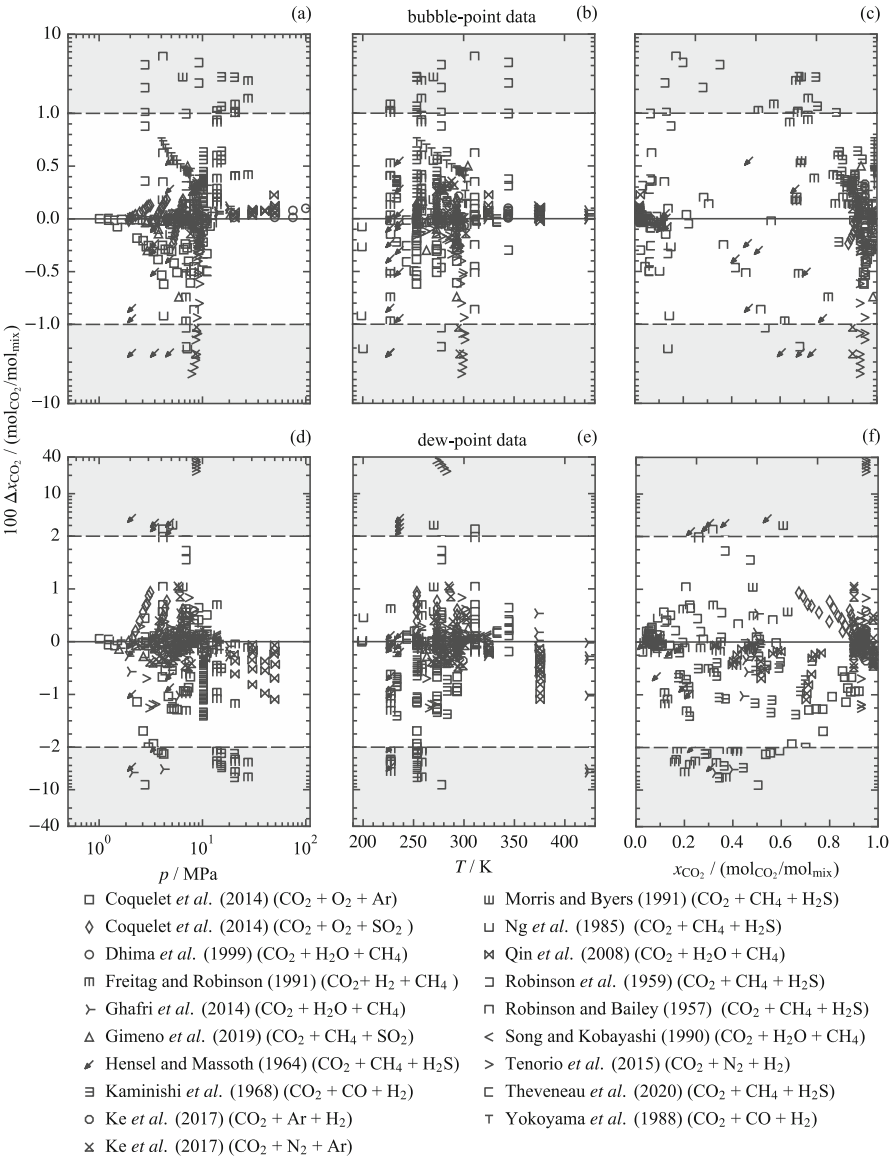


**Fig. 67** Absolute deviations $\Delta x_{CO_2} = (x_{CO_2,data} - x_{CO_2,EOS})$ between bubble- and dew-point data [100, 123, 247–249, 257, 259, 269, 270, 272, 274–279, 281] and values calculated with the EOS of this work as a function of pressure (a,d), temperature (b,e), and composition (c,f) for multicomponent systems containing $CO_2$. The ordinate is linearly scaled between the dashed lines and logarithmically scaled in the gray filled region

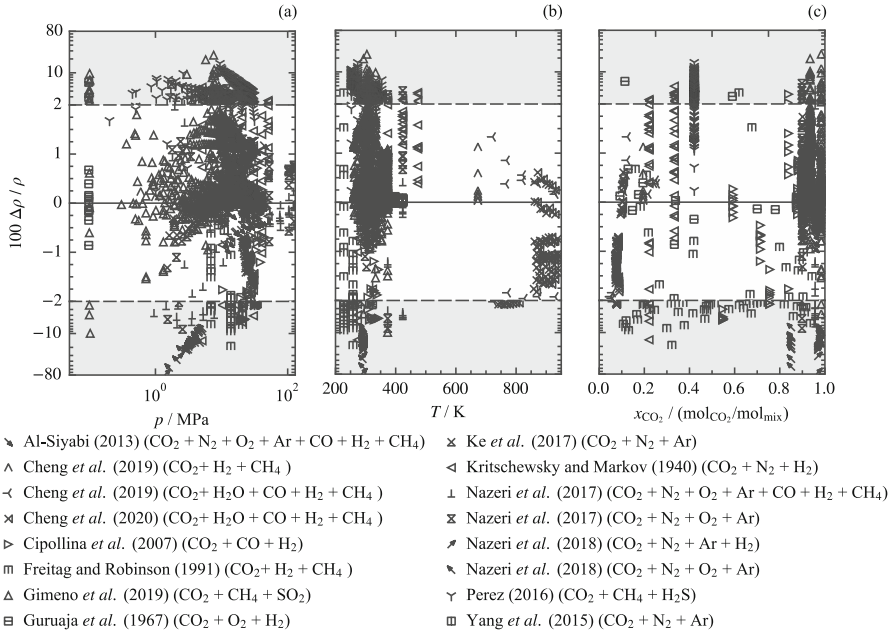


**Fig. 68** Relative deviations $\Delta\rho/\rho=(\rho_{data}-\rho_{EOS})/\rho_{data}$ between experimental homogeneous density data [51, 121, 250, 251, 254, 256–258, 271–273, 280–282] and values calculated with the EOS of this work as a function of pressure (a), temperature (b), and composition (c) for multicomponent mixtures. The dataset of Gimeno et al. [281] is shown in a shortened form. The ordinate is linearly scaled between the dashed lines and logarithmically scaled in the gray filled region

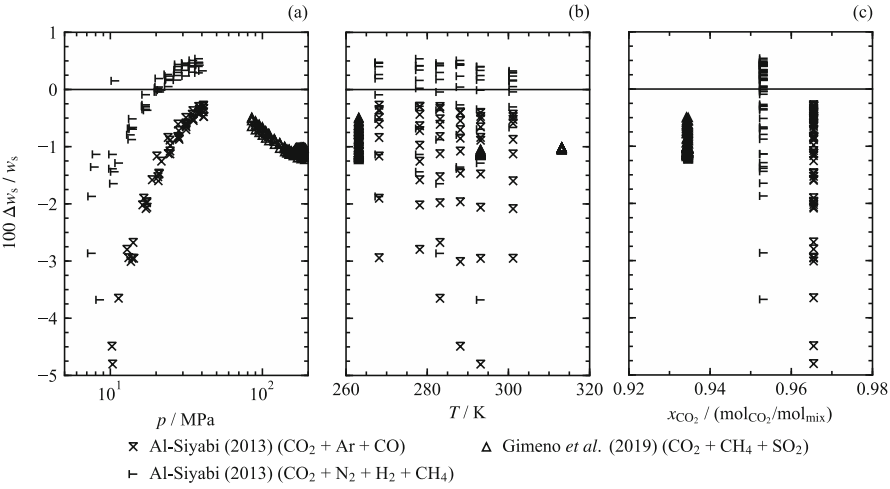


**Fig. 69** Relative deviations $\Delta w_s/w_s=(w_{s,data}-w_{s,EOS})/w_{s,data}$ between experimental homogeneous speed of sound data [51, 281] and values calculated with the EOS of this work as a function of pressure (a), temperature (b), and composition (c) for multicomponent mixtures

for separated bubble and dew points with respect to pressure, temperature, and concentration of $CO_2$.

The dew-point data deviate in general more than the bubble-point data. However, around 80% of all dew-point concentrations and around 90% of the bubble points are represented better than 0.01 $mol_{CO_2}/mol_{mix}$. The order of magnitude of these deviations is similar to the ones in the binary mixtures. Nevertheless, several data points deviate significantly from the EOS.

The homogeneous density data are illustrated in Fig. 68. Gimeno et al. [281] measured almost 19000 data points. Since the pressure steps were small ($<0.02$ MPa), only a reduced dataset was selected for the deviation plots here.

In general, most of the data were measured at temperatures below 400 K and at $CO_2$ concentrations higher than 0.8 $mol_{CO_2}/mol_{mix}$. 75% of the data are represented with deviations less than 2%, which shows the good predictive capabilities of the model, although a few data points have higher deviations. The most significant deviations occur for the data of Nazeri et al. [121]. The authors also measured densities of pure $CO_2$ that deviate by up to 74% with the same trend of increasing deviations for decreasing pressures. Therefore, the accuracy of the mixture data are quite questionable.

Speed of sound data were only measured by two groups. As illustrated in Fig. 69, the data of Gimeno et al. [281] deviate within 1.5%. The data of Al-Siyabi [51] are represented within 5%. The same publication also reports speed of sound data for the binary system $CO_2+Ar$ that deviate by at most 1.5% (cf. Løvseth et al. [87]). The comparably high deviations of the multicomponent data are probably caused by parameters that are larger than necessary in the binary departure functions for $CO_2+H_2$ and $CO_2+CO$ as discussed in Sect. 2.2. Nevertheless, most of the data points deviate by less than 2% from the model.

## 4 Analysis of the Physical and Extrapolation Behavior

Development of equations of state and mixture models is generally based on experimental data. However, for most fluids and mixtures, the data typically cover only small regions of the multidimensional thermodynamic surface. The calculation of reasonable properties in regions without any data are ensured by monitoring and analyzing various thermodynamic properties and derivatives as well as combinations of derivatives of the Helmholtz energy during the fitting process. The extrapolation behavior to extreme regions of temperature and pressure is constantly scrutinized to ensure smooth extrapolation far beyond the fluid limits because perturbations at these states can effect properties such as heat capacities and sound speeds that require multiple derivatives of the Helmholtz energy equation (see Lemmon et al. [283]). For mixtures, the physical and extrapolation behavior are typically more susceptible to erroneous features if a departure function is used because of the high flexibility of the functional form, for example see Rowland et al. [284]. When only reducing parameters are adjusted, all contributions in terms of the Helmholtz energy come from the pure-fluid equations and thus the mixture properties become a function of the quality of the pure-fluid equations, some of which are extremely good but most of

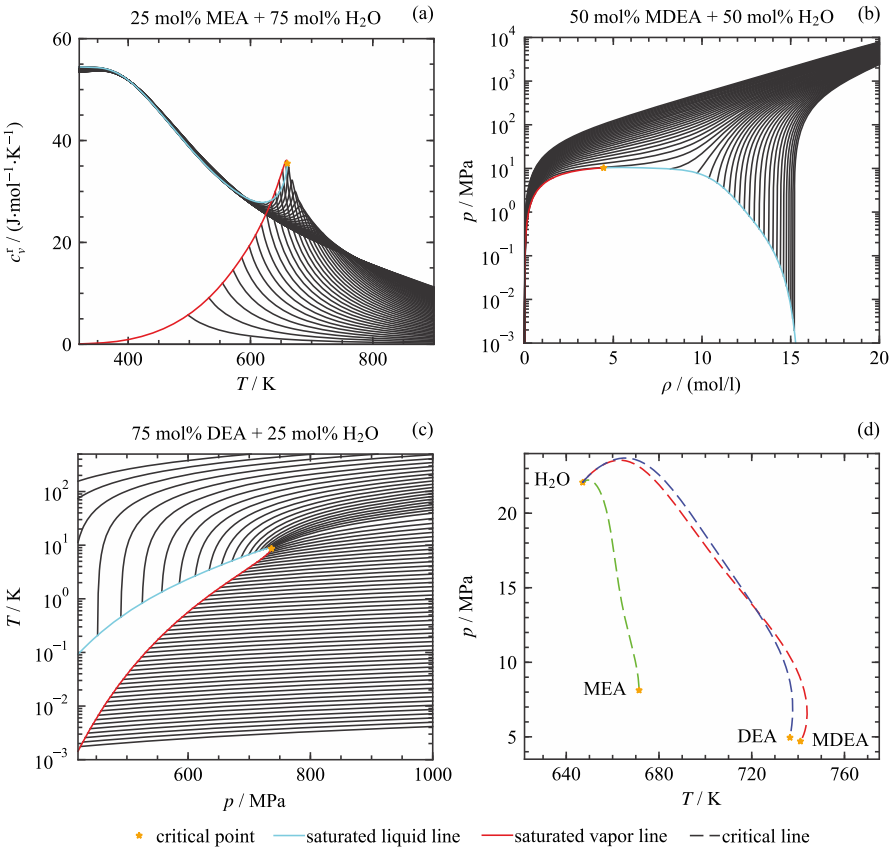


**Fig. 70** Examples of the physical and extrapolation behavior at different compositions of a $c_v^r$,$T$ diagram of the MEA+$H_2O$ system (a), $p$,ρ diagram of the MDEA+$H_2O$ system (b), $T$,$p$ diagram of the DEA+$H_2O$ system (c), and the critical lines of MEA+$H_2O$, DEA+$H_2O$, and MDEA+$H_2O$ in a $p$,$T$ diagram (d)

which are built upon data sets that are generally limited to the liquid-phase only. Figure 70 shows selected diagrams for the three binary mixture models developed with a departure function. The diagrams were calculated at temperatures up to several hundred kelvin and up to pressures of 1 GPa.

For all temperatures and pressures, the shapes of the isolines are smooth and no unreasonable crossing or bumps are detected. In recent publications [7, 50], the course of the critical line has become a topic of interest. Since the experimental VLE data of MEA, DEA, and MDEA mixed with $H_2O$ are far away from critical conditions with regard to temperature and pressure, cf. Figs. 42, 47, and 54, the evaluation of the critical lines is particularly important to ensure reasonable behavior. The critical lines in Fig. 70 were calculated with the teqp software of Bell [19]. Deiters and Bell [50] pointed out that a temperature maximum in the critical line higher than both pure-fluid critical temperatures is physically unsound, which is

caused by the pure-fluid EOS. However, as discussed in Sect. 2.2, this behavior in the MEA + $H_2O$ system could be eliminated by changing the parameters of the departure function. For the DEA + $H_2O$ system, a slight temperature maximum of around 1 K is still apparent. A temperature maximum of around 2 K is apparent for the EOS of MDEA + $H_2O$ and for DEA + $H_2O$. Additional experimental VLE would be beneficial to correct this behavior.

## 5 Extensions of the EOS-CG-2021

The EOS-CG-2021 as presented in this work can describe the thermodynamic properties of most of the mixtures involved in the CCS chain. However, the effects of some process steps and components that require special consideration are outside the typical scope of the EOS-CG-2021 model. This includes reactive mixtures, solid as well as hydrate phase formations, and the solution of gases in seawater as well as other brines. Additional publications discuss these extensions; they cannot be applied to the full EOS-CG-2021 model because they cover only a subset of the required components. All these extensions are based on the EOS reported in this work.

### 5.1 Reactive Mixtures

Reactive mixtures are of great importance in the $CO_2$ capture part of the CCS chain. The most common approach to separate the $CO_2$ from, for example, flue gases is the use of amine solutions, which bind the $CO_2$ by chemical reactions. The EOS-CG-2021 model presented in this work can describe reactive mixtures only empirically if the formed products are present in negligibly small concentrations. In other work, Neumann et al. [8] combined Helmholtz energy equations of state with excess Gibbs energy models. This approach enabled the calculation of phase and chemical equilibria as well as all thermodynamic properties of reactive mixtures. In Neumann et al. [8], the system $H_2O$ + MEA + $CO_2$ is validated with VLE, homogeneous liquid density, and speciation data. The general design of the approach allows its use with other reactive mixtures. However, the choice of the proper excess Gibbs energy model(s) and the validation of experimental data will be topics of future research.

### 5.2 Solid and Hydrate Phase Equilibria

In the $CO_2$ capture and transport segment, the knowledge of solid phases, e.g., ice, dry ice, and hydrates, is essential to avoid clogging of pipelines and valves by accumulated solids. Replacing methane hydrates with $CO_2$ hydrates has been discussed as a potential for $CO_2$ storage. Separate models are typically used to describe solid formation and the properties of the fluid, which leads to inconsistencies at the interfaces. Jäger et al. [285] modeled the phase equilibria, including hydrate formation, of the $H_2O$ + $CO_2$ system with the reference EOS listed in Table 3. This approach was improved and extended to other CCS-relevant gases by a series of three additional publications [286–288]. In Hielscher et al. [289, 290], a model was developed to accuretly describe the thermodynamic properties for mixed hydrates.

The components consisted of CO, $CO_2$, $CH_4$, $C_2H_6$, $C_3H_8$, $N_2$, Ar, and $O_2$ as well as their mixtures. The phase equilibrium algorithm was extended to allow for the calculation of four coexisting phases for ternary mixtures. Based on these models, the dynamics of hydrate formation and the formation of $H_2$-hydrates will be addressed in subsequent projects.

### 5.3 Seawater and Brines

The geological storage sites for separated $CO_2$ are often saline aquifers. Since the thermodynamic properties such as gas solubilities in $H_2O$ change significantly when salt is dissolved, the EOS-CG-2021 is a first step in the model extension to calculate seawater properties with other dissolved gases. Semrau et al. [291] combined the EOS-CG-2021 model in the form of the Helmholtz energy and the Gibbs energy model for seawater of Feistel [292] in a predictive manner. This approach was validated with gas solubilities of $CO_2$, $N_2$, and $O_2$ in seawater. The prediction of the salting out effect is reasonably calculated. To enhance the approach, a Pitzer-based model [293] has been used as the Gibbs energy model [294]. This enables fitting the parameters to experimental data, varying salt concentrations, and the potential description of interactions between the electrolytes as well as neutral species in the brine. However, like the work on reactive mixtures this work still is in an early stage; further research must follow.

## 6 Conclusion

In this work, an extension of the multicomponent mixture model EOS-CG is presented. The equations of state based on the reduced Helmholtz energy were summarized from various sources, and 72 binary mixture models were added within this work. Five departure functions and 14 binary mixture models with adjusted reducing parameters were developed. For the remaining systems, simple combining rules were chosen due to the lack of experimental data. The EOS-CG-2021 can be used to calculate all thermodynamic properties of a mixture consisting of the following 16 components: carbon dioxide, water, nitrogen, oxygen, argon, carbon monoxide, hydrogen, methane, hydrogen sulfide, sulfur dioxide, monoethanolamine, diethanolamine, hydrogen chloride, chlorine, ammonia, and methyl diethanolamine. The resulting 120 binary-specific equations were validated with the available experimental data, and various thermodynamic properties were evaluated to ensure reasonable physical and extrapolation behavior. Chemical reactions between components (e.g., $CO_2+H_2O+$amines or $CO_2+NH_3$) are not considered, except when the amount of products is very limited so that the impact on thermodynamic properties can implicitly be considered by an empirical fit.

The use of models describing the minor components is limited where experimental data are not available, requiring predictive combination rules. These components act

as impurities in CCS applications when the concentrations are low, and the contribution to the mixture model is almost solely based on the pure-fluid equations of state for these minor components. The mixture model uses the most accurate pure-fluid equations, which should result in the lowest uncertainties currently possible.

Nevertheless, new experimental data, in particular for systems without any data, would enable the adjustment of more sophisticated and accurate models. It is unlikely that all systems will be covered with experimental data in the near future; research should address the needs of better predictive models to improve calculations of relevant CCS applications.

The EOS-CG-2021 was validated with data for several multicomponent mixtures to demonstrate its ability to accurately calculate properties for more than just the binary subsets. Since wide temperature, pressure, and composition ranges are covered, reasonable calculations of thermodynamic properties of mixtures can be expected. New experimental data at various states for combinations of components without any data would certainly be of great interest to further validate the model.

## Appendix

See Tables 7, 8 and 9.

**Table 7** Overview of the available thermodynamic property data of binary mixtures and the average absolute relative deviation (AARD) calculated with the corresponding new equation of state

$x$ $H_2O$ + (1 − $x$) $CH_4$

VLE data

| Authors | Year | $N$ | $N_x$ | $N_y$ | $T$/K | $p$/MPa | $x$ | $y$ | $AAD_x$ | $AAD_y$ |
|---|---|---|---|---|---|---|---|---|---|---|
| Campos et al. [102] | 2010 | 18 | 18 | | 303–323 | 0.11–0.64 | 0.99–1.00 | | 0.005 | |
| Chapoy et al. [295] | 2004 | 10 | 10 | | 275–313 | 0.97–18.00 | 0.99–1.00 | | | 0.014 |
| Chapoy et al. [90] | 2005 | 39 | | 39 | 283–318 | 0.99–35.09 | | 0.00–0.01 | | 0.005 |
| Crovetto et al. [296] | 1982 | 7 | 7 | 7 | 297–519 | 1.3–6.5 | 0.99–1.0 | 0.00–0.62 | 0.004 | 0.22 |
| Fenghour and Wakeham [92] | 1996 | 9 | | 9 | 426–596 | 7.43–22.50 | | 0.07–0.68 | | 0.407 |
| Fonseca and von Solms [98] | 2012 | 10 | 10 | 6 | 298–303 | 5.25–12.35 | 0.99–1.00 | 0.99–1.00 | 0.019 | 0.286 |
| Frost et al. [93] | 2014 | 22 | 22 | 22 | 284–324 | 4.78–19.49 | 0.99–1.00 | 0.00–0.01 | 0.028 | 0.16 |
| Gillespie and Wilson [297] | 1982 | 16 | 13 | 16 | 323–589 | 1.38–16.89 | 0.99–1.00 | 0.00–0.84 | 0.019 | 0.015 |
| Kim et al. [99] | 2003 | 5 | 5 | | 298–298 | 2.30–16.60 | 0.99–1.00 | | 0.021 | 0.132 |
| Mohammadi et al. [95] | 2004 | 17 | | 17 | 283–313 | 0.51–2.85 | | 0.01–0.02 | | |
| Olds et al. [96] | 1942 | 78 | | 78 | 311–511 | 2.67–68.88 | | 0.00–0.57 | | 0.005 |
| O'Sullivan and Smith [298] | 1970 | 18 | 18 | | 324–399 | 10.1–60.8 | 0.99–1.00 | | 0.032 | |
| Qin et al. [100] | 2008 | 7 | 7 | | 324–376 | 10.90–49.90 | 0.99–1.00 | | 0.039 | |
| Rigby and Prausnitz [101] | 1968 | 12 | | 12 | 298–373 | 2.35–9.35 | | 0.00–0.02 | | 0.003 |
| Sairanen and Heinonen [97] | 2014 | 135 | | 135 | 253–293 | 0.20–7.00 | | 0.00–0.02 | | 0.023 |
| Yarrison et al. [299] | 2006 | 37 | | 37 | 310–478 | 3.4–111 | | 0.00–0.55 | | 0.31 |

$p\rho T$ data

| Authors | Year | $N$ | $T$/K | $p$/MPa | $x$ | AARD/% |
|---|---|---|---|---|---|---|
| Abdulagatov et al. [104] | 1993 | 64 | 523–653 | 2.24–63.24 | 0.04–0.85 | 3.126 |
| Fenghour and Wakeham [92] | 1996 | 16 | 429–699 | 7.49–12.66 | 0.076 | 0.124 |

**Table 7** continued

| *pρT* data | | | | | | |
|---|---|---|---|---|---|---|
| Authors | Year | *N* | *T*/K | *p*/MPa | *x* | AARD/% |
| | | 14 | 465–699 | 8.96–14.07 | 0.174 | 0.21 |
| | | 12 | 501–699 | 10.72–15.66 | 0.265 | 0.263 |
| | | 11 | 518–699 | 12.09–17.24 | 0.338 | 0.377 |
| | | 9 | 554–699 | 14.18–18.84 | 0.402 | 0.44 |
| | | 8 | 571–699 | 15.84–20.52 | 0.457 | 0.552 |
| | | 6 | 607–699 | 19.32–23.47 | 0.539 | 0.669 |
| | | 5 | 625– 699 | 22.13–26.18 | 0.602 | 0.623 |
| | | 6 | 652–699 | 27.03–30.38 | 0.676 | 0.477 |
| Overall | | 87 | 429–699 | 7.49–30.38 | 0.07–0.68 | 0.352 |
| Joffrion and Eubank [105] | 1989 | 48 | 398–498 | 0.20–12.03 | 0.1 | 0.038 |
| | | 61 | 398–498 | 0.15–8.67 | 0.25 | 0.055 |
| | | 60 | 398–498 | 0.07–4.20 | 0.5 | 0.05 |
| Overall | | 169 | 398–498 | 0.07–12.03 | 0.10–0.50 | 0.049 |
| Shmonov et al. [106] | 1993 | 92 | 626–723 | 10.00–200.00 | 0.20–0.94 | 4.133 |
| Welsch [107] | 1973 | 7 | 626–649 | 22.13—250.0 | 0.00–0.30 | 20.74 |
| Zhang [108] | 1997 | 42 | 662–873 | 17.05–43.14 | 0.05–0.17 | 2.698 |
| $h^E$ data | | | | | | |
| Authors | Year | *N* | *T*/K | *p*/MPa | *x* | AARD/% |
| Lancaster and Wormald [300] | 1990 | 61 | 448–699 | 0.3–12.7 | 0.50 | 12 |
| Smith et al. [301] | 1983 | 69 | 373–423 | 0.30–0.65 | 0.30–0.65 | 55 |
| Wilson and Brady | 1983 | 14 | 583–804 | 3.6–16.6 | 0.48–0.51 | 11 |
| Wormald and Colling [302] | 1984 | 62 | 451–700 | 0.35–12.62 | 0.49–0.51 | 62 |

$c_p$ data

| | | | | | |
|---|---|---|---|---|---|
| Hnědkovský and Wood [109] | 1997 | 15 | 303–704 | 27.98–28.01 | 0.99 995 | 4.645 |

$B$ and $B_{12}$ data

| Authors | Year | $N$ | $T$/K | $p$/MPa | $x$ | AAD/(cm$^3$·mol$^{-1}$) |
|---|---|---|---|---|---|---|
| Abdulagatov et al. [104] | 1993 | 25 | 298–373 | | 0.00–1.00 | 3.896 |
| Abdulagatov et al. [303] | 1996 | 24 | 521–653 | | 0.00–1.00 | 7.611 |
| Akin-Ojo et al. [304] | 2006 | 22 | 233–304 | | – | – |
| Rigby and Prausnitz [101] | 1968 | 4 | 373–423 | | – | – |
| Smith et al. [301] | 1983 | 6 | 233–653 | | – | – |

$x$ $H_2O$+(1−$x$) $H_2S$

VLE data

| Authors | Year | $N$ | $N_x$ | $N_y$ | $T$/K | $p$/MPa | $x$ | $y$ | AAD$_x$ | AAD$_y$ |
|---|---|---|---|---|---|---|---|---|---|---|
| Burgess and Germann [110] | 1969 | 39 | 39 | 39 | 303–443 | 1.72–2.34 | 0.97–1.00 | 0.00–0.33 | 0.064 | 2.423 |
| Chapoy et al. [103, 118] | 2005 | 31 | 31 | 15 | 298–338 | 0.50–3.96 | 0.96–1.00 | 0.00–0.03 | 0.065 | 0.069 |
| Clarke and Glew [114] | 1971 | 36 | 36 | 36 | 273–323 | 0.05–0.10 | 0.99–1.00 | 0.01–0.23 | 0.003 | 0.799 |
| Gillespie and Wilson [94] | 1980 | 17 | 17 | 17 | 310–589 | 0.34–13.79 | 0.95–1.00 | 0.00–0.86 | 0.322 | 2.077 |
| Carroll and Mather [113] | 1989 | 227 | 227 | | 283–453 | 0.13–6.65 | 0.96–1.00 | | 0.07 | |
| Neuburg et al. [111] | 1977 | 651 | 651 | 651 | 298–453 | 1.30–2.30 | 0.96–1.00 | 0.00–0.90 | 0.033 | 0.269 |
| Selleck et al. [115] | 1952 | 67 | 55 | 67 | 310–445 | 0.69–34.47 | 0.84–1.00 | 0.00–0.61 | 0.141 | 0.269 |
| Suleimenov and Krupp [116] | 1994 | 48 | 48 | 48 | 293–585 | 0.22–11.28 | 0.98–1.00 | 0.00–0.93 | 0.048 | 0.278 |
| Yu et al. [117] | 1980 | 39 | 39 | 39 | 286–378 | 0.45–1.73 | 0.97–1.00 | 0.00–0.14 | 0.046 | 0.492 |

$p\rho T$ data

**Table 7** continued

| $p\rho T$ data | | | | | | | | | |
|---|---|---|---|---|---|---|---|---|---|
| Authors | Year | $N$ | | | $T$/K | $p$/MPa | $x$ | AARD/% | |
| Authors | Year | $N$ | | | $T$/K | $p$/MPa | $x$ | AARD/% | |
| Selleck et al. [115] | 1952 | 15 | | | 310–445 | sat. | 0.02–0.06 | 0.657 | |
| Zezin et al. [120] | 2011 | 44 | | | 523–674 | 7.2–23.9 | 0.27–0.95 | 19 | |
| $c_p$ data | | | | | | | | | |
| Authors | Year | $N$ | | | $T$/K | $p$/MPa | $x$ | AARD/% | |
| Hnědkovský and Wood [109] | 1997 | 15 | | | 304–704 | 27.97–28.04 | 0.99–1.00 | 1.996 | |
| $h^E$ data | | | | | | | | | |
| Authors | Year | $N$ | | | $T$/K | $p$/MPa | $x$ | AARD/% | |
| Koschel et al. [305] | 2007 | 204 | | | 323–394 | 1.7–30.9 | 0.76–1.00 | 61 | |
| Wormald [306] | 2003 | 11 | | | 383–484 | 0.101325 | 0.5 | 50 | |
| $x$ $SO_2$+(1−$x$) $CO_2$ | | | | | | | | | |
| VLE data | | | | | | | | | |
| Authors | Year | $N$ | $N_x$ | $N_y$ | $T$/K | $p$/MPa | $x$ | $y$ | $AAD_x$ | $AAD_y$ |
| Blümcke [126] | 1988 | 8 | 8 | | 263 | 0.14–1.18 | 0.70–0.99 | | 2.676 | |
| Caubet [307] | 1902 | 27 | 16 | 27 | 342–364 | 3.26–9.46 | 0.22–0.92 | | | |
| Caubet [125] | 1904 | 10 | 10 | | 332 | 3.17–7.23 | 0.08–0.53 | 0.25–0.78 | | |
| Coquelet et al. [123] | 2014 | 22 | 22 | 22 | 263–334 | 0.10–8.79 | 0.10–0.97 | 0.01–0.80 | 0.845 | 0.737 |
| Lachet et al. [124] | 2009 | 46 | 41 | 46 | 263–333 | 0.12–9.10 | 0.10–1.00 | 0.16–0.58 | 1.461 | 0.898 |
| $p\rho T$ data | | | | | | | | | |

**Table 7** continued

*pρT* data

| Authors | Year | *N* | *T*/K | *p*/MPa | *x* | AARD/% |
|---|---|---|---|---|---|---|
| Authors | Year | *N* | *T*/K | *p*/MPa | *x* | AARD/% |
| Gimeno et al. [122] | 2018 | 200 | 263–304 | 0.10–20.00 | 0.007 | 0.395 |
| | | 200 | 263–304 | 0.10–20.00 | 0.03 | 1.197 |
| | | 200 | 263–304 | 0.10–20.00 | 0.047 | 1.525 |
| | | 200 | 263–304 | 0.10–20.00 | 0.103 | 2.321 |
| | | 200 | 263–304 | 0.10–20.00 | 0.197 | 2.368 |
| Overall | | 1000 | 263–304 | 0.10–20.00 | 0.00–0.20 | 1.561 |
| Nazeri et al. [129] | 2017 | 443 | 273–353 | 0.10–30.00 | 0.05 | 1.168 |
| Wang et al. [128] | 2015 | 12 | 328 | 9.00–20.00 | 0.025 | 3.855 |

$x\ SO_2+(1-x)\ N_2$

VLE data

| Authors | Year | *N* | $N_x$ | $N_y$ | *T*/K | *p*/MPa | *x* | *y* | $AAD_x$ | $AAD_y$ |
|---|---|---|---|---|---|---|---|---|---|---|
| Dean and Walls [133] | 1947 | 6 | 6 | 2 | 241–301 | 1.55–3.55 | 0.98–1.00 | 0.01–0.31 | | |
| Dornte and Ferguson [134] | 1939 | 15 | 15 | | 213–253 | 0.11–0.16 | 0.86–0.95 | | | |
| El Ahmar et al. [130] | 2011 | 46 | 44 | 46 | 323–413 | 1.48–23.53 | 0.82–1.00 | 0.12–1.00 | 0.542 | 1.311 |

*pρT* data

| Authors | Year | *N* | *T*/K | *p*/MPa | *x* | AARD/% |
|---|---|---|---|---|---|---|
| El Ahmar et al. [130] | 2011 | 26 | 323–413 | sat. | 0.53–0.98 | 3.984 |
| Köster and Vrabec [135] | 2017 | 63 | 260–500 | 1.50–40.00 | 0.05–0.95 | 1.107 |

$x\ SO_2+(1-x)\ O_2$

**Table 7** continued

| $x\ SO_2+(1-x)\ O_2$ | | | | | | | | | | |
|---|---|---|---|---|---|---|---|---|---|---|
| VLE data | | | | | | | | | | |
| Authors | Year | $N$ | $N_x$ | $N_y$ | $T$/K | $p$/MPa | $x$ | $y$ | $AAD_x$ | $AAD_y$ |
| VLE data | | | | | | | | | | |
| Authors | Year | $N$ | $N_x$ | $N_y$ | $T$/K | $p$/MPa | $x$ | $y$ | $AAD_x$ | $AAD_y$ |
| El Ahmar et al. [130] | 2011 | 27 | 26 | 27 | 323–413 | 1.47–20.22 | 0.81–1.00 | 0.12–1.00 | 0.756 | 1.723 |
| $pρT$ data | | | | | | | | | | |
| Authors | Year | $N$ | | | $T$/K | $p$/MPa | $x$ | | AARD/% | |
| El Ahmar et al. [130] | 2011 | 26 | | | 323–413 | sat. | 0.62–0.98 | | 5.781 | |
| $x\ SO_2+(1-x)\ CH_4$ | | | | | | | | | | |
| VLE data | | | | | | | | | | |
| Authors | Year | $N$ | $N_x$ | $N_y$ | $T$/K | $p$/MPa | $x$ | $y$ | $AAD_x$ | $AAD_y$ |
| Dean and Walls [133] | 1947 | 5 | 5 | 5 | 241–301 | 1.72–3.55 | 0.96–0.99 | 0.01–0.30 | 0.066 | 0.627 |
| Sayegh et al. [136] | 1981 | 1 | 1 | 1 | 318 | 13.8 | 0.76 | 0.255 | 0.436 | 0.57 |
| $x\ SO_2+(1-x)\ Cl_2$ | | | | | | | | | | |
| VLE data | | | | | | | | | | |
| Authors | Year | $N$ | $N_x$ | $N_y$ | $T$/K | $p$/MPa | $x$ | $y$ | $AAD_x$ | $AAD_y$ |
| Gilot et al. [139] | 1967 | 48 | 18 | 48 | 224–260 | 0.05–0.10 | 0.45–0.99 | 0.16–0.83 | 3.346 | 1.779 |
| Wilson and Wilding [138] | 1994 | 38 | 38 | 38 | 243–324 | 0.06–1.53 | 0.06–0.95 | 0.09–0.84 | 1.15 | 0.605 |
| $x\ SO_2+(1-x)\ HCl$ | | | | | | | | | | |

**Table 7** continued

$x$ $SO_2$+(1−$x$) HCl

VLE data

| Authors | Year | $N$ | $N_x$ | $N_y$ | $T$/K | $p$/MPa | $x$ | $y$ | $AAD_x$ | $AAD_y$ |
|---|---|---|---|---|---|---|---|---|---|---|
| VLE data | | | | | | | | | | |
| Authors | Year | $N$ | $N_x$ | $N_y$ | $T$/K | $p$/MPa | $x$ | $y$ | $AAD_x$ | $AAD_y$ |
| Köster and Vrabec [135] | 2017 | 45 | 45 | 45 | 260–370 | 0.15–7.77 | 0.00–1.00 | 0.00–1.00 | 0.657 | 1.328 |
| Wilson and Wilding [138] | 1994 | 35 | 35 | 35 | 203–273 | 0.00–2.62 | 0.00–1.00 | 0.00–1.00 | 0.713 | 0.165 |

$p\rho T$ data

| Authors | Year | $N$ | $T$/K | $p$/MPa | $x$ | AARD/% |
|---|---|---|---|---|---|---|
| Köster and Vrabec [135] | 2017 | 180 | 200–650 | 0.10–100 | 0.25–0.75 | 1.791 |

$x$ $SO_2$+(1−$x$) DEA

VLE data

| Authors | Year | $N$ | $N_x$ | $N_y$ | $T$/K | $p$/MPa | $x$ | $y$ | $AAD_x$ | $AAD_y$ |
|---|---|---|---|---|---|---|---|---|---|---|
| Li et al. [142] | 2014 | 6 | 6 | | 295–323 | 0.1 | 0.15–0.28 | | 0.296 | |

$x$ $SO_2$+(1−$x$) $H_2O$

VLE data

| Authors | Year | $N$ | $N_x$ | $N_y$ | $T$/K | $p$/MPa | $x$ | $y$ | $AAD_x$ | $AAD_y$ |
|---|---|---|---|---|---|---|---|---|---|---|
| Byerley et al. [159] | 1980 | 2 | 2 | | 298–323 | 0.1 | 0.01–0.03 | | 0.226 | |
| Conrad and Beuschlein [160] | 1934 | 6 | 6 | | 298 | 0.04–0.10 | 0.00–0.01 | | 1.245 | |
| Douabul and Riley [147] | 1979 | 6 | 6 | | 278–303 | 0.1 | 0.02–0.06 | | 0.972 | |
| Hudson [151] | 1925 | 39 | 39 | | 283–353 | 0.07–0.10 | 0.00–0.16 | | 0.776 | |

**Table 7** continued

$x\ SO_2+(1-x)\ H_2O$

VLE data

| Authors | Year | $N$ | $N_x$ | $N_y$ | $T$/K | $p$/MPa | $x$ | $y$ | $AAD_x$ | $AAD_y$ |
|---|---|---|---|---|---|---|---|---|---|---|
| Mondal [153] | 2007 | 19 | 19 | | 293–333 | 0.1 | 0.02–0.10 | | 3.801 | |
| Rabe and Harris [154] | 1963 | 36 | 36 | | 303–333 | 0.00–0.10 | 0.00–0.02 | | 0.011 | |
| Rumpf and Maurer [155] | 1992 | 44 | 44 | | 293–394 | 0.04–1.64 | 0.00–0.10 | | 0.864 | |
| Sherwood [156] | 1925 | 63 | 63 | | 273–323 | 0.00–0.10 | 0.00–0.07 | | 0.58 | |
| Sims [157] | 1862 | 22 | 22 | | 281–323 | 0.1 | 0.01–0.06 | | 0.788 | |
| Smith and Parkhurst [158] | 1922 | 8 | 8 | | 278–333 | 0.1 | 0.00–0.04 | | 0.942 | |
| Spall [148] | 1963 | 19 | 19 | 17 | 373–573 | 0.18–21.85 | 0.06–0.96 | 0.03–0.98 | 3.125 | 4.784 |
| Tokunaga [149] | 1974 | 4 | 4 | | 283–313 | 0.1 | 0.01–0.05 | | 0.588 | |

LLE data

| Authors | Year | $N$ | $N_x$ | $N_y$ | $T$/K | $p$/MPa | $x$ | $y$ | $AAD_x$ | $AAD_y$ |
|---|---|---|---|---|---|---|---|---|---|---|
| van Berkum and Diepen [143] | 1979 | 233 | 233 | | 273–391 | 0.91–345.3 | 0.10–0.36 | | 3.449 | |
| Zhou et al. [162] | 2020 | 45 | 45 | | 263–394 | 1.0–30.0 | 0.04–0.14 | | 2.9 | |

$p\rho T$ data

| Authors | Year | $N$ | $T$/K | $p$/MPa | $x$ | AARD/% |
|---|---|---|---|---|---|---|
| Beuschlein and Simenson [146] | 1949 | 4 | 296 | 0.00–0.11 | 0.00–0.03 | 0.44 |
| Campbell and Maass [152] | 1930 | 37 | 293–383 | 0.05–0.77 | 0.01–0.05 | 0.474 |

$h^E$ data

| Authors | Year | $N$ | $T$/K | $p$/MPa | $x$ | AARD/% |
|---|---|---|---|---|---|---|

**Table 7** continued

| $h^E$ data<br>Authors | Year | $N$ | $T$/K | $p$/MPa | $x$ | AARD/% |
|---|---|---|---|---|---|---|
| Wormald [306] | 2003 | 11 | 383–484 | 0.101 325 | 0.5 | 70 |

$x$ DEA + (1 − $x$) MEA

VLE data

| Authors | Year | $N$ | $N_x$ | $N_y$ | $T$/K | $p$/MPa | $x$ | $y$ | $AAD_x$ | $AAD_y$ |
|---|---|---|---|---|---|---|---|---|---|---|
| Cai et al. [165] | 1996 | 11 | 11 | 11 | 373–459 | 0.007 | 0.00–1.00 | 0.00–1.00 | 1.47 | 2.385 |
| Tsintsarska et al. [192] | 1988 | 15 | 15 | 15 | 354–428 | 0.002 | 0.16–1.00 | 0.00–0.88 | 2.259 | 0.76 |

$x$ $Cl_2$ + (1 − $x$) HCl

VLE data

| Authors | Year | $N$ | $N_x$ | $N_y$ | $T$/K | $p$/MPa | $x$ | $y$ | $AAD_x$ | $AAD_y$ |
|---|---|---|---|---|---|---|---|---|---|---|
| Höchst AG [241] | 1970 | 18 | 18 | 18 | 253–293 | 0.30–3.88 | 0.14–0.95 | 0.03–0.60 | 10.19 | 6.047 |
| Köster and Vrabec [135] | 2017 | 42 | 42 | 42 | 253–370 | 0.27–6.82 | 0.00–1.00 | 0.00–1.00 | 3.33 | 3.814 |
| Wilson and Wilding [138] | 1994 | 36 | 36 | 36 | 213–273 | 0.03–2.49 | 0.00–1.00 | 0.00–1.00 | 0.988 | 0.831 |

$p\rho T$ data

| Authors | Year | $N$ | $T$/K | $p$/MPa | $x$ | AARD/% |
|---|---|---|---|---|---|---|
| Köster et al. [141] | 2023 | 70 | 200–500 | 0.10–101 | 0.25–0.75 | 3.2 |

$x$ MEA + (1 − $x$) $H_2O$

VLE data

| Authors | Year | $N$ | $N_x$ | $N_y$ | $T$/K | $p$/MPa | $x$ | $y$ | $AAD_x$ | $AAD_y$ |
|---|---|---|---|---|---|---|---|---|---|---|

**Table 7** continued

$x$ MEA + $(1-x)$ $H_2O$
VLE data

| Authors | Year | $N$ | $N_x$ | $N_y$ | $T$/K | $p$/MPa | $x$ | $y$ | $AAD_x$ | $AAD_y$ |
|---|---|---|---|---|---|---|---|---|---|---|
| Belabbaci et al. [164] | 2009 | 72 | 72 | | 283–364 | 1E−5–7E−2 | 0.05–0.85 | | 1.9 | |
| Cai et al. [165] | 1996 | 25 | 25 | 25 | 362–432 | 6E−2–0.2 | 0.05–0.93 | 0.00–0.66 | 3.6 | 2.3 |
| Kim et al. [166] | 2008 | 87 | 86 | 86 | 313–374 | 6E−3–7E−2 | 0.00–0.57 | 0.00–0.06 | 1.2 | 0.19 |
| Lenard and Rousseau [172] | 1990 | 13 | 13 | 13 | 343–364 | 5E−3–7E−2 | 0.02–0.74 | 0.00–0.19 | 2.8 | 0.45 |
| Nath and Bender [173] | 1983 | 36 | 36 | | 333–371 | 1E−3–7E−2 | 0.06–0.93 | | 5.2 | |
| Park et al. [169] | 2009 | 33 | 33 | 33 | 355–431 | 5E−2–7E−2 | 0.03–0.99 | 0.00–0.93 | 4.1 | 2.9 |
| Park and Lee [168] | 1997 | 16 | 16 | 16 | 373–444 | 0.101 325 | 0.03–0.98 | 0.00–0.89 | 2.2 | 0.68 |
| Tanaka et al. [170] | 2001 | 11 | 11 | 11 | 373–444 | 0.1 | 0.19–0.97 | 0.01–0.82 | 1.7 | 2.6 |
| Touhara et al. [35] | 1982 | 26 | 26 | | 298–309 | 2E−4–5E−3 | 0.04–0.89 | | 1.4 | |
| Tochigi et al. [171] | 1999 | 9 | 9 | 9 | 363.15 | 4E−3–7E−2 | 0.03–0.89 | 0.00–0.44 | 2.0 | 1.2 |
| Wohland [163] | 1976 | 34 | 34 | | 372–467 | 0.1–0.7 | 0.00–0.86 | | 13 | |

$pρT$ data

| Authors | Year | $N$ | $T$/K | $p$/MPa | $x$ | AARD/% |
|---|---|---|---|---|---|---|
| Amundsen et al. [22] | 2009 | 5 | 298–354 | 0.101325 | 0.0687 | 0.052 |
| | | 5 | 298–354 | 0.101325 | 0.1122 | 0.016 |
| | | 5 | 298–354 | 0.101325 | 0.1643 | 0.11 |
| | | 5 | 298–354 | 0.101325 | 0.2278 | 0.21 |
| | | 5 | 298–354 | 0.101325 | 0.4076 | 0.22 |
| | | 5 | 298–354 | 0.101325 | 0.7264 | 0.12 |
| Overall | | 30 | 298–354 | 0.101325 | 0.07–0.73 | 0.12 |
| Arcis et al. [23] | 2011 | 5 | 298.34 | 0.2–5.0 | 0.0495 | 0.11 |

**Table 7** continued

| *pρT* data | | | | | | |
|---|---|---|---|---|---|---|
| Authors | Year | *N* | *T*/K | *p*/MPa | *x* | AARD/% |
| | | 5 | 298–299 | 0.2–5.0 | 0.1122 | 0.021 |
| Overall | | 10 | 298–299 | 0.2–5.0 | 0.05–0.11 | 0.067 |
| Han et al. [34] | 2012 | 20 | 298–424 | 0.1–0.7 | 0.1122 | 0.034 |
| | | 20 | 298–424 | 0.1–0.7 | 0.1643 | 0.12 |
| | | 20 | 298–424 | 0.1–0.7 | 0.2278 | 0.19 |
| | | 20 | 298–424 | 0.1–0.7 | 0.3067 | 0.2 |
| | | 20 | 298–424 | 0.1–0.7 | 0.4077 | 0.15 |
| | | 20 | 298–424 | 0.1–0.7 | 0.5412 | 0.076 |
| | | 19 | 298–414 | 0.1–0.7 | 0.7264 | 0.15 |
| Overall | | 139 | 298–424 | 0.1–0.7 | 0.11–0.73 | 0.13 |
| Hartono et al. [42] | 2014 | 7 | 293–354 | 0.101325 | 0.0191 | 0.028 |
| | | 19 | 293–354 | 0.101325 | 0.1122 | 0.033 |
| Overall | | 26 | 293–354 | 0.101325 | 0.02–0.11 | 0.031 |
| Hawrylak et al. [43] | 2000 | 69 | 298–319 | 0.101325 | 0.01–0.98 | 0.13 |
| Jamal et al. [44] | 2016 | 5 | 298–319 | 0.101325 | 0.0129 | 0.026 |
| | | 5 | 298–319 | 0.101325 | 0.198 | 0.23 |
| | | 5 | 298–319 | 0.101325 | 0.3 | 0.35 |
| | | 5 | 298–319 | 0.101325 | 0.3989 | 0.39 |
| | | 5 | 298–319 | 0.101325 | 0.4989 | 0.32 |
| | | 5 | 298–319 | 0.101325 | 0.6955 | 0.022 |
| | | 5 | 298–319 | 0.101325 | 0.8012 | 0.1 |
| | | 5 | 298–319 | 0.101325 | 0.8882 | 0.009 |
| Overall | | 40 | 298–319 | 0.101325 | 0.01–0.89 | 0.18 |

**Table 7** continued

| *pρT* data | | | | | | |
|---|---|---|---|---|---|---|
| Authors | Year | *N* | *T*/K | *p*/MPa | *x* | AARD/% |
| Jayarathna et al. [45] | 2013 | 24 | 303–334 | 0.8 | 0.07–0.41 | 0.14 |
| Ju et al. [46] | 2018 | 3 | 293.15 | 0.1 | 0.07–0.16 | 0.096 |
| Kapadi et al. [47] | 2002 | 32 | 303–319 | 0.101325 | 0.11–0.85 | 0.13 |
| Lee and Lin [48] | 1995 | 27 | 303–324 | 0.101325 | 0.10–0.90 | 0.15 |
| Li and Lie [24] | 1994 | 6 | 303–354 | 0.101325 | 0.0687 | 0.035 |
| Ma et al. [25] | 2019 | 5 | 293–334 | 0.1 | 0.1 | 0.031 |
| | | 5 | 293–334 | 0.1 | 0.1999 | 0.22 |
| | | 5 | 293–334 | 0.1 | 0.2998 | 0.3 |
| | | 5 | 293–334 | 0.1 | 0.4 | 0.28 |
| | | 5 | 293–334 | 0.1 | 0.4998 | 0.18 |
| | | 5 | 293–334 | 0.1 | 0.5995 | 0.096 |
| | | 5 | 293–334 | 0.1 | 0.6982 | 0.058 |
| | | 5 | 293–334 | 0.1 | 0.7974 | 0.056 |
| | | 5 | 293–334 | 0.1 | 0.8995 | 0.089 |
| Overall | | 45 | 293–334 | 0.1 | 0.10–0.90 | 0.15 |
| Maham et al. [26] | 1994 | 100 | 298–354 | 0.101325 | 0.01–0.97 | 0.1 |
| Maham et al. [27] | 2002 | 40 | 278–289 | 0.101325 | 0.01–0.97 | 0.17 |
| Mandal et al. [28] | 2003 | 7 | 293–324 | 0.101325 | 0.1122 | 0.096 |
| Muraleedharan et al. [29] | 2012 | 5 | 293–333 | 0.101325 | 0.1122 | 0.28 |
| Page et al. [30] | 1993 | 62 | 283–314 | 0.101325 | 0.00–1.00 | 0.18 |
| Pouryousefi and Idem [31] | 2008 | 80 | 295–334 | 0.101325 | 0.02–0.92 | 0.14 |
| Sobrino et al. [32] | 2016 | 108 | 293–394 | 0.1–120 | 0.0318 | 0.043 |
| | | 108 | 293–394 | 0.1–120 | 0.0687 | 0.059 |

**Table 7** continued

| Authors | Year | $N$ | $T$/K | $p$/MPa | $x$ | AARD/% |
|---|---|---|---|---|---|---|
| *ppT* data | | | | | | |
| | | 108 | 293–394 | 0.1–120 | 0.1125 | 0.02 |
| | | 108 | 293–394 | 0.1–120 | 0.1643 | 0.061 |
| Overall | | 432 | 293–394 | 0.1–120 | 0.03–0.16 | 0.046 |
| Song et al. [33] | 1996 | 5 | 303–344 | 0.101325 | 0.0506 | 0.049 |
| | | 5 | 303–344 | 0.101325 | 0.1122 | 0.031 |
| Overall | | 10 | 303–344 | 0.101325 | 0.05–0.11 | 0.04 |
| Touhara et al. [35] | 1982 | 12 | 298.14 | 0.101325 | 0.02–0.90 | 0.15 |
| Tseng and Thompson [36] | 1964 | 30 | 293–304 | 0.101325 | 0.03–1.00 | 0.18 |
| Wadi and Kathuria [37] | 1992 | 11 | 298.15 | 0.101325 | 0.04–0.73 | 0.16 |
| Weiland et al. [38] | 1998 | 4 | 298.15 | 0.101325 | 0.03–0.16 | 0.15 |
| Yin et al. [39] | 2017 | 5 | 293–334 | 0.1 | 0.0996 | 0.026 |
| | | 5 | 293–334 | 0.1 | 0.1991 | 0.21 |
| | | 5 | 293–334 | 0.1 | 0.2986 | 0.31 |
| | | 5 | 293–334 | 0.1 | 0.3977 | 0.26 |
| | | 5 | 293–334 | 0.1 | 0.4967 | 0.14 |
| | | 5 | 293–334 | 0.1 | 0.5958 | 0.05 |
| | | 5 | 293–334 | 0.1 | 0.6946 | 0.1 |
| | | 5 | 293–334 | 0.1 | 0.7932 | 0.16 |
| | | 5 | 293–334 | 0.1 | 0.8919 | 0.15 |
| Overall | | 45 | 293–334 | 0.1 | 0.10–0.89 | 0.16 |
| Zhang et al. [40] | 2015 | 9 | 298–354 | 0.1 | 0.1122 | 0.004 |
| Zhao et al. [41] | 2010 | 5 | 303–344 | 0.101325 | 0.1123 | 0.49 |
| $w_s$ data | | | | | | |

**Table 7** continued

| $w_s$ data | | | | | | |
|---|---|---|---|---|---|---|
| Authors<br>Authors | Year<br>Year | $N$<br>$N$ | $T$/K<br>$T$/K | $p$/MPa<br>$p$/MPa | $x$<br>$x$ | AARD/%<br>AARD/% |
| Hawrylak et al. [43] | 2000 | 69 | 298–319 | 0.101 325 | 0.01–0.98 | 0.72 |
| Jamal et al. [44] | 2016 | 5 | 298–319 | 0.101 325 | 0.0129 | 4.5 |
| | | 5 | 298–319 | 0.101 325 | 0.198 | 6.2 |
| | | 5 | 298–319 | 0.101 325 | 0.3 | 8 |
| | | 5 | 298–319 | 0.101 325 | 0.3989 | 8.5 |
| | | 5 | 298–319 | 0.101 325 | 0.4989 | 8.3 |
| | | 5 | 298–319 | 0.101 325 | 0.6955 | 6.4 |
| | | 5 | 298–319 | 0.101 325 | 0.8012 | 4.7 |
| | | 5 | 298–319 | 0.101 325 | 0.8882 | 3.1 |
| Overall | | 40 | 298–319 | 0.101 325 | 0.01–0.89 | 6.2 |
| $c_p$ data | | | | | | |
| Authors | Year | $N$ | $T$/K | $p$/MPa | $x$ | AARD/% |
| Page et al. [30] | 1993 | 48 | 283–314 | 0.101 325 | 0.00–1.00 | 1.2 |
| Vega-Maza et al. [174] | 2021 | 24 | 293–354 | 0.1–25 | 0.0318 | 0.91 |
| | | 24 | 293–354 | 0.1–25 | 0.0687 | 0.49 |
| | | 18 | 313–354 | 0.1–25 | 0.1121 | 0.76 |
| | | 24 | 293–354 | 0.1–25 | 0.1644 | 0.64 |
| Overall | | 90 | 293–354 | 0.1–25 | 0.03–0.16 | 0.70 |
| $x$ DEA + $(1-x)$ $H_2O$ | | | | | | |
| VLE data | | | | | | |

**Table 7** continued

$x$ DEA + $(1 - x)$ $H_2O$

VLE data

| Authors<br>Authors | Year<br>Year | $N$<br>$N$ | $N_x$<br>$N_x$ | $N_y$<br>$N_y$ | $T$/K<br>$T$/K | $p$/MPa<br>$p$/MPa | $x$<br>$x$ | $y$<br>$y$ | $AAD_x$<br>$AAD_x$ | $AAD_y$<br>$AAD_y$ |
|---|---|---|---|---|---|---|---|---|---|---|
| Abdi and Meisen [176] | 1999 | 48 | 48 | 5 | 0–446 | 4E−4–3E−2 | 0.34–0.98 | 0.00–0.11 | 3.0 | 0.46 |
| Cai et al. [165] | 1996 | 7 | 7 | 7 | 340–457 | 6.00E−03 | 0.70–0.99 | 0.01–0.74 | 1.8 | 3.0 |
| Horstmann et al. [177] | 2002 | 42 | 42 | 0 | 365.15 | 6E−4–8E−2 | 0.00–0.99 | | 1.4 | |
| Sidi-Boumedine et al. [175] | 2004 | 4 | 4 | 0 | 298–349 | 2E−3–3E−2 | 0.38–0.42 | | 28 | |
| Wilding et al. [178] | 1991 | 26 | 26 | 23 | 373–474 | 3E−3–1.6 | 0.02–0.95 | 0.00–0.14 | 3.2 | 0.063 |

$p\rho T$ data

| Authors | Year | $N$ | $T$/K | $p$/MPa | $x$ | AARD/% |
|---|---|---|---|---|---|---|
| Aguila-Hernandez et al. [186] | 2001 | 9 | 313–334 | 0.101 325 | 0.07–0.15 | 0.084 |
| Alvarez et al. [187] | 2006 | 6 | 298–324 | 0.101 325 | 0.1463 | 0.12 |
| Arcis et al. [179] | 2012 | 6 | 298–299 | 0.2–5.0 | 0.0294 | 0.26 |
| | | 6 | 298–299 | 0.2–5.0 | 0.0684 | 0.29 |
| Overall | | 12 | 298–299 | 0.2–5.0 | 0.03–0.07 | 0.27 |
| Chowdhury et al. [188] | 2010 | 5 | 303–324 | 0.101 325 | 0.0501 | 0.1 |
| | | 5 | 303–324 | 0.101 325 | 0.1004 | 0.089 |
| | | 5 | 303–324 | 0.101 325 | 0.1509 | 0.066 |
| | | 5 | 303–324 | 0.101 325 | 0.2006 | 0.11 |
| | | 5 | 303–324 | 0.101 325 | 0.3008 | 0.23 |
| | | 5 | 303–324 | 0.101 325 | 0.4014 | 0.35 |
| | | 5 | 303–324 | 0.101 325 | 0.5011 | 0.36 |
| | | 5 | 303–324 | 0.101 325 | 0.5957 | 0.28 |

**Table 7** continued

| *pρT* data | | | | | | |
|---|---|---|---|---|---|---|
| Authors | Year | *N* | *T*/K | *p*/MPa | *x* | AARD/% |
| | | 5 | 303–324 | 0.101 325 | 0.6968 | 0.15 |
| | | 5 | 303–324 | 0.101 325 | 0.8034 | 0.061 |
| | | 5 | 303–324 | 0.101 325 | 0.9012 | 0.041 |
| Overall | | 55 | 303–324 | 0.101 325 | 0.05–0.90 | 0.17 |
| Han et al. [189] | 2012 | 20 | 298–424 | 0.1–0.7 | 0.0684 | 0.15 |
| | | 20 | 298–424 | 0.1–0.7 | 0.1025 | 0.18 |
| | | 20 | 298–424 | 0.1–0.7 | 0.1463 | 0.19 |
| | | 20 | 298–424 | 0.1–0.7 | 0.2045 | 0.23 |
| | | 20 | 298–424 | 0.1–0.7 | 0.2856 | 0.3 |
| | | 20 | 298–424 | 0.1–0.7 | 0.4067 | 0.39 |
| | | 20 | 298–424 | 0.1–0.7 | 0.6066 | 0.35 |
| Overall | | 140 | 298–424 | 0.1–0.7 | 0.07–0.61 | 0.26 |
| Hsu and Li [190] | 1997 | 6 | 303–354 | 0.101 325 | 0.0411 | 0.077 |
| | | 6 | 303–354 | 0.101 325 | 0.0684 | 0.13 |
| Overall | | 12 | 303–354 | 0.101 325 | 0.04–0.07 | 0.11 |
| Hawrylak et al. [43] | 2000 | 69 | 298–319 | 0.101 325 | 0.01–0.98 | 0.14 |
| Jayarathna et al. [191] | 2012 | 14 | 293–424 | 0.1–0.8 | 0.1463 | 0.28 |
| | | 14 | 293–424 | 0.1–0.8 | 0.2045 | 0.34 |
| | | 14 | 293–424 | 0.1–0.8 | 0.2856 | 0.43 |
| | | 14 | 293–424 | 0.1–0.8 | 0.4067 | 0.5 |
| Overall | | 56 | 293–424 | 0.1–0.8 | 0.15–0.41 | 0.39 |
| Maham et al. [26] | 1994 | 7 | 298–354 | 0.101 325 | 0.009 | 0.034 |
| | | 7 | 298–354 | 0.101 325 | 0.0188 | 0.054 |

**Table 7** continued

| *pρT* data | | | | | | |
|---|---|---|---|---|---|---|
| Authors | Year | *N* | *T*/K | *p*/MPa | *x* | AARD/% |
| | | 7 | 298–354 | 0.101 325 | 0.0414 | 0.077 |
| | | 7 | 298–354 | 0.101 325 | 0.069 | 0.1 |
| | | 7 | 298–354 | 0.101 325 | 0.1028 | 0.13 |
| | | 7 | 298–354 | 0.101 325 | 0.1469 | 0.15 |
| | | 7 | 298–354 | 0.101 325 | 0.2054 | 0.18 |
| | | 7 | 298–354 | 0.101 325 | 0.2884 | 0.26 |
| | | 7 | 298–354 | 0.101 325 | 0.4026 | 0.37 |
| | | 7 | 298–354 | 0.101 325 | 0.4992 | 0.4 |
| | | 7 | 298–354 | 0.101 325 | 0.6059 | 0.31 |
| | | 7 | 298–354 | 0.101 325 | 0.7764 | 0.15 |
| | | 7 | 298–354 | 0.101 325 | 0.8012 | 0.13 |
| | | 7 | 298–354 | 0.101 325 | 0.8989 | 0.052 |
| | | 7 | 298–354 | 0.101 325 | 0.9438 | 0.025 |
| Overall | | 105 | 298–354 | 0.101 325 | 0.01–0.94 | 0.16 |
| Oyevaar et al. [180] | 1989 | 9 | 298 | 0.101 325 | 0.00–0.05 | 0.46 |
| Rebolledo-Libreros and Trejo [182] | 2006 | 3 | 313–334 | 0.101 325 | 0.0684 | 0.094 |
| Rinker et al. [183] | 1994 | 5 | 293–374 | 0.101 325 | 0.0187 | 0.11 |
| | | 5 | 293–374 | 0.101 325 | 0.0411 | 0.1 |
| | | 5 | 293–374 | 0.101 325 | 0.0684 | 0.14 |
| Overall | | 15 | 293–374 | 0.101 325 | 0.02–0.07 | 0.12 |
| Shojaeian and Haghtalab [184] | 2013 | 6 | 293–344 | 0.101 325 | 0.0684 | 0.12 |
| | | 6 | 293–344 | 0.101 325 | 0.1025 | 0.13 |
| Overall | | 12 | 293–344 | 0.101 325 | 0.07–0.10 | 0.13 |

**Table 7** continued

*pρT* data

| Authors | Year | *N* | *T*/K | *p*/MPa | *x* | AARD/% |
|---|---|---|---|---|---|---|
| Peacock [181] | 1915 | 10 | 298–344 | 0.101 325 | 0.0089 | 0.12 |
| | | 10 | 298–344 | 0.101 325 | 0.0187 | 0.13 |
| | | 10 | 298–344 | 0.101 325 | 0.0294 | 0.14 |
| | | 10 | 298–344 | 0.101 325 | 0.0411 | 0.14 |
| | | 10 | 298–344 | 0.101 325 | 0.054 | 0.14 |
| Overall | | 50 | 298–344 | 0.101 325 | 0.01–0.05 | 0.13 |
| Tseng and Thompson [36] | 1964 | 30 | 293–304 | 0.101 325 | 0.02–0.99 | 0.18 |
| Yang et al. [185] | 2012 | 8 | 283–354 | 0.101 325 | 0.0188 | 0.1 |
| | | 8 | 283–354 | 0.101 325 | 0.0411 | 0.15 |
| | | 8 | 283–354 | 0.101 325 | 0.0683 | 0.18 |
| | | 8 | 283–354 | 0.101 325 | 0.1025 | 0.2 |
| | | 8 | 283–354 | 0.101 325 | 0.1464 | 0.22 |
| | | 8 | 283–354 | 0.101 325 | 0.2061 | 0.27 |
| | | 8 | 283–354 | 0.101 325 | 0.2855 | 0.33 |
| | | 8 | 283–354 | 0.101 325 | 0.4073 | 0.36 |
| | | 8 | 283–354 | 0.101 325 | 0.4994 | 0.34 |
| | | 8 | 283–354 | 0.101 325 | 0.6053 | 0.29 |
| | | 8 | 283–354 | 0.101 325 | 0.7 | 0.23 |
| | | 8 | 283–354 | 0.101 325 | 0.8007 | 0.16 |
| Overall | | 96 | 283–354 | 0.101 325 | 0.02–0.80 | 0.24 |

$w_s$ data

| Authors | Year | *N* | *T*/K | *p*/MPa | *x* | AARD/% |
|---|---|---|---|---|---|---|

**Table 7** continued

| $w_s$ data<br>Authors | Year | $N$ | $T$/K | $p$/MPa | $x$ | AARD/% |
|---|---|---|---|---|---|---|
| Hawrylak et al. [43] | 2000 | 69 | 298–319 | 0.101 325 | 0.01–0.98 | 0.74 |

| $c_p$ data<br>Authors | Year | $N$ | $T$/K | $p$/MPa | $x$ | AARD/% |
|---|---|---|---|---|---|---|
| Vega-Maza et al. [174] | 2021 | 18 | 293–334 | 0.1–25 | 0.0187 | 0.69 |
| | | 24 | 293 354 | 0.1–25 | 0.0413 | 1.0 |
| | | 18 | 313–354 | 0.1–25 | | 0.97 |
| | | 24 | 293–354 | 0.1–25 | | 0.55 |
| Overall | | 84 | 293–354 | 0.1–25 | 0.01–0.11 | 0.81 |

$x$ MDEA + $(1 - x)$ $H_2O$

VLE data

| Authors | Year | $N$ | $N_x$ | $N_y$ | $T$/K | $p$/MPa | $x$ | $y$ | $AAD_x$ | $AAD_y$ |
|---|---|---|---|---|---|---|---|---|---|---|
| Ahmady et al. [193] | 2014 | 6 | 6 | | 303–354 | 4E−3–5E−2 | 0.0672 | | 100 | |
| Barreau et al. [194] | 2007 | 9 | 9 | | 341–404 | 1E−2–9E−2 | 0.60–0.94 | | 4.4 | |
| Dell'Era et al. [195] | 2010 | 29 | 29 | | 333–358 | 4E−3–6E−2 | 0.03–0.76 | | 4.8 | |
| Kim et al. [166] | 2008 | 57 | 57 | 57 | 312–374 | 6E−3–0.2 | 0.00–0.36 | 0.00–0.001 | 2.7 | 0.01 |
| Kuranov et al. [196] | 1996 | 4 | 4 | | 393–414 | 0.2–0.3 | 0.03–0.07 | | 1.2 | |
| Shokouhi and Ahmadi [197] | 2016 | 3 | 3 | | 313–344 | 6E−3–3E−2 | 0.1173 | | 2.1 | |
| Soames et al. [198] | 2018 | 33 | 33 | 33 | 323–459 | 1E−2–4E−2 | 0.07–0.99 | 0.00–0.41 | 4.4 | 0.23 |
| Voutsas et al. [199] | 2004 | 27 | 27 | | 350–459 | 4E−2–7E−2 | 0.06–0.93 | | 6.5 | |
| Xu et al. [200] | 1991 | 34 | 34 | | 326–382 | 1E−2–0.2 | 0.02–0.26 | | 3.4 | |

$p\rho T$ data

**Table 7** continued

| *pρT* data | | | | | | |
|---|---|---|---|---|---|---|
| Authors<br>Authors | Year<br>Year | *N*<br>*N* | *T*/K<br>*T*/K | *p*/MPa<br>*p*/MPa | *x*<br>*x* | AARD/%<br>AARD/% |
| Afkhamipour and Mofarahi [201] | 2018 | 6 | 298–324 | 0.1 | 0.04–0.06 | 0.13 |
| Aguila-Hernandez et al. [186] | 2001 | 9 | 313–334 | 0.101 325 | 0.06–0.13 | 0.12 |
| Al-Ghawas et al. [202] | 1989 | 10 | 288–334 | 0.101 325 | 0.0165 | 0.06 |
| | | 8 | 288–334 | 0.101 325 | 0.0364 | 0.037 |
| | | 8 | 288–334 | 0.101 325 | 0.0609 | 0.15 |
| | | 7 | 288–324 | 0.101 325 | 0.0916 | 0.34 |
| | | 10 | 288–334 | 0.101 325 | 0.1313 | 0.41 |
| Overall | | 43 | 288–334 | 0.101 325 | 0.02–0.13 | 0.2 |
| Alvarez et al. [187] | 2006 | 6 | 298–324 | 0.101 325 | 0.1313 | 0.34 |
| Arcis et al. [203] | 2008 | 5 | 298–299 | 0.2–5.0 | 0.026 | 0.12 |
| | | 5 | 298–299 | 0.2–5.0 | 0.0609 | 0.01 |
| Overall | | 10 | 298–299 | 0.2–5.0 | 0.03–0.06 | 0.063 |
| Bernal-Garcia et al. [204] | 2003 | 17 | 283–364 | 0.101 325 | 0.0168 | 0.034 |
| | | 17 | 283–364 | 0.101 325 | 0.0604 | 0.091 |
| | | 17 | 283–364 | 0.101 325 | 0.0902 | 0.22 |
| | | 17 | 283–364 | 0.101 325 | 0.1293 | 0.33 |
| | | 17 | 283–364 | 0.101 325 | 0.1823 | 0.36 |
| | | 17 | 283–364 | 0.101 325 | 0.2571 | 0.36 |
| | | 17 | 283–364 | 0.101 325 | 0.3715 | 0.37 |
| | | 17 | 283–364 | 0.101 325 | 0.4849 | 0.4 |
| | | 17 | 283–364 | 0.101 325 | 0.5828 | 0.42 |
| | | 17 | 283–364 | 0.101 325 | 0.7175 | 0.39 |
| | | 17 | 283–364 | 0.101 325 | 0.743 | 0.37 |

**Table 7** continued

| *pρT* data | | | | | | |
|---|---|---|---|---|---|---|
| Authors | Year | *N* | *T*/K | *p*/MPa | *x* | AARD/% |
| Overall | | 187 | 283–364 | 0.101 325 | 0.02–0.74 | 0.3 |
| Choi et al. [205] | 2014 | 1 | 313 | 0.101 325 | 0.0609 | 0.21 |
| Chowdhury et al. [188] | 2009 | 5 | 303–324 | 0.101 325 | 0.0501 | 0.025 |
| | | 5 | 303–324 | 0.101 325 | 0.1 | 0.24 |
| | | 5 | 303–324 | 0.101 325 | 0.1501 | 0.32 |
| | | 5 | 303–324 | 0.101 325 | 0.1992 | 0.38 |
| | | 5 | 303–324 | 0.101 325 | 0.2459 | 0.39 |
| | | 5 | 303–324 | 0.101 325 | 0.2961 | 0.33 |
| | | 5 | 303–324 | 0.101 325 | 0.3981 | 0.25 |
| | | 5 | 303–324 | 0.101 325 | 0.5001 | 0.18 |
| | | 5 | 303–324 | 0.101 325 | 0.5938 | 0.14 |
| | | 5 | 303–324 | 0.101 325 | 0.7022 | 0.12 |
| | | 5 | 303–324 | 0.101 325 | 0.7945 | 0.1 |
| | | 5 | 303–324 | 0.101 325 | 0.9015 | 0.074 |
| Overall | | 60 | 303–324 | 0.101 325 | 0.05–0.90 | 0.21 |
| Damanafshan et al. [206] | 2018 | 13 | 298–349 | <0.1 | 0.05–0.13 | 0.2 |
| Das et al. [207] | 2016 | 15 | 298–323 | 0.1 | 0.02–0.08 | 0.075 |
| Derks et al. [208] | 2008 | 20 | 293–324 | 1 | 0.02–0.12 | 0.18 |
| Dey et al. [209] | 2018 | 8 | 303–334 | <0.1 | 0.04–0.06 | 0.19 |
| Fischer et al. [210] | 1999 | 26 | 293–374 | 0.101 325 | 0.01–0.84 | 0.51 |
| Foo et al. [211] | 2015 | 6 | 313–354 | 0.101 325 | 0.04–0.11 | 0.91 |
| Gao et al. [212] | 2013 | 6 | 313–354 | 0.101 325 | 0.04–0.13 | 0.14 |
| Han et al. [189] | 2012 | 20 | 298–424 | 0.1–0.7 | 0.0609 | 0.14 |

**Table 7** continued

| *ppT* data | | | | | | |
|---|---|---|---|---|---|---|
| Authors | Year | *N* | *T*/K | *p*/MPa | *x* | AARD/% |
| | | 20 | 298–424 | 0.1–0.7 | 0.0916 | 0.28 |
| | | 20 | 298–424 | 0.1–0.7 | 0.1313 | 0.34 |
| | | 20 | 298–424 | 0.1–0.7 | 0.1848 | 0.26 |
| | | 20 | 298–424 | 0.1–0.7 | 0.2608 | 0.23 |
| | | 20 | 298–424 | 0.1–0.7 | 0.3768 | 0.3 |
| | | 20 | 298–424 | 0.1–0.7 | 0.5764 | 0.52 |
| Overall | | 140 | 298–424 | 0.1–0.7 | 0.06–0.58 | 0.3 |
| Hawrylak et al. [43] | 2000 | 72 | 298–319 | 0.101 325 | 0.01–0.98 | 0.29 |
| Hawrylak et al. [213] | 2006 | 96 | 283–525 | 0.1–20.2 | 0.00–0.05 | 0.24 |
| Jayarathna et al. [191] | 2012 | 14 | 293–424 | 0.1–0.8 | 0.1313 | 0.27 |
| | | 14 | 293–424 | 0.1–0.8 | 0.1848 | 0.25 |
| | | 14 | 293–424 | 0.1–0.8 | 0.2608 | 0.2 |
| | | 14 | 293–424 | 0.1–0.8 | 0.3768 | 0.34 |
| Overall | | 56 | 293–424 | 0.1–0.8 | 0.13–0.38 | 0.26 |
| Karunarathne et al. [214] | 2020 | 11 | 293–344 | 0.101 325 | 0.0609 | 0.056 |
| Lawal [215] | 2016 | 15 | 293–364 | 0.101 325 | 0.0611 | 0.038 |
| | | 15 | 293–364 | 0.101 325 | 0.0915 | 0.16 |
| | | 15 | 293–364 | 0.101 325 | 0.1313 | 0.23 |
| Overall | | 45 | 293–364 | 0.101 325 | 0.06–0.13 | 0.14 |
| Leo et al. [216] | 2016 | 6 | 313–354 | 0.101 325 | 0.04–0.11 | 0.59 |
| Li and Lie [24] | 1994 | 10 | 303–354 | 0.101 325 | 0.04–0.06 | 0.032 |
| Li and Shen [217] | 1992 | 8 | 303–354 | 0.101 325 | 0.0609 | 0.05 |
| Lu et al. [218] | 2011 | 4 | 288–314 | 0.101 325 | 0.02–0.04 | 0.11 |

**Table 7** continued

| *ppT* data | | | | | | |
|---|---|---|---|---|---|---|
| Authors | Year | *N* | *T*/K | *p*/MPa | *x* | AARD/% |
| Lu et al. [219] | 2012 | 4 | 288–314 | 0.101 325 | 0.02–0.04 | 0.11 |
| Maham et al. [220] | 1995 | 112 | 298–354 | 0.101 325 | 0.01–0.95 | 0.2 |
| Mandal et al. [28] | 2003 | 7 | 293–324 | 0.101 325 | 0.0609 | 0.2 |
| Muhammad et al. [221] | 2008 | 153 | 298–339 | 0.101 325 | 0.01–0.75 | 0.2 |
| Na et al. [222] | 2018 | 40 | 303–334 | 0.101 325 | 0.05–0.90 | 0.23 |
| Paul and Mandal [223] | 2006 | 9 | 288–333 | 0.101 325 | 0.02–0.06 | 0.15 |
| Razavizadeh et al. [224] | 2017 | 8 | 288–324 | 0.101 325 | 0.0079 | 0.42 |
| | | 8 | 288–324 | 0.101 325 | 0.0165 | 0.4 |
| | | 8 | 288–324 | 0.101 325 | 0.0364 | 0.66 |
| | | 8 | 288–324 | 0.101 325 | 0.0609 | 0.52 |
| | | 8 | 288–324 | 0.101 325 | 0.0916 | 0.64 |
| Overall | | 40 | 288–324 | 0.101 325 | 0.01–0.09 | 0.53 |
| Rebolledo-Libreros and Trejo [182] | 2006 | 3 | 313–334 | 0.101 325 | 0.0609 | 0.054 |
| Rinker et al. [183] | 1994 | 15 | 333–374 | 0.101 325 | 0.02–0.13 | 0.091 |
| Rinker et al. [225] | 2000 | 6 | 298–314 | 0.101 325 | 0.02–0.13 | 0.25 |
| Sadegh [226] | 2013 | 47 | 313–354 | 0.101 325 | 0.02–0.58 | 0.15 |
| Sairi et al. [227] | 2015 | 9 | 293–364 | 0.101 325 | 0.0192 | 0.38 |
| | | 9 | 293–364 | 0.101 325 | 0.1168 | 0.28 |
| Overall | | 18 | 293–364 | 0.101 325 | 0.02–0.12 | 0.33 |
| Shojaeian and Haghtalab [184] | 2013 | 6 | 293–344 | 0.101 325 | 0.0609 | 0.46 |
| | | 6 | 293–344 | 0.101 325 | 0.0916 | 0.17 |
| Overall | | 12 | 293–344 | 0.101 325 | 0.06–0.09 | 0.32 |
| Shokouhi and Ahmadi [197] | 2016 | 3 | 313–344 | <0.1 | 0.1173 | 0.25 |

**Table 7** continued

| *pρT* data | | | | | | |
|---|---|---|---|---|---|---|
| Authors | Year | *N* | *T*/K | *p*/MPa | *x* | AARD/% |
| Shokouhi et al. [228] | 2015 | 4 | 303–364 | 0.1 | 0.1101 | 0.44 |
| Sobrino et al. [32] | 2016 | 120 | 293–394 | 0.1–140 | 0.0165 | 0.07 |
| | | 120 | 293–394 | 0.1–140 | 0.0365 | 0.096 |
| | | 120 | 293–394 | 0.1–140 | 0.0609 | 0.09 |
| | | 120 | 293–394 | 0.1–140 | 0.0916 | 0.16 |
| Overall | | 480 | 293–394 | 0.1–140 | 0.02–0.09 | 0.1 |
| Speyer et al. [229] | 2010 | 6 | 293.15 | 0.101 325 | 0.03–0.18 | 0.44 |
| Weiland et al. [38] | 1998 | 4 | 298.15 | 0.101 325 | 0.06–0.18 | 0.61 |
| Welsh and Davis [230] | 1995 | 5 | 283–354 | 0.101 325 | 0.1313 | 0.43 |
| Yin et al. [39] | 2017 | 5 | 293–334 | 0.1 | 0.1 | 0.23 |
| | | 5 | 293–334 | 0.1 | 0.1991 | 0.45 |
| | | 5 | 293–334 | 0.1 | 0.2985 | 0.38 |
| | | 5 | 293–334 | 0.1 | 0.3975 | 0.31 |
| | | 5 | 293–334 | 0.1 | 0.4963 | 0.28 |
| | | 5 | 293–334 | 0.1 | 0.5949 | 0.26 |
| | | 5 | 293–334 | 0.1 | 0.6934 | 0.23 |
| | | 5 | 293–334 | 0.1 | 0.7916 | 0.19 |
| | | 5 | 293–334 | 0.1 | 0.8896 | 0.12 |
| Overall | | 45 | 293–334 | 0.1 | 0.10–0.89 | 0.27 |
| Yusoff et al. [231] | 2013 | 5 | 303–364 | 0.101 325 | 0.0441 | 0.49 |
| | | 5 | 303–364 | 0.101 325 | 0.1137 | 1.3 |
| Overall | | 10 | 303–364 | 0.101 325 | 0.04–0.11 | 0.9 |
| Zhao et al. [41] | 2010 | 5 | 303–344 | 0.1 | 0.0609 | 0.23 |

**Table 7** continued

*ppT* data

| Authors | Year | *N* | *T*/K | *p*/MPa | *x* | AARD/% |
|---|---|---|---|---|---|---|
| Zheng et al. [232] | 2020 | 8 | 303–304 | 0.5–4.0 | 0.06–0.13 | 0.26 |
| Zuniga-Morena et al. [233] | 2007 | 100 | 313–363 | 1.0–20.0 | 0.0369 | 0.28 |
| | | 80 | 313–343 | 1.0–20.2 | 0.0607 | 0.064 |
| | | 120 | 313–363 | 1.0–20.0 | 0.0893 | 0.15 |
| | | 120 | 313–363 | 1.0–20.0 | 0.1302 | 0.2 |
| Overall | | 420 | 313–363 | 1.0–20.2 | 0.04–0.13 | 0.18 |

$w_s$ data

| Authors | Year | *N* | *T*/K | *p*/MPa | *x* | AARD/% |
|---|---|---|---|---|---|---|
| Hawrylak et al. [43] | 2000 | 72 | 298–319 | 0.101325 | 0.01–0.98 | 2.3 |
| Hawrylak et al. [213] | 2006 | 24 | 283–314 | 0.1 | 0.01–0.04 | 2.3 |

$c_p$ data

| Authors | Year | *N* | *T*/K | *p*/MPa | *x* | AARD/% |
|---|---|---|---|---|---|---|
| Chen et al. [235] | 2001 | 11 | 303–354 | 0.101325 | 0.2 | 2.8 |
| | | 11 | 303–354 | 0.101325 | 0.4 | 4.9 |
| | | 11 | 303–354 | 0.101325 | 0.6 | 5.8 |
| | | 11 | 303–354 | 0.101325 | 0.8 | 4.2 |
| Overall | | 44 | 303–354 | 0.101325 | 0.20–0.80 | 4.4 |
| Chiu and Li [236] | 1999 | 11 | 303–354 | 0.101325 | 0.0432 | 0.3 |
| | | 11 | 303–354 | 0.101325 | 0.1313 | 1.3 |
| Overall | | 22 | 303–354 | 0.101325 | 0.04–0.13 | 0.82 |
| Hawrylak et al. [213] | 2006 | 37 | 283–329 | 0.1 | 0.00–0.04 | 79 |

**Table 7** continued

$c_p$ data

| Authors | Year | $N$ | $T$/K | $p$/MPa | $x$ | AARD/% |
|---|---|---|---|---|---|---|
| Hayden et al. [237] | 1983 | 6 | 298–349 | 0.101325 | 0.04–0.13 | 1.9 |
| Vega-Maza et al. [174] | 2021 | 23 | 293–354 | 0.1–25.0 | 0.0365 | 2.7 |
| | | 19 | 313–354 | 0.1–25.0 | 0.0608 | 4.2 |
| Overall | | 42 | 293–354 | 0.1–25.0 | 0.04–0.06 | 3.4 |
| Weiland et al. [238] | 1997 | 4 | 298.15 | 0.101325 | 0.06–0.18 | 1.7 |
| Zhang et al. [234] | 2002 | 19 | 278–369 | 0.101325 | 0.03 | 2 |
| | | 19 | 278–369 | 0.101325 | 0.06 | 2.6 |
| | | 19 | 278–369 | 0.101325 | 0.1001 | 2.8 |
| | | 19 | 278–369 | 0.101325 | 0.1997 | 1.9 |
| | | 19 | 278–369 | 0.101325 | 0.2999 | 0.53 |
| | | 19 | 278–369 | 0.101325 | 0.3992 | 0.73 |
| | | 19 | 278–369 | 0.101325 | 0.4994 | 1.3 |
| | | 19 | 278–369 | 0.101325 | 0.5967 | 1.5 |
| | | 19 | 278–369 | 0.101325 | 0.6978 | 1.5 |
| | | 19 | 278–369 | 0.101325 | 0.8016 | 1.3 |
| | | 19 | 278–369 | 0.101325 | 0.894 | 1.2 |
| | | 19 | 278–369 | 0.101325 | 0.9381 | 1.1 |
| Overall | | 228 | 278–369 | 0.101325 | 0.03–0.94 | 1.5 |

$x$ MDEA + $(1 - x)$ $CO_2$

VLE data

| Authors | Year | $N$ | $N_x$ | $N_y$ | $T$/K | $p$/MPa | $x$ | $y$ | $AAD_x$ | $AAD_y$ |
|---|---|---|---|---|---|---|---|---|---|---|
| Akbar [239] | 2013 | 24 | 24 | | 298–324 | 0.1–2.9 | 0.50–0.97 | | 3.2 | |

**Table 7** continued

| $x$ MDEA + $(1-x)$ $CO_2$ | | | | | | | | | | |
|---|---|---|---|---|---|---|---|---|---|---|
| VLE data | | | | | | | | | | |
| Authors | Year | $N$ | $N_x$ | $N_y$ | $T$/K | $p$/MPa | $x$ | $y$ | $AAD_x$ | $AAD_y$ |
| Sadegh [226] | 2013 | 6 | 6 | | 313–354 | 0.1 | 0.96–0.99 | | 0.76 | |
| $x$ MDEA + $(1-x)$ $CH_4$ | | | | | | | | | | |
| VLE data | | | | | | | | | | |
| Authors | Year | $N$ | $N_x$ | $N_y$ | $T$/K | $p$/MPa | $x$ | $y$ | $AAD_x$ | $AAD_y$ |
| Jou and Mather [240] | 2006 | 47 | 47 | | 298–404 | 0.1–20.3 | 0.91–1.00 | | 0.35 | |
| $x$ MDEA + $(1-x)$ MEA | | | | | | | | | | |
| $c_p$ data | | | | | | | | | | |
| Authors | Year | $N$ | | | $T$/K | $p$/MPa | $x$ | | AARD/% | |
| Chen et al. [235] | 2001 | 11 | | | 303–354 | 0.101325 | 0.2 | | 1.5 | |
| | | 11 | | | 303–354 | 0.101325 | 0.4 | | 2.2 | |
| | | 11 | | | 303–354 | 0.101325 | 0.6 | | 2.5 | |
| | | 11 | | | 303–354 | 0.101325 | 0.8 | | 2.0 | |
| Overall | | 44 | | | 303–354 | 0.101325 | 0.20–0.80 | | 2.0 | |

$AAD_x$ and $AAD_y$ are given with respect to composition in mol% discussed in this work. For the rows labeled "overall", the AARD is calculated between the EOS and the complete dataset. All stated compositions are on a molar basis

**Table 8** Overview of the available thermodynamic property data of ternary mixtures and the average absolute relative deviation (AARD) calculated with the corresponding new equation of state

$x_1$ $CO_2$ + $x_2$ $H_2O$ + $x_3$ $CH_4$

VLE data

| Authors | Year | $N$ | $N_x$ | $N_y$ | $T$/K | $p$/MPa | $x_1$ | $x_2$ | $x_3$ | $y_1$ | $y_2$ | $y_3$ | $AAD_{x_1}$ | $AAD_{x_2}$ | $AAD_{x_3}$ | $AAD_{y_1}$ | $AAD_{y_2}$ | $AAD_{y_3}$ |
|---|---|---|---|---|---|---|---|---|---|---|---|---|---|---|---|---|---|---|
| Dhima et al. [247] | 1999 | 9 | 9 | | 344 | 10.0–100 | 0.00–0.02 | 0.00–0.01 | 0.98–1.00 | | | | 0.039 | 0.081 | 0.041 | | | |
| Ghafri et al. [248] | 2014 | 16 | 16 | 16 | 323–424 | 1.91–18.1 | 0.00–0.02 | 0.98–1.00 | 0.00–0.01 | 0.32–0.51 | 0.00–0.35 | 0.32–0.51 | 0.047 | 0.092 | 0.046 | 0.853 | 1.70 | 0.848 |
| Song and Kobayashi [308] | 1990 | 21 | | 21 | 298–324 | 6.20–13.8 | | | | 0.94–0.95 | 0.00–0.01 | 0.05 | | | | 0.060 | 0.062 | 0.002 |
| Qin et al. 2008 [100] | 2008 | 21 | 21 | 21 | 324–377 | 10.5–50.6 | 0.00–0.03 | 0.97–1.00 | 0.00–0.01 | 0.32–0.77 | 0.00–0.03 | 0.22–0.68 | 0.069 | 0.101 | 0.033 | 0.409 | 0.711 | 0.302 |

$x_1$ $CO_2$ + $x_2$ $N_2$ + $x_3$ Ar

VLE data

| Authors | Year | $N$ | $N_x$ | $N_y$ | $T$/K | $p$/MPa | $x_1$ | $x_2$ | $x_3$ | $y_1$ | $y_2$ | $y_3$ | $AAD_{x_1}$ | $AAD_{x_2}$ | $AAD_{x_3}$ | $AAD_{y_1}$ | $AAD_{y_2}$ | $AAD_{y_3}$ |
|---|---|---|---|---|---|---|---|---|---|---|---|---|---|---|---|---|---|---|
| Ke et al. [257] | 2017 | 63 | 31 | 32 | 267–303 | 3.10–8.96 | 0.89–0.98 | 0.01–0.05 | 0.01–0.05 | 0.89–0.98 | 0.01–0.05 | 0.01–0.05 | 0.267 | 0.413 | 0.459 | 0.302 | 0.297 | 0.223 |

$p\rho T$ data

| Authors | Year | $N$ | $T$/K | $p$/MPa | $x_1$ | $x_2$ | $x_3$ | AARD/% |
|---|---|---|---|---|---|---|---|---|
| Ke et al. [257] | 2017 | 35 | 293 | 10.9–21.9 | 0.89 | 0.05 | 0.06 | 0.358 |
| | | 108 | 303–334 | 1.51–22.6 | 0.90 | 0.05 | 0.05 | 0.458 |
| Overall | | 143 | 293–334 | 1.51–22.6 | 0.89–0.90 | 0.05 | 0.05–0.06 | 0.433 |
| Yang et al. [258] | 2015 | 75 | 323–424 | 2.98–31.0 | 0.90 | 0.05 | 0.05 | 0.122 |
| | | 75 | 323–424 | 2.98–31.0 | 0.95 | 0.04 | 0.01 | 0.074 |

**Table 8** continued

$p\rho T$ data

| Authors | Year | $N$ | $T$/K | $p$/MPa | $x_1$ | $x_2$ | $x_3$ | AARD/% |
|---|---|---|---|---|---|---|---|---|
| Overall | | 150 | 323–424 | 2.98–31.0 | 0.90–0.95 | 0.04–0.05 | 0.01–0.05 | 0.098 |

$x_1$ $CO_2$ + $x_2$ $N_2$ + $x_3$ $H_2$

VLE data

| Authors | Year | $N$ | $N_x$ | $N_y$ | $T$/K | $p$/MPa | $x_1$ | $x_2$ | $x_3$ | $y_1$ | $y_2$ | $y_3$ | $AAD_{x_1}$ | $AAD_{x_2}$ | $AAD_{x_3}$ | $AAD_{y_1}$ | $AAD_{y_2}$ | $AAD_{y_3}$ |
|---|---|---|---|---|---|---|---|---|---|---|---|---|---|---|---|---|---|---|
| Tenorio et al. [259] | 2015 | 71 | 35 | 36 | 252–302 | 2.14–9.82 | 0.93–0.95 | 0.02–0.04 | 0.03 | 0.93–0.95 | 0.02–0.04 | 0.03 | 0.734 | 0.307 | 0.426 | 4.42 | 1.72 | 3.21 |

$p\rho T$ data

| Authors | Year | $N$ | $T$/K | $p$/MPa | $x_1$ | $x_2$ | $x_3$ | AARD/% |
|---|---|---|---|---|---|---|---|---|
| Kritschewsky and Markov [260] | 1940 | 30 | 273–474 | 5.0–50.7 | 0.33 | 0.35 | 0.32 | 1.56 |
| | | 30 | 273–474 | 5.0–50.7 | 0.22 | 0.55 | 0.23 | 2.12 |
| Overall | | 60 | 273–474 | 5.0–50.7 | 0.22–0.33 | 0.35–0.55 | 0.23–0.32 | 1.84 |

$x_1$ $CO_2$ + $x_2$ $O_2$ + $x_3$ $H_2$

$p\rho T$ data

| Authors | Year | $N$ | $T$/K | $p$/MPa | $x_1$ | $x_2$ | $x_3$ | AARD/% |
|---|---|---|---|---|---|---|---|---|
| Guruaja et al. [256] | 1967 | 12 | 296–300 | 0.1 | 0.09–0.78 | 0.12–0.50 | 0.06–0.75 | 1.01 |

$x_1$ $CO_2$ + $x_2$ $O_2$ + $x_3$ Ar

VLE data

| Authors | Year | $N$ | $N_x$ | $N_y$ | $T$/K | $p$/MPa | $x_1$ | $x_2$ | $x_3$ | $y_1$ | $y_2$ | $y_3$ | $AAD_{x_1}$ | $AAD_{x_2}$ | $AAD_{x_3}$ | $AAD_{y_1}$ | $AAD_{y_2}$ | $AAD_{y_3}$ |
|---|---|---|---|---|---|---|---|---|---|---|---|---|---|---|---|---|---|---|

**Table 8** continued

$x_1$ $CO_2$ + $x_2$ $O_2$ + $x_3$ Ar

VLE data

| Authors | Year | $N$ | $N_x$ | $N_y$ | $T$/K | $p$/MPa | $x_1$ | $x_2$ | $x_3$ | $y_1$ | $y_2$ | $y_3$ | $AAD_{x_1}$ | $AAD_{x_2}$ | $AAD_{x_3}$ | $AAD_{y_1}$ | $AAD_{y_2}$ | $AAD_{y_3}$ |
|---|---|---|---|---|---|---|---|---|---|---|---|---|---|---|---|---|---|---|
| Coquelet et al. [123] | 2004 | 28 | 18 | 18 | 253–294 | 2.33–7.64 | 0.94–1.00 | 0.00–0.03 | 0.00–0.03 | 0.53–0.93 | 0.04–0.24 | 0.04–0.23 | 0.354 | 0.174 | 0.179 | 1.360 | 0.685 | 0.675 |

$x_1$ $CO_2$ + $x_2$ $O_2$ + $x_3$ $SO_2$

VLE data

| Authors | Year | $N$ | $N_x$ | $N_y$ | $T$/K | $p$/MPa | $x_1$ | $x_2$ | $x_3$ | $y_1$ | $y_2$ | $y_3$ | $AAD_{x_1}$ | $AAD_{x_2}$ | $AAD_{x_3}$ | $AAD_{y_1}$ | $AAD_{y_2}$ | $AAD_{y_3}$ |
|---|---|---|---|---|---|---|---|---|---|---|---|---|---|---|---|---|---|---|
| Coquelet et al. [123] | 2004 | 31 | 31 | 31 | 253–294 | 1.94–6.47 | 0.88–0.94 | 0.00–0.03 | 0.05–0.12 | 0.67–0.94 | 0.03–0.33 | 0.00–0.04 | 0.095 | 0.165 | 0.128 | 0.337 | 0.508 | 0.235 |

$x_1$ $CO_2$ + $x_2$ Ar + $x_3$ CO

$w_s$ data

| Authors | Year | $N$ | $T$/K | $p$/MPa | $x_1$ | $x_2$ | $x_3$ | AARD/% |
|---|---|---|---|---|---|---|---|---|
| Al-Siyabi [51] | 2013 | 58 | 268–302 | 10.2–41.3 | 0.97 | 0.01 | 0.02 | 1.28 |

$x_1$ $CO_2$ + $x_2$ Ar + $x_3$ $H_2$

VLE data

| Authors | Year | $N$ | $N_x$ | $N_y$ | $T$/K | $p$/MPa | $x_1$ | $x_2$ | $x_3$ | $y_1$ | $y_2$ | $y_3$ | $AAD_{x_1}$ | $AAD_{x_2}$ | $AAD_{x_3}$ | $AAD_{y_1}$ | $AAD_{y_2}$ | $AAD_{y_3}$ |
|---|---|---|---|---|---|---|---|---|---|---|---|---|---|---|---|---|---|---|
| Ke et al. [257] | 2017 | 29 | 12 | 17 | 268–302 | 3.26–9.08 | 0.95 | 0.02 | 0.03 | 0.95 | 0.02 | 0.03 | 0.164 | 0.414 | 0.276 | 0.157 | 2.02 | 2.11 |

**Table 8** continued

$x_1$ $CO_2$ + $x_2$ CO + $x_3$ $H_2$

VLE data

| Authors | Year | $N$ | $N_x$ | $N_y$ | $T$/K | $p$/MPa | $x_1$ | $x_2$ | $x_3$ | $y_1$ | $y_2$ | $y_3$ | $AAD_{x_1}$ | $AAD_{x_2}$ | $AAD_{x_3}$ | $AAD_{y_1}$ | $AAD_{y_2}$ | $AAD_{y_3}$ |
|---|---|---|---|---|---|---|---|---|---|---|---|---|---|---|---|---|---|---|
| Kaminishi et al. [269] | 1968 | 31 | 31 | 31 | 233–284 | 5.06–20.3 | 0.52–0.98 | 0.01–0.34 | 0.00–0.15 | 0.17–0.73 | 0.07–0.57 | 0.03–0.67 | 0.543 | 0.268 | 0.275 | 1.28 | 0.588 | 0.694 |
| Yokoyama et al. [270] | 1988 | 52 | 52 | | 253–304 | 4.02–8.82 | 0.96–0.99 | 0.00–0.04 | 0.00–0.01 | | | | 0.236 | 1.50 | 1.31 | | | |

$p\rho T$ data

| Authors | Year | $N$ | $T$/K | $p$/MPa | $x_1$ | $x_2$ | $x_3$ | AARD/% |
|---|---|---|---|---|---|---|---|---|
| Cipollina et al. [271] | 2007 | 8 | 308–343 | 9.30–12.2 | 0.84 | 0.07 | 0.09 | 1.50 |
| | | 8 | 308–343 | 18.0–22.7 | 0.55 | 0.21 | 0.24 | 4.77 |
| | | 8 | 308–343 | 19.5–27.6 | 0.76 | 0.12 | 0.12 | 1.97 |
| | | 8 | 308–343 | 31.9–41.7 | 0.59 | 0.20 | 0.21 | 0.152 |
| | | 8 | 308–343 | 31.0–43.7 | 0.72 | 0.13 | 0.15 | 0.782 |
| | | 8 | 308–343 | 21.9–36.6 | 0.88 | 0.05 | 0.07 | 0.748 |
| | | 8 | 308–343 | 23.2–38.6 | 0.88 | 0.07 | 0.05 | 0.156 |
| | | 8 | 308–343 | 24.2–41.6 | 0.91 | 0.02 | 0.07 | 0.062 |
| | | 8 | 308–343 | 29.3–48.0 | 0.88 | 0.06 | 0.06 | 0.066 |
| | | 8 | 308–343 | 24.9–43.0 | 0.91 | 0.07 | 0.02 | 0.434 |
| | | 8 | 308–343 | 28.3–49.3 | 0.93 | 0.03 | 0.04 | 0.1255 |
| Overall | | 88 | 308–343 | 9.30–49.3 | 0.55–0.93 | 0.03–0.21 | 0.02–0.24 | 0.979 |

**Table 8** continued

$x_1$ $CO_2$ + $x_2$ $H_2$ + $x_3$ $CH_4$

VLE data

| Authors | Year | $N$ | $N_x$ | $N_y$ | $T$/K | $p$/MPa | $x_1$ | $x_2$ | $x_3$ | $y_1$ | $y_2$ | $y_3$ | $AAD_{x_1}$ | $AAD_{x_2}$ | $AAD_{x_3}$ | $AAD_{y_1}$ | $AAD_{y_2}$ | $AAD_{y_3}$ |
|---|---|---|---|---|---|---|---|---|---|---|---|---|---|---|---|---|---|---|
| Freitag and Robinson [272] | 1986 | 32 | 31 | 32 | 227–259 | 6.89–27.6 | 0.51–0.95 | 0.00–0.23 | 0.02–0.41 | 0.10–0.49 | 0.08–0.83 | 0.05–0.70 | 0.576 | 0.410 | 0.167 | 1.55 | 1.14 | 0.403 |

$p\rho T$ data

| Authors | Year | $N$ | $T$/K | $p$/MPa | $x_1$ | $x_2$ | $x_3$ | AARD/% |
|---|---|---|---|---|---|---|---|---|
| Freitag and Robinson [272] | 1986 | 57 | 227–259 | 6.89–27.6 | 0.10–0.95 | 0.00–0.83 | 0.02–0.70 | 3.30 |
| Cheng et al. [273] | 2019 | 8 | 673 | 0.59–22.1 | 0.195 | 0.603 | 0.202 | 0.299 |

$x_1$ $CO_2$ + $x_2$ $CH_4$ + $x_3$ $H_2S$

VLE data

| Authors | Year | $N$ | $N_x$ | $N_y$ | $T$/K | $p$/MPa | $x_1$ | $x_2$ | $x_3$ | $y_1$ | $y_2$ | $y_3$ | $AAD_{x_1}$ | $AAD_{x_2}$ | $AAD_{x_3}$ | $AAD_{y_1}$ | $AAD_{y_2}$ | $AAD_{y_3}$ |
|---|---|---|---|---|---|---|---|---|---|---|---|---|---|---|---|---|---|---|
| Hensel and Massoth [274] | 1964 | 17 | 17 | 17 | 227–237 | 2.06–4.83 | 0.10–0.78 | 0.04–0.27 | 0.12–0.83 | 0.02–0.55 | 0.38–0.90 | 0.02–0.21 | 0.696 | 1.53 | 0.837 | 1.58 | 3.32 | 1.78 |
| Morris and Byers [275] | 1991 | 3 | 3 | 3 | 270 | 4.10–6.44 | 0.66–0.69 | 0.04–0.12 | 0.19–0.30 | 0.48–0.63 | 0.22–0.41 | 0.11–0.15 | 1.21 | 2.15 | 0.935 | 1.56 | 2.71 | 1.14 |
| Ng et al. [276] | 1985 | 14 | 14 | 14 | 198–286 | 1.50–11.9 | 0.07–0.15 | 0.04–0.38 | 0.49–0.87 | 0.03–0.11 | 0.50–0.95 | 0.02–0.40 | 0.296 | 3.54 | 3.25 | 0.072 | 1.85 | 1.80 |
| Robinson and Bailey [277] | 1957 | 17 | 17 | 17 | 311 | 4.13–12.5 | 0.02–0.57 | 0.00–0.29 | 0.37–0.96 | 0.04–0.58 | 0.05–0.44 | 0.31–0.70 | 0.527 | 0.655 | 1.18 | 0.526 | 1.54 | 2.07 |
| | 1959 | 20 | 20 | 20 | 277–345 | 2.75–11.1 | 0.01–0.68 | 0.01–0.38 | 0.14–0.94 | 0.02–0.51 | 0.03–0.61 | 0.17–0.84 | 1.07 | 2.14 | 2.81 | 0.802 | 2.56 | 2.89 |

**Table 8** continued

$x_1$ $CO_2$ + $x_2$ $CH_4$ + $x_3$ $H_2S$

VLE data

| Authors | Year | $N$ | $N_x$ | $N_y$ | $T$/K | $p$/MPa | $x_1$ | $x_2$ | $x_3$ | $y_1$ | $y_2$ | $y_3$ | $AAD_{x_1}$ | $AAD_{x_2}$ | $AAD_{x_3}$ | $AAD_{y_1}$ | $AAD_{y_2}$ | $AAD_{y_3}$ |
|---|---|---|---|---|---|---|---|---|---|---|---|---|---|---|---|---|---|---|
| Robinson et al. [278] | | | | | | | | | | | | | | | | | | |
| Theveneau et al. [279] | 2020 | 31 | 31 | 31 | 243–334 | 1.01–11.3 | 0.01–0.07 | 0.00–0.52 | 0.42–0.99 | 0.04–0.11 | | 0.06–0.79 | 0.16–0.89 | 0.077 | 2.88 | 2.83 | 0.075 | 1.66 | 1.67 |

$p\rho T$ data

| Authors | Year | $N$ | $T$/K | $p$/MPa | $x_1$ | $x_2$ | $x_3$ | AARD/% |
|---|---|---|---|---|---|---|---|---|
| Perez [280] | 2016 | 352 | 252–354 | 0.20–31.6 | 0.42 | 0.40 | 0.18 | 3.71 |

$x_1$ $CO_2$ + $x_2$ $CH_4$ + $x_3$ $SO_2$

VLE data

| | Year | $N$ | $N_x$ | $N_y$ | $T$/K | $p$/MPa | $x_1$ | $x_2$ | $x_3$ | $y_1$ | $y_2$ | $y_3$ | $AAD_{x_1}$ | $AAD_{x_2}$ | $AAD_{x_3}$ | $AAD_{y_1}$ | $AAD_{y_2}$ | $AAD_{y_3}$ |
|---|---|---|---|---|---|---|---|---|---|---|---|---|---|---|---|---|---|---|
| Gimeno et al. [281] | 2019 | 14 | 7 | 7 | 263–305 | 1.56–7.19 | 0.93–0.99 | 0.01–0.02 | 0.00–0.05 | 0.93–0.99 | 0.01–0.02 | 0.00–0.05 | 0.264 | 0.392 | 0.271 | 0.169 | 0.191 | 0.118 |

$p\rho T$ data

| Authors | Year | $N$ | $T$/K | $p$/MPa | $x_1$ | $x_2$ | $x_3$ | AARD/% |
|---|---|---|---|---|---|---|---|---|
| Gimeno et al. [281] | 2019 | 9369 | 263–374 | 0.10–30.0 | 0.934 | 0.019 | 0.047 | 1.06 |
| | | 9503 | 263–374 | 0.10–30.0 | 0.984 | 0.015 | 0.001 | 0.502 |
| Overall | | 18872 | 263–374 | 0.10–30.0 | 0.93–0.99 | 0.01–0.02 | 0.00–0.05 | 0.781 |

$w_s$ data

**Table 8** continued

| $w_s$ data | | | | | | | | |
|---|---|---|---|---|---|---|---|---|
| Authors | Year | $N$ | $T$/K | $p$/MPa | $x_1$ | $x_2$ | $x_3$ | AARD/% |
| Authors | Year | $N$ | $T$/K | $p$/MPa | $x_1$ | $x_2$ | $x_3$ | AARD/% |
| Gimeno et al. [281] | 2019 | 152 | 263–313 | 84.9–191 | 0.93–0.94 | 0.18–0.19 | 0.04–0.05 | 0.990 |

$AAD_x$ and $AAD_y$ are given with respect to composition in mol% discussed in this work. For the rows labeled "overall", the AARD is calculated between the EOS and the complete dataset. All stated compositions are on a molar basis

**Supplementary Information** The online version contains supplementary material available at https://doi.org/10.1007/s10765-023-03263-6.

**Acknowledgment** We are grateful for Dr. Sebastian Hielscher and Felix Fiedler for providing the software to generate the figures. Our special thanks goes to Sven M. Pohl who helped with the statistical data evaluation. Finally, we thank Joris Scholl and Tan-Trieu-Giang Nguyen for their support in the EOS development and data curation.

**Author Contributions** TN: conceptualization, methodology, software, investigation, data curation, writing—original draft, formal analysis. SH: conceptualization, methodology, software, investigation, data curation, writing—original draft, formal analysis. IHB: methodology, software, writing—review & editing, investigation, validation. RB: conceptualization, methodology, software, investigation, data curation, writing—original draft, formal analysis. EWL: methodology, software, writing—review & editing, formal analysis, validation. MT: conceptualization, methodology, validation, writing—review & editing, formal analysis, supervision. RS: conceptualization, methodology, writing—review & editing, formal analysis, supervision, project administration, funding acquisition.

**Funding** Open Access funding enabled and organized by Projekt DEAL. This publication has been produced with support from various sources, including: The NCCS Research Centre, performed under the Norwegian research program Centres for Environment-friendly Energy Research (FME). The authors acknowledge the following partners for their contributions: Aker Carbon Capture, Allton, Ansaldo Energia, Baker Hughes, CoorsTek Membrane Sciences, Equinor, Fortum Oslo Varme, Gassco, KROHNE, Larvik Shipping, Lundin Norway, Norcem, Norwegian Oil and Gas, Quad Geometrics, Stratum Reservoir, Total, Vår Energi, Wintershall DEA and the Research Council of Norway (257579/E20). The Fraunhofer High-Performance Center DYNAFLEX and the German State of North-Rhine-Westphalia. The European Community's Seventh Framework Programme (FP7-ENERGY-20121-1-2STAGE) under grant agreement n° 308809 (The IMPACTS project) and the following funding partners: Statoil Petroleum AS, Lundin Norway AS, Gas Natural Fenosa, MAN Diesel & Turbo SE and Vattenfall AB. As well as ACT ELEGANCY, Project No 271498, which has received funding from DETEC (CH), BMWi (DE), RVO (NL), Gassnova (NO), BEIS (UK), Gassco, Equinor and Total, and was cofunded by the European Commission under the Horizon 2020 programme, ACT Grant Agreement No 691712. Deutsche Forschungsgemeinschaft (DFG) [Grant Numbers VR6/16 and SP 507/15].

**Data Availability** There are no new datasets available. The investigated data are taken from literature and marked with the corresponding references.

## Declarations

**Conflict of interest** The authors have no competing interests to declare.

**Ethical Approval** Not applicable.



## References

1. UNFCCC, *Kyoto Protocol to the United Nations Framework Convention on Climate Change* (1997)
2. UNFCCC, *Paris Agreement* (2015)
3. IEA. (2019), https://www.iea.org/articles/global-Co2-Emissions-in-2019. Accessed 21 Sept 2022
4. IPCC, *Global Warming of 1.5 °C* (2019), https://www.Ipcc.Ch/Sr15/. Accessed 21 Sept 2022

5. J. Gernert, R. Span, J. Chem. Thermodyn. **93**, 274 (2016). https://doi.org/10.1016/j.jct.2015.05.015
6. O. Kunz, W. Wagner, J. Chem. Eng. Data **57**, 3032 (2012). https://doi.org/10.1021/je300655b
7. R. Beckmüller, M. Thol, I.H. Bell, E.W. Lemmon, R. Span, J. Phys. Chem. Ref. Data **50**, 013102 (2021). https://doi.org/10.1063/5.0040533
8. T. Neumann, J. Poplsteinova Jakobsen, M. Thol, R. Span, Chem. Eng. Sci. **252**, 117261 (2021). https://doi.org/10.1016/j.ces.2021.117261
9. *Thermodynamic Properties of Natural Gas and Related Gases: DETAIL and GROSS Equations of State* (AGA Report No. 8, 2017).
10. *AGA Transmission Measurement Committee, Thermodynamic Properties of Natural Gas and Related Gases: DETAIL and GROSS Equations of State* (AGA Report No. 8, 1992), Part I, 1st edn. Catalog No. XQ1704-1
11. E.W. Lemmon, A Generalized Model for the Predicition of Thermodynamic Properties of Mixtures Including Vapor-Liquid Equilibrium, Ph.D. Thesis, University of Idaho, Idaho, 1996
12. E.W. Lemmon, R. Tillner-Roth, Fluid Phase Equilib. **165**, 1 (1999). https://doi.org/10.1016/S0378-3812(99)00262-9
13. O. Kunz, R. Klimeck, W. Wagner, M. Jaeschke, *The GERG-2004 Wide-Range Equation of State for Natural Gases and Other Mixtures (GERG Technical Monograph)*, vol. 15 (VDI-Verl, Düsseldorf, 2007)
14. D.B. Newell, F. Cabiati, J. Fischer, K. Fujii, S.G. Karshenboim, H.S. Margolis, E. de Mirandés, P.J. Mohr, F. Nez, K. Pachucki, T.J. Quinn, B.N. Taylor, M. Wang, B.M. Wood, Z. Zhang, Metrologia **55**, L13 (2018). https://doi.org/10.1088/1681-7575/aa950a
15. R. Klimeck, Entwicklung Einer Fundamentalgleichung Für Erdgase Für Das Gas- Und Flüssigkeitsgebiet Sowie Das Phasengleichgewicht, Ph.D. Thesis, Ruhr-Universität Bochum, Germany, 2000
16. E.W. Lemmon, R.T. Jacobsen, Int. J. Thermophys. **20**, 825 (1999). https://doi.org/10.1023/A:1022627001338
17. R. Span, *Multiparameter Equations of State—An Accurate Source of Thermodynamic Property Data*, 1st edn. (Springer, Berlin, 2000)
18. J. Gernert, A. Jäger, R. Span, Fluid Phase Equilib. **375**, 209 (2014). https://doi.org/10.1016/j.fluid.2014.05.012
19. I.H. Bell, U.K. Deiters, A.M.M. Leal, Ind. Eng. Chem. Res. **61**, 6010 (2022). https://doi.org/10.1021/acs.iecr.2c00237
20. E.W. Lemmon, R.T. Jacobsen, J. Phys. Chem. Ref. Data **34**, 69 (2005). https://doi.org/10.1063/1.1797813
21. S. Herrig, New Helmholtz-Energy Equations of State for Pure Fluids and CCS-Relevant Mixtures, Ph.D. Thesis, Ruhr-Universität Bochum, Germany, 2018.
22. T.G. Amundsen, L.E. Øi, D.A. Eimer, J. Chem. Eng. Data **54**, 3096 (2009). https://doi.org/10.1021/je900188m
23. H. Arcis, K. Ballerat-Busserolles, L. Rodier, J.-Y. Coxam, J. Chem. Eng. Data **56**, 3351 (2011). https://doi.org/10.1021/je2002946
24. M.H. Li, Y.C. Lie, J. Chem. Eng. Data **39**, 444 (1994). https://doi.org/10.1021/je00015a009
25. D. Ma, C. Zhu, T. Fu, X. Yuan, Y. Ma, J. Chem. Thermodyn. **138**, 350 (2019). https://doi.org/10.1016/j.jct.2019.06.032
26. Y. Maham, T.T. Teng, L.G. Hepler, A.E. Mather, J. Solution Chem. **23**, 195 (1994). https://doi.org/10.1007/BF00973546
27. Y. Maham, T.T. Teng, L.G. Hepler, A.E. Mather, Thermochim. Acta **386**, 111 (2002). https://doi.org/10.1016/S0040-6031(01)00812-7
28. B.P. Mandal, M. Kundu, S.S. Bandyopadhyay, J. Chem. Eng. Data **48**, 703 (2003). https://doi.org/10.1021/je020206a
29. R. Muraleedharan, A. Mondal, B. Mandal, Sep. Purif. Technol. **94**, 92 (2012). https://doi.org/10.1016/j.seppur.2011.10.035
30. M. Pagé, J.-Y. Huot, C. Jolicoeur, Can. J. Chem. **71**, 1064 (1993). https://doi.org/10.1139/v93-142
31. F. Pouryousefi, R.O. Idem, Ind. Eng. Chem. Res. **47**, 1268 (2008). https://doi.org/10.1021/ie0709786
32. M. Sobrino, E.I. Concepción, Á. Gómez-Hernández, M.C. Martín, J.J. Segovia, J. Chem. Thermodyn. **98**, 231 (2016). https://doi.org/10.1016/j.jct.2016.03.021
33. J.H. Song, S.B. Park, J.H. Yoon, H. Lee, K.H. Lee, J. Chem. Eng. Data **41**, 1152 (1996). https://doi.org/10.1021/je9601366

34. J. Han, J. Jin, D.A. Eimer, M.C. Melaaen, J. Chem. Eng. Data **57**, 1095 (2012). https://doi.org/10.1021/je2010038
35. H. Touhara, S. Okazaki, F. Okino, H. Tanaka, K. Ikari, K. Nakanishi, J. Chem. Thermodyn. **14**, 145 (1982). https://doi.org/10.1016/0021-9614(82)90026-X
36. Y.M. Tseng, A.R. Thompson, J. Chem. Eng. Data **9**, 264 (1964). https://doi.org/10.1021/je60021a043
37. R.K. Wadi, P. Kathuria, J. Solution Chem. **21**, 361 (1992). https://doi.org/10.1007/BF00647859
38. R.H. Weiland, J.C. Dingman, D.B. Cronin, G.J. Browning, J. Chem. Eng. Data **43**, 378 (1998). https://doi.org/10.1021/je9702044
39. Y. Yin, T. Fu, C. Zhu, Y. Ma, J. Mol. Liq. **243**, 664 (2017). https://doi.org/10.1016/j.molliq.2017.08.088
40. J. Zhang, P.S. Fennell, J.P.M. Trusler, J. Chem. Eng. Data **60**, 2392 (2015). https://doi.org/10.1021/acs.jced.5b00282
41. Y. Zhao, X. Zhang, S. Zeng, Q. Zhou, H. Dong, X. Tian, S. Zhang, J. Chem. Eng. Data **55**, 3513 (2010). https://doi.org/10.1021/je100078w
42. A. Hartono, E.O. Mba, H.F. Svendsen, J. Chem. Eng. Data **59**, 1808 (2014). https://doi.org/10.1021/je401081e
43. B. Hawrylak, S.E. Burke, R. Palepu, J. Solution Chem. **29**, 575 (2000). https://doi.org/10.1023/A:1005198230692
44. M.A. Jamal, M.K. Khosa, B. Naseem, M. Zaheer-Ud-Din, M. Muneer, Phys. Chem. Liq. **54**, 384 (2016). https://doi.org/10.1080/00319104.2015.1109993
45. S.A. Jayarathna, A. Weerasooriya, S. Dayarathna, D.A. Eimer, M.C. Melaaen, J. Chem. Eng. Data **58**, 986 (2013). https://doi.org/10.1021/je301279x
46. H. Ju, W. Elmoudir, A. Aboudheir, N. Mahinpey, J. Chem. Eng. Data **63**, 1969 (2018). https://doi.org/10.1021/acs.jced.7b01101
47. U.R. Kapadi, D.G. Hundiwale, N.B. Patil, M.K. Lande, Fluid Phase Equilib. **201**, 335 (2002). https://doi.org/10.1016/S0378-3812(02)00095-X
48. M.J. Lee, T.K. Lin, J. Chem. Eng. Data **40**, 336 (1995). https://doi.org/10.1021/je00017a074
49. R. Span, R. Beckmüller, S. Hielscher, A. Jäger, E. Mickoleit, T. Neumann, S. Pohl, B. Semrau, M. Thol, *TREND. Thermodynamic Reference and Engineering Data 5.1* (Lehrstuhl für Thermodynamik, Ruhr-Universität Bochum, Bochum, 2021)
50. U.K. Deiters, I.H. Bell, Int. J. Thermophys. **41**, 169 (2020). https://doi.org/10.1007/s10765-020-02743-3
51. I. Al-Siyabi, Effect of Impurities on $CO_2$ Stream Properties, Ph.D. Thesis, Heriot-Watt University, Scotland, 2013
52. M. Thol, M. Richter, E.F. May, E.W. Lemmon, R. Span, J. Phys. Chem. Ref. Data **48**, 033102 (2019). https://doi.org/10.1063/1.5093800
53. J.A. Beattie, W.H. Stockmayer, H.G. Ingersoll, J. Chem. Phys. **9**, 871 (1941). https://doi.org/10.1063/1.1750859
54. R.T. Ellington, *Personal Communication to Jaeschke et al. 1996* (1996)
55. B.H. Sage, R.A. Budenholzer, W.N. Lacey, Ind. Eng. Chem. **32**, 1262 (1940). https://doi.org/10.1021/ie50369a047
56. J.R. Tomlinson, *Liquid Densities of Ethane, Propane, and Ethane-Propane Mixtures* (NGPA Technical Report No. TP-1, NGPA, Tulsa, OK, 1985)
57. A. Fenghour, J.P. Trusler, W. Wakeham, Fluid Phase Equilib. **163**, 139 (1999). https://doi.org/10.1016/S0378-3812(99)00223-X
58. W. Haynes, J. Chem. Thermodyn. **15**, 903 (1983). https://doi.org/10.1016/0021-9614(83)90123-4
59. M.J. Hiza, W.M. Haynes, W.R. Parrish, J. Chem. Thermodyn. **9**, 873 (1977). https://doi.org/10.1016/0021-9614(77)90173-2
60. M. Jaeschke, A.E. Humphreys, *The GERG Databank of High Accuracy Compressibility Factor Measurements (GERG Technical Monograph 4)* (VDI, Düsseldorf, 1991)
61. M. Jaeschke, H.-M. Hinze, A.E. Humphreys, *Supplement to the GERG Databank of High- Accuracy Compression Factor Measurements. GERG TM7 1996* (Fortschr.-Ber. VDI 6, 355, VDI Verlag, Düsseldorf, 1997)
62. J. Kestin, J. Yata, J. Chem. Phys. **49**, 4780 (1968). https://doi.org/10.1063/1.1669960
63. W.P. Pan, M.H. Mady, R.C. Miller, AIChE J. **21**, 283 (1975). https://doi.org/10.1002/aic.690210209
64. H.H. Reamer, K.J. Korpl, B.H. Sage, W.N. Lacey, Ind. Eng. Chem. **39**, 206 (1947). https://doi.org/10.1021/ie50446a025

65. R. Lentner, M. Richter, R. Kleinrahm, R. Span, J. Chem. Thermodyn. **112**, 68 (2017). https://doi.org/10.1016/j.jct.2017.04.002
66. M. Richter, R. Kleinrahm, R. Lentner, R. Span, J. Chem. Thermodyn. **93**, 205 (2016). https://doi.org/10.1016/j.jct.2015.09.034
67. W. Wagner, A. Pruß, J. Phys. Chem. Ref. Data **31**, 387 (2002). https://doi.org/10.1063/1.1461829
68. E.W. Lemmon, I.H. Bell, M.L. Huber, M.O. McLinden, *NIST Standard Reference Database 23: Reference Fluid Thermodynamic and Transport Properties-REFPROP, 10.0* (Gaithersburg, USA, 2018)
69. I.H. Bell, J. Wronski, S. Quoilin, V. Lemort, Ind. Eng. Chem. Res. **53**, 2498 (2014). https://doi.org/10.1021/ie4033999
70. R. Span, W. Wagner, J. Phys. Chem. Ref. Data **25**, 1509 (1996). https://doi.org/10.1063/1.555991
71. X. Xiao, J.P.M. Trusler, X. Yang, M. Thol, S.Z.S. Al Ghafri, D. Rowland, E.F. May, J. Phys. Chem. Ref. Data (2021). https://doi.org/10.1063/5.0065786
72. R. Span, E.W. Lemmon, R.T. Jacobsen, W. Wagner, A. Yokozeki, J. Phys. Chem. Ref. Data **29**, 1361 (2000). https://doi.org/10.1063/1.1349047
73. R. Schmidt, W. Wagner, Fluid Phase Equilib. **19**, 175 (1985). https://doi.org/10.1016/0378-3812(85)87016-3
74. C. Tegeler, R. Span, W. Wagner, J. Phys. Chem. Ref. Data **28**, 779 (1999). https://doi.org/10.1063/1.556037
75. E.W. Lemmon, R. Span, J. Chem. Eng. Data **51**, 785 (2006). https://doi.org/10.1021/je050186n
76. J.W. Leachman, R.T. Jacobsen, S.G. Penoncello, E.W. Lemmon, J. Phys. Chem. Ref. Data **38**, 721 (2009). https://doi.org/10.1063/1.3160306
77. U. Setzmann, W. Wagner, J. Phys. Chem. Ref. Data **20**, 1061 (1991). https://doi.org/10.1063/1.555898
78. K. Gao, J. Wu, P. Zhang, E.W. Lemmon, J. Chem. Eng. Data **61**, 2859 (2016). https://doi.org/10.1021/acs.jced.6b00195
79. M. Kortmann, Development of Empirical Multiparameter Equations of State for Monoethanolamine and Diethanolamine, Master Thesis, Ruhr-Universität Bochum, Germany, 2016
80. M. Thol, F.H. Dubberke, E. Baumhögger, R. Span, J. Vrabec, J. Chem. Eng. Data **63**, 2533 (2018). https://doi.org/10.1021/acs.jced.7b01031
81. M. Thol, S. Herrig, R. Span, E.W. Lemmon, AIChE J. **67**, 1 (2021). https://doi.org/10.1002/aic.17326
82. K. Gao, J. Wu, I.H. Bell, A.H. Harvey, E.W. Lemmon, J. Phys. Chem. Ref. Data **52**, 013102 (2023). https://doi.org/10.1063/5.0128269
83. T. Neumann, E. Baumhögger, R. Span, J. Vrabec, M. Thol, Int. J. Thermophys. **43**, 10 (2022). https://doi.org/10.1007/s10765-021-02933-7
84. T. Neumann, M. Thol, I.H. Bell, E.W. Lemmon, R. Span, Fluid Phase Equilib. **511**, 112496 (2020). https://doi.org/10.1016/j.fluid.2020.112496
85. T. Neumann, I.M. Bernhardsen, H.K. Knuutila, J. Poplsteinova Jakobsen, R. Span, *Thermodynamic Properties of the Binary Mixture of Monoethanolamine and Carbon Dioxide* (SINTEF Proceedings, 2021)
86. L.F.S. Souza, S. Herrig, R. Span, J.P.M. Trusler, Appl. Energy **251**, 113398 (2019). https://doi.org/10.1016/j.apenergy.2019.113398
87. S.W. Løvseth, A. Austegard, S.F. Westman, H.G.J. Stang, S. Herrig, T. Neumann, R. Span, Fluid Phase Equilib. **466**, 48 (2018). https://doi.org/10.1016/j.fluid.2018.02.009
88. L.F.S. Souza, S.Z.S. Al Ghafri, J.P.M. Trusler, J. Chem. Thermodyn. **126**, 63 (2018). https://doi.org/10.1016/j.jct.2018.06.022
89. A. Chapoy, A.H. Mohammadi, D. Richon, B. Tohidi, Fluid Phase Equilib. **220**, 113 (2004). https://doi.org/10.1016/j.fluid.2004.02.010
90. A. Chapoy, C. Coquelet, D. Richon, Fluid Phase Equilib. **230**, 210 (2005). https://doi.org/10.1016/j.fluid.2004.07.005
91. J.A. Awan, K. Thomsen, C. Coquelet, P.L. Fosbøl, D. Richon, J. Chem. Eng. Data **55**, 842 (2010). https://doi.org/10.1021/je900441f
92. A. Fenghour, W.A. Wakeham, J.T.R. Watson, J. Chem. Thermodyn. **28**, 447 (1996). https://doi.org/10.1006/jcht.1996.0044
93. M. Frost, E. Karakatsani, N. von Solms, D. Richon, G.M. Kontogeorgis, J. Chem. Eng. Data **59**, 961 (2014). https://doi.org/10.1021/je400684k

94. P.C. Gillespie, G.M. Wilson, *Research Report RR-41: Vapor-Liquid Equilibrium Data on Water-Substitute Gas Components:$N_2$-$H_2O$, $H_2$-$H_2O$, CO-$H_2O$, $H_2$-CO-$H_2O$, and $H_2S$-$H_2O$* (Tulsa, OK, 1980)
95. A.H. Mohammadi, A. Chapoy, D. Richon, B. Tohidi, Ind. Eng. Chem. Res. **43**, 7148 (2004). https://doi.org/10.1021/ie049843f
96. R.H. Olds, B.H. Sage, W.N. Lacey, Ind. Eng. Chem. **34**, 1223 (1942). https://doi.org/10.1021/ie50394a018
97. H.A. Sairanen, M.O. Heinonen, Int. J. Thermophys. **35**, 1280 (2014). https://doi.org/10.1007/s10765-014-1720-3
98. J.M.S. Fonseca, N. von Solms, Fluid Phase Equilib. **329**, 55 (2012). https://doi.org/10.1016/j.fluid.2012.05.024
99. Y.S. Kim, S.K. Ryu, S.O. Yang, C.S. Lee, Ind. Eng. Chem. Res. **42**, 2409 (2003). https://doi.org/10.1021/ie0209374
100. J. Qin, R.J. Rosenbauer, Z. Duan, J. Chem. Eng. Data **53**, 1246 (2008). https://doi.org/10.1021/je700473e
101. M. Rigby, J.M. Prausnitz, J. Phys. Chem. **72**, 330 (1968). https://doi.org/10.1021/j100847a064
102. C.E.P. Siqueira Campos, J.R. Penello, F.L. Pellegrini Pessoa, A.M. Cohen Uller, J. Chem. Eng. Data **55**, 2576 (2010). https://doi.org/10.1021/je9007958
103. A. Chapoy, A.H. Mohammadi, B. Tohidi, A. Valtz, D. Richon, Ind. Eng. Chem. Res. **44**, 7567 (2005). https://doi.org/10.1021/ie050201h
104. I.M. Abdulagatov, A.R. Bazaev, A.E. Ramazanova, J. Chem. Thermodyn. **25**, 249 (1993). https://doi.org/10.1006/jcht.1993.1024
105. L.L. Joffrion, P.T. Eubank, Fluid Phase Equilib. **43**, 263 (1988). https://doi.org/10.1016/0378-3812(88)87010-9
106. V.M. Shmonov, R.J. Sadus, E.U. Franck, J. Phys. Chem. **97**, 9054 (1993). https://doi.org/10.1021/j100137a036
107. H. Welsch, H. Welsch, Die Systeme Xenon-Wasser Und Methan-Wasser Bei Hohen Drücken Und Temperaturen, Ph.D. Thesis, Universität Karlsruhe, Germany, 1973
108. Y. Zhang, Chin. J. Geol. **32**, 299 (1997)
109. L. Hnědkovský, R.H. Wood, J. Chem. Thermodyn. **29**, 731 (1997). https://doi.org/10.1006/jcht.1997.0192
110. M.P. Burgess, R.P. Germann, AIChE J. **15**, 272 (1969). https://doi.org/10.1002/aic.690150227
111. H.J. Neuburg, J.F. Atherley, L.G. Walker, *Girdler-Sulfide Process Physical Properties* (Atomic Energy of Canada Limited—Report 5702, Chalk River, Ontario, 1977)
112. J.J. Carroll, A.E. Mather, J. Solution Chem. **21**, 607 (1992)
113. J.J. Carroll, A.E. Mather, Geochim. Cosmochim. Acta **53**, 1163 (1989). https://doi.org/10.1016/0016-7037(89)90053-7
114. E.C.W. Clarke, D.N. Glew, Can. J. Chem. **49**, 691 (1971). https://doi.org/10.1139/v71-116
115. F.T. Selleck, L.T. Carmichael, B.H. Sage, Ind. Eng. Chem. **44**, 2219 (1952). https://doi.org/10.1021/ie50513a064
116. O.M. Suleimenov, R.E. Krupp, Geochim. Cosmochim. Acta **58**, 2433 (1994). https://doi.org/10.1016/0016-7037(94)90022-1
117. Q. Yu, D. Liu, R. Liu, H. Zhou, M. Chen, G. Chen, Chem. Eng. **4** (1980)
118. A. Chapoy, A.H. Mohammadi, B. Tohidi, A. Valtz, D. Richon, Ind. Eng. Chem. Res. **44**, 10021 (2005). https://doi.org/10.1021/ie0511231
119. A. Valtz, A. Chapoy, C. Coquelet, P. Paricaud, D. Richon, Fluid Phase Equilib. **226**, 333 (2004). https://doi.org/10.1016/j.fluid.2004.10.013
120. D.Y. Zezin, A.A. Migdisov, A.E. Williams-Jones, Geochim. Cosmochim. Acta **75**, 5483 (2011). https://doi.org/10.1016/j.gca.2011.07.005
121. M. Nazeri, M.M. Maroto-Valer, E. Jukes, Appl. Energy **212**, 162 (2018). https://doi.org/10.1016/j.apenergy.2017.12.024
122. B. Gimeno, M. Artal, I. Velasco, J. Fernández, S.T. Blanco, Energy Fuels **32**, 8641 (2018). https://doi.org/10.1021/acs.energyfuels.8b01666
123. C. Coquelet, A. Valtz, P. Arpentinier, Fluid Phase Equilib. **382**, 205 (2014). https://doi.org/10.1016/j.fluid.2014.08.031
124. V. Lachet, T. de Bruin, P. Ungerer, C. Coquelet, A. Valtz, V. Hasanov, F. Lockwood, D. Richon, Energy Procedia **1**, 1641 (2009). https://doi.org/10.1016/j.egypro.2009.01.215
125. F. Caubet, Z. Phys, Chem. **49**, 101 (1904)

126. A. Blümcke, Ann. Phys. Chem. **270**, 10–21 (1888)
127. A. Thiel, E. Schulte, Zeitschrift Für Phys Chemie **96U**, 312 (1920). https://doi.org/10.1515/zpch-1920-9611
128. J. Wang, Z. Wang, D. Ryan, C. Lan, Int. J. Greenh. Gas Control **42**, 132 (2015). https://doi.org/10.1016/j.ijggc.2015.08.002
129. M. Nazeri, A. Chapoy, A. Valtz, C. Coquelet, B. Tohidi, Fluid Phase Equilib. **454**, 64 (2017). https://doi.org/10.1016/j.fluid.2017.09.014
130. E. El Ahmar, B. Creton, A. Valtz, C. Coquelet, V. Lachet, D. Richon, P. Ungerer, Fluid Phase Equilib. **304**, 21 (2011). https://doi.org/10.1016/j.fluid.2011.02.008
131. I.H. Bell, U.K. Deiters, AIChE J. **64**, 2745 (2018). https://doi.org/10.1002/aic.16074
132. D.S. Tsiklis, Zh. Fiz. Khim. **20**, 181 (1946)
133. M.R. Dean, W.S. Walls, Ind. Eng. Chem. **39**, 1049 (1947). https://doi.org/10.1021/ie50452a027
134. R.W. Dornte, C.V. Ferguson, Ind. Eng. Chem. **31**, 112 (1939). https://doi.org/10.1021/ie50349a023
135. A. Köster, J. Vrabec, *Personal Communication (Simulated Data)* (2017)
136. S.G. Sayegh, J. Najman, B. Hlavacek, J. Can. Pet. Technol. (1981). https://doi.org/10.2118/81-04-05
137. J. Gross, G. Sadowski, Ind. Eng. Chem. Res. **40**, 1244 (2001). https://doi.org/10.1021/ie0003887
138. H.L. Wilson, W.V. Wilding, Experimental Results for DIPPR 1990-91 Projects on phase equilibria and pure component properties, vapor-liquid and liquid-liquidequilibrium measurements on twenty-two binary mixtures, DIPPR Data Ser. **2**(2), 63–115 (1994)
139. B. Gilot, C. Guiglion, M. Enjabert, Chim. Ind.—Génie Chim. **98**, 1052 (1967)
140. K. Ohgaki, T. Katayama, Fluid Phase Equilib. **1**, 27 (1977). https://doi.org/10.1016/0378-3812(77)80023-X
141. A. Köster, D. Saric, J. Vrabec, *Personal Communication to Monika Thol* (2023)
142. H. Li, X. Jiao, W. Chen, Phys. Chem. Liq. **52**, 349 (2014). https://doi.org/10.1080/00319104.2013.830720
143. J.G. Van Berkum, G.A.M. Diepen, J. Chem. Thermodyn. **11**, 317 (1979). https://doi.org/10.1016/0021-9614(79)90053-3
144. A.F. Hollemann, E. Wiber, N. Wiber, *Lehrbuch Der Anorganischen Chemie* (de Gruyter, Berlin, 1995)
145. C.-M. Hsieh, T. Windmann, J. Vrabec, J. Chem. Eng. Data **58**, 3420 (2013). https://doi.org/10.1021/je400643q
146. W.L. Beuschlein, L.O. Simenson, J. Am. Chem. Soc. **62**, 610 (1940). https://doi.org/10.1021/ja01860a053
147. A. Douabul, J. Riley, J. Chem. Eng. Data **24**, 274 (1979). https://doi.org/10.1021/je60083a014
148. B.C. Spall, Can. J. Chem. Eng. **41**, 79 (1963). https://doi.org/10.1002/cjce.5450410209
149. J. Tokunaga, J. Chem. Eng. Data **19**, 162 (1974). https://doi.org/10.1021/je60061a009
150. L. Gevantman, *CRC Handbook of Chemistry and Physics*, vol. 10, 91st edn. (CRC Press, Boca Raton, 2000), p.80
151. J.C. Hudson, J. Chem. Soc. Trans. **127**, 1332 (1925). https://doi.org/10.1039/CT9252701332
152. W.B. Campbell, O. Maass, Can. J. Res. **2**, 42 (1930). https://doi.org/10.1139/cjr30-006
153. M.K. Mondal, Fluid Phase Equilib. **253**, 98 (2007). https://doi.org/10.1016/j.fluid.2007.01.015
154. A.E. Rabe, J.F. Harris, J. Chem. Eng. Data **8**, 333 (1963). https://doi.org/10.1021/je60018a017
155. B. Rumpf, G. Maurer, Fluid Phase Equilib. **81**, 241 (1992). https://doi.org/10.1016/0378-3812(92)85155-2
156. T.K. Sherwood, Ind. Eng. Chem. **17**, 745 (1925). https://doi.org/10.1021/ie50187a043
157. T.H. Sims, J. Chem. Soc. **14**, 1 (1862)
158. W.T. Smith, R.B. Parkhurst, J. Am. Chem. Soc. **44**, 1918 (1922). https://doi.org/10.1021/ja01430a010
159. J.J. Byerley, G.L. Rempel, V.T. Le, J. Chem. Eng. Data **25**, 55 (1980). https://doi.org/10.1021/je60084a017
160. F.H. Conrad, W.L. Beuschlein, J. Am. Chem. Soc. **56**, 2554 (1934). https://doi.org/10.1021/ja01327a009
161. *International Association for the Properties of Water and Steam, IAPWS R6-95(2016), Revised Release on the IAPWS Formulation 1995 for the Thermodynamic Properties of Ordinary Water Substance for General and Scientific Use* (2016)
162. Q. Zhou, H. Guo, P. Yang, Z. Wang, Ind. Eng. Chem. Res. **59**, 12855 (2020). https://doi.org/10.1021/acs.iecr.9b06242
163. R. Wohland, Leuna Protoc. 6231 (1976)

164. A. Belabbaci, A. Razzouk, I. Mokbel, J. Jose, L. Negadi, J. Chem. Eng. Data **54**, 2312 (2009). https://doi.org/10.1021/je800530u
165. Z. Cai, R. Xie, Z. Wu, J. Chem. Eng. Data **41**, 1101 (1996). https://doi.org/10.1021/je960118o
166. I. Kim, H.F. Svendsen, E. Børresen, J. Chem. Eng. Data **53**, 2521 (2008). https://doi.org/10.1021/je800290k
167. I. Kim, K.A. Hoff, E.T. Hessen, T. Haug-Warberg, H.F. Svendsen, Chem. Eng. Sci. **64**, 2027 (2009). https://doi.org/10.1016/j.ces.2008.12.037
168. S.-B. Park, H. Lee, Korean J. Chem. Eng. **14**, 146 (1997). https://doi.org/10.1007/BF02706075
169. S.J. Park, H.Y. Shin, B. Min, A. Cho, J. Lee, Korean J. Chem. Eng. **26**, 189 (2009). https://doi.org/10.1007/s11814-009-0031-z
170. H. Tanaka, D. Kodama, R. Yaginuma, M. Kato, Jpn. J. Thermophys. Prop. **15**, 182 (2001)
171. K. Tochigi, K. Akimoto, K. Ochi, F. Liu, Y. Kawase, J. Chem. Eng. Data **44**, 588 (1999). https://doi.org/10.1021/je980068i
172. J.-I. Lenard, R.W. Rousseau, A.S. Teja, AIChE Symp. Ser. **86**, 1 (1990)
173. A. Nath, E. Bende, J. Chem. Eng. Data **28**, 370 (1983). https://doi.org/10.1021/je00034a007
174. D. Vega-Maza, *Personal Communication* (2021)
175. R. Sidi-Boumedine, S. Horstmann, K. Fischer, E. Provost, W. Fürst, J. Gmehling, Fluid Phase Equilib. **218**, 85 (2004). https://doi.org/10.1016/j.fluid.2003.11.014
176. M. Abedinzadegan Abdi, A. Meisen, Ind. Eng. Chem. Res. **38**, 3096 (1999). https://doi.org/10.1021/ie980454t
177. S. Horstmann, P. Mougin, F. Lecomte, K. Fischer, J. Gmehling, J. Chem. Eng. Data **47**, 1496 (2002). https://doi.org/10.1021/je020085e
178. W.V. Wilding, L.C. Wilson, G.M. Wilson, AIChE Data Ser. **1**, 6 (1991)
179. H. Arcis, K. Ballerat-Busserolles, L. Rodier, J.-Y. Coxam, J. Chem. Eng. Data **57**, 840 (2012). https://doi.org/10.1021/je201012e
180. M.H. Oyevaar, R.W.J. Morssinkhof, K.R. Westerterp, J. Chem. Eng. Data **34**, 77 (1989). https://doi.org/10.1021/je00055a022
181. D.H. Peacock, J. Chem. Soc. Trans. **107**, 1547 (1915). https://doi.org/10.1039/CT9150701547
182. M.E. Rebolledo-Libreros, A. Trejo, J. Chem. Eng. Data **51**, 702 (2006). https://doi.org/10.1021/je050462y
183. E.B. Rinker, D.W. Oelschlager, A.T. Colussi, K.R. Henry, O.C. Sandall, J. Chem. Eng. Data **39**, 392 (1994). https://doi.org/10.1021/je00014a046
184. A. Shojaeian, A. Haghtalab, J. Mol. Liq. **187**, 218 (2013). https://doi.org/10.1016/j.molliq.2013.07.016
185. F. Yang, X. Wang, Z. Liu, Thermochim. Acta **533**, 1 (2012). https://doi.org/10.1016/j.tca.2012.01.007
186. J. Aguila-Hernández, R. Gómez-Quintana, F. Murrieta-Guevara, A. Romero-Martínez, A. Trejo, J. Chem. Eng. Data **46**, 861 (2001). https://doi.org/10.1021/je0002944
187. E. Álvarez, D. Gómez-Díaz, M.D. La Rubia, J.M. Navaza, J. Chem. Eng. Data **51**, 955 (2006). https://doi.org/10.1021/je050463q
188. F.I. Chowdhury, S. Akhtar, M.A. Saleh, Phys. Chem. Liq. **47**, 638 (2009). https://doi.org/10.1080/00319100802620538
189. J. Han, J. Jin, D.A. Eimer, M.C. Melaaen, J. Chem. Eng. Data **57**, 1843 (2012). https://doi.org/10.1021/je300345m
190. C. Hsu, M.-H. Li, J. Chem. Eng. Data **42**, 502 (1997). https://doi.org/10.1021/je960356j
191. S.A. Jayarathna, D.A. Kottage, D.A. Eimer, M.C. Melaaen, J. Chem. Eng. Data **57**, 2975 (2012). https://doi.org/10.1021/je300530z
192. L. Tsintsarska, S. Dralcheva, P. Petrov, M. Tsvetkova, Khim. Ind. **60**, 164 (1988)
193. A. Ahmady, A. Shamiri, M.A. Hashim, M.K. Aroua, J. Taiwan Inst. Chem. Eng. **45**, 380 (2014). https://doi.org/10.1016/j.jtice.2013.07.004
194. A. Barreau, P. Mougin, C. Lefebvre, Q.M. Luu Thi, J. Rieu, J. Chem. Eng. Data **52**, 769 (2007). https://doi.org/10.1021/je060396f
195. C. Dell'Era, P. Uusi-Kyyny, E.-L.L. Rautama, M. Pakkanen, V. Alopaeus, C. Dell'Era, P. Uusi-Kyyny, E.-L.L. Rautama, M. Pakkanen, V. Alopaeus, Fluid Phase Equilib. **299**, 51 (2010). https://doi.org/10.1016/j.fluid.2010.08.026
196. G. Kuranov, B. Rumpf, N.A. Smirnova, G. Maurer, Ind. Eng. Chem. Res. **35**, 1959 (1996). https://doi.org/10.1021/ie950538r

197. M. Shokouhi, R. Ahmadi, J. Chem. Thermodyn. **102**, 228 (2016). https://doi.org/10.1016/j.jct.2016.06.007
198. A. Soames, A. Al Helal, S. Iglauer, A. Barifcani, R. Gubner, J. Chem. Eng. Data **63**, 1752 (2018). https://doi.org/10.1021/acs.jced.8b00054
199. E. Voutsas, A. Vrachnos, K. Magoulas, Fluid Phase Equilib. **224**, 193 (2004). https://doi.org/10.1016/j.fluid.2004.05.012
200. S. Xu, S. Qing, Z. Zhen, C. Zhang, J.J. Carroll, Fluid Phase Equilib. **67**, 197 (1991). https://doi.org/10.1016/0378-3812(91)90055-C
201. M. Afkhamipour, M. Mofarahi, Fluid Phase Equilib. **457**, 38 (2018). https://doi.org/10.1016/j.fluid.2017.09.019
202. H.A. Al-Ghawas, D.P. Hagewiesche, G. Ruiz-Ibanez, O.C. Sandall, J. Chem. Eng. Data **34**, 385 (1989). https://doi.org/10.1021/je00058a004
203. H. Arcis, L. Rodier, K. Ballerat-Busserolles, J.-Y. Coxam, J. Chem. Thermodyn. **40**, 1022 (2008). https://doi.org/10.1016/j.jct.2008.01.028
204. J. Manuel Bernal-García, M. Ramos-Estrada, G.A. Iglesias-Silva, K.R. Hall, J. Chem. Eng. Data **48**, 1442 (2003). https://doi.org/10.1021/je030120x
205. S.Y. Choi, S.C. Nam, Y. Il Yoon, K.T. Park, S.-J. Park, Ind. Eng. Chem. Res. **53**, 14451 (2014). https://doi.org/10.1021/ie502434m
206. M. Damanafshan, B. Mokhtarani, M. Mirzaei, M. Mafi, A. Sharifi, A.H. Jalili, J. Chem. Eng. Data **63**, 2135 (2018). https://doi.org/10.1021/acs.jced.8b00142
207. B. Das, B. Deogam, Y. Agrawal, B. Mandal, J. Chem. Eng. Data **61**, 2226 (2016). https://doi.org/10.1021/acs.jced.5b00922
208. P.W.J. Derks, E.S. Hamborg, J.A. Hogendoorn, J.P.M. Niederer, G.F. Versteeg, J. Chem. Eng. Data **53**, 1179 (2008). https://doi.org/10.1021/je800031p
209. A. Dey, S.K. Dash, B. Mandal, Fluid Phase Equilib. **463**, 91 (2018). https://doi.org/10.1016/j.fluid.2018.01.030
210. K. Fischer, A. Valtz, D. Richon, ELDATA Int Electron. J. Phys.-Chem. Data **5**, 97 (1999)
211. C.K. Foo, C.Y. Leo, R. Aramesh, M.K. Aroua, N. Aghamohammadi, M.S. Shafeeyan, A. Shamiri, J. Mol. Liq. **209**, 596 (2015). https://doi.org/10.1016/j.molliq.2015.05.041
212. Y. Gao, F. Zhang, K. Huang, J.-W. Ma, Y.-T. Wu, Z.-B. Zhang, Int. J. Greenh. Gas Control **19**, 379 (2013). https://doi.org/10.1016/j.ijggc.2013.09.019
213. B. Hawrylak, R. Palepu, P.R. Tremaine, J. Chem. Thermodyn. **38**, 988 (2006). https://doi.org/10.1016/j.jct.2005.10.013
214. S.S. Karunarathne, D.A. Eimer, K.J. Jens, L.E. Øi, Fluids **5**, 27 (2020). https://doi.org/10.3390/fluids5010027
215. A.A. Lawal, Measurement and Correlation of Data Used for $CO_2$ Absorption in Different Amine Solutions at Various Temperatures, M.Sc.-Thesis, University College of Southeast Norway, 2016
216. C.Y. Leo, A. Shamiri, M.K. Aroua, N. Aghamohammadi, R. Aramesh, E. Natarajan, P. Ganesan, V. Akbari, J. Mol. Liq. **221**, 1155 (2016). https://doi.org/10.1016/j.molliq.2016.06.103
217. M.H. Li, K.P. Shen, J. Chem. Eng. Data **37**, 288 (1992). https://doi.org/10.1021/je00007a002
218. J.-G. Lu, F. Fan, C. Liu, H. Zhang, Y. Ji, M. Chen, J. Chem. Eng. Data **56**, 2706 (2011). https://doi.org/10.1021/je101192x
219. J.-G. Lu, A.-C. Hua, Z.-W. Xu, F. Fan, L. Cheng, F. Lin, Fluid Phase Equilib. **327**, 9 (2012). https://doi.org/10.1016/j.fluid.2012.05.007
220. Y. Maham, T.T. Teng, A.E. Mather, L.G. Hepler, Can. J. Chem. **73**, 1514 (1995). https://doi.org/10.1139/v95-187
221. A. Muhammad, M.I. Abdul Mutalib, T. Murugesan, A. Shafeeq, J. Chem. Eng. Data **53**, 2217 (2008). https://doi.org/10.1021/je800416y
222. J. Na, B.-M. Min, Y.C. Park, J.-H. Moon, D.H. Chun, J.-S. Lee, H.Y. Shin, Korean Chem. Eng. Res **56**, 204 (2018). https://doi.org/10.9713/kcer.2018.56.2.204
223. S. Paul, B. Mandal, J. Chem. Eng. Data **51**, 1808 (2006). https://doi.org/10.1021/je060195b
224. S.A. Razavizadeh, S. Sheikh, Z.N. Gerowgi, Phys. Chem. Res. **5**, 269 (2017). https://doi.org/10.22036/pcr.2017.41046
225. E.B. Rinker, A.T. Colussi, N.L. McKnight, O.C. Sandall, J. Chem. Eng. Data **45**, 254 (2000). https://doi.org/10.1021/je9902286
226. N. Sadegh, Acid Gas Removal from Natural Gas with Alkanolamines: A Modeling and Experimental Study, Ph.D. Thesis, Technical University of Denmark, 2013

227. N.A. Sairi, N.A. Ghani, M.K. Aroua, R. Yusoff, Y. Alias, Fluid Phase Equilib. **385**, 79 (2015). https://doi.org/10.1016/j.fluid.2014.11.009
228. M. Shokouhi, A.H. Jalili, F. Samani, M. Hosseini-Jenab, Fluid Phase Equilib. **404**, 96 (2015). https://doi.org/10.1016/j.fluid.2015.06.034
229. D. Speyer, V. Ermatchkov, G. Maurer, J. Chem. Eng. Data **55**, 283 (2010). https://doi.org/10.1021/je9003383
230. L.M. Welsh, R.A. Davis, J. Chem. Eng. Data **40**, 257 (1995). https://doi.org/10.1021/je00017a055
231. R. Yusoff, M.K. Aroua, A. Shamiri, A. Ahmady, N.S. Jusoh, N.F. Asmuni, L.C. Bong, S.H. Thee, J. Chem. Eng. Data **58**, 240 (2013). https://doi.org/10.1021/je300628e
232. Y. Zheng, E. El Ahmar, M. Simond, K. Ballerat-Busserolles, P. Zhang, J. Chem. Eng. Data **65**, 3784 (2020). https://doi.org/10.1021/acs.jced.9b01163
233. A. Zúñiga-Moreno, L.A. Galicia-Luna, J.M. Bernal-García, G.A. Iglesias-Silva, J. Chem. Eng. Data **52**, 1988 (2007). https://doi.org/10.1021/je700287u
234. K. Zhang, B. Hawrylak, R. Palepu, P.R. Tremaine, J. Chem. Thermodyn. **34**, 679 (2002). https://doi.org/10.1006/jcht.2002.0937
235. Y.-J.J. Chen, T.-W.W. Shih, M.-H.H. Li, J. Chem. Eng. Data **46**, 51 (2001). https://doi.org/10.1021/je0000367
236. L.F. Chiu, H.F. Liu, M.H. Li, J. Chem. Eng. Data **44**, 631 (1999). https://doi.org/10.1021/je980217x
237. T.A. Hayden, T.G.A. Smith, A.E. Mather, J. Chem. Eng. Data **28**, 196 (1983). https://doi.org/10.1021/je00032a020
238. R.H. Weiland, J.C. Dingman, D.B. Cronin, J. Chem. Eng. Data **42**, 1004 (1997). https://doi.org/10.1021/je960314v
239. M.M. Akbar, Studies on $CO_2$ Solubility in N-Methyldiethanolamine and Hydrophobic Ionic Liquid Binary Mixtures, Ph.D.-Thesis, Universiti Teknologi PETRONAS, Malaysia, 2013
240. F.-Y. Jou, A.E. Mather, J. Chem. Eng. Data **51**, 1429 (2006). https://doi.org/10.1021/je060118g
241. A.G. Höchst, Dr.Z/Ho-3484-III.1 (1970)
242. S.M. Lemkowitz, J.C. Van Erp, D.M. Rekers, P.J. Van Den Berg, J. Chem. Technol. Biotechnol. **30**, 85 (1980). https://doi.org/10.1002/jctb.503300112
243. S.M. Lemkowitz, J. Goedegebuur, P.J. Berg, J. Appl. Chem. Biotechnol. **21**, 229 (1971). https://doi.org/10.1002/jctb.5020210803
244. T.R. Briggs, V. Migrdichian, J. Phys. Chem. **28**, 1121 (1924). https://doi.org/10.1021/j150245a001
245. C. Wormald, B. Wurzberger, J. Chem. Thermodyn. **34**, 1567 (2002). https://doi.org/10.1016/S0021-9614(02)00198-2
246. S. Ottøy, T. Neumann, H.G.J. Stang, J.P. Jakobsen, A. Austegard, S.W. Løvseth, Fluid Phase Equilib. **509**, 112444 (2020). https://doi.org/10.1016/j.fluid.2019.112444
247. A. Dhima, J.-C. de Hemptinne, J. Jose, Ind. Eng. Chem. Res. **38**, 3144 (1999). https://doi.org/10.1021/ie980768g
248. S.Z.S. Al Ghafri, E. Forte, G.C. Maitland, J.J. Rodriguez-Henríquez, J.P.M. Trusler, J. Phys. Chem. B **118**, 14461 (2014). https://doi.org/10.1021/jp509678g
249. K.Y. Song, R. Kobayashi, J. Chem. Eng. Data **35**, 320 (1990). https://doi.org/10.1021/je00061a026
250. S. Cheng, F. Shang, W. Ma, H. Jin, N. Sakoda, X. Zhang, L. Guo, J. Chem. Eng. Data **64**, 4024 (2019). https://doi.org/10.1021/acs.jced.9b00399
251. S. Cheng, F. Shang, W. Ma, H. Jin, N. Sakoda, X. Zhang, L. Guo, J. Chem. Eng. Data **65**, 4881 (2020). https://doi.org/10.1021/acs.jced.0c00504
252. N.K. Muirbrook, J.M. Prausnitz, AIChE J. **11**, 1092 (1965). https://doi.org/10.1002/aic.690110624
253. G.H. Zenner, L.I. Dana, Chem. Eng. Prog. Symp. Ser. **59**, 36 (1963)
254. M. Nazeri, A. Chapoy, R. Burgass, B. Tohidi, J. Chem. Thermodyn. **111**, 157 (2017). https://doi.org/10.1016/j.jct.2017.03.036
255. N.K. Muirbrook, Experimental and Thermodynamic Study of the High-Pressure Vapor-Liquid Equilibria for the Nitrogen-Oxygen- Carbon Dioxide System, Ph.D. Thesis, Univ. California Berkeley, 1964
256. G.J. Gururaja, M.A. Tirunarayanan, A. Ramachandran, J. Chem. Eng. Data **12**, 562 (1967). https://doi.org/10.1021/je60035a024
257. J. Ke, N. Suleiman, Y. Sanchez-Vicente, T.S. Murphy, J. Rodriguez, A. Ramos, M. Poliakoff, M.W. George, Int. J. Greenh. Gas Control **56**, 55 (2017). https://doi.org/10.1016/j.ijggc.2016.11.003
258. X. Yang, Z. Wang, Z. Li, J. Chem. Eng. Data **60**, 3353 (2015). https://doi.org/10.1021/acs.jced.5b00625

259. M.-J. Tenorio, A.J. Parrott, J.A. Calladine, Y. Sanchez-Vicente, A.J. Cresswell, R.S. Graham, T.C. Drage, M. Poliakoff, J. Ke, M.W. George, Int. J. Greenh. Gas Control **41**, 68 (2015). https://doi.org/10.1016/j.ijggc.2015.06.009
260. I.R. Kritschewsky, V.P. Markov, Acta Physicochim. URSS **12**, 59 (1940)
261. T.A. Al-Sahhaf, A.J. Kidnay, E.D. Sloan, Ind. Eng. Chem. Fundam. **22**, 372 (1983). https://doi.org/10.1021/i100012a004
262. T.A. Al-Sahhaf, Fluid Phase Equilib. **55**, 159 (1990). https://doi.org/10.1016/0378-3812(90)85010-8
263. E. Sarashina, Y. Arai, S. Saito, J. Chem. Eng. Jpn. **4**, 377 (1971). https://doi.org/10.1252/jcej.4.377
264. F.A. Somait, A.J. Kidnay, J. Chem. Eng. Data **23**, 301 (1978). https://doi.org/10.1021/je60079a019
265. G. Trappehl, H. Knapp, Cryogenics (Guildf) **29**, 42 (1989). https://doi.org/10.1016/0011-2275(89)90010-6
266. N. Xu, J. Dong, Y. Wang, J. Shi, Fluid Phase Equilib. **81**, 175 (1992). https://doi.org/10.1016/0378-3812(92)85150-7
267. J.W. Magee, J.A. Howley, J.F. Ely, Gas Process. Assoc. **RR-136**, 32 (1994)
268. J.C. Seitz, J.G. Blencoe, R.J. Bodnar, J. Chem. Thermodyn. **28**, 539 (1996). https://doi.org/10.1006/jcht.1996.0050
269. G.I. Kaminishi, Y. Arai, S. Saito, S. Maeda, J. Chem. Eng. Jpn. **1**, 109 (1968). https://doi.org/10.1252/jcej.1.109
270. C. Yokoyama, K. Arai, S. Saito, H. Mori, Fluid Phase Equilib. **39**, 101 (1988). https://doi.org/10.1016/0378-3812(88)80006-2
271. A. Cipollina, R. Anselmo, O. Scialdone, G. Filardo, A. Galia, J. Chem. Eng. Data **52**, 2291 (2007). https://doi.org/10.1021/je700307r
272. N.P. Freitag, D.B. Robinson, Fluid Phase Equilib. **31**, 183 (1986). https://doi.org/10.1016/0378-3812(86)90012-9
273. S. Cheng, F. Shang, W. Ma, H. Jin, N. Sakoda, X. Zhang, L. Guo, J. Chem. Eng. Data **64**, 1693 (2019). https://doi.org/10.1021/acs.jced.8b01206
274. W.E. Hensel, F.E. Massoth, J. Chem. Eng. Data **9**, 352 (1964). https://doi.org/10.1021/je60022a011
275. J.S. Morris, C.H. Byers, Fluid Phase Equilib. **66**, 291 (1991). https://doi.org/10.1016/0378-3812(91)85062-Y
276. H.-J. Ng, D.B. Robinson, A.-D. Leu, Fluid Phase Equilib. **19**, 273 (1985). https://doi.org/10.1016/0378-3812(85)87021-7
277. D.B. Robinson, J.A. Bailey, Can. J. Chem. Eng. **35**, 151 (1957)
278. D.B. Robinson, A.P. Lorenzo, C.A. Macrygeorgos, Can. J. Chem. Eng. **37**, 212 (1959). https://doi.org/10.1002/cjce.5450370603
279. P. Theveneau, X. Xu, O. Baudouin, J.-N. Jaubert, P. Ceragioli, C. Coquelet, J. Chem. Eng. Data **65**, 1802 (2020). https://doi.org/10.1021/acs.jced.9b01082
280. A.G. Perez, Etudes Expérimentales et Modélisation Du Comportement de Phase et Des Propriétés de Transport Des Mélanges Liés à La Capture et Au Stockage Du Carbone, Ph.D. Thesis, MINES ParisTech, 2016
281. B. Gimeno, S. Martínez-Casasnovas, I. Velasco, S.T. Blanco, J. Fernández, Fuel **255**, 115800 (2019). https://doi.org/10.1016/j.fuel.2019.115800
282. I.R. Kritschewsky, V.P. Markov, Acta Physicochim. **1**, 56 (1940)
283. E.W. Lemmon, M.O. McLinden, W. Wagner, J. Chem. Eng. Data **54**, 3141 (2009). https://doi.org/10.1021/je900217v
284. D. Rowland, T.J. Hughes, E.F. May, J. Chem. Thermodyn. **97**, 206 (2016). https://doi.org/10.1016/j.jct.2016.01.005
285. A. Jäger, V. Vinš, J. Gernert, R. Span, J. Hrubý, Fluid Phase Equilib. **338**, 100 (2013). https://doi.org/10.1016/j.fluid.2012.10.017
286. V. Vinš, A. Jäger, R. Span, J. Hrubý, Fluid Phase Equilib. **427**, 268 (2016). https://doi.org/10.1016/j.fluid.2016.07.014
287. V. Vinš, A. Jäger, J. Hrubý, R. Span, Fluid Phase Equilib. **435**, 104 (2017). https://doi.org/10.1016/j.fluid.2016.12.010
288. A. Jäger, V. Vinš, R. Span, J. Hrubý, Fluid Phase Equilib. **429**, 55 (2016). https://doi.org/10.1016/j.fluid.2016.08.027
289. S. Hielscher, V. Vinš, A. Jäger, J. Hrubý, C. Breitkopf, R. Span, Fluid Phase Equilib. **459**, 170 (2018). https://doi.org/10.1016/j.fluid.2017.12.015
290. S. Hielscher, B. Semrau, A. Jäger, V. Vinš, C. Breitkopf, J. Hrubý, R. Span, Fluid Phase Equilib. **490**, 48 (2019). https://doi.org/10.1016/j.fluid.2019.02.019

291. B. Semrau, S. Hielscher, M. Thol, R. Span, Int. J. Thermophys. **43**, 43 (2022). https://doi.org/10.1007/s10765-021-02959-x
292. R. Feistel, Deep Sea Res. Part I Oceanogr. Res. Pap. **55**, 1639 (2008). https://doi.org/10.1016/j.dsr.2008.07.004
293. K.S. Pitzer, *Activity Coefficients in Electrolyte Solutions*, 2nd edn. (CRC Press, Boca Raton, 1991)
294. B. Semrau, Combination of Empirical Multi-Parameter Helmholtz-Energy Mixture Models with Gibbs-Energy Based Brine Models, Ph.D. Thesis, Ruhr-Universität Bochum, 2022
295. A. Chapoy, A.H. Mohammadi, A. Chareton, B. Tohidi, D. Richon, Ind. Eng. Chem. Res. **43**, 1794 (2004). https://doi.org/10.1021/ie034232t
296. R. Crovetto, R. Fernández-Prini, M.L. Japas, J. Chem. Phys. **76**, 1077 (1982). https://doi.org/10.1063/1.443074
297. P.C. Gillespie, G.M. Wilson, *Research Report RR-48: Vapor-Liquid and Liquid-Liquid Equilibria: Water-Methane, Water-Carbon Dioxide, Water-Hydrogen Sulfide, Water-NPentane, Water-Methane-NPentane* (Tulsa, OK, 1982)
298. T.D. O'Sullivan, N.O. Smith, J. Phys. Chem. **74**, 1460 (1970). https://doi.org/10.1021/j100702a012
299. M. Yarrison, K.R. Cox, W.G. Chapman, Ind. Eng. Chem. Res. **45**, 6770 (2006). https://doi.org/10.1021/ie0513752
300. N.M. Lancaster, C.J. Wormald, J. Chem. Eng. Data **35**, 11 (1990). https://doi.org/10.1021/je00059a004
301. G. Smith, A. Sellars, T. Yerlett, C. Wormald, J. Chem. Thermodyn. **15**, 29 (1983). https://doi.org/10.1016/0021-9614(83)90101-5
302. C.J. Wormald, C.N. Colling, J. Chem. Thermodyn. **15**, 725 (1983)
303. I.M. Abdulagatov, A.R. Bazaev, R.K. Gasanov, A.E. Ramazanova, J. Chem. Thermodyn. **28**, 1037 (1996). https://doi.org/10.1006/jcht.1996.0089
304. O. Akin-Ojo, A.H. Harvey, K. Szalewicz, J. Chem. Phys. **125**, 014314 (2006). https://doi.org/10.1063/1.2207139
305. D. Koschel, J.Y. Coxam, V. Majer, Ind. Eng. Chem. Res. **46**, 1421 (2007). https://doi.org/10.1021/ie061180+
306. C.J. Wormald, J. Chem. Thermodyn. **35**, 1019 (2003). https://doi.org/10.1016/S0021-9614(03)00044-2
307. F. Caubet, Z. Phys. Chem. **40**, 257 (1902)
308. K.Y. Song, R. Kobayashi, SPE Form. Eval. **2**, 500 (1987)